Fakultät für Chemie

Entwicklung und Optimierung von Anreicherungstechniken zur Bestimmung von Silbernanopartikeln in Umweltproben

Alexander Urstöger

Vollständiger Abdruck der von der Fakultät für Chemie
der Technischen Universität München zur Erlangung des akademischen Grades eines

Doktors der Naturwissenschaften (Dr. rer. nat.)

genehmigten Dissertation.

Vorsitzende/-r: Prof. Dr. Klaus Köhler

Prüfende/-r der Dissertation:

1. Prof. Dr. Michael Schuster

2. Prof. Dr. Martin Elsner

Die Dissertation wurde am 08.02.2021 bei der Technischen Universität München eingereicht und durch die Fakultät für Chemie am 12.05.2021 angenommen.

Die vorliegende Arbeit entstand in der Zeit von Januar 2018 bis Februar 2021 unter Anleitung von Herrn Prof. Dr. Michael Schuster in der Fachgruppe Analytische Chemie an der Fakultät für Chemie der Technischen Universität München.

Everything on the internet is 100% true. – Albert Einstein

Danksagung

Mein größter Dank gilt Herrn Prof. Dr. Michael Schuster für die freundliche Aufnahme in seinen Arbeitskreis und die wissenschaftliche Betreuung der vorliegenden Arbeit. Außerdem möchte ich mich für die überaus interessante Themenstellung, die wertvollen Ratschläge sowie das mir entgegengebrachte Vertrauen bedanken.

Vielen Dank meinen Kolleginnen und Kollegen aus dem Arbeitskreis, Andreas Wimmer, Dominik Huber, Isabelle Dolique, Stephan Fromm, Christine Hutterer, Jasmin Haberl und Stephanie Ferstl. Ihr habt meine Zeit am Arbeitskreis zu einem unvergesslichen Erlebnis werden lassen.

Vielen herzlichen Dank auch an meine Masterandinnen, Forschungspraktikantinnen, und Bachelorandinnen und Bacheloranden, Lilly Zacherl, Christina Glaubitz, Yasmin Selic, Milena Frauenschuh, Marcel Klotz, Simon Reiter und Monika Wenisch. Ohne euch wäre diese Arbeit nicht möglich gewesen.

Ferner gilt mein Dank allen Personen, die mich maßgeblich bei meiner Arbeit unterstützt und vor allem Messungen für mich durchgeführt haben: Maximilian Muhr (Lehrstuhl für Anorganische und Metallorganische Chemie, TUM) für die FTIR Messungen, Carsten Peters (Professur für Elektronenmikroskopie, TUM) für die TEM Messungen, Marina Boyko (Lehrstuhl für Anorganische Chemie mit Schwerpunkt Neue Materialien, TUM) für die SQUID Messungen, Dr. Markus Döblinger (Lehrstuhl für Physikalische Chemie – Physikalische Chemie und Nanowissenschaften, LMU) für die TEM-EDX Messungen und last but not least Dr. Ralf Kaegi (Abteilung Verfahrenstechnik, Eawag) für die TEM-EDX Messungen und die überaus wertvolle Zusammenarbeit, welche maßgeblich zum Gelingen dieser Arbeit beigetragen hat.

Ein ganz besonderer Dank gilt meinen Freunden und meiner Familie, besonders meinen Eltern, die mich immer mit allen Mitteln unterstützt haben, und euch beiden Kindsköpfen Dominik und Max für die zahlreichen erlebten Abenteuer.

Zum Schluss möchte ich noch der wichtigsten Person in meinem Leben danken, Theresa, die immer für mich da ist, besonders auch, wenn es mal gerade nicht so läuft.

Kurzfassung

Durch den zunehmenden Gebrauch von silbernanopartikelhaltigen Erzeugnissen werden diese Nanomaterialien auch als Schadstoffe in die Umwelt freigesetzt. Um deren Auswirkung auf Ökosysteme umfangreich erfassen zu können sind analytische Techniken notwendig, welche eine Charakterisierung von Silbernanopartikeln (AgNP) in Umweltproben erlauben. Erfolgversprechende Techniken, welche auch in Umweltproben anwendbar sind, sind zum einen die magnetische Festphasenextraktion (MSPE) und zum anderen die Cloud Point Extraktion (CPE) von AgNP und deren nachfolgende Charakterisierung mit Einzelpartikelmassenspektrometrie (sp-ICP-MS) und Transmissionselektronenmikroskopie gekoppelt mit energiedispersiver Röntgenfluoreszenzanalyse (TEM-EDX). Für letztere müssen die Partikel allerdings stark angereichert werden.

In der vorliegenden Arbeit wurde die MSPE von AgNP mit verschiedenen chemischen Zusammensetzungen und Beschichtungen bei umweltrelevanten Konzentrationen (unterer ng L^{-1} Bereich) und Bedingungen untersucht. Ag_2S-NP konnten darauffolgend speziesselektiv unter Erhalt ihrer Partikelgrößen eluiert werden. Umweltrelevante Matrixeffekte hatten keine Auswirkung auf die Extraktion oder konnten durch Optimierung der Extraktionsbedingungen umgangen werden.

Die CPE als zweite Extraktionstechnik wurde im Hinblick auf Minimierung der Ag^+ Coextraktion weiter optimiert, wobei der Zusatz von D-Penicillamin eine entscheidende Rolle spielte. Die Ag^+ Coextraktion konnte so bis auf 1.6 % reduziert werden, was zu Partikelgrößennachweisgrenzen bis hinunter zu 4.8 nm für sp-ICP-MS Messungen führte.

Nach der Optimierung und Validierung der CPE wurde diese hinsichtlich einer maximalen Anreicherung und Fokussierung der Partikel für eine nachfolgende TEM-EDX Messung weiterentwickelt. Die CPE wurde hierfür auf einer repetitiven Basis angewandt und mit einer Zentrifugationstechnik kombiniert, um möglichst alle AgNP im CPE Extrakt auf einem TEM-Grid zu abzulagern. Damit konnten AgNP in Realwasserproben bei einer Konzentration von 5 ng L^{-1} mit TEM-EDX sichtbar und charakterisierbar gemacht werden.

AgNP werden durch Flüsse schließlich ins Meer transportiert. Bei Inkubation in Meerwassermatrix lösten sich alle AgNP Spezies, welche in dieser Studie verwendet wurden, nahezu vollständig innerhalb von drei Tagen auf. TEM-EDX Messungen zeigten bei der Inkubation von Ag_2S-NP einen Rückgang des Ag:S Verhältnisses auf 1:1, was auf die Ausbildung einer Schwefelschicht um die sich auflösenden Partikel hindeutet.

Abstract

The increasing use of silver nanoparticles in industrial goods also results in their subsequent release into the environment, thus posing potential harm to ecosystems. Therefore, analytical techniques and procedures are needed for monitoring these nanomaterials in order to fully understand their impact on the environment. Promising techniques which help overcoming several shortcomings when dealing with environmental samples are the magnetic solid phase extraction (MSPE) and the cloud point extraction (CPE) of silver-based nanoparticles (Ag-b-NPs) and their subsequent determination with single particle inductively coupled plasma mass spectrometry (sp-ICP-MS) and transmission electron microscopy coupled with energy dispersive X-ray spectroscopy (TEM-EDX), while great particle enrichment is essential to meet the needs of the latter.

In this work the MSPE of Ag-b-NPs of varying chemical composition and coatings at environmentally relevant concentrations in the low ng L^{-1} range and the subsequent species selective, size preserving elution of Ag_2S-NPs – the predominant Ag-b-NP species in the environment – is presented. Environmentally relevant matrix effects either did not affect the extraction or could be overcome by optimization of the extraction procedure.

CPE as a second extraction technique was optimized further focusing on reducing Ag^+ coextraction to a minimum. The addition of D-penicillamine showed to be a crucial part for achieving coextraction levels as low as 1.6%, thus significantly reducing particle size detection limits down to 4.8 nm with sp-ICP-MS.

After optimization of the CPE and validating its feasibility for subsequent Ag-b-NP characterization with sp-ICP-MS, CPE was developed further towards maximizing enrichment factors for subsequent nanoparticle characterization using TEM-EDX. Therefore, CPE was applied on a repetitive basis and coupled to an on-grid centrifugation technique to ensure nearly complete deposition of all Ag-b-NPs in the CPE extract on the TEM-grid. Following the presented method, Ag-b-NPs at environmentally relevant concentrations of 5 ng L^{-1} could successfully be visualized in environmental water samples and characterized with TEM-EDX.

Ultimately, Ag-b-NPs are transported via rivers into the sea. Incubation studies in seawater matrix showed, that all Ag-b-NP species applied in these studies at environmentally relevant concentrations of 50 ng L^{-1} were nearly completely dissolved within three days. TEM-EDX measurements of Ag_2S-NPs incubated in seawater matrix revealed a decrease of the Ag:S ratio in the particles to 1:1, thus suggesting the formation of a sulfur layer around the particles.

Abkürzungsverzeichnis

AF^4	Asymmetrische Fluss-Feld-Fluss-Fraktionierung
AgNP	Silbernanopartikel
Ag-b-NP	silberbasierte Nanopartikel, engl.: *silver-based nanoparticles*
AgCl-NP	Silberchloridnanopartikel
Ag_2S-NP	Silbersulfidnanopartikel
ATR	abgeschwächte Totalreflexion, engl: *attenuated total reflection*
AuNP	Goldnanopartikel
BET	*Brunauer-Emmet-Teller* Technik
BSA	Rinderserumalbumin, engl: *bovine serum albumine*
CA@Ag-NP	citratstabilisierte Silbernanopartikel
CCD	engl.: *charge coupled device*
cmc	kritische Mizellbildungskonzentration, engl.: *critical micellar concentration*
CPE	Cloud Point Extraktion
DLS	Dynamische Lichtstreuung, engl.: *dynamic light scattering*
EDTA	Ethylendiamintetraacetat
ETAAS	Elektrothermale Atomabsorptionsspektrometrie
FFF	Feld-Fluss-Fraktionierung
FTIR	Fourier-Transform-Infrarotspektroskopie
GFAAS	Grafitofenatomabsorptionsspektroskopie, engl.: *graphite furnace atomic absorption spectrometry*
HAADF	engl.: *high-angle annular dark-field*
HRTEM	Hochauflösende Transmissionselektronenmikroskopie, engl.: *high resolution transmission electron microscopy*
iCPE	engl.: *improved cloud point extraction*
ICP-MS	Massenspektrometrie mit induktiv gekoppeltem Plasma, engl.: *inductively coupled plasma mass spectrometry*
IOMPs	magnetische Eisenoxidpartikel, engl.: *iron oxide magnetic particles*
IR	Infrarotspektroskopie
MSPE	magnetische Festphasenextraktion, engl.: *magnetic solid phase extraction*
NP	Nanopartikel

NOM	natürlich vorkommendes organisches Material, engl.: *natural organic matter*
NTA	Nanopartikel-Tracking-Analyse
PA	D-Penicillamin
$rCPE_x$	repetitive Cloud Point Extraktion mit x = die Anzahl an durchgeführten Extraktionen
SDL	Partikelgrößennachweisgrenze, engl.: *size detection limit*
SQUID	supraleitende Quanteninterferenzeinheit, engl.: *superconducting quantum interference device*
sp-ICP-MS	Einzelpartikelmassenspektrometrie, engl.: *single particle inductively coupled plasma mass spectrometry*
STEM	Rastertransmissionselektronenmikroskopie, engl.: *scanning transmission electron microscopy*
TEM	Transmissionselektronenmikroskop
TEM-EDX	Transmissionselektronenmikroskopie gekoppelt mit energiedispersiver Röntgenfluoreszenzanalyse, engl.: *transmission electron microscopy coupled with energy dispersive X-ray spectroscopy*
TX-114	Triton™ X-114
UPW	Reinstwasser, engl.: *ultra-pure water*

Inhaltsverzeichnis

1. Einleitung

Seit der erstmaligen Erwähnung des Begriffes der „Nanotechnologie“ im Jahr 1974 durch N. Taniguchi im Rahmen der *International Conference on Production Engineering* in Tokyo breitete sich diese vormalige Nischentechnologie in rasantem Tempo aus und wurde letztlich zu einem unverzichtbaren Bestandteil in vielen modernen industriellen Erzeugnissen.[1, 2] Der zunehmende Gebrauch von nanomaterialhaltigen Produkten resultiert allerdings auch in der Freisetzung von Nanomaterialien durch Abwasser und Entsorgung dieser Produkte.[3-6] Einher mit diesem Eintrag in die Umwelt geht eine breit geführte Diskussion über eine mögliche Umweltverschmutzung und daraus resultierenden toxikologisch relevanten Aspekten, welche das gesamte Ökosystem betreffen. Eine Nanomaterialspezies, die dabei besonders im Fokus steht, sind Silbernanopartikel (AgNP).[7] Um eine vollumfängliche Risikoabschätzung des Nanopartikeleintrages in die Umwelt ermöglichen zu können, müssen diese in Umweltproben überwacht und vollständig charakterisiert werden. Dazu werden analytische Techniken benötigt, welche einer Reihe von Herausforderungen gewachsen sind, die im Umgang mit Umweltproben entstehen. Diese sind erstens eine besonders geringe Nanopartikelkonzentration im unteren ng L^{-1}-Bereich, zweitens die Vielzahl an verschiedenen Transformationsprodukten, welche AgNP in der Umwelt unterliegen, und drittens eine sehr anspruchsvolle Probenmatrix.[8-10]

In der vorliegenden Arbeit wurden daher Extraktionstechniken untersucht, welche diesen Einschränkungen gewachsen sind. Dies ist zuerst die magnetische Festphasenextraktion (MSPE, engl.: *magnetic solid phase extraction*) von AgNP mit Eisen(II,III)-oxidpartikeln (IOMPs, engl.: *iron oxide magnetic particles*) in Umweltproben und die nachfolgende Elution der AgNP für eine Charakterisierung mittels Massenspektrometrie mit induktiv gekoppeltem Plasma (ICP-MS, engl.: *inductively coupled plasma mass spectrometry*) und Einzelpartikelmassenspektrometrie (sp-ICP-MS, engl.: *single particle ICP-MS*) (Publikation 1). Die zweite Extraktionstechnik, welche für eine nachfolgende Charakterisierung der AgNP in Umweltproben herangezogen wird, ist die Cloud Point Extraktion (CPE). Diese wurde zunächst im Zusammenhang mit ICP-MS und sp-ICP-MS Messungen optimiert und validiert (Publikation 2) sowie auf einer repetitiven Basis für eine nachfolgende Nanopartikelcharakterisierung mittels Transmissionselektronenmikroskopie (TEM) gekoppelt mit energiedispersiver Röntgenfluoreszenzanalyse (EDX) weiterentwickelt (Publikation 3). Zu guter Letzt wurde noch das Schicksal von AgNP in Meerwasserproben untersucht, wohin diese durch Fließgewässer schließlich transportiert werden (Publikation 4).

2. Nanomaterialien

2.1. Definition, Eigenschaften, Anwendungen und Synthese

Nach Empfehlung der Europäischen Kommission handelt es sich bei Nanomaterialien um Produkte, bei denen mindestens 50 % der Partikel Abmessungen < 100 nm in mindestens eine Raumrichtung aufweisen.[11] Eine weitere Einteilung erfolgt anhand der Anzahl an Raumrichtungen mit Abmessungen < 100 nm dieser Partikel. Unterschieden wird hierbei zwischen 0D, 1D, 2D und 3D Nanomaterialien. Die Abmessungen von 0D Nanomaterialien sind in allen drei Raumrichtungen < 100 nm. 0D Nanomaterialien werden daher auch als Nanopartikel bezeichnet. 1D Nanomaterialien (oder Nanostäbchen) weisen in einer Dimension Abmessungen > 100 nm auf. 2D Nanomaterialien werden als Nanoplättchen bezeichnet mit Abmessungen von > 100 nm in zwei Raumrichtungen. 3D Nanomaterialien schließlich sind in allen drei Raumdimensionen > 100 nm, bestehen allerdings aus Nanostrukturen, wie z.B. Nanostäbchen oder Nanopartikeln.[12]

Aufgrund ihres im Gegensatz zum Grundmaterial deutlich erhöhten Oberflächen-zu-Volumen Verhältnisses zeigen Nanomaterialien gänzlich andere physikalische und chemische Eigenschaften als ersteres. Die Variierung von Größe und Form bei Metallnanopartikeln führt zu einer Veränderung der Oberflächenplasmonenresonanz und folglich zu unterschiedlichen elektronischen und optischen Eigenschaften.[13] Bei maßgeschneiderter Synthese kann damit beispielsweise die Lichtabsorption kontrolliert werden.[14-17] Ferner macht man sich die einzigartigen optischen Eigenschaften von Nanomaterialien zum Beispiel in der Herstellung von Quantenpunkten zunutze.[18] Weitere Anwendungen gehen vom Gebrauch in Katalyse[19] und Sensortechnik[20] über Medizin- und Kosmetikprodukten[21-23] bis hin zu Wandfarben.[19]

Eine der meistgenutzten Spezies in der Nanotechnologie sind Silbernanopartikel. Da auf diesen das Hauptaugenmerk dieser Arbeit liegt, soll im Folgenden noch näher darauf eingegangen werden. Besonders ihren antimikrobiellen Eigenschaften verdanken AgNP ihre Vielzahl an Anwendungen. Diese sind u.a. in Kosmetikprodukten,[4, 24] Sportkleidung,[3, 4] Lebensmittelverpackungen,[25] Medizinprodukten,[19, 26] Wandfarbe[5] oder auch als Additive in Tierfutter[27] enthalten. AgNP werden aber nicht nur wegen ihrer antimikrobiellen Eigenschaften verwendet, sondern finden auch in der Katalyse[28, 29] oder der Krebstherapie[30] – besonders mit verschiedenen Liganden beschichtete AgNP – Anwendung.

Solche beschichteten Nanopartikel werden als Core-Shell Nanopartikel mit der Nomenklatur Shell@Core bezeichnet.[31]

Die Synthese von Nanopartikeln folgt generell zwei verschiedenen Ansätzen, welche als *bottom-up* und *top-down* Synthese bezeichnet werden. *Bottom-up* beschreibt die Herstellung von Nanopartikeln ausgehend von gelöster Spezies durch Reduktion, Gasphasenabscheidung als auch mithilfe von elektrochemischen oder sonochemischen Methoden.[32, 33] *Top-down* Methoden verfolgen hingegen genau den gegenteiligen Ansatz, also die Produktion von Nanomaterialien ausgehend vom Festkörper durch beispielsweise Zermahlen, Photolithographie oder Laserablation.[33-35] Generell führen *top-down* Methoden zu einer engeren Partikelgrößenverteilung und eignen sich daher besser für die Massenproduktion von Nanomaterialien mit einer bestimmten Größe und Form, sind meist allerdings recht kostenintensiv. *Bottom-up* Verfahren resultieren hingegen in kleineren, oft schwer kontrollierbaren Partikelgrößen und -formen. [33, 36] Seit kurzem gewinnt außerdem die Biosynthese von Nanomaterialien zunehmend an Bedeutung.[37]

2.2. Silbernanopartikelproblematik in der Umwelt

Der zunehmende Gebrauch von silbernanopartikelhaltigen Produkten geht allerdings auch mit der Freisetzung dieser Materialien in die Umwelt einher. Die daraus resultierende Diskussion über den Einfluss von AgNP auf das Ökosystem führte zu zahlreichen Studien, welche unterschiedliche Aspekte des Nanopartikeleintrages in die Umwelt beleuchten. Obwohl der Großteil an Nanopartikeln im Klärschlamm von Klärwerken verbleibt, gelangt ein kleiner Teil mit Konzentrationen von 0.7 – 11.1 ng L^{-1} im Ablauf in die Umwelt.[9, 38, 39] Aber auch der größte im Klärschlamm verbleibende Anteil kann durch Felddüngung in der Umwelt landen.[9, 39-41] AgNP werden allerdings nicht nur anthropogen in die Umwelt eingetragen, sondern können dort auch natürlich entstehen. Wimmer *et al.* konnten zeigen, dass AgNP durch Reduktion von gelöstem Ag(I) in Gegenwart von natürlichem organischem Material (NOM, engl.: *natural organic matter*) gebildet werden.[42] Letztendlich gelangen AgNP über Flüsse in das Meer.

Silbernanopartikel interagieren schließlich mit Organismen und werden von ihnen aufgenommen. Aufgrund ihrer Biotoxizität stellen sie daher ein nicht zu unterschätzendes Risiko vor allem für Kleinstlebewesen in Oberflächengewässern dar. Zahlreiche Studien belegen die Toxizität von AgNP auf wirbellose Süßwasserlebewesen[43] und Wirbeltiere,[44-46] Bakterien,[47-49] Algen,[50] Pflanzen,[50, 51] und auch menschliche Zellen.[52-55] Dabei

zeigten nicht nur Silberionen aufgrund deren Freisetzung aus AgNP, sondern auch die Partikel selbst toxische Effekte.[55, 56] Die Toxizität von AgNP ist indessen von verschiedenen Faktoren abhängig. Diese sind neben deren Konzentration vor allem die Partikelgröße, -form und chemische Zusammensetzung. Aufgrund ihrer großen spezifischen Oberfläche dringen kleinere Nanopartikel (< 20 nm) erstens besser in Zellen ein und setzen zweitens deutlich leichter Silberionen frei.[57, 58] Auch die Partikelform hat großen Einfluss auf deren Vermögen, in Organismen und Zellen eindringen zu können. Sphärische Nanopartikel beispielsweise gelangen deutlich leichter durch Zellwände als Nanostäbchen.[59] Einen großen Einfluss auf die Toxizität von AgNP hat außerdem ihre chemische Zusammensetzung. Eine partielle Sulfidierung größer einem Molverhältnis von 0.073 S/Ag zeigte einen signifikanten Rückgang der Nanopartikeltoxizität. Dies kann mit der geringen Löslichkeit von Ag_2S erklärt werden, da durch eine Sulfidschicht auf den AgNP deutlich weniger toxische Silberionen abgegeben werden.[60]

Die chemische Zusammensetzung der Nanopartikel ist insofern von Belang, da AgNP in der Umwelt nicht als statisches Element betrachtet werden können, da sie dort laufend einer Vielzahl an Transformationen unterliegen, welche zum größten Teil auch noch ungeklärt sind. Transformationsmöglichkeiten umfassen dabei sowohl die Adsorption von NOM als auch die Adsorption an in der Umwelt vorhandene Feststoffpartikel, Agglomeration, Oxidation, (partielle) Auflösung der Partikel und auch Reaktionen mit gelösten Spezies, was z.B. in Ag_2S oder AgCl Nanopartikeln oder Beschichtungen (Ag_2S@Ag, AgCl@Ag) resultiert, wobei Silbersulfidnanopartikel (Ag_2S-NP) die in der Umwelt vorherrschende AgNP Spezies darstellen.[7, 38, 40, 61-63]

Um nun eine umfassende Bewertung der Nanopartikelproblematik in der Umwelt vornehmen zu können, sind analytische Techniken und Verfahren notwendig, mit denen die Nanopartikelexposition in der Umwelt verfolgt und beobachtet werden kann. Bei der Handhabung von Umweltproben fallen allerdings eine Reihe von Problemstellungen an, welche mit solchen Methoden bewältigt werden müssen. Dies sind in erster Linie geringe Nanopartikelkonzentrationen im unteren ng L^{-1} Bereich, die Vielzahl an verschieden zusammengesetzten AgNP, welche berücksichtigt werden müssen, und außerdem eine relativ anspruchsvolle Probenmatrix.[2, 8-10]

2.3. Verfahren und aktuelle Entwicklungen in der Nanopartikelanalytik

Die im Zuge dieser Arbeit verwendeten Trenntechniken, wie MSPE, CPE und Dialyse, sowie analytischen Methoden, wie ICP-MS, sp-ICP-MS, TEM-EDX, SQUID (supraleitende Quanteninterferenzeinheit, engl.: *superconducting quantum interference device*) und Infrarotspektroskopie (IR) werden in späteren Kapiteln behandelt. Im Folgenden soll kurz auf aktuelle verschiedene Verfahren zur Charakterisierung von Nanopartikeln eingegangen werden.

Mithilfe der Feld-Fluss-Fraktionierung (FFF) können Nanopartikel von störenden Matrixbestandteilen abgetrennt werden. Innerhalb eines parabolischen Strömungsprofils der FFF-Zelle werden die Partikel anhand ihrer Größe aufgetrennt. Die Größe korreliert dabei mit der Elutionszeit, da kleinere Partikel im Strömungsprofil schneller wandern als größere.[64] Eine Spezialform der FFF stellt die Asymmetrische Fluss-Feld-Fluss-Fraktionierung (AF^4) dar. Hier bedient man sich eines senkrecht zum Strömungsprofil der Probe ausgerichteten Kreuzflusses. Dieser ermöglicht zusätzlich eine dreidimensionale Auftrennung der Partikel, da kleinere Nanopartikel in der Mitte der Zelle verbleiben und außerdem schneller eluiert werden als größere, welche an den Rand der Zelle wandern und zusätzlich später eluiert werden. Zur Detektion der Nanopartikel kann ein Lichtstreudetektor, ein UV/VIS Spektrometer oder ein ICP-MS nachgeschaltet werden. Ein Nachteil dieser Methode sind die hohen Anschaffungskosten, geringe Wiederfindungsraten und lange Messzeiten.[64-67]

Die *Brunauer-Emmet-Teller* (BET) Technik macht sich in der Charakterisierung von Nanomaterialien die Adsorption von Gasatomen und -molekülen wie z.B. N_2 auf festen Oberflächen zu Nutze. Die adsorbierte Gasmenge kann schließlich bestimmt werden und dadurch auf die Oberfläche des Materials rückgeschlossen werden. BET zeichnet sich dabei als eine akkurate, schnelle und einfache Methode zur Oberflächenbestimmung und somit – bei bekannter Partikelform – Partikelgröße von Nanomaterialien aus.[68, 69]

Bei photoaktiven Nanopartikeln, wie dies beispielsweise bei Goldnanopartikeln (AuNP) oder AgNP der Fall ist, kann mithilfe der UV/VIS Spektroskopie die Partikelgröße, Form und Konzentration bestimmt werden. Da die elektronischen und optischen Eigenschaften von photoaktiven Nanopartikeln größen- und formabhängig sind, lässt sich über die Lage des Absorptionsmaximums auf diese Charakteristika schließen. Allerdings stören andere in der

Probe vorhandene photoaktive Stoffe die Messung, weshalb diese Methode nicht für Umweltproben geeignet ist.[69, 70]

Die Dynamische Lichtstreuung (DLS) ist eine weitverbreitete Methode zur Partikelgrößenbestimmung von Nanopartikelsuspensionen. Mithilfe dieser Methode lässt sich aufgrund der Brownschen Molekularbewegung durch die zeitaufgelöste Lichtstreuung an den Partikeln deren hydrodynamischer Durchmesser bestimmen. Dieser bezeichnet den Durchmesser von Nanopartikeln und Solvensmolekülen, welche die gleiche Diffusionsrate wie die Suspension aufweisen.[69, 71]

Eine relativ neue Methode zur Partikelgrößenbestimmung ist die Nanopartikel-Tracking-Analyse (NTA). In dieser Technik wird die Laserlichtstreuungmikroskopie mit einer CCD (charged coupled device) Kamera kombiniert. So können einzelne Nanopartikel anhand ihrer Brownschen Molekularbewegung detektiert werden. Mithilfe der Stokes-Einstein Gleichung kann durch Partikelbewegung auf die Partikelgröße rückgeschlossen werden. Weil mit der NTA im Gegensatz zur DLS einzelne Partikel bestimmt werden, ergibt sich dadurch ein immenser Vorteil, da Begleitsubstanzen die Messung nicht stören.[69, 72]

Die Grafitofenatomabsorptionsspektrometrie (GFAAS, engl.: *graphite furnace atomic absorption spectrometry*) wurde in jüngster Zeit ebenfalls für die Charakterisierung von Nanopartikeln herangezogen. Da Nanopartikel im Vergleich zu gelöster Spezies später atomisiert werden, kann aufgrund der Korrelation der Verzögerungszeit bis das Absorptionsmaximum erreicht ist mit der Nanopartikelgröße eben diese bestimmt werden.[73-77]

3. Anreicherungs- und Aufreinigungstechniken für Silbernanopartikel

Wie schon in Kapitel 2.2. erwähnt, wartet die Analyse von nanopartikelhaltigen Umweltproben mit einigen Herausforderungen auf. Dadurch werden Verfahren benötigt, welche diese bewältigen können. Im Folgenden soll kurz auf die in dieser Arbeit verwendeten Techniken, die MSPE und die CPE, eingegangen werden. Außerdem wird noch kurz die Dialyse als Aufreinigungstechnik für Nanopartikelsuspensionen beschrieben.

3.1. Magnetische Festphasenextraktion

Magnetische Eisenoxidpartikel (IOMPs, engl.: *iron oxide magnetic particles*) werden aufgrund ihrer einfachen Handhabung, geringen Toxizität und vielfältigen Möglichkeiten für Oberflächenmodifikationen in etlichen Disziplinen wie Medizin, Biotechnologie oder Analytischer Chemie für die Festphasenextraktion eingesetzt. Die sogenannte magnetische Festphasenextraktion (MSPE) zeichnet sich dabei besonders durch hohe Selektivität, sowie hohe Anreicherungsfaktoren und hohe Wiederfindungsraten aus. Nach erfolgter Extraktion kann der Analyt schließlich mit einem geeigneten Eluens eluiert werden.[78-80]

Liu *et al.* setzten diese Technik bereits für die Extraktion von AgNP im µg L^{-1} Bereich ein, was allerdings deutlich über umweltrelevanten Konzentrationen liegt.[81] Die Adsorption der AgNP an die IOMP Oberfläche folgt dabei einem Prozess pseudo-zweiter Ordnung, welcher mit der Langmuir Isotherme beschrieben werden kann. Die Adsorption erfolgt dabei hauptsächlich aufgrund von elektrostatischen Wechselwirkungen zwischen den AgNP und der IOMP Oberfläche. Die hohe Verfügbarkeit von Adsorptionsstellen führt dabei in den ersten 15 min zu einer schnellen Adsorption der AgNP, bis die Anzahl der verfügbaren Adsorptionsstellen abnimmt und sich die Reaktion verlangsamt und schließlich ein Adsorptionsgleichgewicht erreicht. Die Adsorption von AgNP an IOMPs ist dabei stark pH- und zeitabhängig.[82] Eine nachfolgende Elution der AgNP erreichten Liu *et al.* durch Auflösung der NP, wodurch allerdings die Information über die ursprüngliche Partikelgröße verloren ging. Nach erfolgreicher Elution konnten die IOMPs regeneriert und wiederverwendet werden.[81, 82]

3.2. Cloud Point Extraktion

Da AgNP in Oberflächengewässerproben im unteren ng L^{-1} Bereich vorkommen, müssen diese für eine weitere Messung von störenden Matrixbestandteilen abgetrennt und angereichert

werden. Dies kann mithilfe der Cloud Point Extraktion bewerkstelligt werden.[83] Ihre Ursprünge hat die CPE in der Biochemie, wo sie angewendet wird, um unpolare organische Moleküle, wie z.B. Proteine oder Metallionen, nach Komplexierung zu unpolaren Verbindungen von polaren Substanzen in wässriger Matrix abzutrennen und anzureichern.[84, 85]

Durch die Zugabe eines Tensids – im Fall der CPE für AgNP Triton X-114 (TX-114) – zu einer wässrigen Probe in einer Konzentration, welche die kritische Mizellbildungskonzentration (cmc, engl.: *critical micellar concentration*) übersteigt, bilden sich nach überschreiten der Cloud Point Temperatur (T_c = 23 °C für TX-114) Mizellen aus. Aufgrund deren amphiphilen Charakters lagern sich hierbei die Tensidmoleküle zu kugelförmigen Gebilden zusammen, wobei ihre hydrophilen Kopfgruppen in Wechselwirkung mit der die Mizellen umgebenden wässrigen Phase treten und die hydrophoben Reste ins Innere der Mizelle ragen. Die Mizellbildung ist dabei entropiegetrieben. Durch die Ausbildung der Mizellen bricht die geordnete Wasserstruktur um die hydrophilen Kopfgruppen der Tensidmonomere zusammen. [86-89] Aufgrund der Abnahme der Dielektrizitätskonstante von Wasser mit steigender Temperatur erfolgt schließlich oberhalb von T_c in der äußersten Schicht der Mizellen ein temperaturgesteuerter Dehydratationsprozess. Dieser verringert die Interaktion der Wassermoleküle mit den hydrophilen Kopfgruppen der Tensidmoleküle, wodurch Wasserstoffbrückenbindungen zwischen eben diesen gebrochen werden. Die Mizellen werden dadurch hydrophober und die Phasenseparierung setzt ein.[90, 91]

Im Inneren der Mizelle können schließlich hydrophobe Substanzen, wie eben auch Silbernanopartikel, eingeschlossen und extrahiert werden. Die nanopartikelhaltige mizellare Phase kann dann aufgrund ihrer höheren Dichte im Vergleich zur wässrigen Phase durch Sedimentation abgetrennt werden. Dieser Prozess kann durch Zentrifugation beschleunigt werden. Da das Volumen der Tensidphase im Vergleich zur wässrigen Phase deutlich kleiner ist, kann so für Silbernanopartikel eine 80-fache Anreicherung erzielt werden.[89] Um eine Coextraktion von störenden Matrixbestandteilen – insbesondere von mit NOM komplexiertem Ag^+ – zu verhindern, müssen der nanopartikelhaltigen Probe Komplexbildner zugesetzt werden. Hartmann *et al.* konnten dabei die besondere Selektivität von Ethylendiamintetraacetet (EDTA) für die Ag^+/AgNP Separation zeigen.[89] Ein großer Vorteil der CPE ist deren Kompatibilität mit Umweltproben, da erstens umweltrelevante Matrixbestandteile keinen Einfluss auf die Extraktionseffizienz zeigen und zweitens die Partikelzusammensetzung die Extraktion nicht beeinflusst. Lediglich AgNP mit einer Rinderserumalbumin (BSA, engl.: *bovine serum*

albumine) Hülle konnten nicht extrahiert werden. Dies hängt damit zusammen, dass BSA sehr gut wasserlöslich ist und daher auch AgNP in der wässrigen Phase hält.[10]

Die Extraktionseffizienz ist bei der CPE stark pH-abhängig, wobei der optimale pH-Wert nahe dem isoelektrischen Punkt des Nanomaterials liegt. Die elektrostatische Abstoßung der am isoelektrischen Punkt ungeladenen Nanopartikel wird dabei minimiert, was eine Einlagerung in die Mizellen erleichtert.[92] Bei einem pH ≥ 5 konnte für AgNP eine Extraktionseffizienz von $\eta > 0{,}9$ erreicht werden.[89] Nach erfolgter CPE müssen die AgNP mit einer selektiven Analysetechnik charakterisiert werden. Dafür haben sich besonders Elektrothermale Atomabsorptionsspektrometrie (ETAAS) und (sp-)ICP-MS Messungen bewährt.[9, 10, 42, 89, 91] In Abbildung 1 ist ein Schema der CPE für Nanopartikel dargestellt.

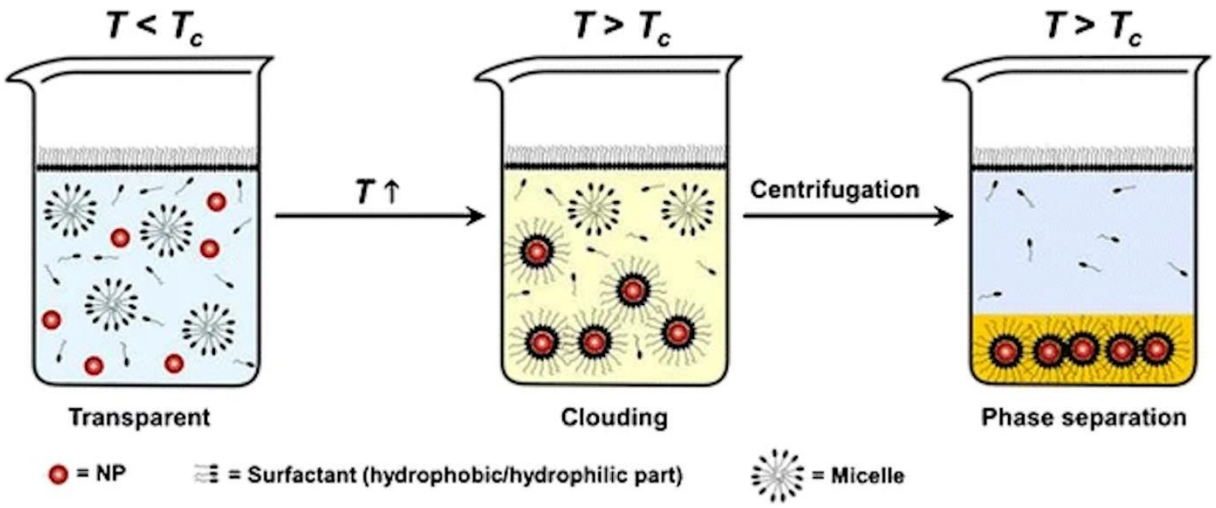

Abbildung 1. Schema der CPE für Nanopartikel nach Duester *et al.*[91]

3.3. Dialyse

Die Dialyse ist eine Technik zur Aufreinigung von hochmolekularen Verbindungen und Partikeln. In der Biochemie wird diese dazu verwendet, um beispielsweise Proteine, DNA oder Polysaccharide von kleineren Molekülen und Ionen abzutrennen. Die Dialyse kann aber auch dazu verwendet werden, Nanopartikelsuspensionen aufzureinigen.[93] Das Prinzip hinter der Dialyse ist die Brownsche Molekularbewegung. Teilchen wandern dadurch entlang eines Konzentrationsgefälles von einem Ort hoher Konzentration zu einem Ort niedriger Konzentration, bis ein Gleichgewicht erreicht ist. Wenn nun ein Ort hoher Konzentration von einem Ort niedriger Konzentration durch eine semipermeable Membran abgegrenzt wird, werden – anhängig von der Porengröße der Membran – größere Moleküle und Teilchen zurückgehalten. Kleinere Teilchen, wie z.B. Ionen und niedermolekulare Verbindungen, hingegen können die Membran passieren. Um den osmotischen Druck auf beiden Seiten der

Membran auszugleichen, wandern diese Teilchen durch die Membran zum Ort niedrigerer Konzentration, bis ein Gleichgewicht erreicht ist. Die Konzentration hinter der Membran verringert sich für diese Teilchen also, während die Anzahl der größeren Moleküle und Teilchen gleichbleibt. [94, 95]

In der Praxis wird dafür die aufzureinigende Nanopartikelsuspension in einen Dialyseschlauch mit definierter Porengröße gegeben und in einem Becherglas mit Reinstwasser (UPW, engl.: *ultra-pure water*) dialysiert. Ionen und kleinere Moleküle, wie z.B. nicht verbrauchtes Reduktionsmittel aus der Nanopartikelsynthese, können den Dialyseschlauch passieren, während die Nanopartikel im Schlauch verbleiben. Da aber auch Wasser die Membran passieren kann, ändert sich die Konzentration der Nanopartikel im Dialyseschlauch leicht, während ihre Anzahl gleichbleibt. Durch mehrmaliges Austauschen des den Dialyseschlauch umgebenden Wassers können somit nahezu alle störenden Ionen und niedermolekularen Verbindungen aus der Nanopartikelsuspension entfernt werden.

4. Analytische Methoden

In den folgenden Abschnitten werden die in dieser Arbeit verwendeten analytischen Methoden beschrieben.

4.1. Massenspektrometrie mit induktiv gekoppeltem Plasma

Die Massenspektrometrie mit induktiv gekoppeltem Plasma (ICP-MS, engl.: *inductively coupled plasma mass spectrometry*) ist eine nachweisstarke Multielementanalysenmethode, die sich besonders durch den hohen linearen Messbereich auszeichnet (pg L^{-1} – g L^{-1}). In dieser Arbeit wurde ein Agilent 7900 Quadrupol ICP-MS mit einem Autosampler SPS4 von Agilent Technologies verwendet. In Abbildung 2 ist das verwendete ICP-MS schematisch dargestellt.

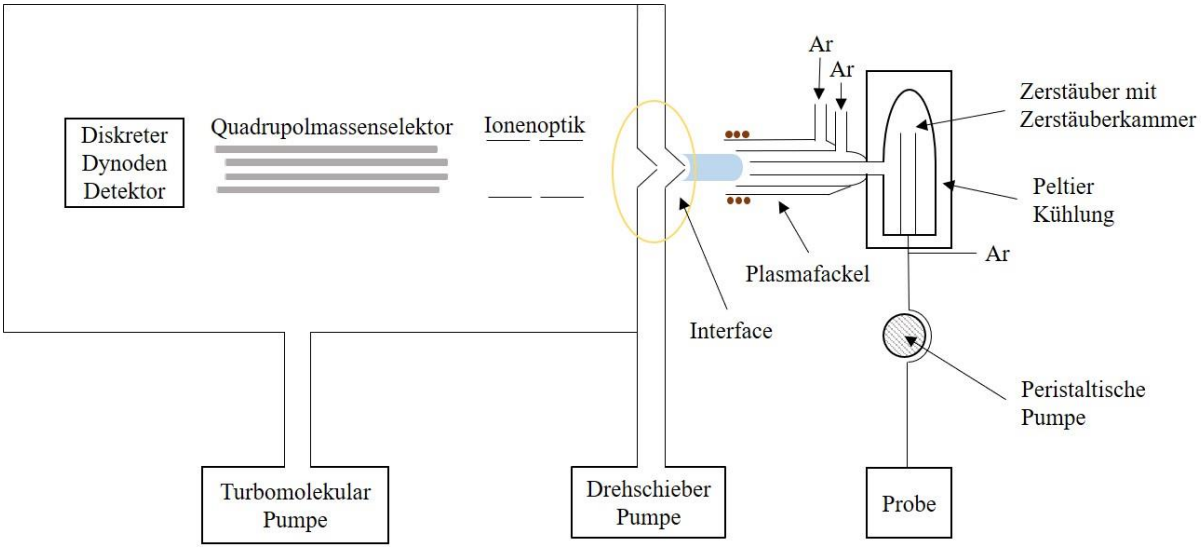

Abbildung 2: Schema des verwendeten Agilent 7900 ICP-MS.

Da im ICP-MS nur flüssige Proben gemessen werden können, muss der Analyt in gelöster Form oder, wie im Fall von nanopartikelhaltigen wässrigen Proben, als Kolloid vorliegen. Die Probe gelangt zunächst über eine peristaltische Pumpe in einen Peltier-gekühlten Zerstäuber, wird dort fein zerstäubt und erreicht schließlich die Plasmafackel. Der größte Teil des Probenaerosols gelangt allerdings in den Abfluss, da die Aerosoltropfen zu groß sind, als dass sie die Zerstäuberkammer in Richtung Plasma passieren können.[96, 97] Dies muss vor allem in der Einzelpartikelmassenspektrometrie berücksichtigt werden (siehe Kapitel 4.1.1.). Die Plasmafackel ist aus drei konzentrischen Quarzrohren aufgebaut, durch welche Argon strömt. Durch die innerste gelangt das Probenaerosol in das Plasma, der Argongasstrom in der mittleren Röhre dient zur Positionierung des Plasmas und derjenige in der äußeren zur Speisung des Plasmas (Plasmagas). Das Plasma wird mithilfe eines Hochspannungspulses aus einer

Teslaspule gezündet und erreicht durch die Kollision von freien Elektronen mit Argonatomen Temperaturen von 8000 – 10000 K. Das Probenaerosol wird im Plasma getrocknet, atomisiert und schließlich durch Kollision mit energiereichen Elektronen (aus Argonatomen) oder einfach positiv geladenen Argonatomen ionisiert.[96, 98] Der Übergang von Atmosphärendruck auf Hochvakuum wird mithilfe des Interface bewerkstelligt. Dieses ist aus zwei aufeinanderfolgenden Konen (Sampler und Skimmer) aufgebaut, wodurch die Teilchenanzahl im Gasstrom reduziert wird. Das Vakuum im Interface wird durch eine Drehschieberpumpe erzeugt.[96, 99] Hinter dem Skimmerkonus wird der Teilchenstrom schließlich durch elektrostatische Linsen fokussiert und leicht gekrümmt, sodass dieser ca. 5 mm oberhalb seiner ursprünglichen Achse in den Quadrupolmassenselektor tritt. Photonen und ungeladene Teilchen werden durch die Ionenlinsen nicht abgelenkt und gelangen daher nicht in den Massenselektor, wodurch das Hintergrundsignal verringert wird. Dadurch wird ein besseres Nachweisvermögen erreicht. Das Hochvakuum wird hier mithilfe einer Turbomolekularpumpe erzeugt.[96, 100] Der Quadrupolmassenselektor ist aus vier parallelen Edelstahlstäben aufgebaut. Durch das Anbringen einer Gleichspannung an einem Stäbepaar und einem Hochfrequenzfeld auf dem gegenüberliegenden Stäbepaar erhalten nur Ionen mit dem gewünschten Masse-zu-Ladungsverhältnis (m/z) eine stabile Flugbahn durch den Quadrupol und treffen auf den Detektor. Alle anderen Ionen weisen eine instabile Flugbahn auf und verlassen den Quadrupol nach außen, woraufhin sie von der Turbomolekularpumpe abgesaugt werden.[96, 101] Die Ionen treffen schließlich auf die erste Dynode des Diskreten Dynoden Detektors und schlagen hier Elektronen heraus. Diese treffen anschließend auf eine zweite Dynode und schlagen dort weitere Elektronen heraus. Dieser Prozess wiederholt sich an jeder Dynode, wodurch eine Elektronenkaskade erzeugt wird, die schließlich an einer Anode detektiert wird. Pro einschlagendem Ion muss dabei stets der gleiche Stromfluss entstehen, um ein reproduzierbares Ergebnis zu erhalten.[96, 102]

Beim ICP-MS können eine Reihe von spektralen Störungen auftreten. Hierbei wird grundsätzlich zwischen drei verschiedenen Störungsarten unterschieden: polyatomare Störungen, doppelt geladene Spektralinterferenzen und isobare Störungen. Die häufigsten Störungen sind polyatomare Störungen. Dies sind Molekülionen, die sich im Plasma meist aus Verbindungen des Plasmagases (Ar) und der Probenmatrix bilden und die gleiche Masse wie der Analyt aufweisen. Polyatomare Störungen können erstens mithilfe von sogenannten kalten Plasmabedingungen, zweitens durch die Verwendung von Reaktions- oder Kollisionszellen und drittens mit hochauflösenden Massenanalysatoren beseitigt werden. Bei kalten Plasmabedingungen wird die Plasmaleistung von 1000 – 1400 W auf 500 – 800 W reduziert.

Dadurch wird die Bildung polyatomarer Ionen verhindert. Allerdings ist diese Technik auf wenige Elemente in einfachen wässrigen Matrices begrenzt, deren Ionisierungstemperaturen deutlich unter normalen Plasmatemperaturen liegen.[103] Bei Reaktions- oder Kollisionszellen wird dem Quadrupolmassenanalysator ein Oktopol vorgeschaltet, in den eine geringe Menge eines Gases eingeleitet wird, welches mit polyatomaren Ionen interagiert. Dabei können sowohl reaktive Gase wie z.B. NH_3, H_2 oder CH_4 aber auch nichtreaktive Gase wie z.B. He verwendet werden. Während erstere mit polyatomaren Ionen entweder zu neutralen Spezies oder Molekülen anderer Masse reagieren und diese dadurch unschädlich machen, kollidieren letztere deutlich häufiger mit Molekülionen aufgrund ihres größeren Wirkungsquerschnittes im Vergleich zu einatomigen Ionen. Dies hat zur Folge, dass Molekülionen abgebremst werden und eine am Ende des Oktopols angelegte Potentialbarriere nicht überwinden können.[104] Die wohl beste Methode, um den Überlapp der Signale von Analyt und Molekülion zu verhindern, ist die Verwendung von hochauflösenden Massenanalysatoren, die die geringen Masseunterschiede zwischen Analyt und Molekülion auflösen können, wie z.B. doppeltfokussierende Sektorfeldmassenanalysatoren. [103] Doppelt geladene Spektralinterferenzen bezeichnen doppelt geladene Ionen, deren m/z Verhältnis dem des Analyten entspricht und daher auch wie die Analytionen den Quadrupolmassenselektor passieren können. Doppelt geladene Spezies können durch Optimierung der Plasmabedingungen verhindert werden. [103] Isobare Störungen sind Isotope anderer Elemente, die eine ähnliche Masse wie das Analytisotop aufweisen, wobei der Massenunterschied vom Massenselektor nicht aufgelöst werden kann. Isobare Störungen können durch die Verwendung hochauflösender Massenselektoren, Messung eines anderen, ungestörten Analytisotops oder mithilfe von mathematischen Korrekturgleichungen vermieden werden. Bei letzterem wird zusätzlich zur gestörten Masse eine andere, ungestörte Masse des störenden Elements gemessen. Anhand der Verhältnisse der Signalintensitäten von Analytmasse und alternativer Masse kann schließlich die Analytmasse um den Betrag des störenden Elements korrigiert werden. Auch durch die Verwendung von Reaktionszellen können eine Vielzahl an isobaren Störungen behoben werden.[103, 104]

4.1.1.Einzelpartikelmassenspektrometrie

Für die Messung von einzelnen Nanopartikeln muss das ICP-MS im Einzelpartikelmodus (sp-ICP-MS) betrieben werden. Der bedeutendste Unterschied zwischen konventioneller ICP-MS Messung und Einzelpartikelmessung ist die Messzeit (engl. *dwell time*). Während diese bei ersterer im Bereich von Sekunden liegt, muss sie bei der Einzelpartikelmessung im Bereich von

µs sein, um einzelne Partikel detektieren zu können. Wenn Nanopartikel im Plasma ionisiert werden, entsteht eine Ionenwolke, die eine bestimmte Zeit braucht, um auf dem Detektor aufzutreffen. Im Vergleich zu einzelnen Ionen, die im Detektor ein kontinuierliches Signal erzeugen, entsteht durch diese Ionenwolke ein Signalpeak. Nun muss die Messzeit allerdings möglichst klein gewählt werden, um einen Partikelzusammenfall in einem Messzeitfenster auszuschließen, was zu einer Überschätzung der Partikelgröße führen würde. Eine Messzeit, die kleiner als die Zeit ist, welche die Ionenwolke benötigt, um auf dem Detektor aufzutreffen, führt allerdings zu einer Fragmentierung des Partikels. Um dennoch die richtige Partikelgröße eruieren zu können, muss dieser fragmentierte Partikelpeak daher integriert werden.[105]

Um nun von den Partikelpeaks auf die Nanopartikelgröße und -konzentration in der Probe schließen zu können, wird die Zerstäubereffizienz η benötigt. Dies ist der Anteil an Partikeln in der Probe, die den Detektor erreichen. Die Zerstäubereffizienz kann mit drei verschiedenen Methoden ermittelt werden. Die einfachste Methode besteht darin, das Probenvolumen, welches die Zerstäuberkammer durch den Abfluss verlässt, vom in die Zerstäuberkammer gepumpten Probenvolumen zu subtrahieren.[106] Nach Methode Zwei kann mithilfe eines Partikelstandards bekannter Konzentration und Partikelgröße anhand der Anzahl an Partikelsignalen der Anteil an Partikeln im Standard berechnet werden, der den Detektor erreicht, was schließlich der Zerstäubereffizienz entspricht.[106] Die dritte Methode zieht das Signal-zu-Masse Verhältnis von gelöstem Analytstandard zu dem eines Nanopartikelstandards für die Ermittlung der Zerstäubereffizienz heran. Das Signal des gelösten Standards ist dabei abhängig von der Zerstäubereffizienz, das Signal eines Nanopartikels dagegen nicht. Nur die Anzahl an detektierten Nanopartikeln hängt von der Zerstäubereffizienz ab. Anhand der Steigung der Massenflussgerade nach Pace *et al.* (1) können die Signalintensitäten in Partikelmassen umgerechnet werden.[107] Der Grenzwert, ab dem Partikelsignale vom Hintergrundsignal unterscheidbar sind, wird dabei anhand einer iterativen Methode oder mittels Signaldekonvolution bestimmt.[107, 108]

$$W = C_{STD} \cdot \eta \cdot Q_{Probe} \cdot t_d \qquad (1)$$

Dabei ist W die Masse pro Messzeitfenster, C_{STD} die Massenkonzentration des Partikelstandards, Q_{Probe} der Probenvolumenstrom in den Zerstäuber und t_d das Messzeitfenster. Die Masse des Nanopartikels kann schließlich unter der Annahme sphärischer Partikel in den Durchmesser des Partikels umgerechnet werden. Bei anderer Partikelgeometrie kann anhand einer geeigneten Gleichung eine entsprechende Größe bestimmt werden. Die eine nanopartikelhaltige wässrige Probe charakterisierende Partikelgrößenverteilung wird

schließlich erhalten, indem der Partikeldurchmesser gegen die Häufigkeit der entsprechenden Partikelgröße aufgetragen wird.[106, 107, 109]

4.2. Elektronenmikroskopie

Wegen ihrer hohen Auflösung und der Möglichkeit, einzelne Partikel abbilden und charakterisieren zu können, sind elektronenmikroskopische Techniken, wie Transmissionselektronenmikroskopie (TEM) oder Rastertransmissionselektronenmikroskopie (STEM, engl.: *scanning transmission electron microscopy*) von besonderer Bedeutung in der Analyse von Nanomaterialien. Mithilfe dieser Methoden lassen sich Aussagen über Partikelgröße, -form, -aggregation und-verteilung machen.[69, 110] Das TEM-Bild wird dabei durch einen Elektronenstrahl generiert, welcher durch einen dünnen Probenfilm transmittiert wird. Die Elektronen interagieren mit der Probe, wobei die elastisch gestreuten Elektronen auf einem Detektor, wie z.B. einem Leuchtschirm oder einer CCD-Kamera, auftreffen und ein Bild erzeugen. Der Bildkontrast hängt dabei von der Absorption des Elektronenstrahles ab und damit von der Elektronendichte im detektierten Partikel (also von der Elementverteilung) und der Dicke bzw. Größe des Partikels. Schwerere Elemente mit höherer Elektronendichte ergeben somit einen stärkeren Kontrast als leichtere. Um organische Materialien detektieren zu können, müssen diese mit schwereren Elementen zuerst angefärbt werden.[111] Beim STEM wird der Elektronenstrahl auf einen kleinen Punkt fokussiert, der dann die Probe abrastert.[69] In Abbildung 3 ist ein Transmissionselektronenmikroskop schematisch dargestellt.

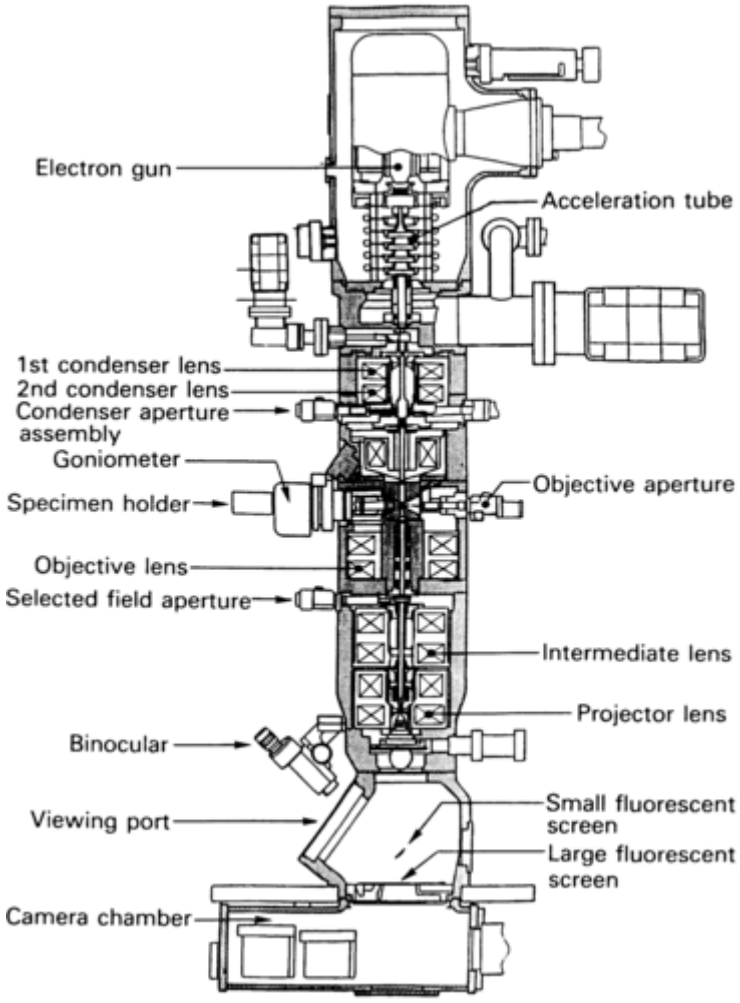

Abbildung 3: Schema eines Transmissionselektronenmikroskops nach Fultz *et al.*[112]

Durch die deutlich kleinere Wellenlänge von Elektronen im Vergleich zu sichtbarem Licht wird in der Elektronenmikroskopie eine erheblich bessere Auflösung als in der Lichtmikroskopie erreicht. Die Wellenlänge von Elektronen hängt dabei von ihrer kinetischer Energie ab.[113] Dies macht man sich in der hochauflösenden Transmissionselektronenmikroskopie (HRTEM, engl.: *high resolution TEM*) zunutze. Indem man die Beschleunigungsspannung im Elektronenmikroskop erhöht, erreichen die Elektronen beinahe Lichtgeschwindigkeit, was Auflösungen bis in den Subnanometerbereich ermöglicht.[111, 113]

Die Elektronen werden mittels Glühemission erzeugt. Dabei überwinden die Elektronen aufgrund ihrer thermischen Energie die Austrittsarbeit des Glühfadenmaterials, meist Wolfram. Eine zweite Möglichkeit, Elektronen zu erzeugen, ist durch Feldemission. Elektronen werden hier durch ein ausreichend starkes elektrisches Feld an einer Kathode erzeugt.[113, 114]

Durch Anlegen einer Spannung werden die ausgestoßenen Elektronen mit mehreren elektrostatischen und elektromagnetischen Linsen auf die Probe beschleunigt und fokussiert und treffen schließlich auf den Detektor, wo das TEM Bild generiert wird.[113]

Bei der Bildgenerierung unterscheidet man zwischen zwei Methoden: Hellfeld und Dunkelfeld. Bei ersterer wird die Objektivöffnung so eingestellt, dass nur elastisch gestreute Elektronen auf dem Detektor auftreffen können. Probenbereiche mit größerer Schichtdicke erscheinen dunkler als solche, wo kein Analyt vorhanden ist, da weniger Elektronen durch die Probe durchtreten können.[113] Bei der Dunkelfeld Methode werden nur von Probenbereichen höherer Dichte gebeugte Elektronen detektiert, weshalb diese Bereiche im TEM Bild heller erscheinen, als analytarme Probenbereiche.[113] In der HRTEM wird das Bild durch Phasenkontrastabbildung generiert, wobei beide, elastisch und inelastisch gestreute, Elektronen detektiert werden.[115] Eine Bildgenerierungstechnik für STEM Messungen ist HAADF (engl.: *high-angle annular dark-field*). Hierbei werden Rutherford-gestreute Elektronen mithilfe eines HAADF Detektors detektiert. Diese Technik ist besonders sensitiv für Elementunterschiede in der Probe.[69]

Im TEM herrscht ein Vakuum von 10^{-4} Pa (10^{-7} – 10^{-9} Pa für Hochspannungs-TEM), um die Kollision von Elektronen mit Luftbestandteilen und so auch die Ausbildung eines Lichtbogens zu vermeiden.[113]

Um die genaue Elementzusammensetzung von Nanopartikeln im TEM bestimmen zu können, kann diese mit einem energiedispersiven Röntgenfluoreszenzspektrometer (EDX, engl.: *energy dispersive X-ray spectroscopy*) kombiniert werden.[69, 111]

4.3. SQUID

Mithilfe eines SQUIDs (supraleitende Quanteninterferenzeinheit, engl.: *superconducting quantum interference device*) lassen sich geringste Magnetfeldänderungen messen. Dies macht es zu einer außerordentlich wichtigen Analysetechnik zur Charakterisierung von magnetischen – besonders von supraleitenden – Materialien.[116, 117] Ein SQUID ist aus einem supraleitenden Ring aufgebaut, der entweder an einer (rf-SQUID, engl.: *radio frequency SQUID*) oder an zwei (dc-SQUID, engl: *direct current SQUID*) Stellen durch einen Isolator unterbrochen ist. Diese Stellen werden Josephson-Kontakte genannt. Elektronen können diese Kontakte mit einer gewissen Wahrscheinlichkeit durchtunneln, was als Flusssprung bezeichnet wird und einen messbaren Stromfluss erzeugt. Wenn sich nun das äußere Magnetfeld ändert, ändert sich auch der Stromfluss und damit die Spannung am SQUID. Dabei wird ein rf-SQUID bei hochfrequenter Wechselspannung und ein dc-SQUID bei Gleichspannung betrieben.

Mithilfe eines SQUID lassen sich allerdings keine absoluten magnetischen Feldstärken messen, sondern nur Feldstärkeänderungen. Ein SQUID wird meist mit flüssigem Helium gekühlt.[117] In Abbildung 4 ist das Ringelement eines dc-SQUID schematisch dargestellt.

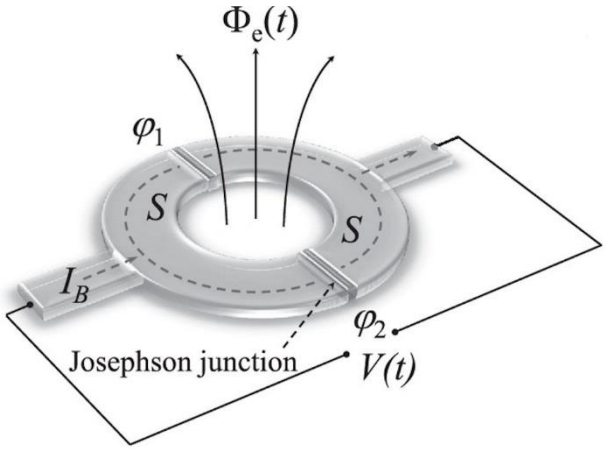

Abbildung 4: Schematische Darstellung des Ringelements eines dc-SQUID nach Bosisio *et al.*.[118]

4.4. Fourier-Transform-Infrarotspektroskopie

Durch Anregung mit Infrarotstrahlung (IR) werden Molekülrotationen und Schwingungen von Molekülbindungen angeregt. Dies macht man sich in der Infrarotspektroskopie zur Strukturaufklärung von Molekülen zunutze. Dabei wird die Probe mit Infrarotstrahlung im Bereich von 4000 – 400 cm^{-1} Wellenzahlen angeregt und deren Absorption bei der jeweiligen Wellenzahl registriert. Diese Absorptionen werden als Banden bezeichnet, welche sich anhand ihrer Lage im IR-Spektrum einzelnen funktionellen Gruppen im Molekül zuordnen lassen. Moleküle müssen dabei einen permanenten oder induzierbaren Dipol aufweisen, um IR aktiv zu sein.[119] Das in dieser Arbeit verwendete Fourier-Transform IR Spektrometer (FTIR) ist mit einer ATR (abgeschwächte Totalreflexion, engl.: *attenuated total reflection*) Einheit ausgestattet. Dabei macht man sich die Totalreflexion in einem ATR-Kristall zunutze. Wenn nun eine Probe an die Oberfläche des ATR-Kristalls gebracht wird, bilden sich in der Probe, hinter der Grenzfläche des ATR-Kristalles, an der die IR Strahlung totalreflektiert wird, evaneszente Wellen aus, mit denen die Probe wechselwirken und einen Teil der Strahlung absorbieren kann.[120] Beim FTIR wird dabei aus einem Interferogramm durch Fourier-Transformation ein IR-Spektrum errechnet, was zu einem deutlich besseren Signal-Rausch Verhältnis und kürzeren Messzeiten im Vergleich zu einem konventionellen IR Spektrometer führt. [120] Mithilfe von FTIR Messungen lassen sich so IR aktive Oberflächenbeschichtungen von Nanopartikeln hervorragend bestimmen.[69, 121]

5. Zusammenfassungen der Publikationen

5.1. Publikation 1: *Magnetic solid phase extraction of silver-based nanoparticles in aqueous samples: Influence of particle composition and matrix effects on its application to environmental samples and species-selective elution and determination of silver sulphide nanoparticles with sp-ICP-MS*

In dieser Studie wurde die magnetische Festphasenextraktion von Silbernanopartikeln mithilfe von IOMPs unterschiedlicher Größe und Form unter umweltrelevanten Bedingungen untersucht. Dazu wurden Silbernanopartikel mit verschiedenen umweltrelevanten Beschichtungen und chemischen Zusammensetzungen im unteren ng L^{-1} Bereich nach einer optimierten Methode von Zhou *et al.* extrahiert.[81] Außerdem wurde der Einfluss von verschiedenen umweltrelevanten Matrixeffekten (anorganische Salze, Silberionen, Feststoffpartikel, NOM) auf die Extraktion untersucht und die Extraktionsbedingungen entsprechend optimiert. Das Ziel war schließlich die speziesselektive Elution von Ag_2S-NP nach erfolgter Extraktion. Dabei lag ein Hauptaugenmerk darauf, die Partikel während des Elutionsprozesses nicht zu verändern, um deren ursprüngliche Größe mittels sp-ICP-MS Messung bestimmen zu können.

Die Studie konnte zeigen, dass die Extraktion von Silbernanopartikeln verschiedener chemischer Zusammensetzungen und Beschichtungen auch bei umweltrelevanten Konzentrationen Extraktionseffizienzen > 80 % lieferte. Die Form der IOMPs hat dabei großen Einfluss auf die Extraktion. Eine raue Oberfläche der Partikel ist dabei einer glatten zu bevorzugen, da diese mehr Adsorptionsstellen für AgNP bietet. Anorganische Salze (PO_4^{3-}, CO_3^{2-}, SO_4^{2-}, NO_3^-, Cl^-, NH_4^+, Na^+, Ca^{2+}, Mg^{2+}, K^+) zeigten ebenso wie Feststoffpartikel (TiO_2-Partikel) bei umweltrelevanten Konzentrationen keine großen Auswirkungen auf die Extraktionseffizienz. Durch den Zusatz von NOM konnte allerdings eine um 50 % schlechtere Extraktionseffizienz beobachtet werden, da NOM AgNP-Bindestellen auf den IOMPs besetzt und dadurch deren Adsorption verhindert. Eine Erhöhung der IOMP Konzentration von 100 mg L^{-1} auf 500 mg L^{-1} konnte diesen Effekt erfolgreich verhindern, da dadurch mehr Adsorptionsstellen für AgNP verfügbar gemacht werden. Der Zusatz von Ca^{2+}, wie von Zhou *et al.*[81] vorgeschlagen, ist hingegen nicht zu empfehlen, da dies mit einer erhöhten Coextraktion von Ag^+ einhergeht. Die Coextraktion von Ag^+ kann außerdem durch den Zusatz

von NOM unterbunden werden, was diese Extraktionstechnik besonders für Umweltproben interessant macht.

Im weiteren Verlauf der Studie wird die Optimierung der speziesselektiven, Partikelgröße bewahrenden Elution von Ag_2S-NP basierend auf EDTA beschrieben. Hierbei konnte festgestellt werden, dass ein basischer pH von 9 sowie die Erhöhung der Inkubationstemperatur auf 40 °C wesentlich zu einer besseren Desorptionseffizienz der Ag_2S-NP beiträgt. Außerdem lieferte die Zugabe des Tensids TX-114 in Konzentrationen oberhalb der kritischen Mizellbildungskonzentration und die Zugabe von D-Penicillamin eine enorme Steigerung der Desorptionseffizienz auf 76 ± 6 %. Die Partikelgröße änderte sich durch diese modifizierte Cloud Point Extraktion für Ag_2S-NP nicht. Silberkernnanopartikel und Silberchloridnanopartikel (AgCl-NP) lösten sich allerdings infolge dieser Elution auf, was das große Potential dieser Methode aufzeigt, Silbernanopartikel anhand ihrer chemischen Zusammensetzung mithilfe dieser Elution unterscheiden zu können.

Eigener Beitrag:

- *Entwurf und Ausarbeitung des Versuchskonzeptes*
- *Planung und Durchführung der Experimente*
- *Auswertung und Interpretation der Ergebnisse*
- *Schreiben der Publikation*

5.2. Publikation 2: *Separating dissolved silver from nanoparticulate silver is the key: Improved cloud-point-extraction hyphenated to single particle ICP-MS for comprehensive analysis of silver-based nanoparticles in real environmental samples down to single-digit nm particle sizes*

Das Ziel dieser Studie war die Reduzierung der Partikelgrößennachweisgrenze (SDL, engl.: *size detection limit*) für Silbernanopartikel für sp-ICP-MS Messungen. Ag^+ führt in sp-ICP-MS Messungen zu einem deutlich erhöhten Hintergrundsignal. Damit einher gehen SDL > 20 nm, was für Umweltproben deutlich zu hoch ist.[122] So fanden Kim *et al.* beispielsweise Silbernanopartikel im Bereich von 5 – 20 nm in Klärschlammproben.[123]

Die CPE ist eine vielversprechende Methode zur Separierung von AgNP und Ag^+ Spezies in wässrigen Proben. Um solch niedrige SDL zu erreichen, mit denen auch Nanopartikel in Umweltproben charakterisiert werden können wurde die CPE weiterentwickelt (iCPE) und die Kopplung an sp-ICP-MS Messungen untersucht und validiert.

Durch die Zugabe von D-Penicillamin (PA) konnte eine deutliche Reduzierung der Coextraktion von Ag^+ erreicht werden. Die Zugabe von 1000 µL PA (bei einem Probenvolumen von 40 mL) erniedrigte die Coextraktion von Ag^+ bei einer Ag^+-Konzentration von 500 ng L^{-1} (1000 ng L^{-1}) auf 1.6 % (3.1 %). Außerdem konnte keine Abhängigkeit der Nanopartikelgröße auf die Extraktionseffizienz festgestellt werden. Nanopartikel jeder Größe wurden also gleich gut extrahiert. Bei Zugabe von Ag^+ in verschiedenen Konzentrationen zu nanopartikelhaltigen Proben konnte außerdem gezeigt werden, dass die iCPE zu einer deutlich geringeren Signalzunahme führte, als dies für die ursprüngliche CPE der Fall war. Dies ist vor allem auf die geringere Coextraktion von Ag^+ im Vergleich zur CPE zurückzuführen. Versuche in Flusswasserproben lieferten Extraktionseffizienzen > 96 %, womit die iCPE auch hervorragend für Umweltproben geeignet ist.

Infolge der Kopplung der iCPE an sp-ICP-MS Messungen wurde zunächst die Konstanz der Zerstäubereffizienz η untersucht. Weder die Messzeit noch die Partikelgröße der Nanopartikel, welche für die Bestimmung von η verwendet wurde, zeigte einen Einfluss darauf.

Ein weiterer wichtiger Punkt ist die richtige Wahl der Messzeit, um Nanopartikelproben korrekt charakterisieren zu können. Dabei stellte sich heraus, dass solche Proben mit verschiedenen

Messzeiten untersucht und die Ergebnisse miteinander verglichen werden müssen, um eine bestmöglich genaue Charakterisierung gewährleisten zu können.

Infolge der Separierung von AgNP und Ag^+ konnten mithilfe der iCPE und nachfolgender sp-ICP-MS Messung SDL von 4.8 – 5.2 nm bei einer Ag^+ Konzentration von 0 – 100 ng L^{-1} erreicht werden. sp-ICP-MS Messungen ohne vorherige Extraktion der AgNP mithilfe der iCPE lieferten dagegen eine SDL von 23.1 nm.

Schließlich wurde die iCPE-(sp-)ICP-MS noch validiert und mit der bereits etablierten Methode basierend auf ETAAS-Messungen verglichen. Diese Versuchsreihe zeigte eine hervorragende Korrelation der Ergebnisse und belegt damit das große Potential der entwickelten Methode, um nanopartikelhaltige Umweltproben erfolgreich und genau charakterisieren zu können.

Eigener Beitrag:

- *Entwicklung und Durchführung der Studien zur Kopplung von iCPE und sp-ICP-MS*
- *Auswertung und Interpretation der Ergebnisse*
- *Schreiben der Publikation (Kapitel 2.2.4 sowie Kapitel 3.8)*

Wesentliche Beiträger Dritter:

- *A. Wimmer: Entwurf und Ausarbeitung des Versuchskonzeptes*
- *A. Wimmer: Entwicklung der iCPE*
- *A. Wimmer: Durchführung der Kopplungsstudien von iCPE und sp-ICP-MS*
- *A. Wimmer: Bestimmung der SDL*
- *A. Wimmer: Schreiben der Publikation (ausgenommen eigene Beiträge)*

5.3. Publikation 3: *Looking at Silver-Based Nanoparticles in Environmental Water Samples: Repetitive Cloud Point Extraction Bridges Gaps in Electron Microscopy for Naturally Occurring Nanoparticles*

Partikelgröße, -form und -zusammensetzung sind wichtige Parameter, um eine Risikoabschätzung des Silbernanopartikeleintrages in die Umwelt tätigen zu können. Eine dafür besonders gut geeignete Technik ist TEM-EDX. Da Silbernanopartikel im unteren ng L^{-1} Bereich in Umweltproben vorkommen, müssen diese für eine erfolgreiche Charakterisierung mit TEM-EDX stark angereichert werden.

In dieser Studie wurde die Cloud Point Extraktion hin zu einer repetitiven Extraktionstechnik (rCPE) weiterentwickelt, um die Anreicherung von Silbernanopartikeln zu maximieren. Diese Methode wurde schließlich mit einer Zentrifugationstechnik gekoppelt, um möglichst alle AgNP im Extrakt auf ein TEM-Grid zu zentrifugieren. Ein kritischer Schritt ist dabei, das Tensid vom TEM-Grid zu entfernen, um eine Charakterisierung der AgNP zu ermöglichen. Hierfür wurde ein Waschverfahren für das TEM-Grid – nach erfolgter Zentrifugation – basierend auf Cyclohexan und Ethanol untersucht. Die rCPE wurde dabei in Reinstwasserproben entwickelt und deren Tauglichkeit für Umweltproben anhand der Extraktion in Flusswasserproben dargelegt. Als Modellpartikel dienten Ag_2S-NP und Silberkernnanopartikel.

Die Verwendung von Cyclohexan für das TEM-Grid Waschverfahren führte zu einer erhöhten Filmbildung auf dem TEM-Grid. Ethanol zeigte diesen Effekt hingegen nicht, sondern vermochte bei sechsmaligem Waschen zuverlässig störende Tensidreste zu entfernen.

ICP-MS Messungen zeigten Extraktionseffizienzen > 73 % für AgNP mit einer ursprünglichen Ag-Konzentration von 5 bzw. 50 ng L^{-1} nach erfolgter fünfmaliger repetitiver CPE ($rCPE_5$). Die Partikel änderten durch die Extraktionstechnik weder ihre Form, Größe noch Zusammensetzung und konnten mit TEM-EDX charakterisiert werden. Das große Potential dieser Methode konnte schließlich anhand von Versuchen in Realwasserproben bestätigt werden. Auch hier konnten Ag_2S-NP mit einer ursprünglichen Konzentration von 5 ng L^{-1} zuverlässig mit TEM-EDX nachgewiesen werden. Eine Veränderung der Größe, Form und chemischen Zusammensetzung der Nanopartikel konnte auch in solch anspruchsvoller Matrix nicht beobachtet werden.

Eigener Beitrag:

- *Entwurf und Ausarbeitung des Versuchskonzeptes*
- *Synthese der AgNP*
- *Entwicklung und Optimierung der rCPE*
- *Realwasserprobenahme und Charakterisierung*
- *Auswertung und Interpretation der Ergebnisse*
- *Schreiben der Publikation (ausgenommen Beiträge von A. Wimmer, s. u.)*

Wesentliche Beiträger Dritter:

- *R. Kaegi: Entwicklung der Zentrifugationstechnik und TEM Messungen*
- *A. Wimmer: Optimierung der Zentrifugationstechnik und des TEM-Grid Waschverfahrens*
- *A. Wimmer: Schreiben der Publikation (Optimierung der Zentrifugationstechnik und des Waschverfahrens, Überlegungen zur Partikelanzahl auf dem TEM-Grid)*

5.4. Publikation 4: *What happens to silver-based nanoparticles if they meet seawater?*

Silbernanopartikel gelangen nach deren Freisetzung in die Umwelt infolge des Transportes durch Flüsse schlussendlich ins Meer, weshalb deren Schicksal in solchen Probenmatrices besonderer Aufmerksamkeit bedarf. Bisher wurde beobachtet, dass Silbernanopartikel in Meerwasser einerseits aggregieren und sich andererseits auflösen. Allerdings lagen die eingesetzten Konzentrationen im unteren µg L^{-1} bis mg L^{-1} Bereich und damit um viele Größenordnungen über umweltrelevanten Konzentrationen im unteren ng L^{-1} Bereich.[124-126] Der hohe Chloridgehalt in Meerwassermatrices verhinderte bisher den Einsatz höherer Konzentrationen, da die Proben für eine nachfolgende instrumentelle Messung verdünnt werden müssen, was zu schlechteren Nachweisgrenzen führt.

In dieser Studie wurden 50 ng L^{-1} citratstabilisierte Silbernanopartikel (CA@Ag-NP), Ag_2S-NP und AgCl-NP mit variierender Partikelgröße in künstlich hergestelltem als auch natürlichem Meerwasser bei verschiedenen Temperaturen und Zeiten inkubiert. Außerdem wurde der Einfluss von NOM auf das Schicksal der Nanopartikel in Meerwassermatrices untersucht. Die AgNP wurden daraufhin mit der CPE extrahiert, was zur Abtrennung der störenden Chloridmatrix einerseits und einer Anreicherung der Nanopartikel andererseits führte. Die Nanopartikel wurden schließlich mit (sp-)ICP-MS quantifiziert. Außerdem wurden TEM-EDX Messungen durchgeführt, um die erhaltenen Ergebnisse zu validieren und mögliche Änderungen der Partikelzusammensetzung zu detektieren. Das Schicksal von Silbernanopartikeln in Meerwasser wurde schließlich noch anhand real existierender Silbernanopartikel in Klärwerksablaufproben untersucht, indem diese mit einer entsprechenden Menge Natriumchlorid versetzt wurden.

Unabhängig von ihrer Zusammensetzung konnte eine fast vollständige Auflösung der AgNP nach drei Tagen in künstlichem als auch natürlichem Meerwasser beobachtet werden. Die Auflösung der Partikel war dabei in realem Meerwasser noch stärker ausgeprägt als in künstlich hergestelltem. Durch die Ausbildung von Silberchlorokomplexen der Zusammensetzung $AgCl_x^{1-x}$ ($x > 1$) wird dem Reaktionsgleichgewicht Ag^+ entzogen, was die Auflösung der Partikel verstärkt. TEM-EDX Messungen zeigten, dass sich bei der Inkubation von Ag_2S-NP in Meerwasser das Ag:S Verhältnis auf 1:1 erniedrigte. Silber wurde also aus den Nanopartikeln gelöst, während sich Schwefel um die Partikel ansammelte. Auch in Klärwerksablaufproben konnte eine fast vollständige Auflösung der Nanopartikel beobachtet werden.

Ein Einfluss der Inkubationstemperatur auf die Auflösung der Nanopartikel konnte nicht festgestellt werden. Der Zusatz von NOM führte hingegen zu einer verstärkten Auflösung der Nanopartikel. Dies kann damit erklärt werden, dass NOM mit Ag(I) Komplexe bildet und dadurch Ag(I) dem Reaktionsgleichgewicht entzieht, was die Auflösung der Partikel begünstigt.

Eigener Beitrag:

- *Synthese und Charakterisierung der eingesetzten AgNP*
- *Auswertung und Diskussion der TEM-EDX Aufnahmen*
- *Schreiben der Publikation (Einleitung Absätze 1-3 und 6-9, Kapitel 2.2. Absatz 3, Kapitel 3.1, Kapitel 3.2. letzter Absatz)*

Wesentliche Beiträger Dritter:

- *A. Wimmer: Versuchsplanung und Konzipierung der Studie*
- *A. Wimmer: Durchführung und Auswertung der Inkubationsstudien*
- *A. Wimmer: Schreiben der Publikation (ausgenommen eigene Beiträge)*

6. Schlussfolgerungen und Ausblick

Die vorliegende Arbeit liefert schnelle und aussichtsreiche Methoden, um Silbernanopartikel in Umweltproben umfangreich nachweisen und charakterisieren zu können. Insbesondere die repetitive Cloud Point Extraktion und deren Kopplung mit TEM-EDX Messungen verspricht ein großes Potential, da damit einzelne Partikel aus realen Proben extrahiert und charakterisiert werden können.

Außerdem konnte das Schicksal von Silbernanopartikeln in Meerwasser aufgeklärt werden, wo diese zuletzt hingelangen. Nachdem sich diese nahezu vollständig auflösen, sind kaum relevante Folgen für das Ökosystem Ozean zu erwarten.

Da in weiterer Zukunft eine stetige Zunahme von nanoskaligen Industrieprodukten zu erwarten ist, muss auch mit einem erhöhten Eintrag von Nanomaterialien in die Umwelt gerechnet werden. Die in dieser Arbeit präsentierten Methoden geben dazu einen vielversprechenden Ansatz, um Nanomaterialien in Umweltproben effizient nachweisen und charakterisieren und so ihre Auswirkungen auf relevante Ökosysteme abschätzen zu können. Das enorme Potential dieser analytischen Techniken kann nicht hoch genug eingeschätzt werden, da diese auch relativ leicht auf andere metallische als auch nichtmetallische Nanopartikel, wie z.B. sogar Mikro- oder Nanoplastik, angepasst und weiterentwickelt werden können, wofür indes weitere Forschungsarbeit nötig ist.

7. Abdruckgenehmigungen

7.1. Abbildung 1

Copyright Clearance Center RightsLink®

? Help | Email Support

SPRINGER NATURE

Can cloud point-based enrichment, preservation, and detection methods help to bridge gaps in aquatic nanometrology?

Author: Lars Duester et al

Publication: Analytical and Bioanalytical Chemistry

Publisher: Springer Nature

Date: Aug 24, 2016

Copyright © 2016, The Author(s)

Creative Commons

This is an open access article distributed under the terms of the Creative Commons CC BY license, which permits unrestricted use, distribution, and reproduction in any medium, provided the original work is properly cited.

You are not required to obtain permission to reuse this article.

To request permission for a type of use not listed, please contact Springer Nature

7.2. Abbildung 3

SPRINGER NATURE LICENSE
TERMS AND CONDITIONS

Jan 28, 2021

This Agreement between Technical University of Munich -- Alexander Urstoeger ("You") and Springer Nature ("Springer Nature") consists of your license details and the terms and conditions provided by Springer Nature and Copyright Clearance Center.

License Number	4997621413558
License date	Jan 28, 2021
Licensed Content Publisher	Springer Nature
Licensed Content Publication	Springer eBook
Licensed Content Title	The TEM and Its Optics
Licensed Content Author	Brent Fultz, James Howe
Licensed Content Date	Jan 1, 2013
Type of Use	Thesis/Dissertation
Requestor type	academic/university or research institute
Format	print and electronic
Portion	figures/tables/illustrations
Number of figures/tables /illustrations	1
Will you be translating?	no

Circulation/distribution	1 - 29
Author of this Springer Nature content	no
Title	Entwicklung und Optimierung von Anreicherungstechniken zur Bestimmung von Silbernanopartikeln in Umweltproben
Institution name	Technische Universität München
Expected presentation date	Feb 2021
Portions	Figure on page 59
Requestor Location	Technical University of Munich Lichtenbergstraße 4 AK Prof. Schuster Garching, 85748 Germany Attn: Technical University of Munich
Total	0.00 EUR

Terms and Conditions

Springer Nature Customer Service Centre GmbH
Terms and Conditions

This agreement sets out the terms and conditions of the licence (the **Licence**) between you and **Springer Nature Customer Service Centre GmbH** (the **Licensor**). By clicking 'accept' and completing the transaction for the material (**Licensed Material**), you also confirm your acceptance of these terms and conditions.

1. Grant of License

1. 1. The Licensor grants you a personal, non-exclusive, non-transferable, world-wide licence to reproduce the Licensed Material for the purpose specified in your order only. Licences are granted for the specific use requested in the order and for no other use, subject to the conditions below.

1. 2. The Licensor warrants that it has, to the best of its knowledge, the rights to license reuse of the Licensed Material. However, you should ensure that the material you are requesting is original to the Licensor and does not carry the copyright of another entity (as credited in the published version).

1. 3. If the credit line on any part of the material you have requested indicates that it was reprinted or adapted with permission from another source, then you should also seek permission from that source to reuse the material.

2. Scope of Licence

2. 1. You may only use the Licensed Content in the manner and to the extent permitted by these Ts&Cs and any applicable laws.

2. 2. A separate licence may be required for any additional use of the Licensed Material, e.g. where a licence has been purchased for print only use, separate permission must be obtained for electronic re-use. Similarly, a licence is only valid in the language selected and does not apply for editions in other languages unless additional translation rights have been granted separately in the licence. Any content owned by third parties are expressly excluded from the licence.

2. 3. Similarly, rights for additional components such as custom editions and derivatives require additional permission and may be subject to an additional fee. Please apply to Journalpermissions@springernature.com/bookpermissions@springernature.com for these rights.

2. 4. Where permission has been granted **free of charge** for material in print, permission may also be granted for any electronic version of that work, provided that the material is incidental to your work as a whole and that the electronic version is essentially equivalent to, or substitutes for, the print version.

2. 5. An alternative scope of licence may apply to signatories of the STM Permissions Guidelines, as amended from time to time.

3. Duration of Licence

3. 1. A licence for is valid from the date of purchase ('Licence Date') at the end of the relevant period in the below table:

Scope of Licence	Duration of Licence
Post on a website	12 months
Presentations	12 months
Books and journals	Lifetime of the edition in the language purchased

4. Acknowledgement

4. 1. The Licensor's permission must be acknowledged next to the Licenced Material in print. In electronic form, this acknowledgement must be visible at the same time as the figures/tables/illustrations or abstract, and must be hyperlinked to the journal/book's homepage. Our required acknowledgement format is in the Appendix below.

5. Restrictions on use

5. 1. Use of the Licensed Material may be permitted for incidental promotional use and minor editing privileges e.g. minor adaptations of single figures, changes of format, colour and/or style where the adaptation is credited as set out in Appendix 1 below. Any other changes including but not limited to, cropping, adapting, omitting material that affect the meaning, intention or moral rights of the author are strictly prohibited.

5. 2. You must not use any Licensed Material as part of any design or trademark.

5. 3. Licensed Material may be used in Open Access Publications (OAP) before publication by Springer Nature, but any Licensed Material must be removed from OAP sites prior to final publication.

6. Ownership of Rights

6. 1. Licensed Material remains the property of either Licensor or the relevant third party and any rights not explicitly granted herein are expressly reserved.

7. Warranty

IN NO EVENT SHALL LICENSOR BE LIABLE TO YOU OR ANY OTHER PARTY OR ANY OTHER PERSON OR FOR ANY SPECIAL, CONSEQUENTIAL, INCIDENTAL OR INDIRECT DAMAGES, HOWEVER CAUSED, ARISING OUT OF OR IN CONNECTION WITH THE DOWNLOADING, VIEWING OR USE OF THE MATERIALS REGARDLESS OF THE FORM OF ACTION, WHETHER FOR BREACH OF CONTRACT, BREACH OF WARRANTY, TORT, NEGLIGENCE, INFRINGEMENT OR OTHERWISE (INCLUDING, WITHOUT LIMITATION, DAMAGES BASED ON LOSS OF PROFITS, DATA, FILES, USE, BUSINESS OPPORTUNITY OR CLAIMS OF THIRD PARTIES), AND
WHETHER OR NOT THE PARTY HAS BEEN ADVISED OF THE POSSIBILITY OF SUCH DAMAGES. THIS LIMITATION SHALL APPLY NOTWITHSTANDING ANY FAILURE OF ESSENTIAL PURPOSE OF ANY LIMITED REMEDY PROVIDED HEREIN.

8. Limitations

8. 1. ***BOOKS ONLY:*** Where **'reuse in a dissertation/thesis'** has been selected the following terms apply: Print rights of the final author's accepted manuscript (for clarity, NOT the published version) for up to 100 copies, electronic rights for use only on a personal website or institutional repository as defined by the Sherpa guideline (www.sherpa.ac.uk/romeo/).

8. 2. For content reuse requests that qualify for permission under the STM Permissions Guidelines, which may be updated from time to time, the STM Permissions Guidelines supersede the terms and conditions contained in this licence.

9. Termination and Cancellation

9. 1. Licences will expire after the period shown in Clause 3 (above).

9. 2. Licensee reserves the right to terminate the Licence in the event that payment is not received in full or if there has been a breach of this agreement by you.

Appendix 1 — Acknowledgements:

For Journal Content:
Reprinted by permission from [**the Licensor**]: [**Journal Publisher** (e.g. Nature/Springer/Palgrave)] [**JOURNAL NAME**] [**REFERENCE CITATION** (Article name, Author(s) Name), [**COPYRIGHT**] (year of publication)

For **Advance Online Publication papers:**
Reprinted by permission from [**the Licensor**]: [**Journal Publisher** (e.g. Nature/Springer/Palgrave)] [**JOURNAL NAME**] [**REFERENCE CITATION** (Article name, Author(s) Name), [**COPYRIGHT**] (year of publication), advance online publication, day month year (doi: 10.1038/sj.[JOURNAL ACRONYM].)

For Adaptations/Translations:
Adapted/Translated by permission from [**the Licensor**]: [**Journal Publisher** (e.g. Nature/Springer/Palgrave)] [**JOURNAL NAME**] [**REFERENCE CITATION** (Article name, Author(s) Name), [**COPYRIGHT**] (year of publication)

Note: For any republication from the British Journal of Cancer, the following credit line style applies:

Reprinted/adapted/translated by permission from [**the Licensor**]: on behalf of Cancer Research UK: : [**Journal Publisher** (e.g. Nature/Springer/Palgrave)] [**JOURNAL NAME**] [**REFERENCE CITATION** (Article name, Author(s) Name), [**COPYRIGHT**] (year of publication)

For **Advance Online Publication** papers:
Reprinted by permission from The [**the Licensor**]: on behalf of Cancer Research UK: [**Journal Publisher** (e.g. Nature/Springer/Palgrave)] [**JOURNAL NAME**] [**REFERENCE CITATION** (Article name, Author(s) Name), [**COPYRIGHT**] (year of publication), advance online publication, day month year (doi: 10.1038/sj.[JOURNAL ACRONYM])

For Book content:
Reprinted/adapted by permission from [**the Licensor**]: [**Book Publisher** (e.g. Palgrave Macmillan, Springer etc) [**Book Title**] by [**Book author**(s)] [**COPYRIGHT**] (year of publication)

Other Conditions:

Version 1.3

Questions? customercare@copyright.com or +1-855-239-3415 (toll free in the US) or +1-978-646-2777.

7.3. Abbildung 4

AIP PUBLISHING LICENSE
TERMS AND CONDITIONS

Jan 28, 2021

This Agreement between Technical University of Munich -- Alexander Urstoeger ("You") and AIP Publishing ("AIP Publishing") consists of your license details and the terms and conditions provided by AIP Publishing and Copyright Clearance Center.

License Number	4997630842220
License date	Jan 28, 2021
Licensed Content Publisher	AIP Publishing
Licensed Content Publication	Journal of Applied Physics
Licensed Content Title	Parasitic effects in superconducting quantum interference device-based radiation comb generators
Licensed Content Author	R. Bosisio, F. Giazotto, P. Solinas
Licensed Content Date	Dec 7, 2015
Licensed Content Volume	118
Licensed Content Issue	21
Type of Use	Thesis/Dissertation
Requestor type	Student
Format	Print and electronic

Portion	Figure/Table
Number of figures/tables	1
Title	Entwicklung und Optimierung von Anreicherungstechniken zur Bestimmung von Silbernanopartikeln in Umweltproben
Institution name	Technische Universität München
Expected presentation date	Feb 2021
Portions	Figure 1(a)
Requestor Location	Technical University of Munich Lichtenbergstraße 4 AK Prof. Schuster Garching, 85748 Germany Attn: Technical University of Munich
Total	0.00 EUR

Terms and Conditions

AIP Publishing -- Terms and Conditions: Permissions Uses

AIP Publishing hereby grants to you the non-exclusive right and license to use and/or distribute the Material according to the use specified in your order, on a one-time basis, for the specified term, with a maximum distribution equal to the number that you have ordered. Any links or other content accompanying the Material are not the subject of this license.

1. You agree to include the following copyright and permission notice with the reproduction of the Material:"Reprinted from [FULL CITATION], with the permission of AIP Publishing." For an article, the credit line and permission notice must be printed on the first page of the article or book chapter. For photographs, covers, or tables, the notice may appear with the Material, in a footnote, or in the reference list.
2. If you have licensed reuse of a figure, photograph, cover, or table, it is your responsibility to ensure that the material is original to AIP Publishing and does not contain the copyright of another entity, and that the copyright notice of the figure, photograph, cover, or table does not indicate that it was reprinted by AIP Publishing, with permission, from another source. Under no circumstances does AIP Publishing purport or intend to grant permission to reuse material to which it does not hold

appropriate rights.
You may not alter or modify the Material in any manner. You may translate the Material into another language only if you have licensed translation rights. You may not use the Material for promotional purposes.

3. The foregoing license shall not take effect unless and until AIP Publishing or its agent, Copyright Clearance Center, receives the Payment in accordance with Copyright Clearance Center Billing and Payment Terms and Conditions, which are incorporated herein by reference.
4. AIP Publishing or Copyright Clearance Center may, within two business days of granting this license, revoke the license for any reason whatsoever, with a full refund payable to you. Should you violate the terms of this license at any time, AIP Publishing, or Copyright Clearance Center may revoke the license with no refund to you. Notice of such revocation will be made using the contact information provided by you. Failure to receive such notice will not nullify the revocation.
5. AIP Publishing makes no representations or warranties with respect to the Material. You agree to indemnify and hold harmless AIP Publishing, and their officers, directors, employees or agents from and against any and all claims arising out of your use of the Material other than as specifically authorized herein.
6. The permission granted herein is personal to you and is not transferable or assignable without the prior written permission of AIP Publishing. This license may not be amended except in a writing signed by the party to be charged.
7. If purchase orders, acknowledgments or check endorsements are issued on any forms containing terms and conditions which are inconsistent with these provisions, such inconsistent terms and conditions shall be of no force and effect. This document, including the CCC Billing and Payment Terms and Conditions, shall be the entire agreement between the parties relating to the subject matter hereof.

This Agreement shall be governed by and construed in accordance with the laws of the State of New York. Both parties hereby submit to the jurisdiction of the courts of New York County for purposes of resolving any disputes that may arise hereunder.

V1.2

Questions? customercare@copyright.com or +1-855-239-3415 (toll free in the US) or +1-978-646-2777.

7.4. Publikation 1

Magnetic solid phase extraction of silver-based nanoparticles in aqueous samples: Influence of particle composition and matrix effects on its application to environmental samples and species-selective elution and determination of silver sulphide nanoparticles with sp-ICP-MS

Author:
Alexander Urstoeger,Lilly Zacherl,Maximilian Muhr,Yasmin Selic,Monika Wenisch,Marcel Klotz,Michael Schuster

Publication: Talanta
Publisher: Elsevier
Date: 1 April 2021

7.5. Publikation 2

Separating dissolved silver from nanoparticulate silver is the key: Improved cloud-point-extraction hyphenated to single particle ICP-MS for comprehensive analysis of silver-based nanoparticles in real environmental samples down to single-digit nm particle sizes

Author:
Andreas Wimmer,Alexander Urstoeger,Tobias Hinke,Margit Aust,Philipp J. Altmann,Michael Schuster

Publication: Analytica Chimica Acta

Publisher: Elsevier

Date: 15 March 2021

7.6. Publikation 3

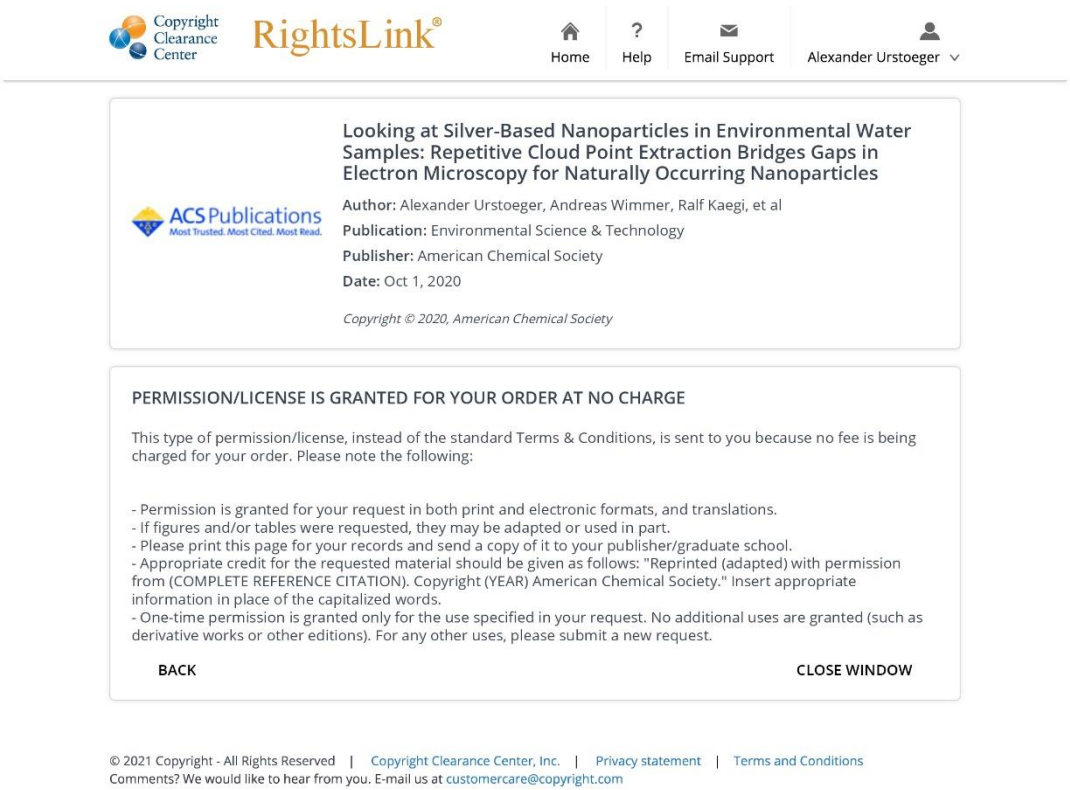

7.7. Publikation 4

What happens to silver-based nanoparticles if they meet seawater?

Author:
Andreas Wimmer,Alexander Urstoeger,Nils Christoph Funck,Franziska Petra Adler,Leonhard Lenz,Markus Doeblinger,Michael Schuster

Publication: Water Research

Publisher: Elsevier

Date: 15 March 2020

8. Bibliografische Angaben und Abdruck der Publikationen

8.1. Publikation 1

Magnetic solid phase extraction of silver-based nanoparticles in aqueous samples: Influence of particle composition and matrix effects on its application to environmental samples and species-selective elution and determination of silver sulphide nanoparticles with sp-ICP-MS

Alexander Urstoeger [a], Lilly Zacherl [a], Maximilian Muhr [b], Yasmin Selic [a], Monika Wenisch [a], Marcel Klotz [a], Michael Schuster [a,*]

[a] Division of Analytical Chemistry, Department of Chemistry, Technical University of Munich, Lichtenbergstraße 4, 85748, Garching, Germany

[b] Chair of Inorganic and Metal-Organic Chemistry, Department of Chemistry and Catalysis Research Center, Technical University of Munich, Ernst-Otto-Fischer-Straße 1, 85748, Garching, Germany

* Corresponding author

E-Mail: michael.schuster@tum.de

Abdruck des Artikels mit Genehmigung von Elsevier (siehe Kapitel 7.4) aus

Talanta, 2021, 225, 12202028.

Talanta 225 (2021) 122028

Contents lists available at ScienceDirect

Talanta

journal homepage: www.elsevier.com/locate/talanta

Magnetic solid phase extraction of silver-based nanoparticles in aqueous samples: Influence of particle composition and matrix effects on its application to environmental samples and species-selective elution and determination of silver sulphide nanoparticles with sp-ICP-MS

Alexander Urstoeger [a], Lilly Zacherl [a], Maximilian Muhr [b], Yasmin Selic [a], Monika Wenisch [a], Marcel Klotz [a], Michael Schuster [a,*]

[a] Division of Analytical Chemistry, Department of Chemistry, Technical University of Munich, Lichtenbergstraße 4, 85748, Garching, Germany
[b] Chair of Inorganic and Metal-Organic Chemistry, Department of Chemistry and Catalysis Research Center, Technical University of Munich, Ernst-Otto-Fischer-Straße 1, 85748, Garching, Germany

ARTICLE INFO

Keywords:
Magnetic solid phase extraction
Silver nanoparticles
sp-ICP-MS
Environmental water samples
Matrix effect study
Particle size preserving elution

ABSTRACT

Silver-based nanoparticles (Ag-b-NPs) are currently a cause for concern because they are being produced in increasing quantities for use in industrial goods and consumer products. This goes hand in hand with their release to the environment and the resultant risks for the entire ecosystem. Therefore, it is essential that these materials are monitored. A promising technique that overcomes a number of shortcomings in handling environmental samples is magnetic solid phase extraction (MSPE) of Ag-b-NPs, which is applied in this study. It has been possible to extract different kinds of Ag-b-NPs at environmentally relevant concentrations in the low ng L^{-1} range using iron oxide magnetic particles (IOMPs) of different size and shape with efficiencies in the range from 80 to 100%. Furthermore, environmentally relevant inorganic ions and TiO_2 particles exhibited no major effect on the extraction efficiency. However, natural organic matter (NOM) exhibited a significant influence from 1 mg L^{-1} resulting in a 50% drop in extraction efficiency. This effect could be overcome by adding 10 mM Ca^{2+} or increasing the iron oxide magnetic particle (IOMP) concentration to 500 mg L^{-1}. Applying the presented procedure, Ag-b-NPs added to a river water sample at β_{Ag} = 50 ng L^{-1} were successfully extracted. We also investigated the coextraction of Ag^+, demonstrating that NOM could eliminate coextraction. The subsequent species-selective elution of Ag_2S-NPs after MSPE, was carried out based on ethylene diamine tetraacetate (EDTA) as eluent in different matrices. A desorption efficiency of 76 ± 6% could be achieved while preserving the Ag_2S-NPs' size. By contrast, core Ag-NPs and AgCl-NPs are dissolved if the presented method is followed.

1. Introduction

Since the first use of the term "nanotechnology" in 1974 by N. Taniguchi [1], this former niche technique has grown to make an indispensable contribution to today's industrial production [2]. Silver-based nanoparticles (Ag-b-NPs) are one of the most widely used nanomaterial species and are found in a wide range of applications such as catalysts [3], biosensors [4,5], and medical and antibacterial products [5,6]. However, the increasing use of those products is also associated with their disposal and the subsequent release of the nanomaterials to the environment [7]. This has given rise to a discussion about environmental nanomaterial pollution, accompanied by concerns about toxic effects on the whole ecosystem [2,8]. Factors that greatly influence nanoparticle toxicity are their chemical composition, size, and concentration in the environment. For example, far fewer Ag^+ ions are released from Ag_2S because of its lower solubility in comparison with other Ag species [9]. Once in the environment, Ag-b-NPs are likely to transform and interact with environmentally relevant species typically resulting in adsorption onto organic molecules and materials, oxidation, followed by dissolution of the particles and reactions with dissolved species, thus changing the chemical composition of the whole nanoparticle or its coating to e.g. Ag_2S or AgCl. This makes it inevitable to assess the impact of pristine as well as transformed Ag-b-NPs on the environment [10,11]. However, silver sulphide nanoparticles (Ag_2S-NPs) represent the predominant silver-based nanoparticular species in the environment [9,

* Corresponding author.
E-mail address: michael.schuster@tum.de (M. Schuster).

https://doi.org/10.1016/j.talanta.2020.122028
Received 26 October 2020; Received in revised form 11 December 2020; Accepted 14 December 2020
Available online 17 December 2020

Abbreviations

Ag-b-NPs	silver-based nanoparticles
BSA	bovine serum albumine
CA	citrate
CPE	cloud point extraction
Cys	cysteine
DL	detection limit
IOMPs	iron oxide magnetic particles
Lys	L-lysine
MSA	mercaptosuccinic acid
MSPE	magnetic solid phase extraction
MUA	mercaptoundecanoic acid
NOM	natural organic matter
PVP	polyvinylpyrrolidone
SPE	solid phase extraction
sp-ICP-MS	single particle inductively coupled plasma mass spectrometry
SR-NOM	Suwannee River natural organic matter
TOC	total organic carbon
TX-114	Triton X-114
UPW	ultra-pure water

12–14]. Engineered Ag-b-NPs are commonly stabilised through the adsorption or covalent binding of organic molecules, such as polyvinylpyrrolidone (PVP), citrate (CA), starch and many more to prevent aggregation and allow for the control of particle size and shape [9]. The desired Ag-b-NP coating is typically established via ligand exchange mechanisms or *in-situ* reduction of Ag^+ and functionalisation in the presence of $NaBH_4$ or glucose (in the case of starch coated Ag-b-NPs) and the desired coating agent. As the coating agents differ greatly in molecular weight and chemical structure, this will also have an impact on their fate in the environment [9]. An overview over the Ag-b-NPs used in this study and their preparation method can be found in Table 1. Another parameter which is essential to consider when dealing with environmental nanoparticle exposure is the particle size. Smaller particles exhibit enhanced dissolution properties because of their intrinsically high surface area, thus increasing their environmental impact [15,16]. To fully assess their fate in the environment for a comprehensive risk evaluation, Ag-b-NPs need to be monitored. This calls for analytical techniques and procedures that are able to overcome a number of shortcomings when dealing with environmental samples. These are firstly, as mentioned above, considering the very number of silver-based nanoparticular species in industrial products and present in the environment, secondly, their low concentration in the environment in the range of sub ng L^{-1} to 100 ng L^{-1}, and thirdly, the rather challenging sample matrix [2,17,18].

Magnetic solid phase extraction (MSPE) using iron oxide magnetic particles (IOMPs) of Ag-b-NPs has been shown to be a promising technique when handling environmental samples [19–23]. IOMPs have been widely used for solid phase extraction (SPE) in many fields such as medicine, biotechnology and analytical chemistry because of their high selectivity, enrichment factors and recovery rates as well as their simple handling and their ease of use for surface modifications [24–26]. Zhou et al. also presented this method for the extraction of Ag-b-NPs [20,21]. They found that the extraction is based on a pseudo-second-order physisorption process controlled by intraparticle diffusion and weak interactions. The adsorption process follows three different stages, which can be described as firstly, rapid external diffusion and adsorption at the IOMP surface, secondly, slow intraparticle diffusion and thirdly, a much slower intraparticle diffusion until an adsorption equilibrium is reached. The process can be described with the Langmuir isotherm model, assuming specific homogeneous adsorption sites on the IOMPs. Further analysis using a Dubinin-Radushkevich isotherm model showed that the adsorption of Ag-b-NPs onto IOMPs is mainly driven by physisorption [21]. At sample pH 6.2, IOMPs are positively charged on their surface, whereas Ag-b-NPs exhibit a negative surface charge. The resultant electrostatic interactions between IOMPs and Ag-b-NPs are therefore critical for an efficient extraction of the latter and, thus, show a maximum at said pH [20]. However, the Ag-b-NP concentrations (μg L^{-1} – mg L^{-1}) Zhou et al. used in their experiments exceeded by far the environmentally relevant concentrations, which are in the ng L^{-1} range, as stated earlier [2,18,20,21]. Furthermore, Ag concentration recovery was determined by the elution of Ag-b-NPs as Ag(I) from the IOMPs, thus, leading to a loss of information on particle size, which is an important aspect for a proper risk assessment of Ag-b-NPs as environmental pollutants [15,16,20].

Our aim was to provide a broadly applicable method for the extraction of Ag-b-NPs of various industrially and environmentally relevant compositions (Ag_2S-NPs and AgCl-NPs) and coatings, at environmentally relevant concentrations in the ng L^{-1} range for Ag-b-NP/Ag^+ separation, matrix interference elimination and subsequent Ag-b-NP speciation [13,27–29]. We also investigated the influence of IOMP concentration, size and surface shape on the extraction efficiency. When dealing with environmental water samples, relevant matrix effects have to be considered as stated above. Therefore, we will discuss possible effects of environmentally relevant matrix constituents on the MSPE of Ag-b-NPs and how to overcome them. We have also investigated the coextraction of Ag^+ at such low Ag-b-NP concentrations as those found in the environment, because coextracted Ag^+ may lead to false positive nanoparticle concentrations after elution and subsequent concentration determination with ICP-MS. Ultimately, the aim was to separate the Ag-b-NPs from the IOMPs and, in particular, to preserve the size of the Ag_2S-NPs, because they represent the predominant species of Ag-b-NPs in the environment [9,12–14], for subsequent species selective particle size determination via sp-ICP-MS measurement. This approach covered the elution of Ag-b-NPs from the IOMPs using ethylene diamine

Table 1
Ag-b-NPs used in this study including their corresponding nomenclature and coating.

Ag-b-NPs	coating	preparation method
AgCl-NPs	–	coprecipitation [20]
Ag_2S-NPs	–	coprecipitation [32]
BSA@Ag-NPs	bovine serum albumin (BSA)	*in-situ* reduction [33]
CA@Ag-NPs	citrate (CA)	*in-situ* reduction [31]
Cys@Ag-NPs	cysteine (Cys)	ligand exchange [34]
Lys@Ag-NPs	L-lysine (Lys)	ligand exchange [35]
MSA@Ag-NPs	mercaptosuccinic acid (MSA)	ligand exchange [36]
MUA@Ag-NPs	mercaptoundecanoic acid (MUA)	ligand exchange [36]
PVP_{10}@Ag-NPs	polyvinylpyrrolidone (PVP_{10}, M = 10 kDa)	ligand exchange [37]
Starch@Ag-NPs	starch	*in-situ* reduction [38]

tetraacetate disodium salt (EDTA) to induce the adsorption of EDTA onto the IOMPs [30] and thus the desorption of the Ag-b-NPs. EDTA was chosen as eluent, as it is already known to have no influence on the particle size, shape and composition of Ag-b-NPs [17,31]. Furthermore, we modified the cloud point extraction (CPE) [31], a method developed in our group for Ag-b-NP extraction from environmental samples where the addition of EDTA and sample pH are both crucial in desorbing the Ag-b-NPs from the IOMPs. The size of the Ag-b-NPs was subsequently determined with sp-ICP-MS.

2. Materials and Methods

2.1. Chemicals and reagents

Acetic acid (glacial), Ag(I) ICP-Standard ($AgNO_3$ in 3% HNO_3, β_{Ag} = 1000 mg L^{-1}), calcium nitrate tetrahydrate, cysteine (Cys), ethanol, ethylenediaminetetraacetate (EDTA) disodium salt, ethylene glycol, D-(+)-glucose, L-lysine (Lys), nitric acid (suprapure, 65%), potassium nitrate, silver(I) nitrate, sodium acetate anhydrous, sodium chloride and starch were obtained from Merck (Darmstadt, Germany). Bovine serum albumin (BSA), citrate stabilised silver nanoparticles (CA@AgNPs, 40 nm), iron (III) chloride hexahydrate, iron (II,III) oxide nanopowder (50–100 nm), magnesium sulphate, mercaptosuccinic acid (MSA), mercaptoundecanoic acid (MUA), D-penicillamine, polyvinylpyrrolidone (PVP_{10}, M = 10 kDa) and sodium sulphide were purchased from Sigma-Aldrich Corp. (St. Louis, MO, USA). Sodium hydroxide solution (1 mol L^{-1}) was obtained from VWR (Ismaning, Germany) and Triton™ X-114 (TX-114) was purchased from AppliChem (Darmstadt, Germany). Iron (II,III) oxide nanopowder (<50 nm) was obtained from American Elements (Los Angeles, CA, USA) and iron (II, III) oxide powder was purchased from Alfa Aesar (Haverhill, MA, USA). Suwannee River natural organic matter (SR-NOM) was provided by the International Humic Substance Society, IHSS (Saint Paul, MN, USA). Since Ag-b-NP dispersions contain impurities of dissolved Ag, the stock dispersions were purified from dissolved Ag species by dialysis (3.5 kDa regenerated cellulose membrane by ZelluTrans, Carl Roth, Karlsruhe, Germany) before use. A citrate-stabilised gold nanoparticle dispersion (CA@Au-NPs, NIST reference material RM 8013, 56 nm, β_{Au} = 52 mg L^{-1}) was purchased from the National Institute of Standards and Technology (Gaithersburg, MD, USA). All chemicals were at least of analytical grade and were checked for Ag contamination by ICP-MS measurements before use. Ultra-pure water (UPW, resistivity of 18.2 MΩcm) was obtained by a Milli-Q-Gradient System (Millipore GmbH, Schwalbach, Germany).

2.2. Instrumentation

ICP-MS and sp-ICP-MS measurements were conducted on a quadrupole mass spectrometer 7900 ICP-MS (Agilent, Santa Clara, CA, USA) equipped with an autosampler SPS4 (Agilent) and a MicroMist nebuliser (Glass Expansion, Melbourne, Australia). Argon 4.8 (Westfalen, Münster, Germany) was used as plasma gas.

For Ag quantification, ICP-MS measurements were carried out targeting ^{107}Ag as the analyte mass in He collision cell (He-CCT) mode to avoid possible polyatomic interferences. ^{115}In was used as an internal standard. The measurement time was set to 1 s for the analyte and 0.1 s for the internal standard. The nebuliser gas pressure was 429 kPa. Calibration was performed using aqueous Ag(I) solutions of known concentrations ranging from 5 to 200 ng L^{-1}. For Ag quantification, Ag-b-NP containing samples were acidified with HNO_3 yielding 1.625% (v/v) to dissolve the Ag-b-NPs to increase the analyte stability and homogeneity. The detection limit for ^{107}Ag was 0.5 ng L^{-1}.

For particle size determination using sp-ICP-MS, ^{107}Ag was also chosen as the target mass. The dwell time was set to 500 µs with an acquisition time of 60 s, which results in 120,000 data points. The pump rate was gravimetrically determined as 0.310 mL min^{-1}. To enable correct determination of the particles' sizes, the transport efficiency η, the proportion of initial particles in the sample which finally reach the detector, must be determined. CA@Au-NP dispersions (RM 8013) [39] at a concentration of β_{Au} = 52 ng L^{-1} were used for the determination of η following an already approved procedure [40,41]. η was determined to be 0.08. The Ag(I) standard solution, diluted to β_{Ag} = 1 µg L^{-1} was used to calibrate the elemental sensitivity. The particle size distributions were evaluated using MassHunter Workstation 4.4, version C.01.04 (Agilent) equipped with the Single Nanoparticle Application Module. Particle size distributions are presented, unless stated otherwise, as normalised particle number frequency throughout the text. Background equivalent diameters were determined using MassHunter Workstation 4.4 (yielding 12 nm for core Ag-NPs, 14 nm for Ag_2S-NPs and 14 nm for AgCl-NPs).

Additional instrumental parameters and analytical performance data for ICP-MS and sp-ICP-MS measurements can be found in the SI, Table S4 and Figures S22 and S23.

2.3. Synthesis and characterisation of IOMPs and Ag-b-NPs

IOMP and Ag-b-NP synthesis and characterisation as well as purification of Ag-b-NPs are described in the Supplementary Information (SI). The sizes of the IOMPs were determined by TEM using a JEM-2010 (JEOL) instrument operating at an acceleration voltage of 120 kV. Their magnetisation hysteresis curves were determined using an MPMS 5 XL SQUID magnetometer (Quantum Design Inc., San Diego, CA, USA). Ag-b-NP concentrations were quantified with ICP-MS measurements and the Ag-b-NP sizes were determined using sp-ICP-MS. Particle size distributions of the pristine Ag-b-NPs are presented in the SI, Figures S1 and S2. The compositions of Ag_2S-NPs and AgCl-NPs were determined using a scanning transmission electron microscope (STEM, HD-2700-Cs, Hitachi, Chiyoda, Japan) operated at an acceleration voltage of 200 kV fitted with an energy dispersive X-ray detector (EDAX, Mahwah, NJ, USA). Ag-b-NP coatings were evaluated by conducting FTIR measurements on a Bruker Alpha FTIR spectrometer with an ATR geometry, using a diamond ATR unit (Bruker Corporation, Billerica, MA, USA). The coated core silver nanoparticles are nomenclated as shell@core nanoparticles in the following. The Ag-b-NPs used in this study are presented in Table 1. To obtain a sufficient amount of Ag-b-NP powder for a proper characterisation of their coating, the stock dispersions were centrifuged several times at 10,000 g for 10 min. The surfactant was then removed via pipetting and the particles were dried under vacuum before carrying out FTIR measurements.

2.4. Extraction of Ag-b-NPs with IOMPs

For the detailed extraction study, the extraction efficiency for the extraction of Ag_2S-NPs, CA@Ag-NPs and AgCl-NPs at concentrations ranging from 5 to 200 ng L^{-1} was determined using IOMP concentrations from 1 to 500 mg L^{-1}. Table 2 gives an overview of the Ag-b-NP concentrations and corresponding IOMP concentrations used for these extraction experiments. The working solutions were prepared by dilution of the initial stock solutions of IOMPs of different concentrations (10 g L^{-1} and 1 g L^{-1}). In a first step, UPW was provided in glass bottles with snap-on caps. Then the initial pH was adjusted to 6.2 with 1.25 M acetic acid and 1 M sodium acetate solution, as this pH enhances the interaction of IOMPs and Ag-b-NPs as described in the Section 1. IOMP stock solutions were ultrasonicated for 1 min to ensure homogeneous

Table 2
Ag-b-NP concentrations and corresponding IOMP concentrations for the MSPE of Ag-b-NPs with IOMPs.

Ag-b-NP concentrations [ng L^{-1}]	IOMP concentrations [mg L^{-1}]					
5	1	10	25	50	100	–
50	5	25	50	100	250	500
200	5	25	50	100	250	500

dispersion of the particles and to prevent particle aggregation. Equivalent volumes of IOMP stock solutions were added to each sample and finally, the corresponding volume of the Ag-b-NP working solution was added. The Ag-b-NP stock solution was also sonicated for 1 min before usage for the same reasons as with the IOMP stock solutions. The final sample volume was 40 mL. The mixture was shaken for 60 min at 300 rpm at ambient temperature on a IKA KS501 digital shaker (IKA Labortechnik, Staufen, Germany). Afterwards, the magnetic particles were collected by an external NdFeB magnet (IBS magnet, Berlin, Germany). The supernatant was collected for further analysis. The extraction efficiency (*e.e.*) was calculated using equation (1).

$$e.e.\ [\%] = 100 \cdot (c_0 - c_e)/c_0 \quad (1)$$

with c_0 the initial Ag concentration in the Ag-b-NP suspension and c_e the Ag concentration after the extraction in the supernatant, determined by ICP-MS measurements.

To provide a method suitable for a wide range of Ag-b-NPs, we further investigated the optimised MSPE in respect of its applicability to Ag-b-NPs with seven industrially and environmentally relevant coatings. These Ag-b-NPs were extracted at $\beta_{Ag} = 50$ ng L^{-1} and the IOMP concentration was 50 mg L^{-1}. The further extraction procedure corresponds to the above described method.

2.5. Matrix Effect Study and Application of MSPE to a river water sample

To provide a method capable of extracting Ag-b-NPs from environmental samples, a thorough examination of the influence of potential matrix constituents on the MSPE is needed. Our objective was to assess their influence at environmentally relevant concentrations as well as concentrations exceeding these to establish a robust method for the extraction of Ag-b-NPs using MSPE. Those potential matrix constituents include inorganic ions (phosphate, carbonate, sulphate, nitrate, chloride, and ammonium, sodium, calcium, magnesium, potassium), TiO_2-particles as an example of solid material suspended in environmental water samples, and NOM (SR-NOM). The samples, containing these matrix constituents in different amounts, and Ag_2S-NPs at a concentration of $\beta_{Ag} = 50$ ng L^{-1} were subjected to MSPE (with 100 mg L^{-1} IOMPs) as described above (2.4. Extraction of Ag-b-NPs with IOMPs). Ag_2S-NPs were chosen as model particles, as they represent the greatest fraction of environmentally occurring Ag-b-NPs [9,12–14]. Furthermore, no major differences could be found in the extraction efficiencies of the various Ag-b-NPs, as is shown later in the Results and Discussion section (3.2. Extraction of Ag-b-NPs using IOMPs). Consequently, the sole use of Ag_2S-NPs for this study is justified. To improve the extraction efficiency in samples containing NOM, Ca^{2+} was added at different concentrations as proposed by Zhou et al. [20].

The river water sample was taken from the river Wiesäckerbach (Garching, Germany) in January under dry weather conditions. The sample was collected in a polyvinyl chloride container (0.5 L), with the container being rinsed three times using the sample water, before being filled finally. The sample was filtered with a syringe filter (0.45 μm, cellulose acetate, VWR, Ismaning, Germany) and checked for Ag content with ICP-MS. The sample characteristics (T, pH, TOC, O_2 content) are shown in the SI, Table S1. Aliquots of the river water sample were then spiked with Ag_2S-NPs with a final concentration of $\beta_{Ag} = 50$ ng L^{-1} and subjected to MSPE. Therefore, IOMPs were added with a final concentration of 100 and 500 mg L^{-1}, respectively. To possibly improve the extraction efficiency, $Ca(NO_3)_2$ was added at different concentrations to some samples as proposed by Zhou et al. [20]. The final sample volume was 40 mL.

2.6. Coextraction of Ag^+

In order to evaluate Ag^+ coextraction, MSPE was conducted with samples with concentrations of 5, 50 and 500 ng L^{-1} Ag^+ containing 5 and 50 ng L^{-1} Ag_2S-NPs, respectively. The influence of natural organic matter on the coextraction was determined by the addition of SR-NOM (10 mg L^{-1} total organic carbon, TOC). Moreover, the effect of the addition of Ca^{2+} 10 mM on the coextraction of Ag^+, as proposed by Zhou et al. was studied [20]. Ag_2S-NPs were chosen for this experiment as model particles because they represent the majority of naturally occurring Ag-b-NPs [9,12–14]. The extraction procedure follows the method described in section 2.4. Extraction of Ag-b-NPs with IOMPs.

2.7. Recovery of Ag-b-NPs after SPE

In order to determine the size of extracted Ag-b-NPs, the IOMPs and Ag-b-NPs must be separated. This was done by eluting the Ag-b-NPs using EDTA in varying matrices. To do so, the previously collected IOMPs with adsorbed Ag-b-NPs were redispersed in UPW. Saturated EDTA solution ($EDTA_{aq,\ sat.}$) was added in volumes ranging from 0.5 to 3 mL and afterwards, the pH was adjusted with 1.25 M acetic acid, 1 M sodium acetate solution and/or 1 M sodium hydroxide solution. The pH ranged from 4.7 to 10. A pH < 4 was not chosen, as Ag-b-NP dissolution increases with lower pH [42,43]. For elution experiments in surfactant matrix, Triton™ X-114 (TX-114) 10% (v/v) was added in volumes of 30 μL (0.1 mM; < critical micellar concentration (cmc); cmc = 0.2 mM for TX-114) and 1 mL (4.9 mM; > cmc). The final volume of the samples was 40 mL. The samples were then sonicated for 1 min to prevent particle aggregation and afterwards shaken on a shaker IKA KS501 digital for 60 min at 300 rpm, unless otherwise stated. Elution experiments were carried out at ambient temperature, 30 °C, 40 °C and 50 °C.

To improve the elution process further, we investigated whether CPE can desorb the Ag-b-NPs from the IOMPs. $EDTA_{aq,\ sat.}$ was added in varying amounts to the IOMP dispersions for a better comparison of the results and the pH was adjusted, as stated above. Then, 1 mL of TX-114 10% (v/v) (4.9 mM) and additionally 1 mL of D-penicillamine 0.1 M were added to the IOMP dispersion. The final sample volume was 40 mL. After adding the additives, the samples were sonicated for 1 min to prevent particle aggregation and then incubated at 40 °C for 30 min in a water bath. The samples were sonicated every 5 min to prevent particle aggregation.

IOMPs were then collected using a handheld magnet and the Ag-b-NP containing supernatant was measured with ICP-MS and sp-ICP-MS. For experiments containing TX-114, the same amount of ethanol as TX-114 (10% (v/v)) was added in advance to decrease the viscosity of the sample before measurement.

The desorption efficiency (*d.e.*) was calculated using equation (2).

$$d.e.\ [\%] = 100 \cdot c_d/(c_0 - c_e) \quad (2)$$

with c_0 the initial Ag concentration in the Ag-b-NP suspension and c_e the Ag concentration after the extraction procedure in the supernatant, where $c_0 - c_e$ represents the concentration of extracted Ag-b-NPs. c_d is the final Ag concentration in the supernatant after the desorption process. c_0, c_e and c_d were determined based on ICP-MS measurements.

2.8. Error calculations

Three independent sample replicates were prepared and measured individually for all measurements. Five measurement replicates were conducted for each sample. Uncertainties were calculated using Gaussian error propagation, including pipetting uncertainties and standard deviations of the independently measured sample replicates.

The Ag concentrations were blank-corrected by measurement of blank samples.

3. Results and Discussion

3.1. Characterisation of IOMPs

Magnetisation hysteresis curves of the IOMPs are presented in the SI, Figure S3 and S4. The aged IOMPs show slightly lower saturation magnetisation values than in their pristine state, suggesting superficial oxidation of the IOMPs. Furthermore, there are great differences in the saturation magnetisation values of the various IOMPs. While the IOMPs <50 nm show values of 74.5 emu g^{-1}, they increase for synthesised IOMPs (85.9 emu g^{-1}), milled IOMPs (96.1 emu g^{-1}) and IOMPs 50–100 nm (98.5 emu g^{-1}). TEM images of the IOMPs revealed great differences in aggregation state, size and surface shape. IOMPs <50 nm tended to aggregate into large particle clusters, while the other IOMPs showed much less aggregation. Furthermore, the synthesised IOMPs exhibited fissured surfaces, while the surfaces of other IOMPs were rather smooth. Ageing of the IOMPs did not lead to a change in size or shape of the particles. TEM images of IOMPs are shown in the SI, Figure S5 and S6. Particle diameter ranges, derived from TEM images, are also shown in the SI, Table S2.

3.2. Extraction of Ag-b-NPs using IOMPs

The objective of the extraction studies was to provide a MSPE of Ag-b-NPs for a broad range of Ag-b-NPs at environmental conditions and concentrations in the low ng L^{-1} range. Ag_2S-NPs, CA@Ag-NPs and AgCl-NPs could be successfully extracted using all IOMP types. However, synthesised IOMPs exhibited the best extraction efficiencies. The addition of 50 mg L^{-1} of the synthesised IOMPs ensured complete extraction of all Ag-b-NPs at initial concentrations of 5, 50 and 200 ng L^{-1} Ag. The fissured surface structure of the synthesised IOMPs leads to a much higher surface-to-volume ratio in comparison with the other IOMPs and their smooth surface. Combined with low particle aggregation, this might lead to more adsorption sites for Ag-b-NPs, therefore significantly reducing the number of particles required to ensure the complete extraction of Ag-b-NPs. The extraction efficiencies of different IOMPs at varying IOMP concentrations for the extraction of Ag_2S-NPs, CA@Ag-NPs and AgCl-NPs are presented in the SI, Figures S7-S9. Ageing of the IOMPs showed that there was little influence on the extraction efficiency for Ag_2S-NPs and CA@Ag-NPs. The ageing of the IOMPs slightly improved the extraction performance for AgCl-NPs. A comparison of the extraction efficiencies of the IOMPs in their pristine and aged state for all Ag-b-NPs is presented in the SI, Figure S10. Owing to their superior extraction capacity in comparison with the other IOMPs, synthesised IOMPs were used for the following experiments, where not otherwise stated.

To establish a method that is suitable for extraction of a wide range of Ag-b-NPs from aqueous samples, it is crucial that Ag-b-NPs of different composition and coating can be quickly extracted. Therefore, we conducted the extraction on Ag-b-NPs with various industrially and environmentally relevant coatings and determined the corresponding extraction efficiencies. All particles could be extracted with extraction efficiencies ranging from 80 to 98% for environmentally relevant concentrations (β_{Ag} = 50 ng L^{-1}), thus emphasising the applicability of MSPE to various kinds of Ag-b-NPs (SI, Figure S11).

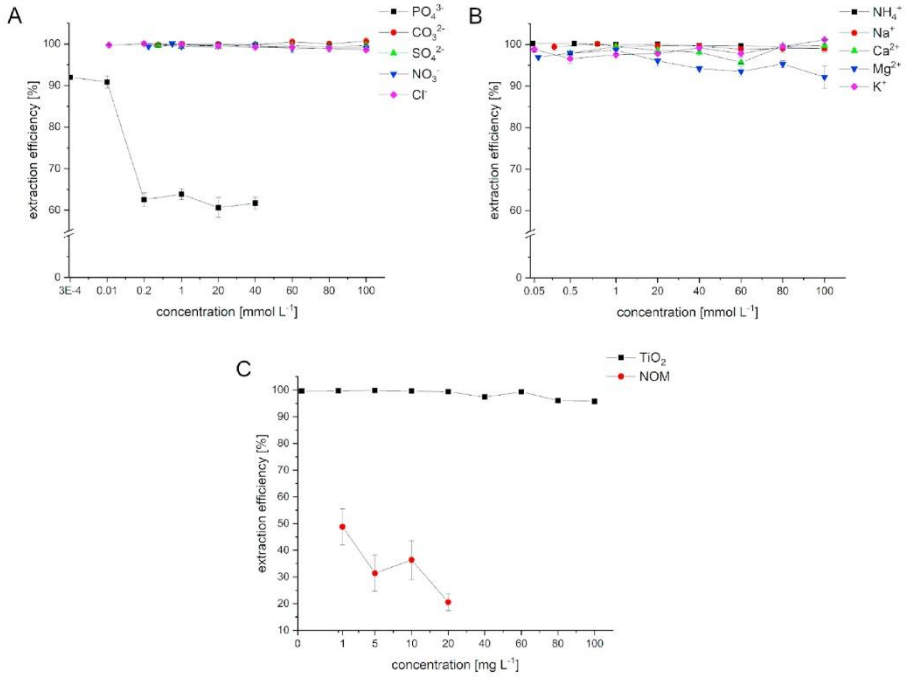

Fig. 1. Influence of environmentally relevant inorganic anions (A) and cations (B), TiO_2 particles and NOM (B) on the MSPE of Ag-b-NPs.

3.3. Examination of Matrix Effects and Optimisation of the MSPE

To investigate the applicability of the MSPE of Ag-b-NPs to environmental samples, we tested the influence of environmentally relevant inorganic ions (PO_4^{3-}, CO_3^{2-}, SO_4^{2-}, NO_3^-, Cl^-, and NH_4^+, Na^+, Ca^{2+}, Mg^{2+}, K^+) as well as TiO_2 particles as an example of solid matter occurring in environmental water samples and NOM. As stated in the Materials and Methods section (2.5. Matrix Effect Study and Application of MSPE to a River Water Sample), Ag_2S-NPs were chosen as model particles for this study, as they represent the majority of naturally occurring Ag-b-NPs and no major differences in the extraction efficiency of various Ag-b-NPs using MSPE could be detected [9,12–14]. The inorganic ions showed little influence on the extraction efficiency of Ag_2S-NPs, except PO_4^{3-} (Fig. 1A and B). Samples containing >0.01 mmol phosphate exhibited a significant decrease in extraction efficiency. Phosphate is also known to readily adsorb onto iron oxides. Therefore, an excess of phosphate might block adsorption sites for Ag-b-NPs, and thus, impeding their adsorption onto the IOMPs [44–46]. However, where the environmentally relevant phosphate concentrations (0.1–3 μmol L^{-1}) [47] are concerned, no major influence of PO_4^{3-} on the MSPE of Ag-b-NPs in environmental water samples is expected. For improved clarity, the graphs for each individual inorganic ion component are presented in the SI, Figure S12 and S13. Also, no influence of TiO_2 particles could be detected (Fig. 1C). However, the addition of even 1 mg L^{-1} SR-NOM resulted in a decrease of 50% in the extraction efficiency (Fig. 1C). This can either be explained by the ability of NOM to bind Ag-b-NPs and therefore prevent their adsorption onto the IOMPs or the binding of NOM onto the IOMPs thus blocking the Ag-b-NP adsorption sites [48,49]. One possibility for overcoming these shortcomings is the addition of Ca^{2+} to environmental water samples for the MSPE of Ag-b-NPs. NOM is known to bind to Ca^{2+}, consequently resulting in the release of Ag-b-NPs to make them available for MSPE or preventing the adsorption of NOM onto IOMPs therefore make them available for Ag-b-NP binding [50]. Fig. 2 shows that the addition of 10 mM Ca^{2+} results in a large increase in the extraction efficiency. Increasing the Ca^{2+} concentration to 100 mM enhances the positive effect on the MSPE of Ag-b-NPs.

In a last step we investigated the applicability of the MSPE of Ag-b-NPs under real conditions in surface water samples (river Wiesäckerbach, Garching, Germany). The presence of NOM greatly influences the extraction efficiency and drops to 40 ± 4% for the MSPE with 100 mg L^{-1} IOMPs. This correlates with our results presented above. Also, the addition of Ca^{2+} greatly increases the extraction efficiency by up to 102% (Figure S14). We also investigated the influence of an increase in IOMP concentration to 500 mg L^{-1}, which led to an increase in the extraction efficiency to 98 ± 1% (Figure S14, sample 2). This result supports our suggestion, that NOM blocks the Ag-b-NP adsorption sites on the IOMPs and therefore hinders their extraction. Increasing the quantity of IOMPs added to the sample also leads to a blocking of some adsorption sites by NOM to some extent. However, the availability of a greater number of IOMPs ensures an efficient extraction of Ag-b-NPs from environmental water samples, as more adsorption sites on the IOMPs are available, which are not blocked by NOM.

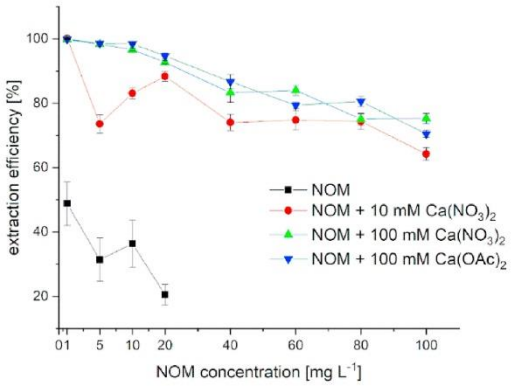

Fig. 2. Influence of the addition of Ca^{2-} to NOM containing water samples on the MSPE of Ag-b-NPs. Ca^{2+} has been added as either $Ca(NO_3)_2$ or calcium acetate ($Ca(OAc)_2$) in concentrations of 10 mM and 100 mM respectively.

3.4. Coextraction of Ag^+

As coextraction of Ag^+ may lead to false positive nanoparticle concentrations after elution and subsequent concentration determination with ICP-MS, this effect also needs to be taken into account. The extraction procedure showed high Ag^+-coextraction factors for Ag_2S-NP containing samples also containing Ag^+ at concentrations of 5, 50 and 500 ng L^{-1} (up to 70%), respectively. However, the addition of SR-NOM significantly reduced coextraction to levels <10% for samples containing Ag^+ at environmentally relevant concentrations of 5 ng L^{-1} [51]. This can be explained by the ability of NOM to complex noble metals [50] and therefore prevent the adsorption of Ag^+ onto the IOMPs. Coextraction may further be reduced if the extraction procedure is performed with aged IOMPs. However, the addition of Ca^{2+}, as proposed by Zhou et al. for overcoming environmental matrix effects [20] increased the coextraction, especially for higher Ag^+ concentrations (50 ng L^{-1} and 500 ng L^{-1}, respectively; up to 60%). Coextraction levels of Ag^+ for different sample matrices are presented in the SI, Figure S15. However, Zhou et al. found Ag^+ coextraction levels of 4.65% in their study [20]. The contradiction between our findings and those of the previous study by Zhou et al. [20] may be a consequence of the environmentally relevant concentrations in the ng L^{-1} range used in our studies. There is a possibility that adsorption/desorption processes of Ag^+ onto/from IOMPs become more dominant at such low concentrations as for concentrations in the μg L^{-1} range. Therefore, when dealing with environmental samples and considering the effect of NOM on the extraction efficiency (3.3. Examination of Matrix Effects and Optimisation of the MSPE), increasing the IOMP concentration is to be preferred over the addition of Ca^{2+} for the MSPE of Ag-b-NPs.

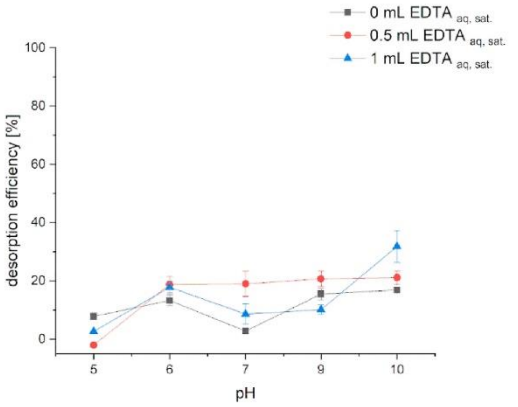

Fig. 3. Influence of sample pH and amount of $EDTA_{aq,\ sat.}$ added to the sample on the elution of Ag_2S-NPs from IOMPs at RT. Incubation time was 60 min. Pristine synthesised IOMPs were used for the prior extraction of Ag_2S-NPs with an initial Ag concentration of 50 ng L^{-1}. The IOMP concentration was 100 mg L^{-1}.

3.5. Recovery of Ag-b-NPs after MSPE

To determine the Ag-b-NPs' sizes, they must be separated from the IOMPs after their extraction by elution from the IOMPs. As Ag_2S-NPs represent the majority of naturally occurring Ag-b-NPs [9,12–14], the aim was to develop a method for species-selective size determination of Ag_2S-NPs. To this end, we developed an elution process based on EDTA as eluent added to the samples at varying amounts of a saturated solution. In a first attempt, we investigated the effect of sample pH on the elution of Ag_2S-NPs from IOMPs to identify an optimal pH (range) for the elution process (Fig. 3). As sample pH affects the surface charge of IOMPs and Ag-b-NPs and therefore their interaction, this is a crucial parameter for an effective elution of Ag-b-NPs. It is worth noting that desorption efficiencies were <30%, thus indicating the need of further improvement in the desorption process. However, when working in this aqueous sample matrix, a slight increase in the desorption efficiency could be observed when the pH was increased. Possibly, the electrostatic repulsion between the negative surface charges of Ag_2S-NPs and IOMPs at higher pH leads to weaker binding, thereby facilitating their desorption from the IOMPs [42,52–54]. Therefore, for our next studies, pH = 7 and pH = 9 were chosen in order to compare the desorption efficiencies at neutral and basic pH.

Our next step was to evaluate the influence of incubation temperature on the elution process and therefore provide an optimal temperature for the elution process for maximum desorption of Ag_2S-NPs from IOMPs. As an increase of incubation temperature leads to higher particle diffusion rates, this might also enhance the desorption process further. However, applying a too high temperature might also affect Ag-b-NP stability. As before for the pH study, the incubation temperature study was performed at varying amounts of $EDTA_{aq,\ sat.}$ for a better comparison and classification of the obtained results. As can be seen from Fig. 4, increasing the incubation temperature to 40 °C leads to an increase in the desorption efficiency with 0.5 mL $EDTA_{aq,\ sat.}$ added to the sample. However, exceeding a temperature of 40 °C leads to a decrease in desorption efficiency. Conducting sp-ICP-MS measurements showed no change in particle size for an incubation temperature of T = 40 °C (SI, Figure S16). However, conduction of sp-ICP-MS measurements for T = 50 °C showed no particle signals, thus indicating particle dissolution. The corresponding number of measured particles for all particle size distributions for the elution process optimisation are presented in the SI, Table S3. As a result, for our further studies we chose an incubation temperature of 40 °C. The previously made observation, that an increase in sample pH results in an increase in the desorption efficiency could be confirmed at an incubation temperature of 40 °C (SI, Figure S17). However, the desorption efficiency is still not much greater than 30%, making further optimisation steps necessary.

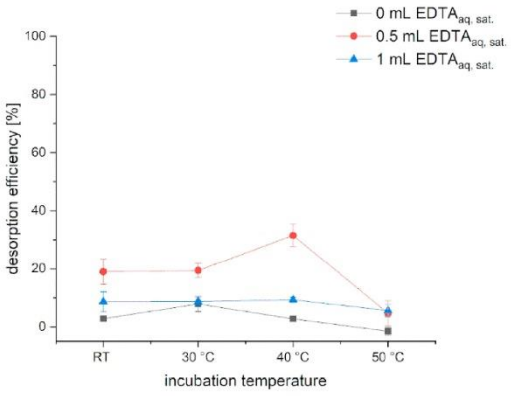

Fig. 4. Influence of incubation temperature on the elution of Ag_2S-NPs from IOMPs. Sample pH was set to 7. Incubation time was 60 min. Pristine synthesised IOMPs were used for the prior extraction of Ag_2S-NPs, with an initial Ag concentration of 50 ng L^{-1}. The IOMP concentration was 100 mg L^{-1}.

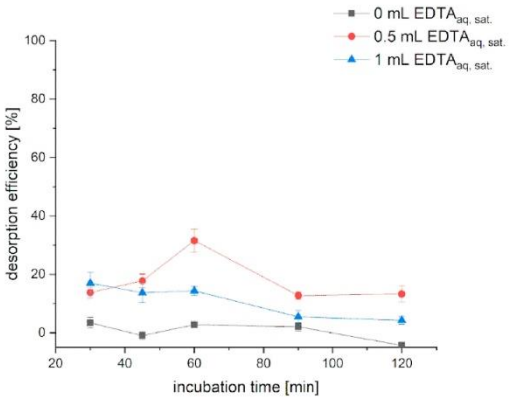

Fig. 5. Influence of incubation temperature on the elution of Ag_2S-NPs from IOMPs. Sample pH was set to 7. Incubation time was 60 min. Pristine synthesised IOMPs were used for the prior extraction of Ag_2S-NPs, with an initial Ag concentration of 50 ng L^{-1}. The IOMP concentration was 100 mg L^{-1}.

Next, we investigated the influence of the incubation time on the elution of Ag_2S-NPs and evaluate a possible optimal incubation time to improve the desorption efficiency. The incubation time also is a key parameter, as re-adsorption of Ag-b-NPs onto IOMPs might occur at some point. Here too, to improve comparison, we presented our findings in relation to the amount of $EDTA_{aq,\ sat.}$ added to the sample. Fig. 5 shows an increase in the desorption efficiency until a maximum is observed for 60 min and 0.5 mL $EDTA_{aq,\ sat.}$. For longer incubation times, the desorption efficiency decreases. One possibility is that previously eluted Ag_2S-NPs tend, after some time, to once again be

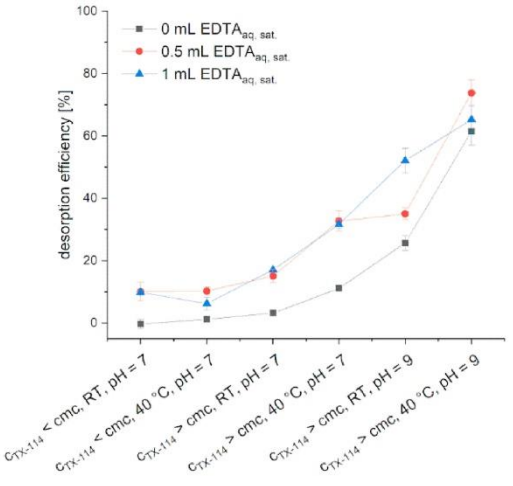

Fig. 6. Influence of the surfactant concentration of TX-114, incubation temperature and sample pH on the desorption of Ag_2S-NPs from IOMPs while varying the amounts of $EDTA_{aq,\ sat.}$ added to the samples.

adsorbed onto the surfaces of the IOMPs. Therefore, for the next optimisation steps of the elution process, we used an incubation time of 60 min.

To optimise the elution process of Ag_2S-NPs from IOMPs further and thus maximise the desorption efficiency, we evaluated the influence of the addition and concentration of the surfactant TX-114 to the samples in concentrations below (0.15 mM, $c_{TX\text{-}114} < cmc$) and above (4.93 mM, $c_{TX\text{-}114} > cmc$) the critical micelle concentration (cmc = 0.23 mM for TX-114). Elution experiments were carried out below (RT) and above (40 °C) the cloud point temperature of TX-114 (23 °C) to evaluate the influence of micelle formation on the process. Fig. 6 shows that exceeding both the cmc and cloud point temperature, which occurs in the formation of micelles, greatly enhanced the desorption of Ag_2S-NPs from the IOMPs. Furthermore, the previously observed influence of sample pH resulting in a maximum desorption of Ag_2S-NPs at pH 9 was also observed here. In Fig. 6, the abscissa extends from $c_{TX\text{-}114} < cmc$ at RT and pH = 7 to $c_{TX\text{-}114} > cmc$ at 40 °C and pH = 9, so that the influence of those factors (i.e. sample pH, incubation temperature and TX-114 concentration) on the increase in desorption efficiency is clearly visible. The formation of micelles clearly improved the elution of Ag-b-NPs from the IOMPs, suggesting that the nanoparticles were encapsulated which therefore prevented their repeat adsorption onto the IOMPs. It is also worthy of note, that the addition of $EDTA_{aq,\ sat.}$ further enhanced the desorption process by approximately 10%. This can be explained as being due to the adsorption of EDTA onto the IOMPs, therefore enhancing Ag-b-NP elution. However, when applying a higher IOMP concentration in the previous extraction step, which is necessary when dealing with environmental samples (see section 3.3. Examination of Matrix Effects and Optimisation of the MSPE), a large decrease in desorption efficiency to 51 ± 2% was observed as a result of doubling the IOMP concentration. Therefore, to improve the desorption efficiency when dealing with environmental samples, which requires higher IOMP concentrations, we applied a modified version of the CPE in a subsequent step. The conduction of sp-ICP-MS measurements also showed no change in particle size following this method (pH = 9), which is crucial for an accurate particle size determination for unknown samples (SI, Figure S18). A TX-114 concentration of 4.93 mM ($c_{TX\text{-}114} > cmc$), incubation temperature of 40 °C and sample pH = 9 therefore represents a promising combination for the elution of Ag_2S-NPs from IOMPs after extraction.

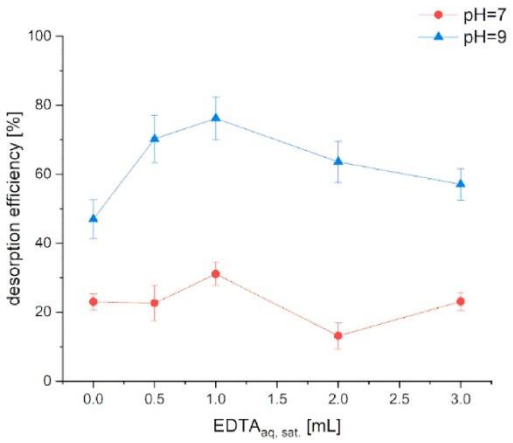

Fig. 7. Desorption efficiencies of the elution of Ag_2S-NPs from IOMPs using modified CPE as the desorption method with varying volumes of $EDTA_{aq,\ sat.}$ added to the sample. Elution was carried out at pH 7 and pH 9. Pristine synthesised IOMPs were used for the prior extraction of Ag_2S-NPs with an initial Ag concentration of 50 ng L^{-1}. IOMP concentration was 100 mg L^{-1}.

The elution process based on the modified CPE procedure indicated a maximum efficiency for pH = 9 and 1.0 mL $EDTA_{aq,\ sat.}$ added to the sample, resulting in a desorption efficiency of 76 ± 6% (Fig. 7), determined with ICP-MS measurements. Furthermore, increasing IOMP concentration, previously applied for the Ag-b-NP extraction, which is necessary when dealing with environmental water samples (see 3.3. Examination of Matrix Effects and Optimisation of the MSPE) did not lead to a major decrease in the desorption efficiency (SI, Figure S19A). We also investigated the influence of the surface structure on the elution process. Ageing of the IOMPs lead to a 10% increase in the desorption efficiency, whereas using 50–100 nm IOMPs for the extraction-elution process resulted in lower desorption efficiencies (SI, Figure S19B), thus suggesting that firstly, the fissured surface of the synthesised IOMPs and secondly, the oxidised surface, further enhance the desorption of Ag_2S-NPs from IOMPs. It is possible that the oxidised surface of aged IOMPs leads to a weaker interaction with Ag-b-NPs than in their pristine state, thus facilitating their elution. Aged synthesised IOMPs are therefore suggested as the best choice for the extraction-elution procedure. In addition, sp-ICP-MS measurements of eluted Ag_2S-NPs following this optimised method also showed no change in particle size, thus highlighting the potential of this method, based on MSPE and the subsequent elution of Ag_2S-NPs, for preserving the particles' size (SI, Figure S20).

As our goal was to establish a method for the species selective determination of Ag_2S-NPs, we also investigated the stability of core Ag-b-NPs (CA@Ag-NPs) and AgCl-NPs during the elution process. Examining the optimised elution method based on CPE at pH = 9 and 1.0 mL $EDTA_{aq,\ sat.}$ added to the sample based on CA@Ag-NPs and AgCl-NPs, ICP-MS measurement showed desorption efficiencies of 71 ± 12% (CA@Ag-NPs) and 79 ± 5% (AgCl-NPs). However, sp-ICP-MS measurements revealed that the NPs were dissolved during the elution step (SI, Figure S21). The presented method, based on CPE at pH = 9, 40 °C and 1 mL $EDTA_{aq,\ sat.}$ added to the sample, therefore offers an effective approach for the extraction of Ag-b-NPs from environmental samples and subsequent species-selective, size-preserving elution of Ag_2S-NPs, which are the largest fraction of naturally occurring Ag-b-NPs [9, 12–14]. Therefore, our unique findings provide a fast and simple method capable of distinguishing between Ag-b-NPs in environmental samples based on their chemical composition.

4. Conclusions

MSPE represents an efficient tool for the extraction of Ag-b-NPs of various chemical compositions and coatings from environmental water samples. It was shown that Ag-b-NPs could be extracted at environmentally relevant concentrations in the low ng L^{-1} range with efficiencies of 80–100%. However, the surface shape and agglomeration state of the IOMPs were shown to have a great influence on the extraction efficiency. A fissured surface enhances the extraction, possibly owing to an increased number of adsorption sites. Furthermore, it was shown that environmentally relevant matrix constituents, such as inorganic ions and solids had no major influence on the extraction efficiency at environmentally relevant concentrations. However, the presence of NOM lead to a 50% decrease in extraction efficiency. However, addition of Ca^{2+} or increasing the IOMP concentration were shown to overcome this effect efficiently, resulting in extraction efficiencies >97%, thus suggesting that NOM blocks Ag-b-NP binding sites on the IOMPs and therefore hinders their efficient extraction. Moreover, we were successful in extracting Ag-b-NPs added to a river water sample at an environmentally relevant concentration of β_{Ag} = 50 ng L^{-1}. Also, Ag^+ coextraction was eliminated when adding SR-NOM at environmentally relevant concentrations to the sample. As particle size is an important factor in respect of Ag-b-NP toxicity, its preservation during the elution of the particles from the IOMPs is crucial. Ag_2S-NPs, which are the predominant species in environmental samples, are of great

interest. Our method provides an approach for preserving the size of Ag_2S-NPs for an accurate particle size determination, while core silver nanoparticles and AgCl-NPs are dissolved during the process, thus underlining the huge potential of our method for species-selective size determination of Ag_2S-NPs using sp-ICP-MS in aqueous samples. The MSPE of Ag-b-NP therefore proves to be a valuable tool for Ag-b-NP analysis in environmental samples. Future studies should address possible pathways towards species-selective, size-preserving elution of other environmentally relevant Ag-b-NP compounds to establish a method that is capable of species-selective determination of various kinds of Ag-b-NPs in environmental samples.

Credit author statement

A. Urstoeger: Conceptualisation, Methodology, Validation, Formal analysis, Investigation, Writing – Original Draft, Writing – Review & Editing, Visualisation. **L. Zacherl**: Formal analysis, Investigation. **M. Muhr**: Investigation. **Y. Selic**: Investigation. **M. Wenisch**: Investigation. **M. Klotz**: Investigation. **M. Schuster**: Supervision, Project administration, Funding acquisition.

Funding sources

This research project was financed by the Bavarian State Ministry for the Environment and Consumer Protection (TNT01NaT-73602).

Declaration of competing interest

The authors declare that they have no known competing financial interests or personal relationships that could have appeared to influence the work reported in this paper.

Appendix A. Supplementary data

Supplementary data to this article can be found online at https://doi.org/10.1016/j.talanta.2020.122028.

References

[1] N. Taniguchi, On the basic concept of nanotechnology, in: Proc. Int. Conf. Prod. Eng. Tokyo, Part II, Japan Society of Precision Engineering, Tokyo, 1974.
[2] F. Gottschalk, T. Sun, B. Nowack, Environmental concentrations of engineered nanomaterials: review of modeling and analytical studies, Environ. Pollut. 181 (2013) 287–300, https://doi.org/10.1016/j.envpol.2013.06.003.
[3] Q. Ye, J. Zhao, F. Huo, J. Wang, S. Cheng, T. Kang, H. Dai, Nanosized Ag/α-MnO2 catalysts highly active for the low-temperature oxidation of carbon monoxide and benzene, Catal. Today 175 (2011) 603–609, https://doi.org/10.1016/j.cattod.2011.04.008.
[4] A. Loiseau, V. Asila, G. Boitel-Aullen, M. Lam, M. Salmain, S. Boujday, Silver-based plasmonic nanoparticles for and their use in biosensing, Biosensors 9 (2019) 78, https://doi.org/10.3390/bios9020078.
[5] G.A. Sotiriou, S.E. Pratsinis, Engineering nanosilver as an antibacterial, biosensor and bioimaging material, Curr. Opin. Chem. Eng. 1 (2011) 3–10, https://doi.org/10.1016/j.coche.2011.07.001.
[6] H.F. Krug, Nanosafety research—are we on the right track? Angew. Chem. Int. Ed. 53 (2014) 12304–12319, https://doi.org/10.1002/anie.201403367.
[7] N.C. Mueller, B. Nowack, Exposure modeling of engineered nanoparticles in the environment, Environ. Sci. Technol. 42 (2008) 4447–4453, https://doi.org/10.1021/es7029637.
[8] M.A. Maurer-Jones, I.L. Gunsolus, C.J. Murphy, C.L. Haynes, Toxicity of engineered nanoparticles in the environment, Anal. Chem. 85 (2013) 3036–3049, https://doi.org/10.1021/ac303636s.
[9] C. Levard, E.M. Hotze, G.V. Lowry, G.E. Brown, Environmental transformations of silver nanoparticles: impact on stability and toxicity, Environ. Sci. Technol. 46 (2012) 6900–6914, https://doi.org/10.1021/es2037405.
[10] W. Zhang, B. Xiao, T. Fang, Chemical transformation of silver nanoparticles in aquatic environments: mechanism, morphology and toxicity, Chemosphere 191 (2018) 324–334, https://doi.org/10.1016/j.chemosphere.2017.10.016.
[11] P.M. Potter, J. Navratilova, K.R. Rogers, S.R. Al-Abed, Transformation of silver nanoparticle consumer products during simulated usage and disposal, Environ. Sci.: Nano 6 (2019) 592–598, https://doi.org/10.1039/C8EN00958A.
[12] R. Kaegi, A. Voegelin, C. Ort, B. Sinnet, B. Thalmann, J. Krismer, H. Hagendorfer, M. Elumelu, E. Mueller, Fate and transformation of silver nanoparticles in urban wastewater systems, Water Res. 47 (2013) 3866–3877, https://doi.org/10.1016/j.watres.2012.11.060.
[13] B. Nowack, J.F. Ranville, S. Diamond, J.A. Gallego-Urrea, C. Metcalfe, J. Rose, N. Horne, A.A. Koelmans, S.J. Klaine, Potential scenarios for nanomaterial release and subsequent alteration in the environment, Environ. Toxicol. Chem. 31 (2012) 50–59, https://doi.org/10.1002/etc.726.
[14] B. Nowack, Nanosilver revisited downstream, Science 330 (2010) 1054–1055, https://doi.org/10.1126/science.1198074.
[15] Y.M. Cho, Y. Mizuta, J.I. Akagi, T. Toyoda, M. Sone, K. Ogawa, Size-dependent acute toxicity of silver nanoparticles in mice, J. Toxicol. Pathol. 31 (2018) 73–80, https://doi.org/10.1293/tox.2017-0043.
[16] A. Wimmer, A. Urstoeger, N.C. Funck, F.P. Adler, L. Lenz, M. Doeblinger, M. Schuster, What happens to silver-based nanoparticles if they meet seawater? Water Res. 171 (2020) 115399, https://doi.org/10.1016/j.watres.2019.115399.
[17] G. Hartmann, T. Baumgartner, M. Schuster, Influence of particle coating and matrix constituents on the cloud point extraction efficiency of silver nanoparticles (Ag-NPs) and application for monitoring the formation of Ag-NPs from Ag^+, Anal. Chem. 86 (2014) 790–796, https://doi.org/10.1021/ac403289d.
[18] F. Gottschalk, T. Sonderer, R.W. Scholz, B. Nowack, Modeled environmental concentrations of engineered nanomaterials (TiO(2), ZnO, Ag, CNT, Fullerenes) for different regions, Environ. Sci. Technol. 43 (2009) 9216–9222, https://doi.org/10.1021/es9015553.
[19] S.K. Mwilu, E. Siska, R.B.N. Baig, R.S. Varma, E. Heithmar, K.R. Rogers, Separation and measurement of silver nanoparticles and silver ions using magnetic particles, Sci. Total Environ. 472 (2014) 316–323, https://doi.org/10.1016/j.scitotenv.2013.10.077.
[20] X. Zhou, J. Liu, C. Yuan, Y. Chen, Speciation analysis of silver sulfide nanoparticles in environmental waters by magnetic solid-phase extraction coupled with ICP-MS, J. Anal. At. Spectrom. 31 (2016) 2285–2292, https://doi.org/10.1039/C6JA00243A.
[21] X.-x. Zhou, Y.-j. Li, J.-f. Liu, Highly efficient removal of silver-containing nanoparticles in waters by aged iron oxide magnetic particles, ACS Sustain. Chem. Eng. 5 (2017) 5468–5476, https://doi.org/10.1021/acssuschemeng.7b00797.
[22] T. Tolessa, X.-X. Zhou, M. Amde, J.-F. Liu, Development of reusable magnetic chitosan microspheres adsorbent for selective extraction of trace level silver nanoparticles in environmental waters prior to ICP-MS analysis, Talanta 169 (2017) 91–97, https://doi.org/10.1016/j.talanta.2017.03.064.
[23] I. Hagarová, Magnetic solid phase extraction as a promising technique for fast separation of metallic nanoparticles and their ionic species: a review of recent advances, Journal of Analytical Methods in Chemistry 2020 (2020) 8847565, https://doi.org/10.1155/2020/8847565.
[24] M. Wierucka, M. Biziuk, Application of magnetic nanoparticles for magnetic solid-phase extraction in preparing biological, environmental and food samples, TrAC Trends Anal. Chem. (Reference Ed.) 59 (2014) 50–58, https://doi.org/10.1016/j.trac.2014.04.007.
[25] M. Mahmoudi, S. Sant, B. Wang, S. Laurent, T. Sen, Superparamagnetic iron oxide nanoparticles (SPIONs): development, surface modification and applications in chemotherapy, Adv. Drug Deliv. Rev. 63 (2011) 24–46, https://doi.org/10.1016/j.addr.2010.05.006.
[26] J.-f. Liu, Z.-s. Zhao, G.-b. Jiang, Coating Fe3O4 magnetic nanoparticles with humic acid for high efficient removal of heavy metals in water, Environ. Sci. Technol. 42 (2008) 6949–6954, https://doi.org/10.1021/es800924c.
[27] B. Kim, C.-S. Park, M. Murayama, M.F. Hochella, Discovery and characterization of silver sulfide nanoparticles in final sewage sludge products, Environ. Sci. Technol. 44 (2010) 7509–7514, https://doi.org/10.1021/es101565j.
[28] T.M. Tolaymat, A.M. El Badawy, A. Genaidy, K.G. Scheckel, T.P. Luxton, M. Suidan, An evidence-based environmental perspective of manufactured silver nanoparticle in syntheses and applications: a systematic review and critical appraisal of peer-reviewed scientific papers, Sci. Total Environ. 408 (2010) 999–1006, https://doi.org/10.1016/j.scitotenv.2009.11.003.
[29] M.P. Monopoli, D. Walczyk, A. Campbell, G. Elia, I. Lynch, F.B. Bombelli, K. A. Dawson, Physical-chemical aspects of protein corona: relevance to in vitro and in vivo biological impacts of nanoparticles, J. Am. Chem. Soc. 133 (2011) 2525–2534, https://doi.org/10.1021/ja107583h.
[30] M.A. Blesa, E.B. Borghi, A.J.G. Maroto, A.E. Regazzoni, Adsorption of EDTA and iron—EDTA complexes on magnetite and the mechanism of dissolution of magnetite by EDTA, J. Colloid Interface Sci. 98 (1984) 295–305, https://doi.org/10.1016/0021-9797(84)90155-3.
[31] G. Hartmann, C. Hutterer, M. Schuster, Ultra-Trace determination of silver nanoparticles in water samples using cloud point extraction and ETAAS, J. Anal. At. Spectrom. 28 (2013) 567–572, https://doi.org/10.1039/C3JA30365A.
[32] J.M. Pettibone, J. Liu, In situ methods for monitoring silver nanoparticle sulfidation in simulated waters, Environ. Sci. Technol. 50 (2016) 11145–11153, https://doi.org/10.1021/acs.est.6b03023.
[33] L. Garza-Ocañas, D.A. Ferrer, J. Burt, L.A. Diaz-Torres, M. Ramírez Cabrera, V. T. Rodríguez, R. Luján Rangel, D. Romanovicz, M. Jose-Yacaman, Biodistribution and long-term fate of silver nanoparticles functionalized with bovine serum albumin in rats, Metall 2 (2010) 204–210, https://doi.org/10.1039/B916107D.
[34] S. Mandal, A. Gole, N. Lala, R. Gonnade, V. Ganvir, M. Sastry, Studies on the reversible aggregation of cysteine-capped colloidal silver particles interconnected via hydrogen bonds, Langmuir 17 (2001) 6262–6268, https://doi.org/10.1021/la010536d.
[35] D.R. Bae, W.S. Han, J.M. Lim, S. Kang, J.Y. Lee, D. Kang, J.H. Jung, Lysine-Functionalized silver nanoparticles for visual detection and separation of histidine and histidine-tagged proteins, Langmuir 26 (2010) 2181–2185, https://doi.org/10.1021/la9026865.

[36] L. Li, G. Hartmann, M. Döblinger, M. Schuster, Quantification of nanoscale silver particles removal and release from municipal wastewater treatment plants in Germany, Environ. Sci. Technol. 47 (2013) 7317–7323, https://doi.org/10.1021/es3041658.
[37] D. Mahl, C. Greulich, W. Meyer-Zaika, M. Köller, M. Epple, Gold nanoparticles: dispersibility in biological media and cell-biological effect, J. Mater. Chem. 20 (2010) 6176–6181, https://doi.org/10.1039/C0JM01071E.
[38] P. Vasileva, B. Donkova, I. Karadjova, C. Dushkin, Synthesis of starch-stabilized silver nanoparticles and their application as a surface plasmon resonance-based sensor of hydrogen peroxide, Colloids Surf., A 382 (2011) 203–210, https://doi.org/10.1016/j.colsurfa.2010.11.060.
[39] National Institute of Standards & Technology, Report of Investigation: Reference Material® 8013, National Institute of Standards and Technology, Gaithersburg, 2015, pp. 1–10.
[40] T.Y. Sun, N.A. Bornhöft, K. Hungerbühler, B. Nowack, Dynamic probabilistic modeling of environmental emissions of engineered nanomaterials, Environ. Sci. Technol. 50 (2016) 4701–4711, https://doi.org/10.1021/acs.est.5b05828.
[41] M.D. Montaño, J.W. Olesik, A.G. Barber, K. Challis, J.F. Ranville, Single Particle ICP-MS: advances toward routine analysis of nanomaterials, Anal. Bioanal. Chem. 408 (2016) 5053–5074, https://doi.org/10.1007/s00216-016-9676-8.
[42] J.-f. Liu, J.-b. Chao, R. Liu, Z.-q. Tan, Y.-g. Yin, Y. Wu, G.-b. Jiang, Cloud point extraction as an advantageous preconcentration approach for analysis of trace silver nanoparticles in environmental waters, Anal. Chem. 81 (2009) 6496–6502, https://doi.org/10.1021/ac900918e.
[43] T.S. Peretyazhko, Q. Zhang, V.L. Colvin, Size-controlled dissolution of silver nanoparticles at neutral and acidic pH conditions: kinetics and size changes, Environ. Sci. Technol. 48 (2014) 11954–11961, https://doi.org/10.1021/es5023202.
[44] Z. Ajmal, A. Muhmood, M. Usman, S. Kizito, J. Lu, R. Dong, S. Wu, Phosphate removal from aqueous solution using iron oxides: adsorption, desorption and regeneration characteristics, J. Colloid Interface Sci. 528 (2018) 145–155, https://doi.org/10.1016/j.jcis.2018.05.084.
[45] L. Weng, W.H. Van Riemsdijk, T. Hiemstra, Factors controlling phosphate interaction with iron oxides, J. Environ. Qual. 41 (2012) 628–635, https://doi.org/10.2134/jeq2011.0250.
[46] M. Li, J. Liu, Y. Xu, G. Qian, Phosphate adsorption on metal oxides and metal hydroxides: a comparative review, Environ. Rev. 24 (2016) 319–332, https://doi.org/10.1139/er-2015-0080.
[47] R. Pohling, Chemische Reaktionen in der Wasseranalyse, Springer Spektrum, Wiesbaden, 2015, https://doi.org/10.1007/978-3-642-36354-2.
[48] A.T. Sutton, R.D. Arrua, S.C. Thickett, E. Lombi, E.F. Hilder, Understanding the interaction of gold and silver nanoparticles with natural organic matter using affinity capillary electrophoresis, Environ. Sci.: Nano 6 (2019) 1351–1362, https://doi.org/10.1039/C9EN00014C.
[49] B. Gu, J. Schmitt, Z. Chen, L. Liang, J.F. McCarthy, Adsorption and desorption of natural organic matter on iron oxide: mechanisms and models, Environ. Sci. Technol. 28 (1994) 38–46, https://doi.org/10.1021/es00050a007.
[50] E. Tipping, Cation Binding by Humic Substances, Cambridge University Press, Cambridge, 2002, https://doi.org/10.1017/CBO9780511535598.
[51] A. Peters, P. Simpson, G. Merrington, K. Rothenbacher, L. Sturdy, Occurrence and concentration of dissolved silver in rivers in England and Wales, Bull. Environ. Contam. Toxicol. 86 (2011) 637–641, https://doi.org/10.1007/s00128-011-0288-x.
[52] J.-f. Liu, R. Liu, Y.-g. Yin, G.-b. Jiang, Triton X-114 based cloud point extraction: a thermoreversible approach for separation/concentration and dispersion of nanomaterials in the aqueous phase, Chem. Commun. (2009) 1514–1516, https://doi.org/10.1039/B821124H.
[53] D.F. Lawler, A.M. Mikelonis, I. Kim, B.L.T. Lau, S. Youn, Silver nanoparticle removal from drinking water: flocculation/sedimentation or filtration? Water Supply 13 (2013) 1181–1187, https://doi.org/10.2166/ws.2013.125.
[54] V. Sharma, Tarachand, V. Ganesan, G.S. Okram, Zeta-potential and particle size studies of silver sulphide nanoparticles, AIP Conference Proceedings 1731 (2016), 050087, https://doi.org/10.1063/1.4947741.

Supplementary Information (SI)

Magnetic solid phase extraction of silver-based nanoparticles in aqueous samples: Influence of particle composition and matrix effects on its application to environmental samples and species-selective elution and determination of silver sulphide nanoparticles with sp-ICP-MS

Alexander Urstoeger,[a] Lilly Zacherl,[a] Maximilian Muhr,[b] Yasmin Selic,[a] Monika Wenisch,[a] Marcel Klotz[a] and Michael Schuster[a,*]

[a] Division of Analytical Chemistry, Department of Chemistry, Technical University of Munich, Lichtenbergstraße 4, 85748 Garching, Germany

[b] Chair of Inorganic and Metal-Organic Chemistry, Department of Chemistry and Catalysis Research Center, Technical University of Munich, Ernst-Otto-Fischer-Straße 1, 85748 Garching, Germany

* Corresponding Author. E-mail: michael.schuster@tum.de

20 pages

23 figures

4 tables

Synthesis of IOMPs and Ag-b-NPs

IOMPs

IOMPs were synthesised based on a solvothermal reaction whose description has been published previously [1, 2]. In brief, 5.4 g $FeCl_3 \cdot 6\ H_2O$ was dissolved in 200 mL of ethylene glycol while vigorously stirring. After complete dissolution of the $FeCl_3 \cdot 6\ H_2O$, 14.4 g of sodium acetate was added within 20 min while stirring continuously. The orange suspension was then transferred to a Teflon-lined stainless-steel autoclave (OFI Testing Equipment, Inc., Houston TX, USA) and sealed before being maintained at 200 °C for 10 h. Then the black particles were collected with a handheld magnet and washed five times with ultra-pure water (UPW) and ethanol, individually, to remove non-magnetic by-products. The particles were dried under vacuum for 6 h resulting in 2.4 g of IOMPs and stored at 5 °C in a glass bottle. Milled IOMPs were obtained by milling Fe_3O_4 powder for 1 min at 67 g in a PM 100 ball mill (Retsch, Haan, Germany). The particles were treated at 90 °C overnight to age the IOMPs.

AgCl-NPs

The AgCl-NPs were synthesised according to a previously published method [1]. In brief, 1 mL of a solution of 50 mM NaCl in UPW was added dropwise to a solution containing 0.05 mM $AgNO_3$ and 25 mg TX-114 while stirring constantly. The mixture was then stirred for 30 min in the dark at RT. TEM-EDX measurements confirmed the presence of AgCl-NPs (data not shown).

Ag_2S-NPs

Ag_2S-NPs were synthesised according to a procedure published by Pettibone *et al.* [3]. In brief, 0.16 mL of a 0.5 M Na_2S solution was added to 40 mL of a solution of 2 mM $AgNO_3$ in UPW all at once while stirring constantly. The mixture was then stirred for 1 h in the dark at room temperature (RT). TEM-EDX measurements confirmed the presence of Ag_2S-NPs (data not shown).

BSA@Ag-NPs

BSA@Ag-NPs were synthesised according to a procedure reported by Garza-Ocañas *et al.* [4]. In brief, 153 mg $AgNO_3$ and 943 mg BSA were dissolved in 38 mL UPW and 2 mL of a 0.6 M $NaBH_4$ solution was added. BSA@Ag-NPs form quickly under foam generation. The solution was stirred for 30 min at RT and afterwards left in the dark for 5 h to allow ageing.

$\tilde{\nu}$ [cm^{-1}] = 3000-3500 (O-H, N-H), 1650 (C=O), 1530 (N-H), 1392 (C-O)

Cys@Ag-NPs

According to a procedure reported by Mandal *et al.* [5]. 5 mL of a CA@Ag-NP suspension (40 nm, β_{Ag} = 10 mg L^{-1}) was mixed with 100 µL of a cysteine solution (1 mM in UPW) and stirred for 10 min. The mixture was then left in the dark for 24 h to allow ageing.

$\tilde{\nu}$ [cm^{-1}] = 3350 (O-H), 2900 (N-H), 1619 (C=O), 1363 (C-O)

Lys@Ag-NPs

Lys@Ag-NPs were synthesised according to a procedure reported by Bae *et al.* [6]. In brief, 5 mL of a CA@Ag-NP suspension (40 nm, β_{Ag} = 10 mg L^{-1}) was mixed with 500 µL of a L-lysine solution (4 mM in UPW) and stirred for 24 h at RT.

$\tilde{\nu}$ [cm^{-1}] = 2800 (C-H), 1560 (C=O), 1370 (C-O)

MSA@Ag-NPs

MSA@Ag-NPs were prepared as described by Li *et al.* [7]. In brief, 5 mL of a CA@Ag-NP suspension (40 nm, β_{Ag} = 10 mg L^{-1}) was mixed with 50 µL of a mercaptosuccinic acid solution (10 mM in UPW) and stirred for 3 h. Then the mixture was left in the dark for 15 h to allow ageing.

$\tilde{\nu}$ [cm^{-1}] = 1100 (C-N), 1360 (C-H, O-H), 1652 (C=O), 2918 (C-H), 3353 (O-H)

MUA@Ag-NPs

MUA@Ag-NPs were prepared as described by Li *et al.* [7]. In brief, 5 mL of a CA@Ag-NP suspension (40 nm, β_{Ag} = 10 mg L^{-1}) was mixed with 50 µL of a mercaptoundecanoic acid solution (10 mM in UPW) and stirred for 3 h. Then the mixture was left in the dark for 15 h to allow ageing.

$\tilde{\nu}$ [cm^{-1}] = 3335 (O-H), 2848, 2921 (C-H), 1617 (C=O), 1293 (C-O)

PVP_{10}@Ag-NPs

PVP_{10}@Ag-NPs were synthesised according to a procedure reported by Hartmann *et al.* [8]. In brief, 5 mL of a CA@Ag-NP suspension (40 nm, β_{Ag} = 10 mg L^{-1}) was mixed with 250 µL of a PVP solution (PVP_{10}, M = 10 kDa, 0.02 mM in UPW) and stirred for 19 h at RT.

$\tilde{\nu}$ [cm^{-1}] = 2960 (C-H), 1600 (C=O), 1420 (C-H), 1260 (C-N)

Starch@Ag-NPs

Starch@Ag-NPs were prepared following a procedure reported by Vasileva *et al.* [9]. In brief, 32 mL of UPW containing 2 % (w/v) starch was mixed with 16 mL of a $AgNO_3$ solution (1 mM in UPW) and sonicated at 30 °C. Then 10 min 480 µL of a D-(+)-glucose solution (0.1 M in UPW) and 2.4 mL of 0.1 M NaOH were added simultaneously. The mixture was sonicated for another 60 min.

$\tilde{\nu}$ [cm^{-1}] = 3337 (O-H), 2925, 2886 (C-H), 1419, 1359 (C-H), 1013 (C-O)

Purification of Ag-b-NPs

To remove Ag^+ and possible soluble by-products Ag-b-NP dispersions were dialysed (3.5 kDa regenerated cellulose membrane by ZelluTrans, Carl Roth, Karlsruhe, Germany) in the dark for three days, with the water being changed twice a day. After dialysis, the Ag-b-NP suspensions were stored in the dark at 5 °C and were stable for several days.

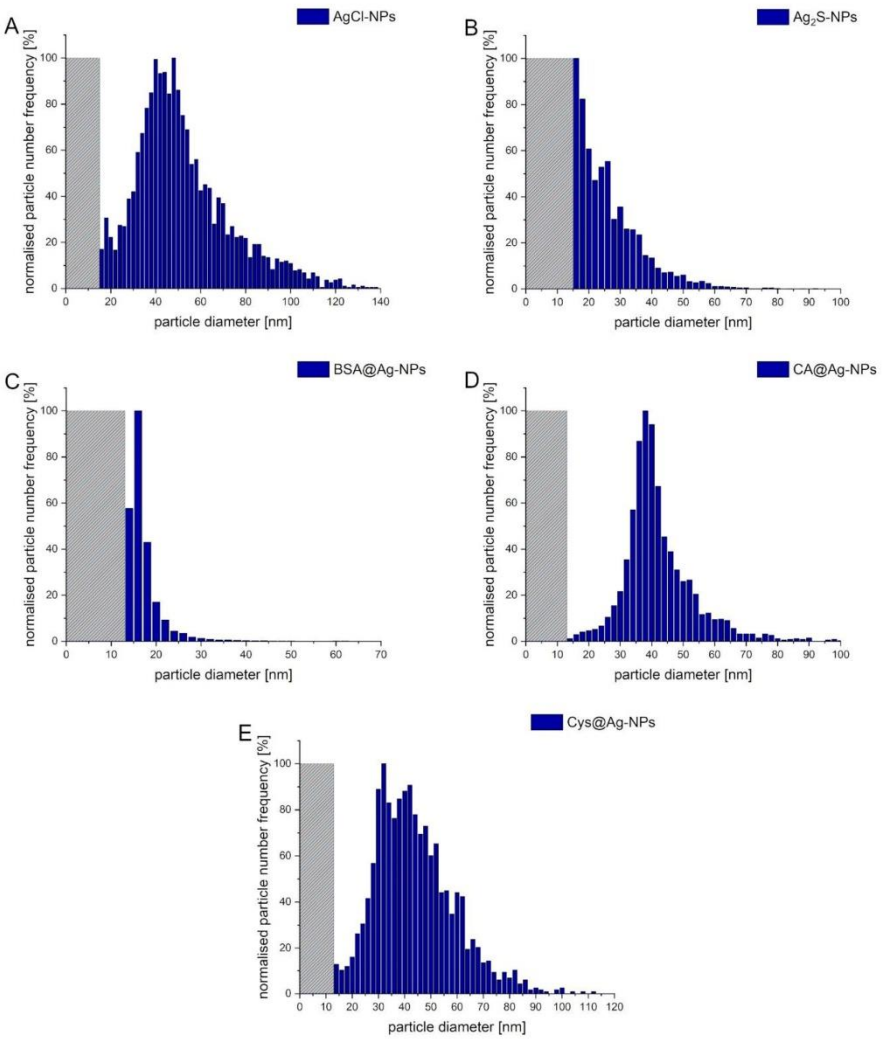

Figure S1. Particle size distributions of AgCl-NPs (A), Ag_2S-NPs (B), BSA@Ag-NPs (C), CA@Ag-NPs (D) and Cys@Ag-NPs (E). The particle size distributions were obtained by sp-ICP-MS measurement based on normalised particle number frequencies. The grey dashed bars indicate the BED, i.e. the threshold at which NP signals overlap with background signal and therefore can no longer be identified as NPs.

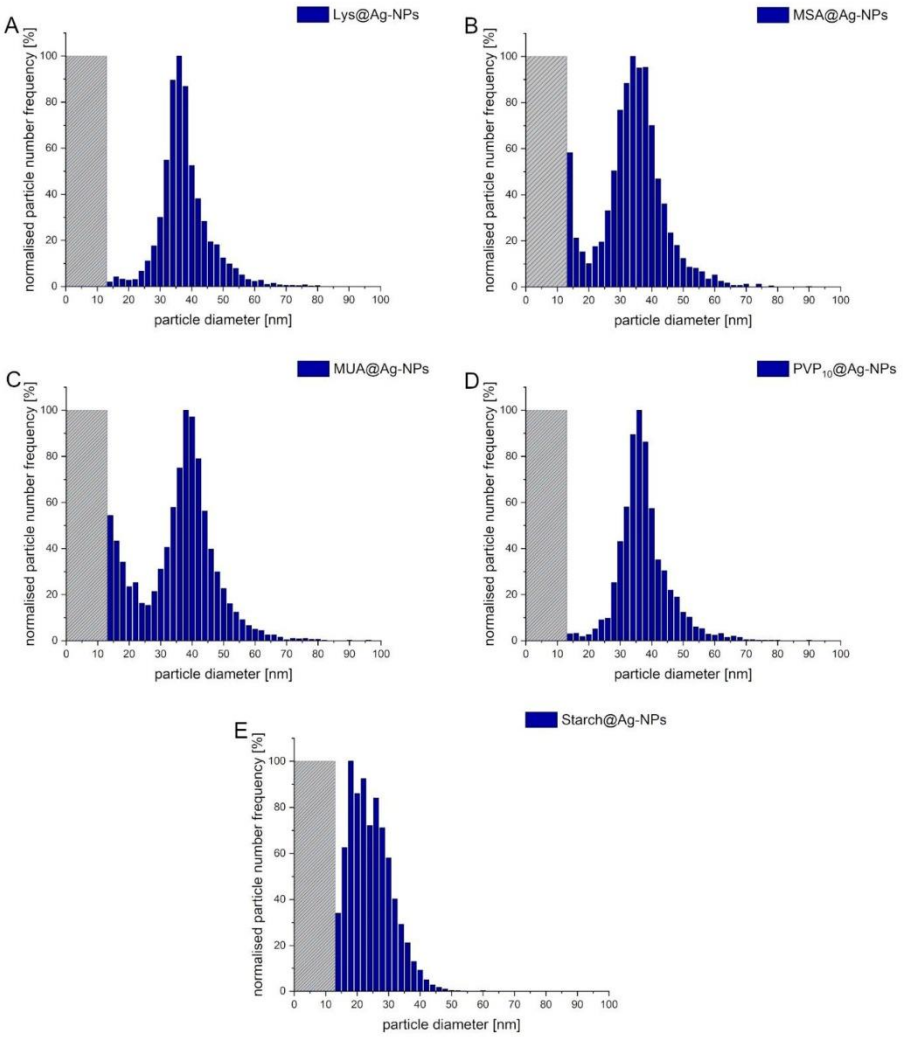

Figure S2. Particle size distributions of Lys@Ag-NPs (A), MSA@Ag-NPs (B), MUA@Ag-NPs (C), PVP_{10}@Ag-NPs (D) and Starch@Ag-NPs (E). The particle size distributions were obtained by sp-ICP-MS measurement based on normalised particle number frequencies. The grey dashed bars indicate the BED, i.e. the threshold at which NP signals overlap with background signal and therefore can no longer be identified as NPs.

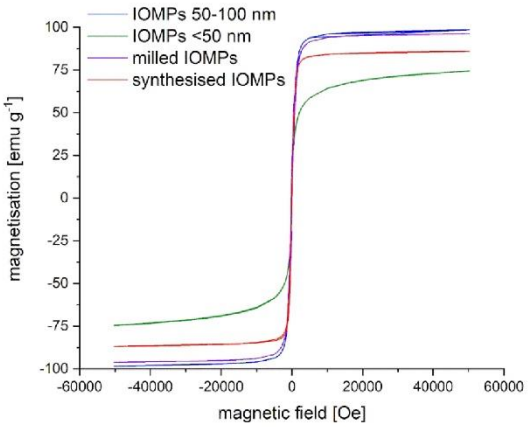

Figure S3. Magnetisation hysteresis curves of IOMPs.

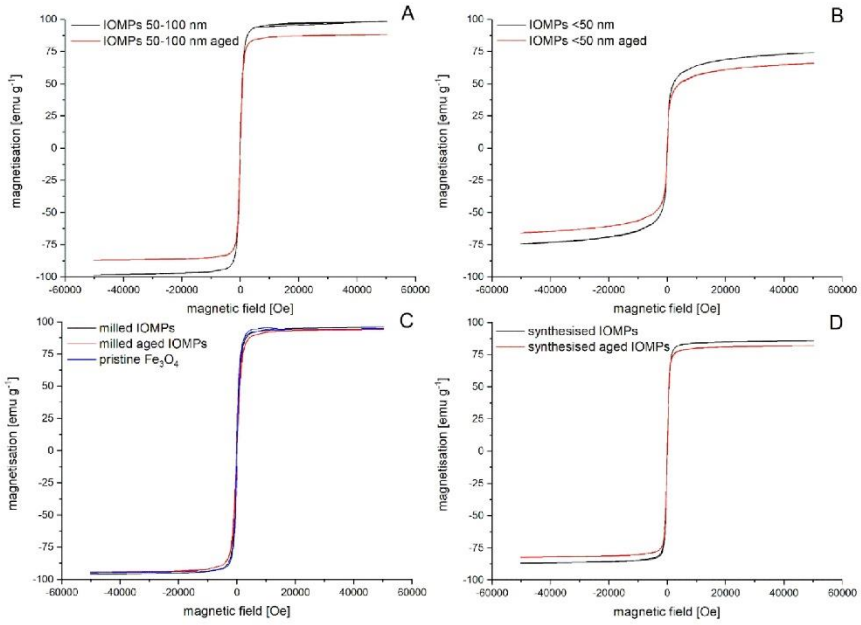

Figure S4. Comparison of magnetisation hysteresis curves of IOMPs 50 – 100 nm (A), IOMPs <50 nm (B), milled IOMPs and pristine Fe_3O_4 (C) and synthesised IOMPs (D) in their pristine and aged state. The magnetisation hysteresis curve of pristine Fe_3O_4 has been added to C to make comparison easier.

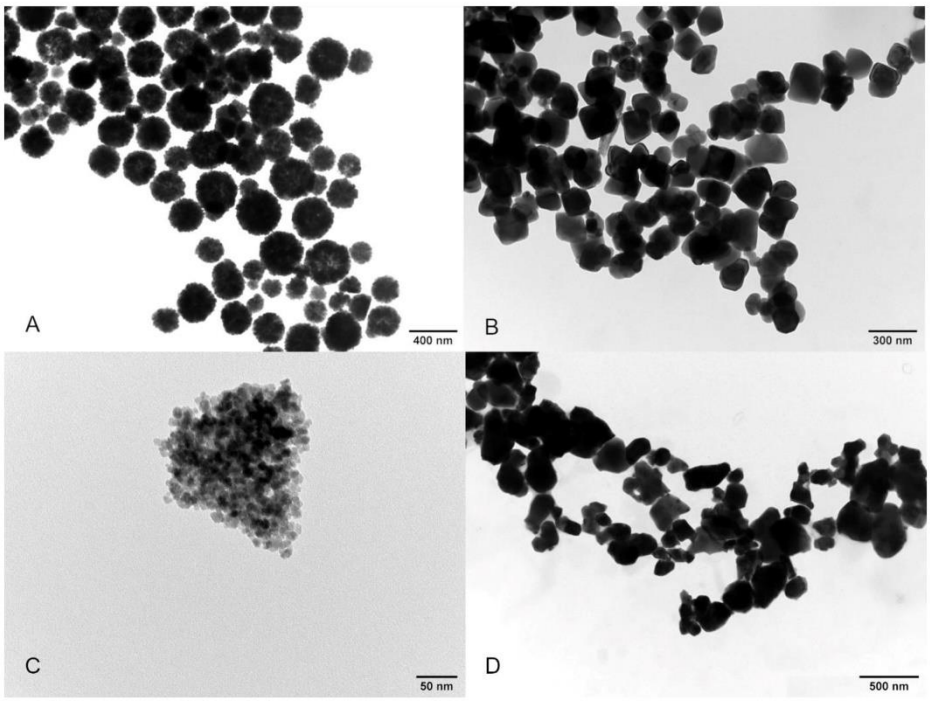

Figure S5. TEM images of synthesised IOMPs (A), IOMPs 50 – 100 nm (B), IOMPs <50 nm (C) and milled IOMPs (D).

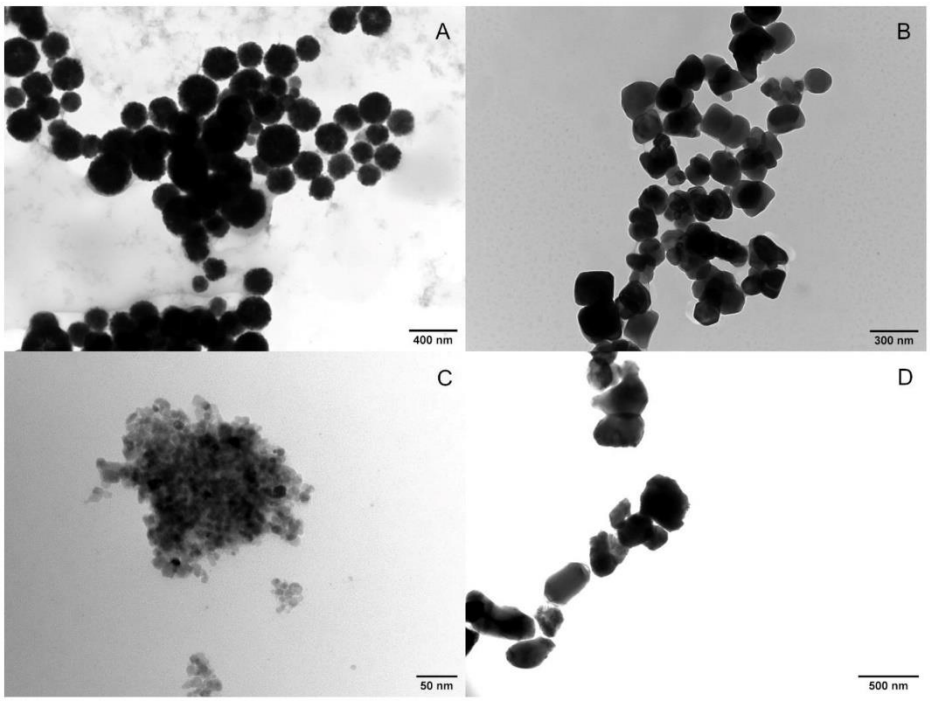

Figure S6. TEM images of aged synthesised IOMPs (A); aged IOMPs 50-100 nm (B), aged IOMPs <50 nm (C) and milled aged IOMPs (D).

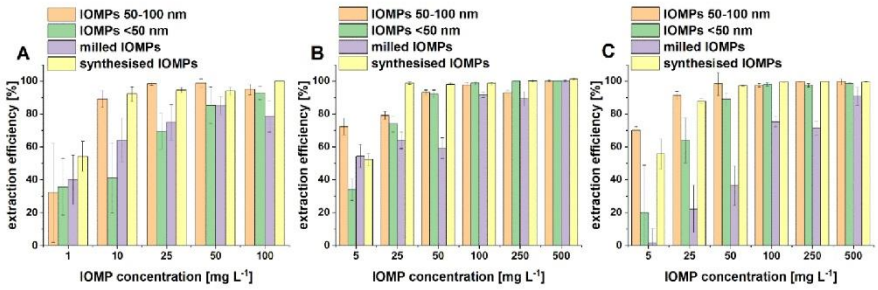

Figure S7. Extraction efficiencies of different IOMPs for the extraction of Ag_2S-NPs at an Ag concentration of 5 ng L^{-1} (A), 50 ng L^{-1} (B) and 200 ng L^{-1} (C).

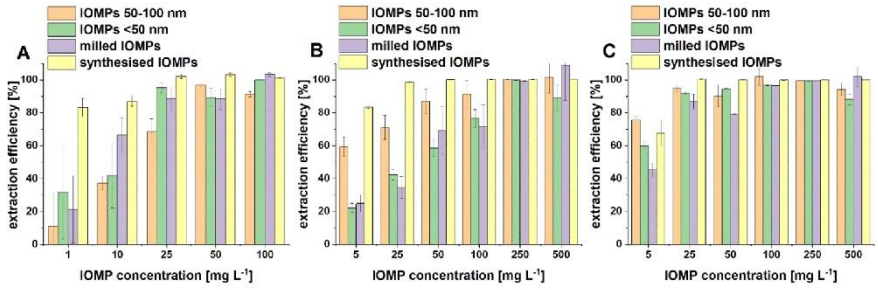

Figure S8. Extraction efficiencies of different IOMPs for the extraction of CA@Ag-NPs at an Ag concentration of 5 ng L^{-1} (A), 50 ng L^{-1} (B) and 200 ng L^{-1} (C).

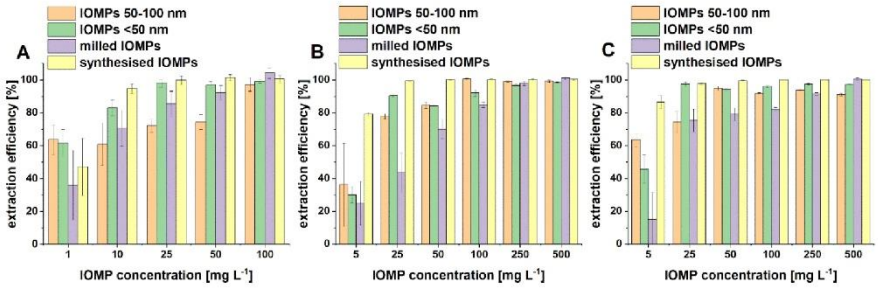

Figure S9. Extraction efficiencies of different IOMPs for the extraction of AgCl-NPs at an Ag concentration of 5 ng L^{-1} (A), 50 ng L^{-1} (B) and 200 ng L^{-1} (C).

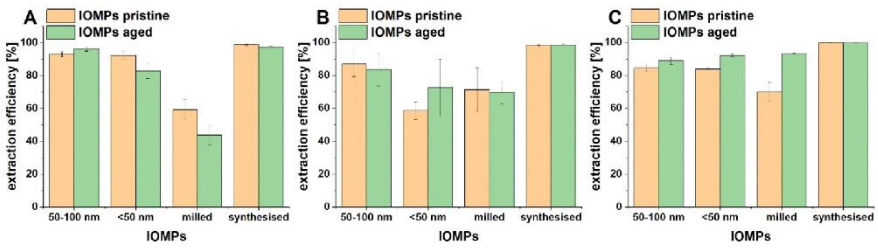

Figure S10. Comparison of the extraction performance of pristine and aged IOMPs used in the extraction of Ag_2S-NPs (A), CA@Ag-NPs (B) and AgCl-NPs (C). The initial Ag concentration was set to 50 ng L^{-1}. The IOMP concentration was set to 50 mg L^{-1} for IOMPs 50-100 nm, IOMPs <50 nm and milled IOMPs and to 25 mg L^{-1} for synthesised IOMPs.

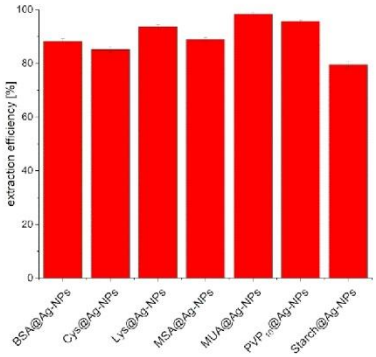

Figure S11. MSPE extraction efficiency for differently coated Ag-b-NPs. The initial Ag-b-NP concentration was β_{Ag} = 50 ng L^{-1} and the IOMP concentration was 50 mg L^{-1}.

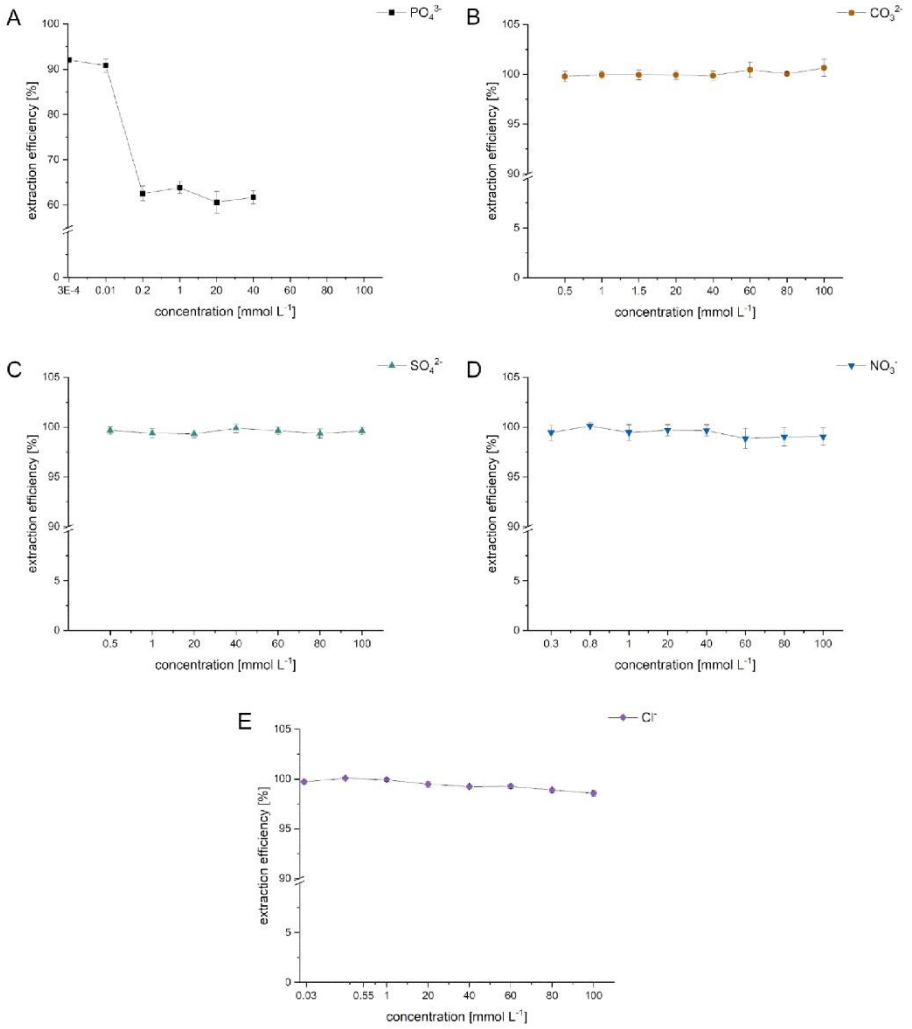

Figure S12. Influence of the presence of PO_4^{3-} (A), CO_3^{2-} (B), SO_4^{2-} (C), NO_3^- (D) and Cl^- (E) at varying concentrations on the MSPE of Ag-b-NPs.

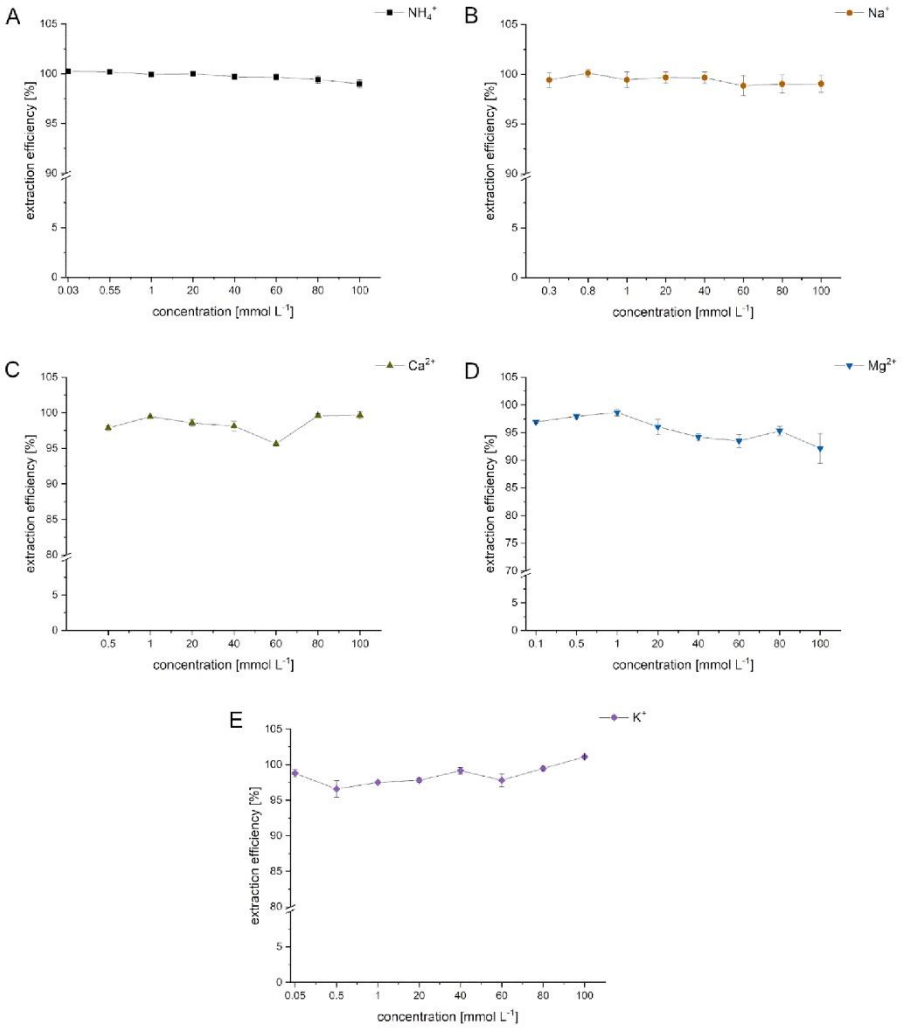

Figure S13. Influence of the presence of NH_4^+ (A), Na^+ (B), Ca^{2+} (C), Mg^{2+} (D) and K^+ (E) at varying concentrations on the MSPE of Ag-b-NPs.

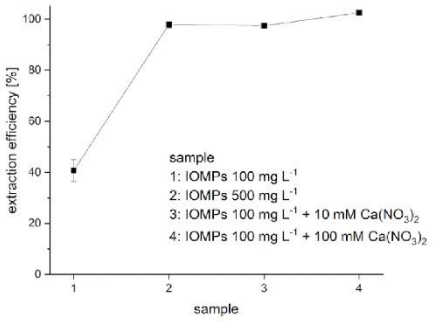

Figure S14. Extraction of Ag_2S-NPs (β_{Ag} = 50 ng L^{-1}) with MSPE from surface water samples (river Wiesäckerbach, Garching, Germany). Samples were prepared with 100 mg L^{-1} or 500 mg L^{-1} IOMPs and the addition of $Ca(NO_3)_2$, respectively.

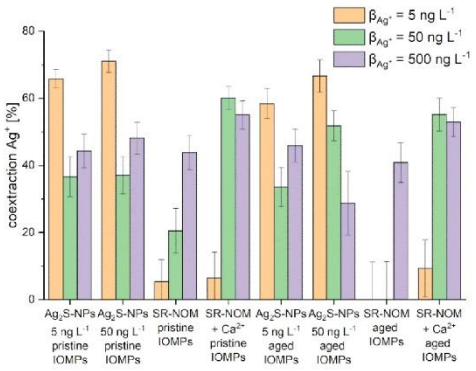

Figure S15. Coextraction of Ag^+ at concentrations of β_{Ag} = 5, 50 and 500 ng L^{-1} with the addition of Ag_2S-NPs at an Ag concentration of 5 and 50 ng L^{-1}, respectively and the addition of SR-NOM at a concentration of 10 mg L^{-1} (TOC). $Ca(NO_3)_2$ concentration was set to 10 mM in samples containing Ca^{2+}. Extraction was performed with 100 mg L^{-1} synthesised IOMPs in their pristine as well as aged state.

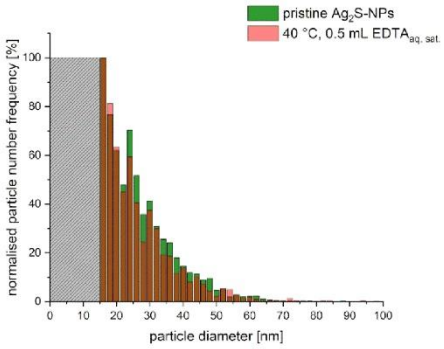

Figure S16. Comparison of particle size distributions of Ag_2S-NPs after elution with $EDTA_{aq, sat.}$ at sample pH = 7 and 40 °C for 60 min. Pristine synthesised IOMPs were used for the prior extraction of Ag_2S-NPs with an initial Ag concentration of 50 ng L^{-1}. IOMP concentration was 100 mg L^{-1}. The brownish colour indicates the overlap of the two size distributions. The grey dashed bar indicates the BED, i.e. the threshold at which NP signals overlap with background signal and therefore can no longer be identified as NPs.

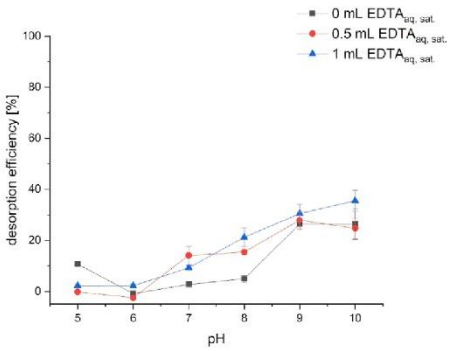

Figure S17. Influence of sample pH and amount of $EDTA_{aq, sat.}$ added to the sample on the elution of Ag_2S-NPs from IOMPs at 40 °C. Incubation time was 60 min. Pristine synthesised IOMPs were used for the prior extraction of Ag_2S-NPs with an initial Ag concentration of 50 ng L^{-1}. The IOMP concentration was 100 mg L^{-1}.

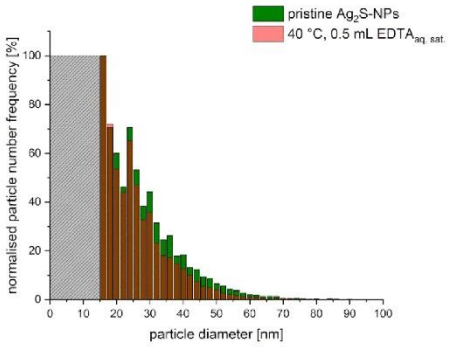

Figure S18. Particle size distribution of Ag_2S-NPs after the desorption from IOMPs at pH = 9 and 40 °C with a TX-114 concentration of 4.9 mM ($c_{TX\text{-}114}$ > cmc) and the addition of 0.5 mL $EDTA_{aq,\ sat.}$ in comparison with the particle size distribution of pristine Ag_2S-NPs. Pristine synthesised IOMPs were used for the prior extraction of Ag_2S-NPs with an initial Ag concentration of 50 ng L^{-1}. The IOMP concentration was 100 mg L^{-1}. The brownish colour indicates the overlap of the two size distributions. The grey dashed bar indicates the BED, i.e. the threshold at which NP signals overlap with background signal and therefore can no longer be identified as NPs.

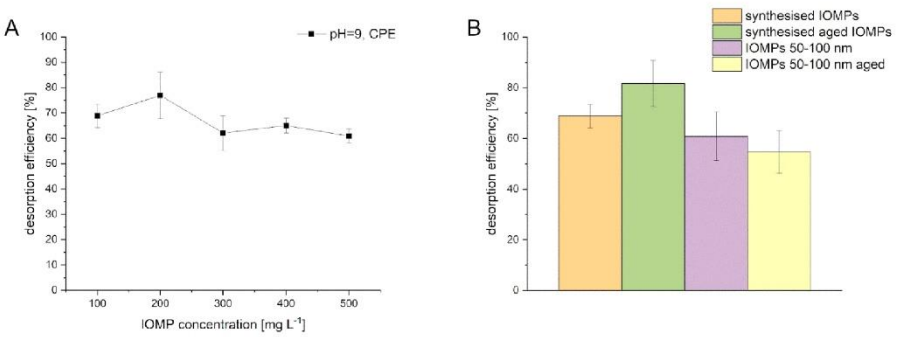

Figure S19. Influence of the IOMP concentration of the preceding extraction procedure on the desorption efficiency of the elution of Ag_2S-NPs using CPE as the desorption method at pH = 9 and with 1 mL of $EDTA_{aq,\ sat.}$ added to the sample (A), and influence of IOMP type (IOMP concentration was 100 mg L^{-1}) on the desorption efficiency (B). The prior extraction of Ag_2S-NPs was carried out with an initial Ag concentration of 50 ng L^{-1}.

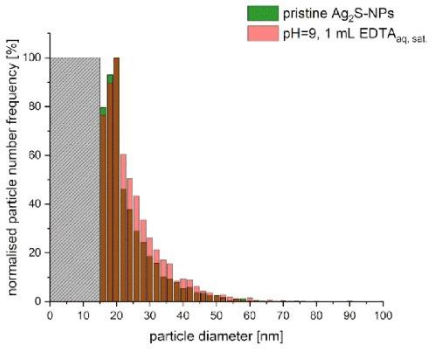

Figure S20. Particle size distribution of Ag_2S-NPs after the desorption from IOMPs using CPE as the desorption method at pH = 9 and with 1 mL of $EDTA_{aq, sat.}$ added to the sample in comparison with the particle size distribution of pristine Ag_2S-NPs. Pristine synthesised IOMPs were used for the prior extraction of Ag_2S-NPs with an initial Ag concentration of 50 ng L^{-1}. IOMP concentration was 100 mg L^{-1}. The brownish colour indicates the overlap of the two size distributions. The grey dashed bar indicates the BED, i.e. the threshold at which NP signals overlap with background signal and therefore can no longer be identified as NPs.

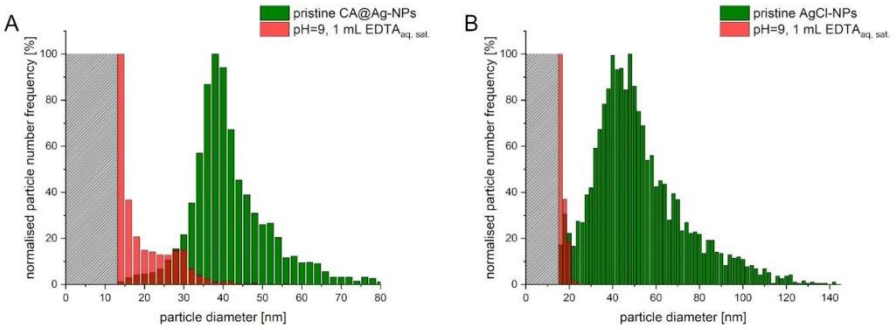

Figure S21. Particle size distribution of CA@Ag-NPs (A) and AgCl-NPs (B) after their desorption from IOMPs using CPE as the desorption method at pH = 9 and with 1 mL of $EDTA_{aq, sat.}$ added to the sample in comparison with the particle size distribution of pristine CA@Ag-NPs and AgCl-NPs. Pristine synthesised IOMPs were used for the prior extraction of CA@Ag-NPs with an initial Ag concentration of 50 ng L^{-1}. The IOMP concentration was 100 mg L^{-1}. The grey dashed bars indicate the BED, i.e. the threshold at which NP signals overlap with background signal and therefore can no longer be identified as NPs.

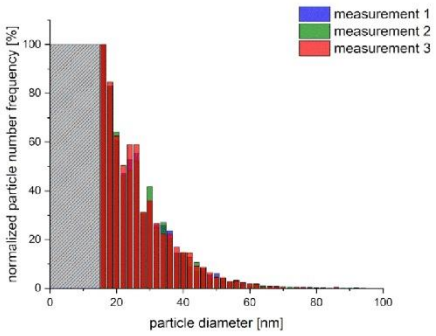

Figure S22. Particle size distributions of a Ag_2S-NP containing sample of three independent sp-ICP-MS measurements. The grey dashed bar indicates the BED, i.e. the threshold at which NP signals overlap with background signal and therefore can no longer be identified as NPs.

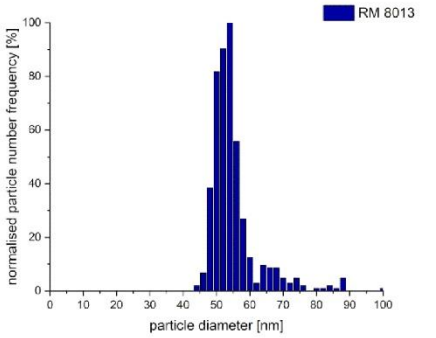

Figure S23. Particle size distribution of the Reference Material RM 8013 used for nebulisation efficiency determination for sp-ICP-MS measurement.

Table S1. River Wiesäckerbach water sample characteristics.

pH	7.9
temperature	2.1 °C
O_2 content	16.35 mg L^{-1}
TOC	20.36 ± 0.64 mg L^{-1}

Table S2. Particle diameter ranges of IOMPs.

IOMPs	particle diameter range [nm]
50-100 nm	123 - 179
<50 nm	9 - 12
milled	174 - 382
synthesised	182 - 315

Table S3. Numbers of measured Ag-b-NPs of presented particle size distributions for the elution process.

Figure	Pristine particles	After desorption
S16	6352	1343
S18	6826	4678
S20	5743	4233
S21 A	2727	301
S21 B	2326	258

Table S4. Instrumental parameters and analytical performances of ICP-MS measurements.

	ICP-MS
RF power [W]	1550
plasma gas flow [L min^{-1}]	15
analyser pressure [Pa]	$7.55*10^{-5}$
R^2 of calibration	0.9996 ± 0.0003
standard deviation of measurement values [%]	1.3 ± 0.5
deviation of measurement values from reference value [%]	0.9 ± 0.8

References

[1] X. Zhou, J. Liu, C. Yuan, Y. Chen, Speciation analysis of silver sulfide nanoparticles in environmental waters by magnetic solid-phase extraction coupled with ICP-MS, J. Anal. At. Spectrom. 31 (2016) 2285-2292. https://doi.org/10.1039/C6JA00243A.

[2] Y. Deng, D. Qi, C. Deng, X. Zhang, D. Zhao, Superparamagnetic High-Magnetization Microspheres with an Fe3O4@SiO2 Core and Perpendicularly Aligned Mesoporous SiO2 Shell for Removal of Microcystins, J. Am. Chem. Soc. 130 (2008) 28-29. https://doi.org/10.1021/ja0777584.

[3] J.M. Pettibone, J. Liu, In Situ Methods for Monitoring Silver Nanoparticle Sulfidation in Simulated Waters, Environ. Sci. Technol. 50 (2016) 11145–11153. https://doi.org/10.1021/acs.est.6b03023.

[4] L. Garza-Ocañas, D.A. Ferrer, J. Burt, L.A. Diaz-Torres, M. Ramírez Cabrera, V.T. Rodríguez, R. Luján Rangel, D. Romanovicz, M. Jose-Yacaman, Biodistribution and long-term fate of silver nanoparticles functionalized with bovine serum albumin in rats, Metallomics 2 (2010) 204-210. https://doi.org/10.1039/B916107D.

[5] S. Mandal, A. Gole, N. Lala, R. Gonnade, V. Ganvir, M. Sastry, Studies on the Reversible Aggregation of Cysteine-Capped Colloidal Silver Particles Interconnected via Hydrogen Bonds, Langmuir 17 (2001) 6262-6268. https://doi.org/10.1021/la010536d.

[6] D.R. Bae, W.S. Han, J.M. Lim, S. Kang, J.Y. Lee, D. Kang, J.H. Jung, Lysine-Functionalized Silver Nanoparticles for Visual Detection and Separation of Histidine and Histidine-Tagged Proteins, Langmuir 26 (2010) 2181-2185. 10.1021/la9026865.

[7] L. Li, G. Hartmann, M. Döblinger, M. Schuster, Quantification of Nanoscale Silver Particles Removal and Release from Municipal Wastewater Treatment Plants in Germany, Environ. Sci. Technol. 47 (2013) 7317-7323. https://doi.org/10.1021/es3041658.

[8] G. Hartmann, T. Baumgartner, M. Schuster, Influence of Particle Coating and Matrix Constituents on the Cloud Point Extraction Efficiency of Silver Nanoparticles (Ag-NPs) and Application for Monitoring the Formation of Ag-NPs from Ag^+, Anal. Chem. 86 (2014) 790–796. https://doi.org/10.1021/ac403289d.

[9] P. Vasileva, B. Donkova, I. Karadjova, C. Dushkin, Synthesis of starch-stabilized silver nanoparticles and their application as a surface plasmon resonance-based sensor of hydrogen peroxide, Colloids Surf., A 382 (2011) 203-210. https://doi.org/10.1016/j.colsurfa.2010.11.060.

8.2. Publikation 2

Separating dissolved silver from nanoparticulate silver is the key: Improved cloud-point-extraction hyphenated to single particle ICP-MS for comprehensive analysis of silver-based nanoparticles in real environmental samples down to single-digit nm particle sizes

Andreas Wimmer[a,1], Alexander Urstoeger[a,1], Tobias Hinke[a], Margit Aust[a], Philipp J. Altmann[b], Michael Schuster[a,*]

[a] Division of Analytical Chemistry, Department of Chemistry, Technical University of Munich, Garching, 85748, Germany

[b] Catalysis Research Center, Technical University of Munich, Garching, 85748, Germany

* Corresponding author

E-Mail: michael.schuster@tum.de

[1] These authors contributed equally to the present study.

Abdruck des Artikels mit Genehmigung von Elsevier (siehe Kapitel 7.5) aus

Analytica Chimica Acta, 2021, 1150, 238198

Analytica Chimica Acta 1150 (2021) 238198

Contents lists available at ScienceDirect

Analytica Chimica Acta

journal homepage: www.elsevier.com/locate/aca

Separating dissolved silver from nanoparticulate silver is the key: Improved cloud-point-extraction hyphenated to single particle ICP-MS for comprehensive analysis of silver-based nanoparticles in real environmental samples down to single-digit nm particle sizes

Andreas Wimmer [a, 1], Alexander Urstoeger [a, 1], Tobias Hinke [a], Margit Aust [a], Philipp J. Altmann [b], Michael Schuster [a, *]

[a] Division of Analytical Chemistry, Department of Chemistry, Technical University of Munich, Garching, 85748, Germany
[b] Catalysis Research Center, Technical University of Munich, Garching, 85748, Germany

GRAPHICAL ABSTRACT

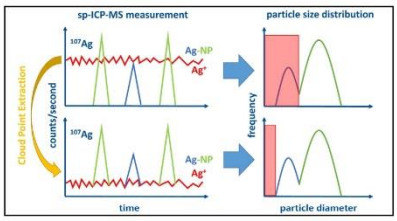

ARTICLE INFO

Article history:
Received 15 October 2020
Received in revised form
21 December 2020
Accepted 2 January 2021
Available online 5 January 2021

Keywords:
Silver based nanoparticles
Cloud point extraction
Single particle ICP-MS
Size detection limit
Real environmental samples

ABSTRACT

Investigating silver-based nanoparticles (Ag-b-NPs) in environmental samples is challenging with current analytical techniques, owing to their low concentrations (ng L^{-1}) in the presence of high quantities of dissolved Ag(I) species. sp-ICP-MS is a promising technique able to simultaneously determine the concentration and particle sizes of Ag-b-NPs even at concentrations of several ng L^{-1}. However, sp-ICP-MS suffers from the coexistence of dissolved analyte species causing high background signals. These background signals cover particle signals and therefore limit the size detection limit (SDL) in sp-ICP-MS. Ag-b-NPs in environmental samples exhibit diameters of < 20 nm, whereas the current sp-ICP-MS approaches barely reach an SDL as low as 20 nm. Using a surfactant-mediated sample pre-treatment (improved cloud point extraction, iCPE), we were able to separate Ag-b-NPs in aqueous samples from dissolved Ag(I) species and enrich the NPs in the extract. By hyphenating iCPE to sp-ICP-MS, we were able to reach SDL values as low as 4.5 nm, thus paving the way for the successful monitoring of Ag-b-NPs in the environment.

* Corresponding author.
E-mail address: michael.schuster@tum.de (M. Schuster).
[1] These authors contributed equally to the present study.

https://doi.org/10.1016/j.aca.2021.01.001
0003-2670/

1. Introduction

Silver-based nanoparticles (Ag-b-NPs) are being widely applied due to their antimicrobial properties, such as in consumer products, fabrics, and surgery products [1–9]. However, concerns are being raised about the threats NPs might present to the environment. During usage of such products or their disposal, Ag-b-NPs may be released into (waste)water streams, pass wastewater treatment plants [10,11], and finally reach natural water bodies [12,13]. Moreover, it has recently been shown that Ag-b-NPs even occur for natural reasons to a very slight extent in lakes due to a reduction of dissolved Ag(I) species [14].

Despite benefits of Ag-b-NPs, emerging technologies should always go hand-in-hand with a balanced risk assessment. In general, the risk of Ag-b-NPs in the environment is derived from three main features: the elemental composition, the concentration and the size distribution. Since Ag^+ deriving from Ag-b-NPs is assumed to be the relevant toxic agent in the environment, Ag species having a lower solubility, such as Ag_2S, exhibit a limited environmental impact [15]. Furthermore, smaller particles have a higher intrinsic surface and therefore exhibit an enhanced release of Ag^+ eventually increasing the NPs' environmental impact [16].

Literature reports toxicity of Ag-b-NPs and Ag(I) to human and environmental health in the μg L^{-1} range and above [1]. To the best of the authors knowledge, no toxic effects of ng L^{-1} traces of Ag-b-NPs and Ag(I) have been reported so far. However, Ag-b-NP and Ag(I) traces are prone to accumulation in the environment and may eventually represent a potential threat to human and environmental health.

Therefore, establishing an analytical approach that is able to simultaneously determine the concentration and size distribution of Ag-b-NPs is regarded essential. Electron microscopy, for instance, enables the determination of particle size distributions. However, such measurements are time-consuming and require extensive sample pretreatment and instrumental effort, resulting in distributions based on only several hundred NPs. In contrast, single particle inductively coupled plasma mass spectrometry (sp-ICP-MS) allows for a fast and simultaneous determination of concentration and particle size distribution. This approach leads to results within minutes, with distributions being based on large numbers of particles. Consequently, size distributions measured by sp-ICP-MS are much more reliable and practicable than those acquired by electron microscopy.

In sp-ICP-MS, the analyte mass is recorded in a time-resolved manner. Instrument noise and dissolved ionic analyte species lead to a continuous signal in the mass spectra representing a background signal. As to the particulate analytes, they are atomized to an ion cloud in the plasma, whereas ions derived from one single particle reach the detector of the mass spectrometer more or less simultaneously. Since sp-ICP-MS detectors record signal intensity consecutively and with very short detection times (the so-called dwell time), NP atomization events in the plasma are recorded as time-resolved transient peaks. Once separated from the background signal, these peaks are eventually converted into particle size distributions and mass concentration of the nanoparticulate analyte [17,18].

However, sp-ICP-MS suffers from some limitations – especially regarding environmental samples. The size detection limit (SDL) in sp-ICP-MS represents the minimum particle size detectable at a reasonable confidence level. The peak signal area is proportional to the size of the corresponding particle ionized in the plasma. Smaller particles cause signals that are not distinguishable from the background signal anymore. Therefore, high background signals lead to an increase of the SDL. Environmental samples containing Ag-b-NPs regularly also contain significant traces of dissolved Ag(I) species resulting in high background signals overlapping the NP peaks. Ag(I) concentration, thus, correlates with the size detection limit (SDL) of Ag-b-NPs [19]. The current literature regards 20 nm as the minimum SDL for Ag-b-NPs [19]. This is insufficient for environmental analysis because Ag-b-NPs in environmental samples are assumed to be smaller than this 20 nm limit. In fact, Kim et al. have reported on Ag-b-NPs in sewage sludge at the 5–20 nm size [20]. The literature suggests diluting the sample in order to decrease the background signal, which is, however, counterproductive to analysis sensitivity, especially in view of the low analyte concentration [17,19,21–23]. In fact, Ag-b-NPs in natural water bodies are present at the level of several ng L^{-1} [11,12,24], which is far beyond the limit of detection (LOD) in current sp-ICP-MS approaches. Finally, additional environmental constituents in real water samples have to be separated prior to measurement in order to avoid cone clogging of the ICP instrument. Therefore, in order to achieve environmental applicability of sp-ICP-MS, it is essential to both enrich Ag-b-NPs and to separate them from the matrix constituents and dissolved Ag(I) species so as to obtain proper LODs in the low ng L^{-1} range and an SDL < 20 nm.

In order to separate the NP signal in sp-ICP-MS from the background signal, various approaches have been suggested, mainly based on mathematical models. Mozhyeva et al., for instance, presented a data deconvolution approach for the extraction of such peaks in the presence of high background signals using microsecond time resolved signals [25]. In order to achieve SDL values sufficient for environmental analysis, we sought to physically separate dissolved Ag(I) species from NPs prior to the measurement, without the need of mathematical discrimination techniques. Therefore, we hyphen a new coacervate-based technique, namely cloud point extraction (CPE), to (sp)-ICP-MS in order to overcome the aforementioned limitations by enriching and separating Ag-b-NPs from aqueous media. Recently, Torrent et al. applied CPE hyphenated to sp-ICP-MS for detection of Ag-b-NPs in soil leachates. A limited background elimination, however, resulted in SDL values of 40 nm, which is insufficient for environmental water samples of the present study [26].

CPE is a sample pretreatment method able to species-selectively enrich and extract Ag-b-NPs from aqueous (environmental) samples. In the 1970s, Watanabe et al. were the first to describe CPE for the extraction of metals from aqueous samples [27] and, thereafter, Liu et al. applied this technique to the extraction of NPs [28]. The samples are mixed with non-ionic surfactants at concentrations exceeding their critical micellar concentration and heated above the respective cloud point temperature. This results in the formation of micells and, thus, a two-phase system comprising aqueous and surfactant rich phase. Ag-b-NPs are "trapped" in the micelles and separated together with the surfactant rich phase. Owing to the volume reduction during extraction in the surfactant rich phase, high enrichment rates can be achieved (approximately factor of 80 considering a 500 μL surfactant rich extract from an initial aqueous phase of 40 mL) [29–32]. The use of CPE for Ag-b-NPs has been thoroughly investigated and validated by our group, whereas quantification of the extracted Ag-b-NPs was achieved by hyphenation to electro thermal atomic spectrometry (ET-AAS), which is a solely quantitative technique [11,29–32]. However, this approach lacks information about the size distribution of Ag-b-NPs.

Therefore, we are in this study (i) presenting an improved version of CPE (hereinafter called iCPE) which exhibits improved species selectivity. In order to obtain size information of nanoparticulate analytes, (ii) iCPE extracts are measured using sp-ICP-MS. Owing to the significantly reduced co-extraction of dissolved Ag(I) species into the surfactant rich phase, (iii) we also studied improvements regarding the SDL of sp-ICP-MS measurements. We further (iv) examined iCPE-sp-ICP-MS with regard to particle size

distribution and parameters influencing the size results, with a special focus on the dwell-time. We finally (v) compared the quantitative results of iCPE-(sp)-ICP-MS hyphenation to the previously validated and established CPE-ET-AAS approach [30,32].

2. Experimental section

2.1. Materials

This study was conducted using citrate-stabilized silver (CA@AgNPs) and gold nanoparticles (CA@AuNPs) of different size. Experiments including dissolved Ag(I) species applied a dissolved Ag(I) ICP-standard ($AgNO_3$ in 3% HNO_3). Main reagents for iCPE are acetic acid and sodium acetate anhydrous and the complexing agents ethylenediaminetetraacetate disodium salt dihydrate ($Na_2EDTA{\cdot}2H_2O$; $C_{10}H_{14}N_2Na_2O_8{\cdot}2H_2O$) and D-penicillamine (PA, $C_5H_{11}NO_2S$). All chemicals were of at least analytical grade and ultra pure water (UPW) was used as diluent. For details regarding used materials, please see the Appendix.

The natural water was sampled in Garching, Germany, from the "*Wiesäckerbach*" stream in June 2016. According to the conventional ICP-MS quantification of Ag in the stream water, the samples contained no Ag beyond the limit of detection (0.15 ng L^{-1}). The water samples were thus used as blank matrix for the further experiments.

2.2. Instrumentation

In essence, the Ag quantification in this study was performed using two different measurement approaches: (i) ET-AAS and (ii) ICP-MS. The latter can be run in conventional ICP-MS mode for the Ag quantification, and in single-particle mode (sp-ICP-MS) for the simultaneous determination of particle size distribution and concentration of nanoparticulate Ag.

2.2.1. ET-AAS

Ag quantification was conducted with a Zeeman-corrected ET-AAS instrument (AAnalyst 800, PerkinElmer, Waltham, MA, USA) equipped with a transversally heated THGA 800 graphite tube atomizer and an AS-72 autosampler. Highly pure Argon 4.8 (Westfalen, Münster, Germany) served as the inert gas during measurements. A silver hollow cathode lamp (Photron, Victoria, Australia) was operated at the recommended current of 10 mA, and the silver quantification was based on the absorption line at $\lambda = 328.1$ nm at an integration time of 5 s. The temperature program of the graphite furnace for the quantification Ag in organic extracts of iCPE followed an approach previously developed in our working group [32].

2.2.2. (sp)-ICP-MS

(sp)-ICP-MS measurements were performed on a quadrupole mass spectrometer 7900 ICP-MS (Agilent, Santa Clara, CA, USA) equipped with a SPS4 autosampler (Agilent) and a MicroMist nebulizer (Glass Expansion, Melbourne, Australia). Argon 4.8 (Westfalen, Münster, Germany) was used as the plasma gas.

Regarding ICP-MS, the Ag quantification was performed by targeting ^{107}Ag (no isobaric interferences) in He collision cell (CCT) mode in order to reduce polyatomic interferences via kinetically energy discrimination. ^{115}In was used as the internal standard.

In sp mode, the dwell time was set to a value ranging from 100 μs to 1000 μs for an acquisition time of 60–90 s. ^{107}Ag was chosen as the target mass, and the pump rate was gravimetrically determined as 0.310 mL min^{-1}. The transport efficiency η describes the proportion of initial particles in the sample finally reaching the detector. CA@Au-NP dispersions (RM 8012, 8013) were used for determining η, following a previously approved procedure [17,33]. Elemental sensitivity was calibrated using a 1 μg L^{-1} Ag(I) standard solution to compensate for an element-specific signal intensity. Particle size distributions were evaluated using Agilent's MassHunter Workstation 4.4 (version C.01.04, build 544.3) software equipped with the Single Nanoparticle Application Module. sp-ICP-MS analysis relies on certain approximations: the investigated CA@Ag-NPs are assumed to be of a spherical shape exhibiting the density of the bulk material Ag ($\rho = 10.49$ g cm^{-3}). See Table A.1 for further instrumental details on sp-ICP-MS measurements.

2.2.3. Total organic carbon (TOC) measurements

The TOC of real water samples was determined using a TOC-L CSH/CSN analyzer (Shimadzu, Kyoto, Japan). All samples were measured in undiluted form without filtration and mixed thoroughly seconds before starting the TOC analysis. For calibration, standard solutions containing 10–100 mg L^{-1} TOC in UPW were prepared from potassium hydrogen phthalate solutions.

2.2.4. Electron microscopy

Transmission Electron Microscopy (TEM) was applied as a supplementary technique for particle size determination. TEM measurements were conducted using a TEM Jeol 1400 plus instrument equipped with a LaB_6 filament at an operating voltage of 120 kV along with a CCD-camera. (JEOL, Freising, Germany). Samples were measured on a copper grid covered with a continuous carbon film (Micro to Nano, Haarlem, the Netherlands).

2.2.5. X-ray diffractometry

Regarding the crystal structure analysis, the X-ray intensity data were measured on a Bruker (Billerica, MA, USA) D8 Venture Duo IMS system equipped with a Helios optic monochromator and a Mo IMS microsource ($\lambda = 0.71073$ Å). CCDC 2006750 contains the supplementary crystallographic data for this paper. These data can be obtained free of charge from The Cambridge Crystallographic Data Centre. Please see the Appendix for further crystallographic details.

2.3. Cloud point extraction (CPE)

This study seeks to further improve CPE, i.e. maximally reduce the co-extraction of dissolved Ag species without affecting the extraction efficiency (EE) of Ag-b-NPs [30–32]. In brief, 40 mL of an aqueous sample containing Ag-b-NPs was mixed with 400 μL of 1 M sodium acetate solution, 1 mL of 1.25 M acetic acid, and 1 mL of 10% TX-114 (w/w) [9–31]. In addition to the established CPE approach, a mixture of the multidental ligands EDTA and PA was applied in iCPE. Like EDTA, PA is able to complex Ag(I) and form highly hydrophilic complexes. For method development, 1–5 mL of saturated EDTA and 1–3 mL of 0.1 M aqueous PA solution were added to the aforementioned CPE mixture (best results were achieved for 3 mL of saturated EDTA solution and 1 mL of 0.1 M PA; see results below). The iCPE mixture was thoroughly mixed and incubated at 40 °C for 30 min. Afterwards, phase separation was accelerated by means of centrifugation (4500 g, 12 min), and both phases were separated by decanting the aqueous phase. The remaining Ag-b-NP-containing organic phase was mixed with 100 μL of EtOH in case the extract was forwarded to ET-AAS measurement or mixed with 500 μL of EtOH and UPW to reach a final volume of 10 mL in case the extract was forwarded to conventional ICP-MS and sp-ICP-MS techniques.

2.4. Hyphenation of iCPE to quantitative analytical techniques

As presented above, the iCPE extract was investigated by means

of ET-AAS and ICP-MS. Since the extract consisted mainly of the surfactant and was highly viscous, the sample introduction was challenging.

2.4.1. iCPE-ET-AAS

ET-AAS tolerates high concentrations of organic matrix constituents. The organic extract was mixed with only 100 μL of EtOH (to reduce sample viscosity) and transferred via a low-volume pipette (20 μL) into the graphite furnace of the ET-AAS instrument. Considering an initial sample volume of 40 mL and 500 μL of resulting extract, an enrichment factor of 80 was achieved.

2.4.2. iCPE-ICP-MS and iCPE-sp-ICP-MS

ICP-MS instruments are more sensitive to highly viscous samples. Therefore, the iCPE extracts were mixed with 500 μL of EtOH and gravimetrically filled with UPW to a total volume of 10 mL. The samples intended for sp-ICP-MS analysis were forwarded to measurement without further treatment. Samples intended for conventional ICP-MS analysis further contained 3.25% HNO_3 (v/v) in order to dissolve NPs and increase sample homogeneity. An enrichment factor of approximately 4 was achieved.

2.5. iCPE method development

ET-AAS and ICP-MS are not able to distinguish between particulate and dissolved Ag, and sp-ICP-MS results are distorted by dissolved Ag traces in the sample. Thus, species selectivity during iCPE is crucial. Therefore, we focused on (i) minimizing the co-extraction of dissolved Ag(I) into the organic phase, (ii) improving size selective EE for Ag-b-NPs, and (iii) reducing the influence of the natural water matrix on the iCPE outcome.

2.5.1. Co-extraction of dissolved Ag(I)

Several solutions containing ng L^{-1} amounts of Ag(I) in 40 mL UPW were prepared. iCPE was applied to all of the samples, whereas the amount of EDTA and PA was varied. As comparison, CPE without ligand addition was carried out (hereinafter referred to as CPE^0). The iCPE and CPE^0 extracts were measured by means of ET-AAS. The signal intensities measured relate to the co-extraction of dissolved Ag(I) species into the organic phase.

2.5.2. Size dependency of the extraction efficiency (EE)

Calibration of iCPE-ET-AAS or iCPE-ICP-MS can be performed using calibration samples containing Ag-b-NPs of known concentration forwarded to the same extraction procedure as the unknown samples. It is intended that the system can be calibrated using Ag-b-NPs of arbitrary size (within a broad range of 10 to 100 nm diameter). This is only valid if there is no size dependent EE. To investigate potential size effects, 40 mL of UPW were mixed with CA@AgNPs of varying size (10, 20, 40, 60, 80, 100, 200 nm) and forwarded to iCPE. To mimic the case of 100% EE, the same type and amount of NPs were added to the organic extracts after iCPE of UPW-only samples (reference). The extracts were measured by means of ET-AAS. The EE can be calculated by dividing the signal intensities measured for the NP-containing extracts by the signal intensities measured for the reference.

2.5.3. Influence of the natural water matrix

Freshly sampled river water (TOC 2.5 mg L^{-1}; initial β_{Ag} < 0.15 ng L^{-1}) was spiked with specific amounts of dissolved Ag(I) standard, yielding in final concentrations of 5, 10 and 50 ng L^{-1} Ag(I). Further, a non-spiked blank river water sample was also subjected to iCPE as basis for evaluation. Moreover, the same amount of Ag(I) as used in the spiked samples was added to the organic extracts after iCPE of blank river water, thus mimicking the case of 100% co-extraction. Spiked samples and samples mimicking 100 % co-extraction were measured by ET-AAS and signal intensities were divided by the signal intensities measured for blank samples to gain the factor for signal increase compared to the blank sample.

2.6. Calibration approaches

As relative quantification techniques, ET-AAS and (sp)-ICP-MS require calibration samples of known analyte concentration. If calibration samples are not pre-treated similar to unknown samples, potential enrichment factors occurring during the sample pretreatment must be considered for data evaluation. sp-ICP-MS requires a calibration approach which significantly differs from the conventional techniques [17].

2.6.1. iCPE-ET-AAS/AgNPs as the calibrant

All experiments were related to iCPE-ET-AAS, a hyphenation which has already been thoroughly developed and validated in our working group [30–32]. It is noted, that no influence of using the iCPE approach instead of the CPE approach could be observed for (i) CPE-ET-AAS (data not shown). The calibration samples containing 60 nm CA@AgNPs of known concentration in the range of β_{Ag} = 5–30 ng L^{-1} were subjected to iCPE together with the unknown samples. This offered the advantage that both the calibration and the unknown samples undergo the same enrichment and are present in the same matrix. The iCPE extracts were diluted as described above in section 2.4.1 and forwarded to ET-AAS.

2.6.2. iCPE-ICP-MS/AgNPs as the calibrant

Calibration samples of iCPE-ICP-MS/AgNP were identical to those for iCPE-ET-AAS/AgNP. The iCPE extracts were diluted as described above in section 2.4.2 and forwarded to ICP-MS. Nebulization in the ICP-MS process was highly dependent on the viscosity of the sample. Given that both the calibration and the unknown samples were present in the same matrix, the nebulization required no correction.

2.6.3. iCPE-ICP-MS/Ag(I) as the calibrant

Here, solutions of dissolved Ag(I) (5–150 ng L^{-1}) served as the calibrant instead of NPs. Since these solutions underwent no iCPE, they were prepared in a UPW matrix (acidified to 3.25% (v/v) HNO_3) including 5% (v/v) of 10% TX-114 (w/w) and 5% (v/v) ethanol to mimic iCPE extract matrix. Samples of 40 mL resulted in a 10 mL diluted iCPE extract forwarded to measurement. Since the calibration solutions were not subjected to the iCPE enrichment, this enrichment factor must be considered in the data evaluation (division by a factor of 4).

2.6.4. iCPE-sp-ICP-MS/AuNPs + Ag(I) as the calibrant

According to Peters et al. [17], all calculations were based on the pump rate, which has been gravimetrically determined as 0.310 mL min^{-1}. The nebulization efficiency η was calculated on the basis of a dispersion containing CA@Au-NPs (RM 8012 and 8013) [17,33]. The elemental sensitivity was calibrated using a 1 μg L^{-1} Ag(I) solution. All calibration samples used were prepared in a matrix consisting of 5% (v/v) TX-114 (10% (w/w)) and 5% (v/v) ethanol. This ensured that both the calibration and the unknown samples were of the same matrix and behaved similarly during nebulization and atomization in the plasma. We investigated the influence of different dwell times (100–1000 μs). We also investigated the consistency of η and how it is influenced by surfactant content. Therefore, η was determined on the basis of several independently prepared CA@AuNP calibration samples containing various quantities of TX-114 and EtOH ranging from 0.5% (v/v) to

1.0% (v/v) (TX-114 10% (w/w)) and 5% (v/v) to 10% (v/v) (EtOH), respectively.

2.7. Determining the SDL of iCPE-sp-ICP-MS

As explained above, the SDL of sp-ICP-MS is highly dependent on the constant background signal overlapping with the transient particle signals. In order to determine the SDL, we mixed UPW with increasing amounts of dissolved Ag(I) (0, 10, 50, 100, 500 ng L^{-1}), carried out sp-ICP-MS measurements with and without iCPE prior to measurement and compared the received single particle mass spectra. The Ag(I) concentrations were chosen so as to represent environmentally-relevant levels (~0–100 ng L^{-1}) [11,12] and a concentration exceeding environmental scenarios (500 ng L^{-1}).

2.8. Error calculations

Three independent aliquots were treated and measured individually in all of the measurements conducted. Each sample was measured using three replicates (U, n = 3). The uncertainty U was calculated via Gaussian error propagation in consideration of pipetting uncertainties and standard deviations of the independently measured aliquots. Blank samples were used to correct Ag concentrations in all incubation experiments.

3. Results and discussion

3.1. Crystal structure of $C_{10}H_{14}Ag_2N_2O_8$

During iCPE, the dissolved Ag(I) species were complexed both by EDTA and PA. The crystal structure of Ag(I)-PA complexes is well known in the literature [34] and is described as eight Ag(I)-PA monomers connected with a nearly linear AgS_2-coordination. Two intertwined polymeric strands in a double helix assembly are formed as a result [34]. As,- to the best of the authors' knowledge- no structure for Ag(I)-EDTA complexes has yet been published, we investigated the corresponding crystal structure. This is especially interesting because complexation of the d^{10} metal species Ag(I) in the octaedric coordination sphere of EDTA may be challenging. The preparation of the crystallized Ag-EDTA complex is presented in the Appendix. The elemental analysis revealed a sum formula of $C_{10}H_{14}Ag_2N_2O_8$, indicating that the Ag(I)-EDTA complex comprises two Ag(I) ions for each EDTA molecule. The Ag(I)-EDTA complex crystallizes in spacegroup C2/c from UPW. The Ag(I) ions are coordinated by three oxygen atoms of adjacent carboxylate groups in a distorted trigonal fashion (Ag1–O1 2.178(2) Å, Ag1–O4 2.220(2) Å, Ag1–O4' 2.506(2) Å). Two silver ions form handles which are held together by argentophilic interactions [35] at an Ag–Ag distance of 3.2005(6) Å, which is well below the sum of their van der Waals radii (3.44 Å). Both amine groups of the EDTA ligand are protonated, so they do not participate in metal coordination. The *N*-bound protons form intramolecular H-bonds to the non-coordinating oxygen atoms of the spatially closest carboxyl group. These properties result in an overall three dimensional polymeric structure, as shown in Fig. A.1.

3.2. Reducing the co-extraction rates of Ag(I) by means of iCPE

The previously developed CPE approach indeed exhibits good species selectivity for Ag-b-NPs [30,32]. However, coupling CPE to ICP-MS, and especially sp-ICP-MS places even greater demands on species selectivity. We developed iCPE to reduce the co-extraction of dissolved Ag(I) species into the organic extract to an absolute minimum by applying a mixture of EDTA and PA during the iCPE process. To investigate the optimum amount and ratio of both ligands, co-extraction for solutions initially containing 500 and 1000 ng L^{-1} Ag(I), respectively, underwent iCPE using a varying amount of EDTA and PA (see section 2.5.1). The Ag(I) concentrations were chosen to represent the upper limit of environmentally-relevant Ag traces [11,12]. If co-extraction is minimized for such relatively high values, then the approach is even more suitable for environmentally-relevant Ag traces in the low ng L^{-1} range.

The Ag signal measured in an iCPE extract (intensity I_{iCPE}) was related to the (higher) signal intensity measured for the same initial sample, which, however, underwent a CPE approach without added ligands (hereinafter referred to as CPE^0; intensity I_{CPE^0}). The latter represents the worst case of maximized co-extraction. Fig. 1 shows the remaining Ag signal (in percent), which equals to $\frac{I_{iCPE}}{I_{CPE^0}} \cdot 100\%$. Increasing the amount of EDTA added during iCPE from 2 to 3 mL led to a reduction of the co-extraction. A further increase to 4 mL no longer affected the co-extraction rates (data not shown). Therefore, it appears that co-extraction can be minimized only to a certain extent by applying solely EDTA during iCPE. It is very likely that the Ag(I)-EDTA system is running into a state of equilibrium at this stage. However, it was surprisingly found that 500 and 1000 μL of 0.01 M PA in addition to 3 mL of EDTA caused a further significant reduction of co-extraction. Using 2000 μL of PA did not further reduce the co-extraction, possibly again due to an equilibrium situation due to the PA-Ag(I) system or a partition equilibrium of the Ag(I) complexes between the aqueous and organic phases. In sum, using a combination of 3 mL of saturated EDTA solution and 1 mL of 0.01 M PA solution in iCPE is optimal for further reducing the co-extraction, namely to only 1.6% (3.1%) for aqueous samples initially containing 500 ng L^{-1} (1000 ng L^{-1}) of dissolved Ag(I). Combining EDTA and PA during iCPE is a powerful tool to significantly reduce the co-extraction of dissolved Ag(I) species. However, we do not recommend completely replacing EDTA with PA since PA is much more expensive than EDTA. Furthermore, EDTA readily complexes dissolved species of alkaline earth metals which are usually present in natural water samples, and, therefore, serves as kind of a wideband complexing agent.

3.3. The influence of incubation time during iCPE on Ag-b-NP EE and Ag(I) co-extraction rates

Similar to the already established CPE approach [32], 30 min incubation time is the optimum for iCPE. For more details, please see the Appendix.

3.4. The influence of iCPE on the Ag-b-NPs being extracted

Particles to be extracted were not affected by iCPE. For more details, please see the Appendix.

3.5. The influence of particle size on the EE of Ag-b-NPs during iCPE

We also investigated whether the EE depends on the size of the Ag-b-NPs (see section 2.5.2). This outcome is crucial with regard to NP-based calibration approaches. If the EE was size-dependent, then the calibration particles should have the same size as the sample particles. However, the particle size of sample particles is the object of the analysis itself and, thus, unknown. Fig. A.2 summarizes the EEs for CA@AgNPs during iCPE at increasing CA@AgNP concentrations (A: 5, B: 50, C: 300 ng L^{-1} nanoparticulate Ag) as a function of the particle size. Overall, particles at sizes from 10 nm to 100 nm were equally well extracted – i.e., within a range from approximately 80–110% EE. Lowest EE of approximately 80% could be observed for 40 nm NPs at 50 ng L^{-1}, 60 nm NPs at 300 ng L^{-1} and 100 nm NPs at all investigated concentrations. As to the 100 nm

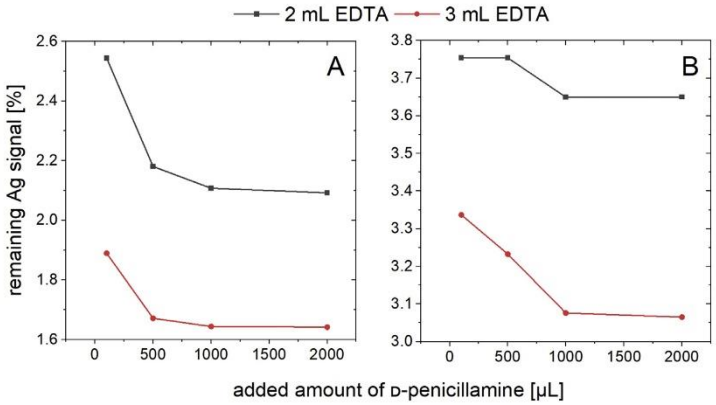

Fig. 1. Reduction of the Ag signal measured for iCPE extracts of samples initially containing 500 (A) and 1000 (B) ng L^{-1} Ag(I) with increasing amounts of EDTA and PA added during iCPE. The calculations are related to CPE^0.

NPs, we thus assume that EE is reduced due to an increasing particle size which inhibits proper arrangement of the NPs in the iCPE-induced micelles. This, however, differs from the observations made for 40 nm and 60 nm NPs. Lower EE values were only observable for some of the investigated concentrations, which is probably caused by inconsistencies in the experimentation. In particular, samples initially containing 5 ng L^{-1} (50 ng L^{-1}, resp. 300 ng L^{-1}) CA@AgNPs resulted in an EE ranging from approximately 91–112% (81–109%, resp. 77–109%). Consequently, particles which are by definition nanoparticles [36] (i.e., exhibiting diameters from 1 to 100 nm), are almost quantitatively extracted. In this context, it should be noted that CPE is feasible for the purpose of nanoparticle enrichment regardless of their chemical composition and coating [30]. Therefore, the aforementioned high EE can be applied to a wide variety of Ag-b-NP compositions and coatings. In contrast to the foregoing, significantly lower EE levels were obtained for particle sizes of 200 nm, in particular 33% (5 ng L^{-1}), 39% (50 ng L^{-1}), and 24% (300 ng L^{-1}). The decrease in EE for particles of >100 nm particle size corresponds to earlier observations made by our working group [31] and continues the trend started for 100 nm particles as noted above. This may possibly occur due to improper NP inclusion in the micelles and limitations of the partition equilibrium between the two phases. However, this decrease in EE for particles exceeding 100 nm is acceptable since, according to the IUPAC, particles > 100 nm are not considered to be nanoparticles given that their properties no longer differ from the corresponding bulk material to any significant degree [36]. However, it should be noted that currently there is no consensus on this boundary between nano and non-nano. Nevertheless, the proposed iCPE approach is able to reproducibly and quantitatively extract Ag-b-NPs of a certain range of particle size, whereas the extraction gives satisfactory results up to a size of 100 nm with EE of 80–110%.

3.6. Comparing CPE to iCPE

Further, we compared the extent of reduced co-extraction of dissolved Ag(I) species in iCPE extracts to CPE extracts. Therefore, aqueous samples containing 100 ng L^{-1} 60 nm CA@AgNPs and increasing amounts of dissolved Ag(I) (1000, 2000, and 4000 ng L^{-1}) were subjected to CPE^0 (i.e., without added ligands), CPE (i.e., 1 mL EDTA) [30–32], and iCPE (i.e., 3 mL EDTA, 1 mL PA). Samples were supplemented by reference samples only containing Ag-b-NPs (i.e. 0 ng L^{-1} Ag(I)) to mimic the case in which no Ag(I) co-extraction into the organic phase occurs. ET-AAS measurements of CPE^0, CPE and iCPE extracts resulted in measured intensities I_{CPE^0}, I_{CPE} and I_{iCPE}, respectively. Further it is to be noted that ET-AAS measurements of CPE and iCPE extracts of the reference samples resulted in comparable signal intensities $I_{reference}$. Fig. 2 depicts the factor of ET-AAS signal increase, which equals to $\frac{I_{CPE^0}}{I_{reference}}$, $\frac{I_{CPE}}{I_{reference}}$ or $\frac{I_{iCPE}}{I_{reference}}$, respectively. The red dotted line represents the case without signal increase, i.e. the optimum case without any co-extraction of Ag(I) species into the extract at all (i.e. signal increase factor of 1.0). The presence of 1000 ng L^{-1} Ag(I) species led to an undesirable increase of the measured signal intensity by factors of 1.05 (iCPE), 1.12 (CPE), and 1.27 (CPE^0). These findings indicate a distinct co-extraction effect of dissolved species into the organic phase. In case 2000 ng L^{-1} dissolved Ag(I) species were added to the aqueous sample prior to extraction, the signal intensity increased by factors of 1.11 (iCPE), 1.35 (CPE), and 1.34 (CPE^0). Very interestingly, iCPE was able to significantly reduce co-extraction even for 2000 or 4000 ng L^{-1} Ag(I), whereas CPE did not show any advantageous effect as compared to CPE^0. Although co-extraction was visible for iCPE, the measured signal was only increased by a factor of 1.50. Since a concentration of 4000 ng L^{-1} Ag(I) is far from any environmentally relevant scenario, the co-extraction measured was not considered to be problematic. In sum, it was shown that only iCPE was capable of reducing the co-extraction of dissolved silver traces for samples containing 1000 and 2000 ng L^{-1} Ag(I) to a marginally remaining value, which is due to an increased amount of chelating agents compared to CPE.

3.7. The applicability of iCPE to real environmental samples

As already shown in section 3.6, iCPE worked well in model systems. However, the next step was applying the method to real environmental systems. River water contains considerable amounts of natural organic matter in either dissolved or dispersed form. Conceivably, dissolved Ag(I) species may adsorb thereto and form potentially poorly hydrophilic species. Therefore, these species may have the tendency to be undesirably co-extracted into the organic iCPE extract. In order to evaluate potential limitations regarding the applicability of iCPE to environmental samples, river

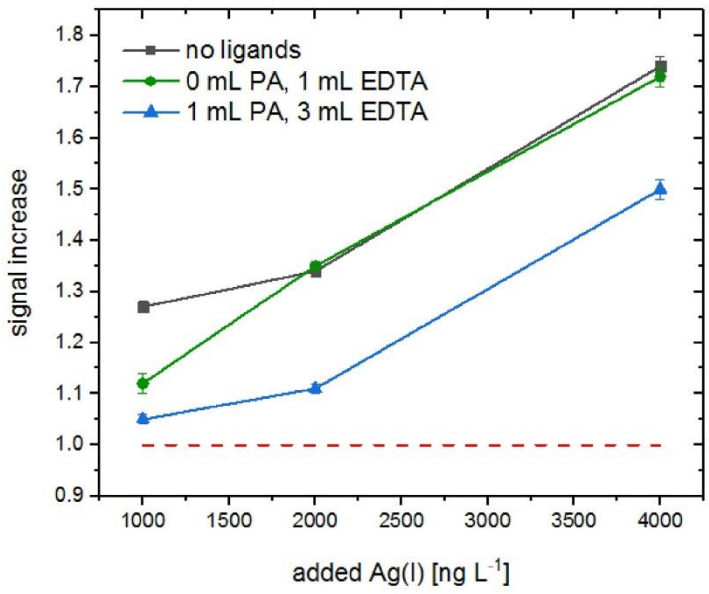

Fig. 2. Factor by which the measured signal intensity increased for samples initially containing 100 ng L^{-1} Ag-b-NPs mixed with 1000, 2000, and 4000 ng L^{-1} dissolved Ag(I) species, related to reference samples only containing 100 ng L^{-1} Ag-b-NPs. Ideal case with no signal increase is represented by the red dotted line. Prior to the measurements, the samples underwent iCPE (▲), CPE (●) and CPE^0 (■).

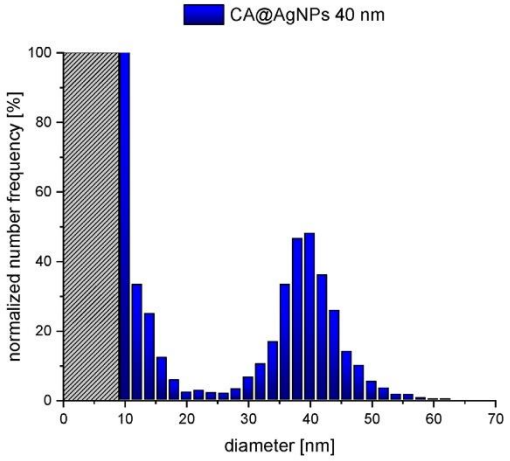

Fig. 3. Particle size distribution of Ag-b-NPs with a medium diameter of 40 nm measured at a dwell time of 100 μs. The grey dashed bar in the particle size distribution indicates the SDL, i.e., the cutoff at which NPs can no longer be identified as NPs. For reasons of comparison, we chose an SDL similar to that applied for measurements with a dwell time of 500 μs.

water (TOC 2.5 mg L^{-1}; initial β_{Ag} < 0.15 ng L^{-1}) was spiked with 5, 10, and 50 ng L^{-1} dissolved Ag(I) species, and the co-extraction during iCPE was examined (see also section 2.5.3).

As presented in Fig. A.3, iCPE significantly reduced the amount of co-extracted Ag(I) species into the organic phase to negligible levels. Whereas a 100% co-extraction would lead to an increase of the blank signal by a factor of 2 (5 ng L^{-1} Ag(I)), 4 (10 ng L^{-1}Ag(I)), and 17 (50 ng L^{-1} Ag(I)), almost no signal increase was observed for samples that underwent iCPE. Only co-extraction rates as low as 3% (5, 10 ng L^{-1} Ag(I)) or 5% (50 ng L^{-1} Ag(I)) were calculated.

Comparable experiments using river water spiked with 60 nm CA@Ag-NPs resulted in EEs of 97% (5 ng L^{-1} CA@Ag-NP), 96% (10 ng L^{-1} CA@Ag-NP) and 98% (50 ng L^{-1} CA@Ag-NP). Thus, iCPE is perfectly suited for selectively separating dissolved Ag(I) species from their nanoparticulate counterparts in real environmental matrices, whereas Ag-b-NPs were extracted with a high EE.

3.8. iCPE-sp-ICP-MS

3.8.1. η consistency and the influence of surfactant content

We further intended to measure iCPE extracts with sp-ICP-MS. Even though the extracts were diluted as described above, they were highly viscous. Therefore, sample introduction and measurement using a conventional ICP-MS system might be challenging. In sp-ICP-MS, especially η is crucial for data evaluation and is supposed to be strongly influenced by the sample's viscosity. However, our results showed a good consistency for η over several measurements. Neither the dwell time nor the size of the particles used for the determination of η showed an influence on η itself (see Table A.3). The samples containing surfactant resulted in a higher η of ~0.08 than those prepared in UPW with a η of ~0.06.

3.8.2. Influences on particle size distribution: sample matrix

The overall particle number concentration in the measured sample (sp-ICP-MS) showed no influence on particle size distribution (Fig. A.4 A). This presumes a number of particles being not so

low as to give enough particle signals for being sufficiently informative (< 2000 particles mL^{-1}) or so high that particle signal coincidence occurred, which broadens the particle size distribution (> 1.600.000 particles mL^{-1}) (see Fig. A.4).

The particle size distribution was slightly shifted to higher diameters for samples prepared in a surfactant matrix instead of UPW (see Fig. A.5). This shift increased with the size of the particles. While no shift was observable for small particles (see Fig. A.6 A), one was apparent for larger particles (see Fig. A.6 B). However, this discrepancy between smaller and larger particles might be a consequence of reaching the SDL for the smaller particles, thus veiling this shift to some extent. A comparison with TEM measurement shows that the particle size distribution obtained from sp-ICP-MS measurement in surfactant matrix matched that obtained from TEM measurement (see Fig. A.7). This observation indicates that the nebulization efficiency calculated in an UPW matrix is somewhat underestimated.

3.8.3. Influences on particle size distribution: dwell time

Commercially available instruments allow for dwell times in the microsecond to millisecond range [18]. In particular, high dwell times may result in unwanted situations, e.g., particle coincidence (two or more particles recorded within one single dwell time, thus resulting in one bigger NP instead of two or more smaller NPs) [18]. To overcome this limitation, modern instruments use very short dwell times (in the µs range). However, we report that it is not recommended to use the lowest dwell time allowed by the instrument and respective vendor software, but rather to consider each measurement and the specific requirements thereof. We sought to elucidate the correct choice of appropriate dwell times adjusted to a certain measurement situation.

Once a nanoparticle is atomized and ionized in the plasma, an ion cloud is generated exhibiting an average duration in the order of a few hundreds of microseconds [18]. Using dwell times shorter than this ion cloud event results in the observation of the particle event as transient signal comprising several data points. It is noted that on the one hand, it is theoretically favorable to use dwell times as short as possible to improve the resolution of the investigated transient signal [37–39]. On the other hand, however, we observed for dwell times as short as 100 µs that current data evaluation approaches struggle with the differentiation between noise and actual particle signal. (Just for the sake of completeness, it is noted that samples have not been spiked with ionic species in these experiments.) In particular, we found that a "virtual" fragmentation occurs for a dwell time of 100 µs. First and last portions of a certain transient signal are difficult to be sufficiently recognized as signal boundaries and, thus, ascribed to the whole transient signal (see Fig. A.8). Consequently, the nanoparticle size is underestimated and respective first and last signal portions are considered as separate, small particles. This resulted in a false particle size distribution and, consequently, a too small medium particle diameter. As can be seen in Fig. 3, a large quantity of very small particles occurred for CA@Ag-NPs, which should measure about 40 nm in diameter. Such small particles could not be found in the particle size distribution obtained from the TEM measurement. This indicates that these signals derived from heavy particle fragmentation, a potential result of incorrect data processing by the data evaluation approach. The grey dashed bar in Fig. 3 indicates the diameter, whereas below particles were identified as a background signal in the sp-ICP-MS measurement. Thus, these signals could thus no longer be identified as particles (SDL). Particle fragmentation even occurred at dwell times of 500 µs and 800 µs (Fig. A.9 A). However, if the particle number frequency is converted into mass distribution, the high number of small particles only negligibly contributed to the distribution (Fig. A.9 B). Further examples are shown in Fig. A.10. Therefore, no generally applicable dwell time can be defined for samples having unknown particle diameters, i.e., natural samples. It is necessary to measure these samples with various dwell times and to then choose the most suitable dwell time on the basis of a comparison of the particle size distributions obtained. If a broad particle size distribution is obtained, it may even be possible to consider various dwell times and compare the particle size distributions to each other for an ideal characterization of the sample.

Of course, this software issue can be overcome by using proper data evaluation tools and software settings. However, users of sp-ICP-MS should always consider and double-check this issue with their instrument and software – especially for dwell times as short as 100 µs. Given our data evaluation approach, we did not apply such short dwell times since heavy particle fragmentation did occur.

3.9. Determining the SDL of iCPE-sp-ICP-MS

It is well known that Ag-b-NPs in the aquatic environment usually size 20 nm or less [20]. Current state of the art sp-ICP-MS approaches are not applicable to such samples as they only reach a size detection limit (SDL) above 20 nm, mainly due to coexisting dissolved Ag(I) causing high background signals [19]. Thus, it is crucial to lower the SDL accordingly. We used iCPE prior to analysis in order to quantitatively separate the dissolved Ag(I) fraction from Ag-b-NPs. As a result, the background signal was significantly reduced and the SDL massively improved. The SDL was then only affected by instrument noise, and not by the interferences caused by dissolved Ag(I) species.

According to literature, SDL can be calculated as follows [19,40] (see the Appendix for more information on the development of the following equation), with the median of all the signal intensities throughout an entire measurement I_{median} [cps], the dwell time t_d [µs], the pump rate ν [ml min^{-1}] of the nebulizer, the nebulizing efficiency η, the ratio of molar masses of the whole nanoparticle and the analyte element $\frac{M_{NP}}{M_e}$ (which is 1 for AgNPs), and the elemental sensitivity ES_{ion} [cps/(µg/L)] and the density ρ [g cm^{-3}] of the material the NPs are composed of:

$$SDL = \sqrt[3]{\frac{18}{\pi \cdot \rho} \cdot \frac{I_{median} \cdot t_d \cdot \nu \cdot \eta}{ES_{ion}} \cdot \frac{M_{NP}}{M_e}}$$

Fig. 4 A-E depicts mass spectra acquired by sp-ICP-MS (t_d=100 µs) of aqueous samples with initial amounts of dissolved Ag(I) with and without iCPE prior to the measurement. It clearly shows that the background signal was massively increased at an increasing Ag(I) content. However, this increase can be significantly reduced after performing iCPE prior to sp-ICP-MS.

Using iCPE, the corresponding SDL was in a range from 4.8 nm to 5.2 nm for samples initially containing 0–100 ng L^{-1} Ag(I) (Fig. 4 F). Increasing this concentration up to 500 ng L^{-1} resulted in an SDL of 8.0 nm. Although it is obvious that slight traces of Ag(I) were co-extracted by iCPE, the SDL remained at very low values. In contrast, measurements without iCPE prior sp-ICP-MS showed SDL values of up to 23.1 nm. Since I_{median} is directly proportional to the Ag(I) concentration and further, $SDL \sim \sqrt[3]{I_{median}}$ is derived from the equation given above, SDL should be a cubic root function of the Ag(I) concentration. This is perfectly displayed in the measurement itself (Fig. 4 F, Fig. A.11 F).

Obviously, initial Ag(I) concentrations in the aqueous samples influence the amount of co-extracted Ag(I) and, thus, SDL. Therefore, it is not possible to present a universally valid SDL. However, in the case of environmentally relevant dissolved Ag(I) concentrations (typically up to 100 ng L^{-1}) [11,12] coexisting in the aqueous

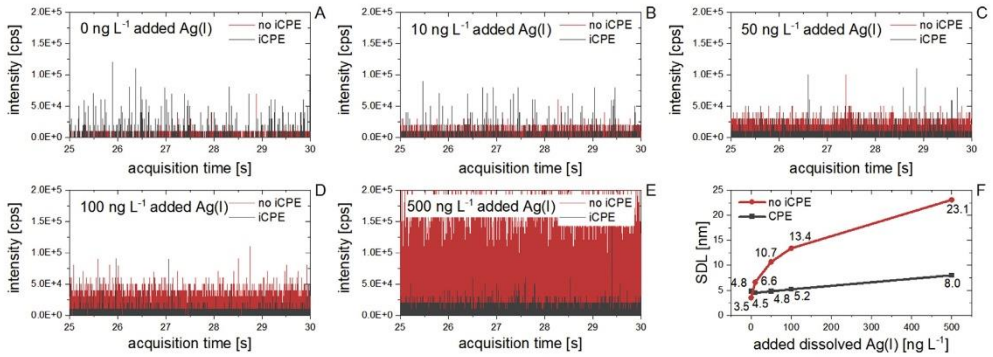

Fig. 4. Mass spectra obtained by sp-ICP-MS (t_d = 100 µs) in presence of increasing amounts of dissolved Ag(I) with and without iCPE prior to measurement (A–E). SDL as a function of Ag(I) added to samples (F).

sample, a SDL ranging from 4.8 to 5.2 nm can be assumed.

The measurements were repeated with t_d = 500 µs. According to above given equation, SDL should be increased by a factor of $\sqrt[3]{500/100} \approx 1.7$ compared to experiments with t_d = 100 µs. As shown in Fig. A.11, this factor was fairly accurately depicted in the experiments. In the case of initial Ag(I) concentrations of 0–100 ng L^{-1}, the SDL was determined as 5.9–23.5 nm without iCPE and 4.8–8.5 nm with iCPE prior to sp-ICP-MS measurement. For 500 ng L^{-1} Ag(I), SDL was increased to 39.6 nm (without iCPE) and 13.8 nm (with iCPE), respectively. It should be noted that the aforementioned advantages of higher dwell times should be assessed in consideration of slightly higher SDLs. Nonetheless, an SDL of 8.5 nm for t_d = 500 µs is still sufficient for environmental analysis when assuming a maximum dissolved Ag(I) concentration of 100 ng L^{-1}, which is typical for environmental samples [11,12].

Of course, the exact concentrations of coexisting dissolved Ag(I) species in the sample are not accessible prior to analysis. Therefore, a more conservative but more reliable SDL of approximately 5.2 nm (t_d=100 µs) and 8.5 nm (t_d=500 µs) has to be assumed instead of the lowest SDL values representing the ideal case with no coexisting Ag(I).

Owing to the influence on SDL by the concentration of coexisting Ag(I), it is simply not possible to present a universally valid SDL value.

3.10. Determination of the concentration of nanoparticulate Ag using all investigated measurement approaches

After optimizing the iCPE and successfully transferring this technique to ICP-MS and sp-ICP-MS, the final step was the quantification of unknown samples by means of (sp)-ICP-MS and relating these values to the previously established approach based on ET-AAS as reference [30–32]. The calibration differed significantly among the approaches and was performed as presented above in section 2.6.

Determined concentrations of nanoparticulate Ag were in good agreement with one another, independent of the utilized approach (see Table 1). Deviations from the reference values determined by ET-AAS were randomly distributed. According to the mean recovery rates, all approaches were excellently suitable for reproducing the reference results. As for the ICP-MS measurements, it should be noted that the calibration using dissolved Ag(I) species was much less time-consuming and therefore preferable over calibration using CA@AgNPs. Moreover, it is favourable that the analyte homogeneity was much higher for dissolved Ag(I) species, and Ag(I) species can be handled and diluted much more easily than CA@AgNPs (for instance, no sonication step for Ag(I)).

The excellent consistency among all of the three above methods was surprising but very pleasing given that the methods are based on entirely different physical and mathematical principles: ET-AAS

Table 1
Compilation of measured concentrations (incl. corresponding standard deviations) of nanoparticulate Ag in aqueous samples initially containing approximately 25 ng L^{-1} 40/60 nm CA@Ag-NPs using iCPE followed by quantification via ET-AAS, ICP-MS and sp-ICP-MS. All results are related to the validated ET-AAS approach [30–32]. rr represents the calculated recovery rate based on the concentrations measured by ET-AAS as reference. The calibration was performed using either aqueous dispersions of CA@AgNP of known concentrations or aqueous solutions of dissolved Ag(I) of known concentrations. The dwell time for sp-ICP-MS measurement was set to 500 µs. All measurements were performed in triplicate (n = 3).

Measurement approach	ET-AAS (reference)	ICP-MS		ICP-MS		sp-ICP-MS	
Calibrant	AgNP	Ag(I)		AgNP		AuNP/Ag(I)	
LOD [ng L^{-1}]	0.20[a]	0.15[b]		0.15[c]		0.25[d]	
Diameter [nm]	conc.	conc.	rr [%]	conc.	rr [%]	conc.	rr [%]
40	**25.95 ± 3.63**	24.8 ± 2.01	95	22.96 ± 2.26	88	27.49 ± 1.96	106
40	**26.05 ± 2.31**	23.5 ± 2.34	90	22.93 ± 2.18	88	23.77 ± 2.03	91
60	**24.32 ± 2.47**	25.5 ± 0.63	105	25.5 ± 5.27	105	25.35 ± 1.45	104
60	**22.51 ± 2.00**	24.9 ± 3.54	111	24.92 ± 3.54	111	26.74 ± 1.56	119
Mean recovery rate relative to reference [%]		**100**		**98**		**105**	

[a, b, c] calculated from the calibration curve [32].
[d] completely different calibration approach; approximated LOD is derived from blank measurements (blank-limited LOD).

measures light absorption, whereas in ICP-MS, masses of ions formed in the plasma are detected. Furthermore, sp-ICP-MS does not at first glance measure the concentration but measures the masses of each single particle by mathematically transferring the acquired data in a separate data evaluation step into concentration values based on certain assumptions as presented above. Fortunately, the LODs for all the approaches were very low and were therefore well-suited for the purpose of quantifying Ag-b-NPs in real environmental samples. The LOD for iCPE-sp-ICP-MS was, rather, a blank-limited approximation. iCPE-sp-ICP-MS measurements within the magnitude of the LOD should therefore be supplemented by iCPE-ICP-MS measurements exhibiting a more reliable LOD. However, such supplementary measurements are not particularly disadvantageous since both approaches can be performed subsequently on the same instrument using the same sample within acceptable measurement times.

4. Conclusion

We presented an improved CPE approach applying highly argentophilic complexing agents able to species-selectively extract and enrich Ag-b-NPs from aqueous samples. The method was developed using model systems of dissolved and nanoparticulate Ag species in UPW and was successfully applied to real environmental samples. Species selectivity allows hyphenation of iCPE to ICP-MS and even sp-ICP-MS, the latter being very sensitive to traces of dissolved Ag(I) species causing undesired background signals. Reducing this background by iCPE is a key in sp-ICP-MS in order to achieve a SDL as low as 4.5 nm, instead of the > 20 nm as discussed in the literature [19]. However, a single-digit SDL is essential for environmental samples, because Ag-b-NPs in natural waters usually measure < 20 nm. Finally, we were able to demonstrate perfect accordance between the quantitative results obtained by iCPE-(sp)-ICP-MS and a previously established hyphenation of CPE to ET-AAS. iCPE-(sp)-ICP-MS is a fast, cheap and easy applicable approach to nanoparticle analysis. Once established in a lab, this approach is capable of running hundreds of samples per day and can be performed by lab technicians after moderate training. Therefore, iCPE-(sp)-ICP-MS represents a key technique for the routine environmental monitoring of transport and fate of Ag-b-NPs in the aquatic environment. Application examples are presented in a parallel study of our working group addressing the fate of Ag-b-NPs in seawater by iCPE-(sp)-ICP-MS [41].

Funding source

This research project was financed by the Bavarian State Ministry for the Environment and Consumer Protection (TNT01NaTFuE69458).

CRediT authorship contribution statement

Andreas Wimmer: Conceptualization, Methodology, Validation, Formal analysis, Investigation, Writing - original draft, Writing - review & editing, Visualization. **Alexander Urstoeger:** Methodology, Validation, Formal analysis, Investigation, Writing - original draft, Writing - review & editing, Visualization. **Tobias Hinke:** Investigation. **Margit Aust:** Investigation. **Philipp J. Altmann:** Validation, Formal analysis, Investigation, Writing - original draft, Visualization. **Michael Schuster:** Supervision, Project administration, Funding acquisition.

Declaration of competing interest

The authors declare that they have no known competing financial interests or personal relationships that could have appeared to influence the work reported in this paper.

Appendix A. Supplementary data

Supplementary data to this article can be found online at https://doi.org/10.1016/j.aca.2021.01.001.

References

[1] H.F. Krug, Nanosafety research—are we on the right track? Angew. Chem. Int. Ed. 53 (46) (2014) 12304–12319.
[2] P. Krystek, A. Ulrich, C.C. Garcia, S. Manohar, R. Ritsema, Application of plasma spectrometry for the analysis of engineered nanoparticles in suspensions and products, J. Anal. At. Spectrom. 26 (9) (2011) 1701–1721.
[3] R. Kessler, Engineered nanoparticles in consumer products: understanding a new ingredient, Environ. Health Perspect. 119 (3) (2011) A120–A125.
[4] T.M. Benn, P. Westerhoff, Nanoparticle silver released into water from commercially available sock fabrics, Environ. Sci. Technol. 42 (11) (2008) 4133–4139.
[5] L. Geranio, M. Heuberger, B. Nowack, The behavior of silver nanotextiles during washing, Environ. Sci. Technol. 43 (21) (2009) 8113–8118.
[6] D.M. Mitrano, P. Limpiteeprakan, S. Babel, B. Nowack, Durability of nano-enhanced textiles through the life cycle: releases from landfilling after washing, Environ. Sci.: Nano 3 (2) (2016) 375–387.
[7] D.M. Mitrano, E. Rimmele, A. Wichser, R. Erni, M. Height, B. Nowack, Presence of nanoparticles in wash water from conventional silver and nano-silver textiles, ACS Nano 8 (7) (2014) 7208–7219.
[8] D. Jiang, L. Chen, J. Xie, M. Chen, Ag2S/g-C3N4 composite photocatalysts for efficient Pt-free hydrogen production. The co-catalyst function of Ag/Ag2S formed by simultaneous photodeposition, Dalton Trans. 43 (12) (2014) 4878–4885.
[9] A.P. Richter, J.S. Brown, B. Bharti, A. Wang, S. Gangwal, K. Houck, E.A. Cohen Hubal, V.N. Paunov, S.D. Stoyanov, O.D. Velev, An environmentally benign antimicrobial nanoparticle based on a silver-infused lignin core, Nat. Nanotechnol. 10 (2015) 817.
[10] L. Li, G. Hartmann, M. Döblinger, M. Schuster, Quantification of nanoscale silver particles removal and release from municipal wastewater treatment plants in Germany, Environ. Sci. Technol. 47 (13) (2013) 7317–7323.
[11] L. Li, M. Stoiber, A. Wimmer, Z. Xu, C. Lindenblatt, B. Helmreich, M. Schuster, To what extent can full-scale wastewater treatment plant effluent influence the occurrence of silver-based nanoparticles in surface waters? Environ. Sci. Technol. 50 (12) (2016) 6327–6333.
[12] T.Y. Sun, N.A. Bornhöft, K. Hungerbühler, B. Nowack, Dynamic probabilistic modeling of environmental emissions of engineered nanomaterials, Environ. Sci. Technol. 50 (9) (2016) 4701–4711.
[13] M. Troester, H.-J. Brauch, T. Hofmann, Vulnerability of drinking water supplies to engineered nanoparticles, Water Res. 96 (2016) 255–279.
[14] A. Wimmer, A. Kalinnik, M. Schuster, New insights into the formation of silver-based nanoparticles under natural and semi-natural conditions, Water Res. 141 (2018) 227–234.
[15] C. Levard, E.M. Hotze, G.V. Lowry, G.E. Brown, Environmental transformations of silver nanoparticles: impact on stability and toxicity, Environ. Sci. Technol. 46 (13) (2012) 6900–6914.
[16] Y.-M. Cho, Y. Mizuta, J.-i. Akagi, T. Toyoda, M. Sone, K. Ogawa, Size-dependent acute toxicity of silver nanoparticles in mice, J. Toxicol. Pathol. 31 (1) (2018) 73–80.
[17] R.J.B. Peters, Z.H. Rivera, G. van Bemmel, H.J.P. Marvin, S. Weigel, H. Bouwmeester, Development and validation of single particle ICP-MS for sizing and quantitative determination of nano-silver in chicken meat, Anal. Bioanal. Chem. 406 (16) (2014) 3875–3885.
[18] D. Mozhayeva, C. Engelhard, A critical review of single particle inductively coupled plasma mass spectrometry – a step towards an ideal method for nanomaterial characterization, J. Anal. At. Spectrom. 35 (2020) 1740–1783.
[19] S. Lee, X. Bi, R.B. Reed, J.F. Ranville, P. Herckes, P. Westerhoff, Nanoparticle size detection limits by single particle ICP-MS for 40 elements, Environ. Sci. Technol. 48 (17) (2014) 10291–10300.
[20] B. Kim, C.-S. Park, M. Murayama, M.F. Hochella, Discovery and characterization of silver sulfide nanoparticles in final sewage sludge products, Environ. Sci. Technol. 44 (19) (2010) 7509–7514.
[21] C. Degueldre, P.Y. Favarger, Colloid analysis by single particle inductively coupled plasma-mass spectroscopy: a feasibility study, Colloid. Surface. Physicochem. Eng. Aspect. 217 (1–3) (2003) 137–142.
[22] F. Laborda, E. Bolea, G. Cepriá, M.T. Gómez, M.S. Jiménez, J. Pérez-Arantegui, J.R. Castillo, Detection, characterization and quantification of inorganic engineered nanomaterials: a review of techniques and methodological approaches for the analysis of complex samples, Anal. Chim. Acta 904 (2016) 10–32.
[23] M.D. Montano, H.R. Badiei, S. Bazargan, J.F. Ranville, Improvements in the detection and characterization of engineered nanoparticles using spICP-MS with microsecond dwell times, Environ. Sci.: Nano 1 (4) (2014) 338–346.
[24] R. Vogt, D. Mozhayeva, B. Steinhoff, A. Schardt, B.T.F. Spelz, A. Philippe,

S. Kurtz, G.E. Schaumann, C. Engelhard, H. Schönherr, D.K. Lamatsch, J. Wanzenböck, Spatiotemporal distribution of silver and silver-containing nanoparticles in a prealpine lake in relation to the discharge from a wastewater treatment plant, Sci. Total Environ. 696 (2019) 134034.
[25] D. Mozhayeva, C. Engelhard, A quantitative nanoparticle extraction method for microsecond time resolved single-particle ICP-MS data in the presence of a high background, J. Anal. At. Spectrom. 34 (8) (2019) 1571–1580.
[26] L. Torrent, F. Laborda, E. Marguí, M. Hidalgo, M. Iglesias, Combination of cloud point extraction with single particle inductively coupled plasma mass spectrometry to characterize silver nanoparticles in soil leachates, Anal. Bioanal. Chem. 411 (20) (2019) 5317–5329.
[27] H. Watanabe, H. Tanaka, A non-ionic surfactant as a new solvent for liquid—liquid extraction of zinc(II) with 1-(2-pyridylazo)-2-naphthol, Talanta 25 (10) (1978) 585–589.
[28] J.-f. Liu, R. Liu, Y.-g. Yin, G.-b. Jiang, Triton X-114 based cloud point extraction: a thermoreversible approach for separation/concentration and dispersion of nanomaterials in the aqueous phase, Chem. Commun. (12) (2009) 1514–1516.
[29] L. Duester, A.-L. Fabricius, S. Jakobtorweihen, A. Philippe, F. Weigl, A. Wimmer, M. Schuster, M.F. Nazar, Can cloud point-based enrichment, preservation, and detection methods help to bridge gaps in aquatic nanometrology? Anal. Bioanal. Chem. 408 (27) (2016) 7551–7557.
[30] G. Hartmann, T. Baumgartner, M. Schuster, Influence of particle coating and matrix constituents on the cloud point extraction efficiency of silver nanoparticles (Ag-NPs) and application for monitoring the formation of Ag-NPs from Ag+, Anal. Chem. 86 (1) (2014) 790–796.
[31] G. Hartmann, M. Schuster, Species selective preconcentration and quantification of gold nanoparticles using cloud point extraction and electrothermal atomic absorption spectrometry, Anal. Chim. Acta 761 (2013) 27–33.
[32] G. Hartmann, C. Hutterer, M. Schuster, Ultra-trace determination of silver nanoparticles in water samples using cloud point extraction and ETAAS, J. Anal. At. Spectrom. 28 (4) (2013) 567–572.
[33] M.D. Montano, J.W. Olesik, A.G. Barber, K. Challis, J.F. Ranville, Single Particle ICP-MS: advances toward routine analysis of nanomaterials, Anal. Bioanal. Chem. 408 (19) (2016) 5053–5074.
[34] B.O. Leung, F. Jalilehvand, V. Mah, M. Parvez, Q. Wu, Silver(I) complex formation with cysteine, penicillamine, and glutathione, Inorg. Chem. 52 (8) (2013) 4593–4602.
[35] H. Schmidbaur, A. Schier, Argentophilic interactions, Angew. Chem. Int. Ed. 54 (3) (2015) 746–784.
[36] J.H. Duffus, M. Nordberg, D.M. Templeton, Glossary of Terms Used in Toxicology, 2nd Edition (IUPAC Recommendations 2007), vol. 79, 2007, p. 1153, 7.
[37] R. Aznar, F. Barahona, O. Geiss, J. Ponti, T. José Luis, J. Barrero-Moreno, Quantification and size characterisation of silver nanoparticles in environmental aqueous samples and consumer products by single particle-ICPMS, Talanta 175 (2017) 200–208.
[38] D. Mozhayeva, I. Strenge, C. Engelhard, Implementation of online preconcentration and microsecond time resolution to capillary electrophoresis single particle inductively coupled plasma mass spectrometry (CE-SP-ICP-MS) and its application in silver nanoparticle analysis, Anal. Chem. 89 (13) (2017) 7152–7159.
[39] I. Strenge, C. Engelhard, Single particle inductively coupled plasma mass spectrometry: investigating nonlinear response observed in pulse counting mode and extending the linear dynamic range by compensating for dead time related count losses on a microsecond timescale, J. Anal. At. Spectrom. 35 (1) (2020) 84–99.
[40] H.E. Pace, N.J. Rogers, C. Jarolimek, V.A. Coleman, E.P. Gray, C.P. Higgins, J.F. Ranville, Single particle inductively coupled plasma-mass spectrometry: a performance evaluation and method comparison in the determination of nanoparticle size, Environ. Sci. Technol. 46 (22) (2012) 12272–12280.
[41] A. Wimmer, A. Urstoeger, N.C. Funck, F.P. Adler, L. Lenz, M. Doeblinger, M. Schuster, What happens to silver-based nanoparticles if they meet seawater? Water Res. 171 (2020) 115399.

Appendix A

Separating Dissolved Silver from Nanoparticulate Silver is the Key: Improved Cloud-Point-Extraction Hyphenated to Single Particle ICP-MS for Comprehensive Analysis of Silver-Based Nanoparticles in Real Environmental Samples Down to Single-Digit nm Particle Sizes

Andreas Wimmer [1,#], Alexander Urstoeger [1,#], Tobias Hinke [1], Margit Aust [1], Philipp J. Altmann[2], Michael Schuster [1,*]

[1] Division of Analytical Chemistry, Department of Chemistry, Technical University of Munich, Garching 85748, Germany
[2] Catalysis Research Center, Technical University of Munich, Garching, 85748, Germany
[#] These Authors contributed equally to the present study.

22 pages
11 figures
5 tables

Author contribution:

M.S. supervised the study. A.W. designed the study and its experimental set-up. A.W. carried out the iCPE development assisted by T.H. and M.A.. A.W. synthesized the Ag(I)-EDTA complex assisted by T.H.. P.A. carried out the X-ray diffractometry and evaluated the crystal structure. A.U. and A.W. carried out the CPE-sp-ICP-MS hyphenation. A.W. determined the SDL of sp-ICP-MS and carried out comparative measurements of all investigated measurement approaches. The manuscript was written through the contributions of all authors. All authors have given approval to the final version of the manuscript.

Detailed information on the materials used in this study:

The dissolved Ag(I) ICP-standard ($AgNO_3$ in 3% HNO_3, β_{Ag} = 1000 mg L^{-1}) and dissolved In(III) ICP-standard ($In(NO_3)_3$ in 2-3% HNO_3, β_{In} = 1000 mg L^{-1}) used as an internal standard were obtained from Merck (Darmstadt, Germany). $AgNO_3$ was obtained from Merck. Dispersions of citrate-stabilized silver nanoparticles (CA@AgNPs) sizing 10, 20, 40, 60, 80, 100 and 200 nm (mass concentration β_{Ag} ~ 20 mg L^{-1}) were purchased from Sigma-Aldrich (St. Louis, MO, USA). Gold nanoparticle (CA@AuNP) dispersions (reference material RM 8012, 8013, 28 nm, 58 nm, β_{Au} ~ 50 mg L^{-1}, citrate stabilized) and silver nanoparticle (PVP@AgNP) dispersions (reference material RM 8017, 75 nm, pressed powder) were supplied by the National Institute of Science and Technology (NIST) (Gaithersburg, MD, USA). iCPE reagents, e.g., acetic acid (glacial), ethanol (Emsure®), ethylenediaminetetraacetate disodium salt dihydrate ($Na_2EDTA{\cdot}2H_2O$; $C_{10}H_{14}N_2Na_2O_8{\cdot}2H_2O$), sodium acetate anhydrous ($C_2H_3NaO_2$), and nitric acid (HNO_3, 65%, suprapure) were purchased from Merck. Triton X-114 ($(C_2H_4O)_nC_{14}H_{22}O$, n = 7 or 8) was obtained from AppliChem (Darmstadt, Germany). D-Penicillamine (PA, $C_5H_{11}NO_2S$) was purchased from Sigma Aldrich. Potassium hydrogen phthalate used as a calibrant for TOC measurements was obtained from Naclai Tesque Inc. (Kyoto, Japan). All chemicals were of at least analytical grade and were checked for contamination via ICP-mass spectrometry (ICP-MS) analysis prior to use. Ultrapure water (UPW, resistivity of 18.2 MΩ cm^{-1}) was obtained using a Milli-Q-Gradient-System (Millipore GmbH, Schwalbach, Germany). All solutions and dilutions were prepared in UPW unless otherwise indicated.

CA@Ag-NP dispersions were freed from impurities of dissolved Ag by dialysis (3.5 kDa regenerated cellulose membrane by ZelluTrans, Carl Roth, Karlsruhe, Germany) prior to use. Aliquots of the purified NP dispersions were dissolved in 3.25% (v/v) HNO_3 to ensure sample homogeneity and subjected to Ag quantification by ICP-MS. Before usage and each dilution step, CA@AgNP dispersions were ultrasonicated for 1 min in an ultrasonic bath (Ulsonix Proclean 3.0DSP; Ulsonix, Berlin, Germany) to prevent particle aggregation.

All glass vessels were rinsed three times with 6.5% HNO_3 (w/w), steamed with HNO_3 vapor for at least 4 h, rinsed three times with UPW, and then stored in a particle-free environment until use.

Table A.1. Compilation of instrumental details of the sp-ICP-MS measurements.

acquisition time	60 s
dwell time	100 - 1000 µs
analyte mass	^{107}Ag
RF power	1550 W
RF matching	1.80 V
sample depth	8.0 mm
nebulizer gas	1.05 L min^{-1}
S/C temperature	2 °C

Preparation of crystalline Ag(I)-EDTA

To prepare crystalline Ag(I)-EDTA, we mixed 2 mL of an aqueous Na_2EDTA ($C_{10}H_{14}N_2Na_2O_8$) solution (8 g $Na_2EDTA{\cdot}2H_2O$ in 100 mL UPW) dropwise with 3 mL of an aqueous $AgNO_3$ solution (15 g $AgNO_3$ in 100 mL UPW) at room temperature within a time period of 1 h. After stirring for another 1 h at room temperature, a colorless, flaked solid was formed. After separation from the reaction mixture by filtration, the solid was washed carefully with EtOH and dried in the vacuum. The colorless crystalline solid was forwarded to CHN analysis supplemented by Ag and Na elemental analysis and X-ray crystallographic analysis. A clear colorless plate-like specimen of the Ag(I)-EDTA complex, approximate dimensions 0.047 mm x 0.070 mm x 0.116 mm, was used for the X-ray crystallographic analysis.

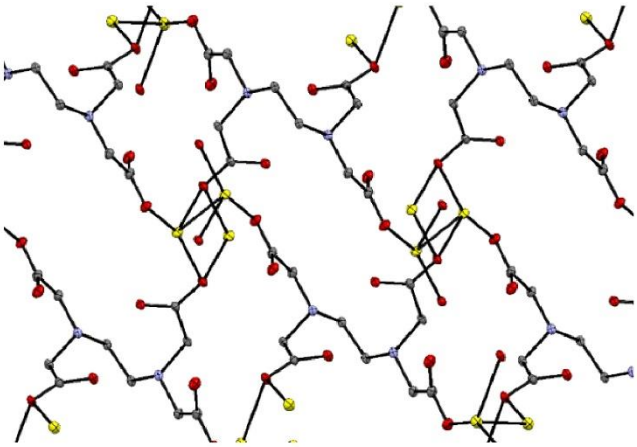

Figure A.1. Detail of the ORTEP representation of the Ag(I)-EDTA complex ($C_{10}H_{14}Ag_2N_2O_8$). Ellipsoids are shown at 70% probability. Color code: C = grey, N = blue, O = red, Ag = yellow.

For more details, please see Crystallographic Details attached to the end of Appendix A.

iCPE development

The influence of incubation time during iCPE on Ag-b-NP EE and Ag(I) co-extraction rates. Similar to the already established CPE approach[3], 30 min incubation time is the optimum for iCPE. We further examined whether the EE of Ag-b-NPs and the co-extraction of Ag(I) are influenced when the incubation time exceeds the suggested 30 min at 40 °C.[3] Therefore, solutions containing either 50 ng L^{-1} 60 nm CA@AgNP or 50 ng L^{-1} dissolved Ag(I) in UPW were subjected to iCPE, whereas the incubation time was set to 10, 20, 30, 60, and 90 min at 40 °C. The EE for Ag-b-NPs was determined as described in sections 2.5.2 in conjunction with 3.5 and the co-extraction of dissolved Ag(I) species determined as described in sections 2.5.1 in conjunction with 3.2. The maximum EE was reached after 30 min of incubation and was not further affected by increasing the incubation time, even by up to 90 min (see Table A.2). This is in line with the findings of our former CPE study.[3] However, the co-extraction rates were consistently low for incubation times of 10, 20, and 30 min, but they were increased in an unreproducible manner for incubation times of 60 and 90 min. This increase was possibly due to the formation of Ag-b-NPs from dissolved Ag(I) species after long incubation times, which has already been proven for naturally-occurring Ag(I).[4] These Ag-b-NPs were then transferred into the organic phase during iCPE. Therefore, in order to achieve the maximum EE along with maximally reduced co-extraction of dissolved Ag(I) species, it must be ensured that incubation times of exactly 30 min are adhered to.

Table A.2. Effect of iCPE incubation time on extraction efficiency (EE) of Ag-b-NPs and the remaining Ag signal as a measure of co-extraction rates of Ag(I)

incubation time	10 min	20 min	30 min	60 min	90 min
EE (Ag-b-NPs)	57 %	78 %	95 %	89 %	93 %
remaining Ag signal (Ag(I))	0.9%	0.9%	1.2%	4.7%	3.4%

The influence of iCPE on the Ag-b-NPs being extracted. Particles to be extracted were not affected by iCPE. It has already been shown that CPE applying 1 mL EDTA and no PA has no influence on the particle size of Ag-b-NPs during the extraction procedure.[3] This is an essential prerequisite for the use of CPE in environmental nanoparticle analysis, because it is possible to 'freeze' the particles in environmental samples in their current state. Samples containing 100 ng L^{-1} of 60 nm CA@AgNP were subjected to iCPE in order to investigate whether iCPE

also has no effect on particle sizes. Similar samples were analyzed by sp-ICP-MS without conducting iCPE. The corresponding particle size distributions were determined by means of sp-ICP-MS. Measured particle sizes were marginally reduced from 60.16 nm before CPE to 59.9 nm after CPE, indicating that the particle sizes were not affected by iCPE.

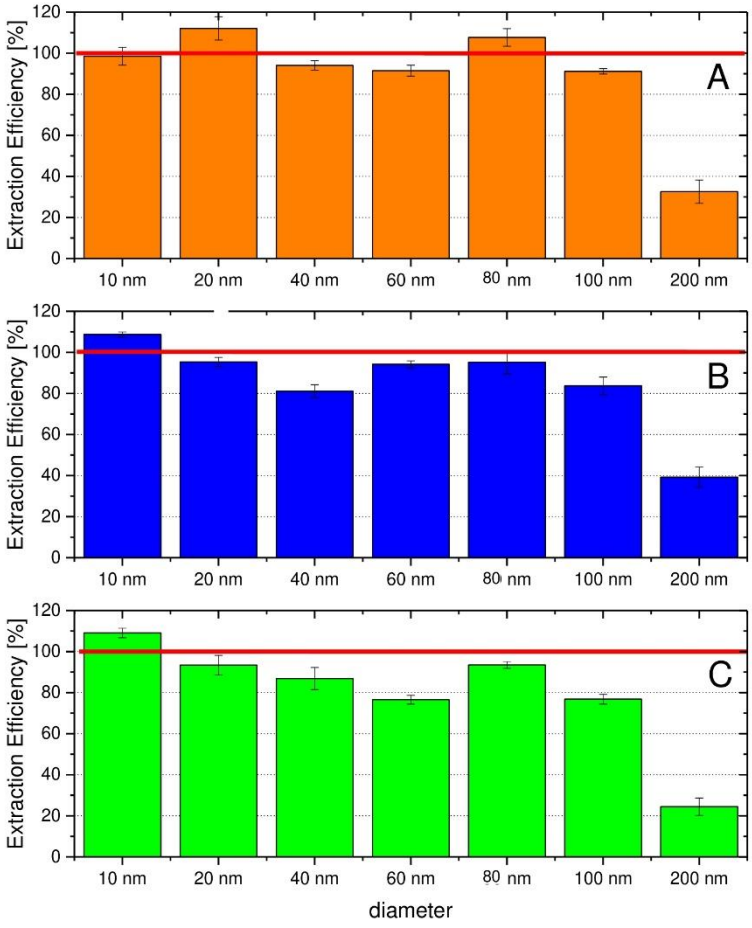

Figure A.1: EE for CA@AgNPs dependent of their mean particle size for samples initially containing 5 (A), 50 (B), and 300 ng L^{-1} (C) nanoparticulate Ag prior to iCPE.

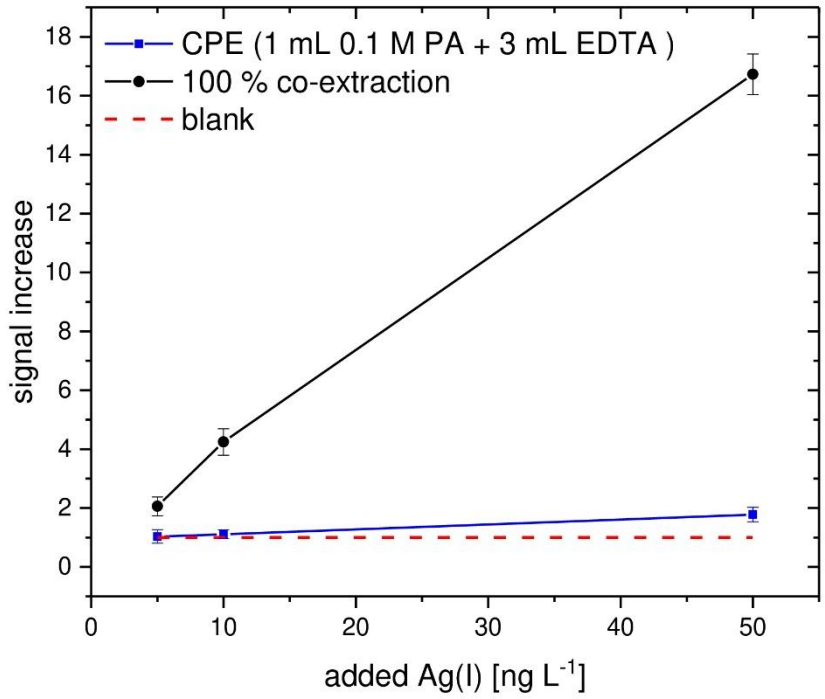

Figure A.3: Factor by which the measured signal intensity increased for river water samples initially containing 5, 10, and 50 ng L^{-1} dissolved Ag(I) mimicking 100% co-extraction (●) and after performing iCPE (■) compared to the blank measurement (i.e. a iCPE extract of river water containing no Ag at all). Assuming the ideal case of no Ag(I) co-extraction into the iCPE extract, the signal increase factor should be 1.0 (red dotted line).

Table A.3. Nebulization efficiencies at different dwell times in UPW and surfactant matrix determined with RM 8012 and RM 8013.

RM	**η**	**Matrix**	**Dwell time**
8012	0.064 ± 0.006	UPW	100 µs
8012	0.075 ± 0.000	surfactant	100 µs
8012	0.068 ± 0.004	UPW	500 µs
8012	0.080 ± 0.004	surfactant	500 µs
8013	0.060 ± 0.004	UPW	100 µs
8013	0.058 ± 0.002	UPW	500 µs

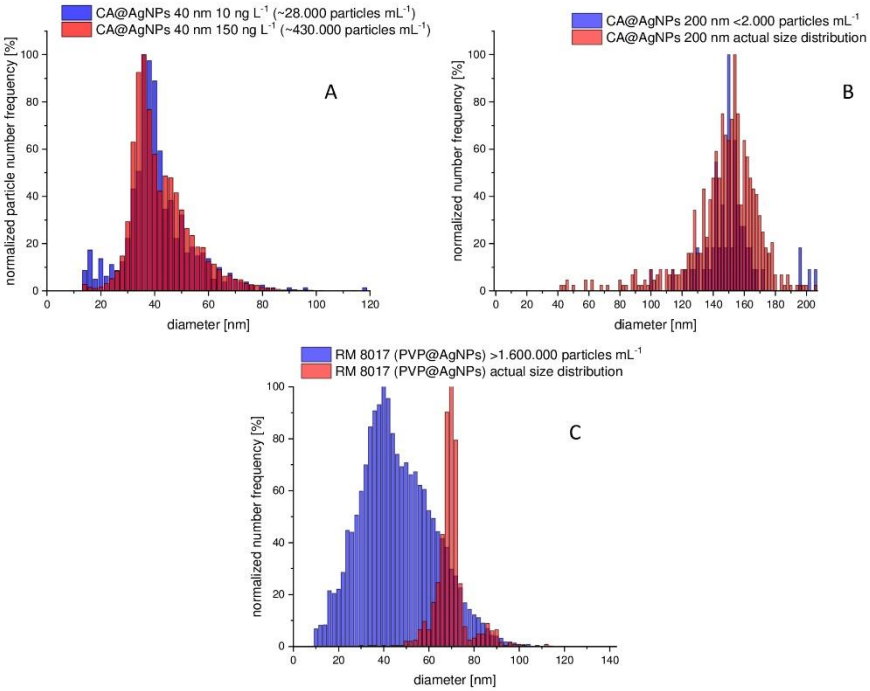

Figure A.4. Stability of particle size distributions over concentration range (A) and particle size distribution at a too low (B) and too high particle number concentration (C) in comparison to the actual size distributions.

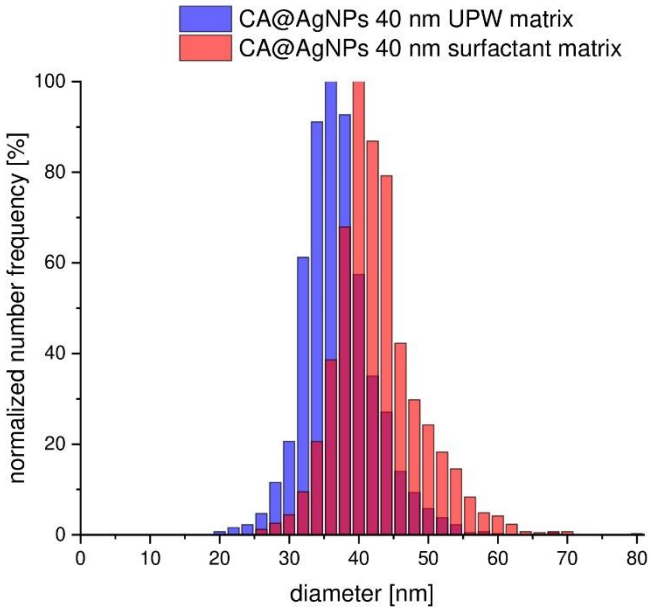

Figure A.5. Comparison of the particle size distribution obtained from sp-ICP-MS measurement in UPW and surfactant matrix.

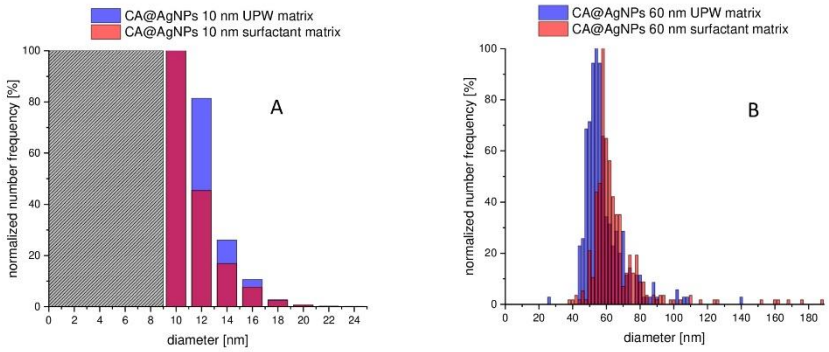

Figure A.6. Comparison of the particle size distributions obtained from sp-ICP-MS measurement of CA@Ag-NP dispersions prepared in UPW and surfactant matrix (A, B). In sp-ICP-MS measurement, t_d was set 100 µs for CA@AgNPs 10 nm (A) and 500 µs for CA@AgNPs 60 nm (B). The grey dashed bar in the particle size distribution A indicates the SDL, i.e. the cutoff, where NPs cannot be identified as NPs anymore. For reasons of comparison, we chose similar SDL values for both dwell times.

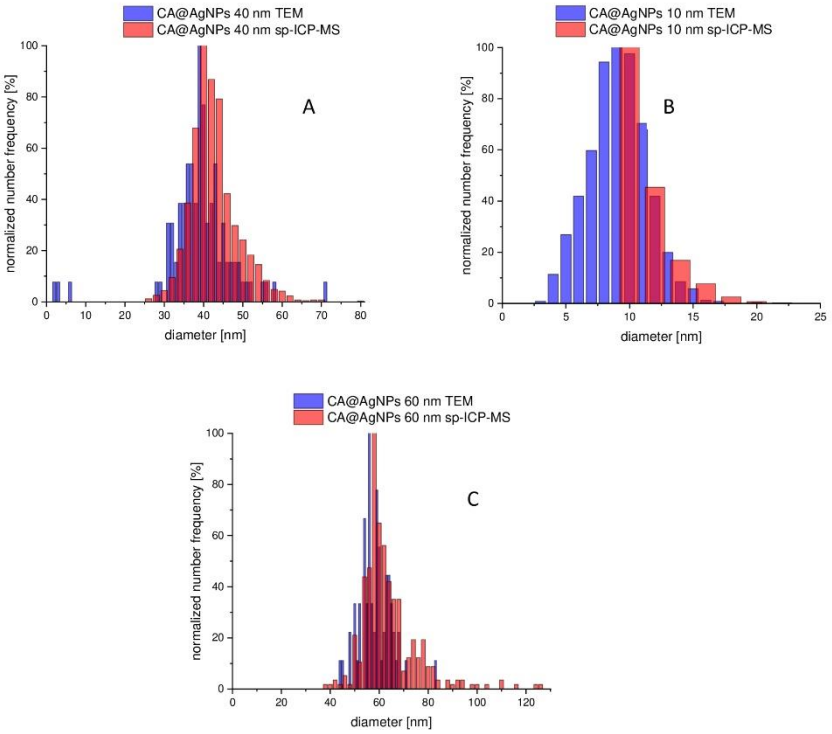

Figure A.7. Comparison of the particle size distributions obtained from sp-ICP-MS measurement in surfactant matrix and TEM measurement of CA@AgNP 40 nm (A), CA@AgNP 10 nm (B) and CA@AgNP 60 nm (C) dispersions.

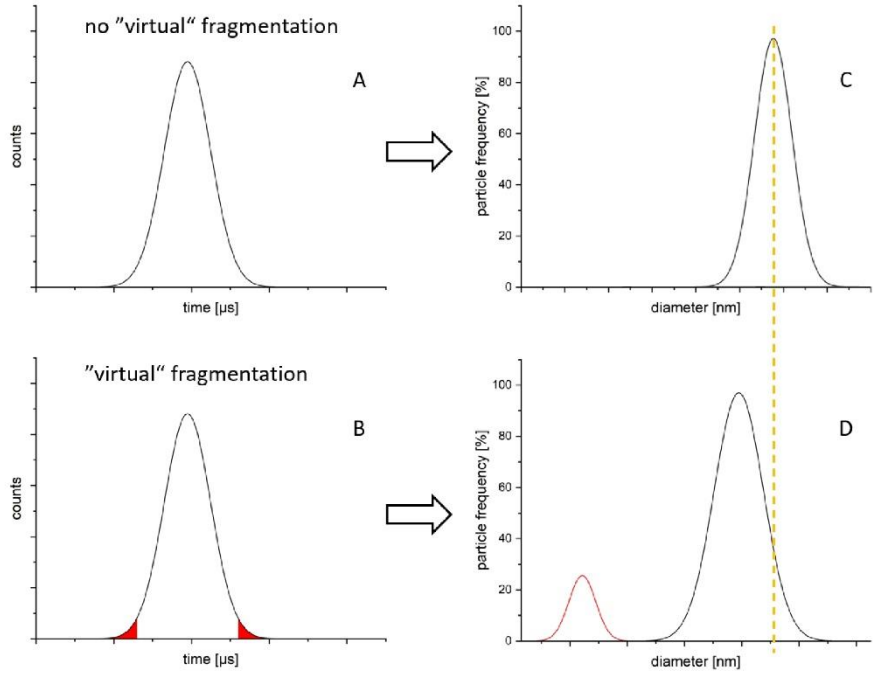

Figure A.8. Data processing struggling with correct evaluation of boundaries of the transient NP signal leading to ideal situation with correct particle boundary evaluation (A, C) and virtual particle fragmentation (B, D).

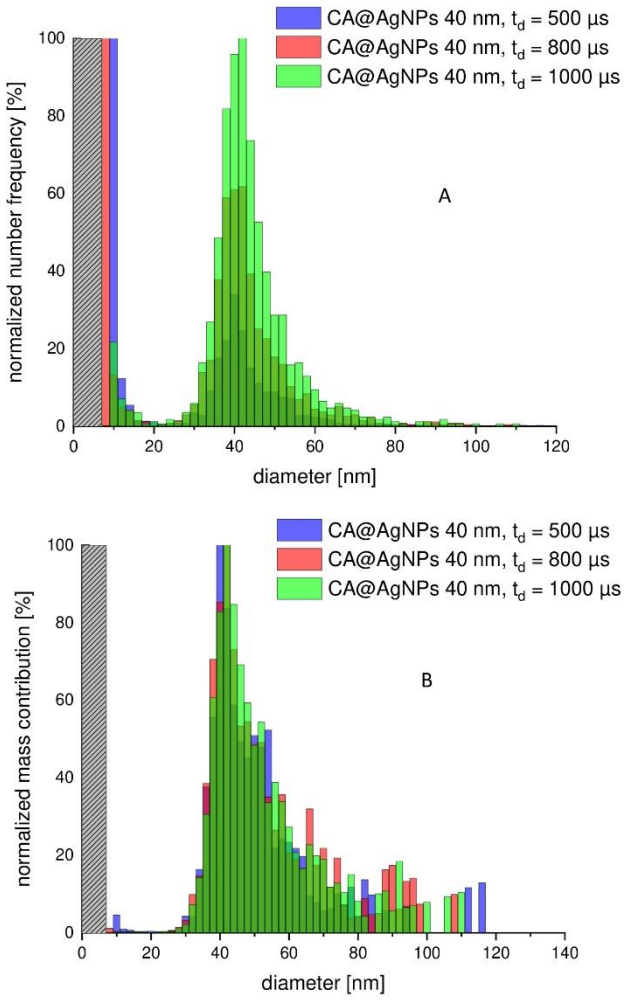

Figure A.9. Particle size distribution on a number frequency basis (A) and a mass contribution basis (B) of 40 nm CA@AgNPs measured by sp-ICP-MS applying different dwell times (t_d). The grey dashed bar in the particle size distributions indicates the SDL.

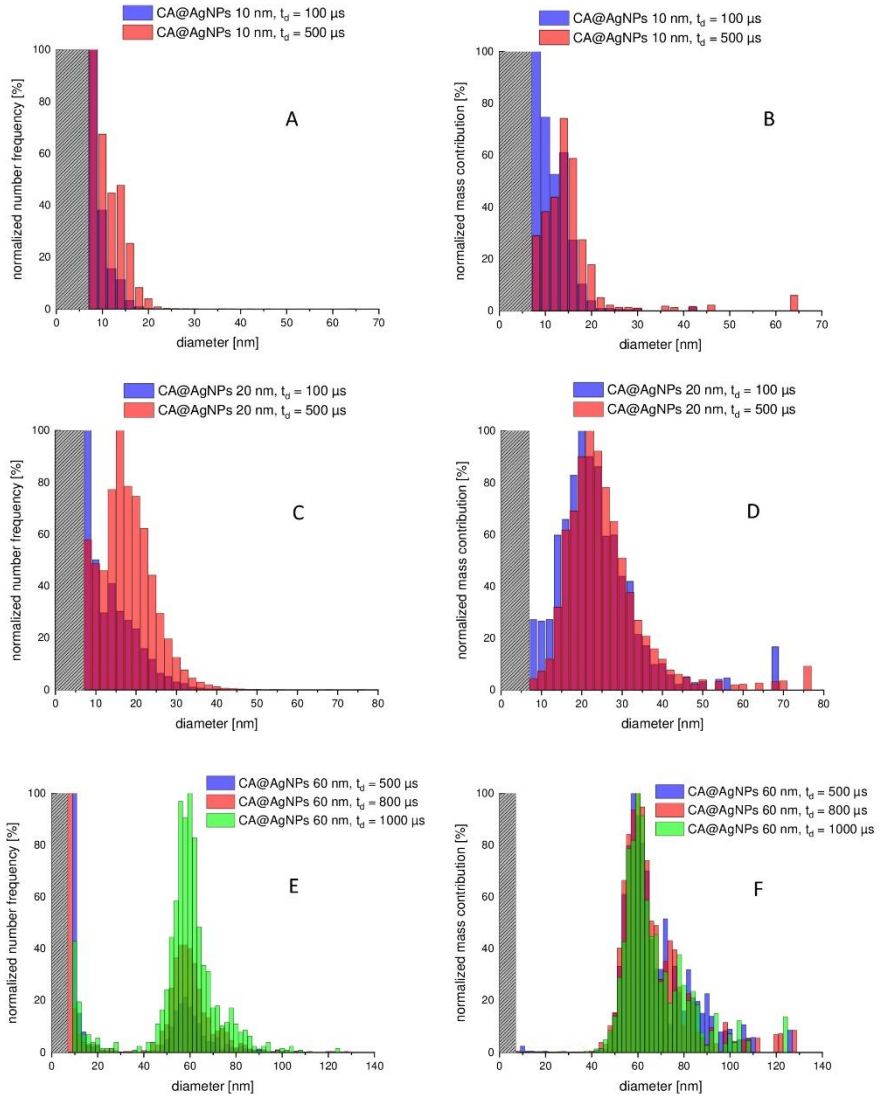

Figure A.10. Comparison of particle size distributions depicted as number frequency and mass contribution for CA@AgNP with a medium diameter of 10 nm (A, B), 20 nm (C, D) and 60 nm (E, F) at different dwell times (t_d). The grey dashed bar in the particle size distributions indicates the SDL, i.e. the cutoff, where NPs cannot be identified as NPs anymore. For reasons of comparison, we chose similar SDL values for both dwell times.

Determination of the size detection limit (SDL) in sp-ICP-MS:

In sp-ICP-MS, peak signals can be transformed into information on masses of each single nanoparticle causing the corresponding peak in the mass spectra. Following the calculations of Pace at al., the mass m_{NP} of a nanoparticle is calculated as follows from the signal intensity I_{NP} [cps] of the corresponding peak, the dwell time t_d [µs], the pump rate ν [ml min^{-1}] of the nebulizer, the nebulizing efficiency η, the ratio of molar masses of the whole nanoparticle and the analyte element $\frac{M_{NP}}{M_e}$ (which is 1 for AgNPs), and the elemental sensitivity ES_{ion} [cps/(µg/L)] correlating a signal intensity to a certain analyte concentration:[5]

$$m_{NP} = \frac{I_{NP} \cdot t_d \cdot \nu \cdot \eta}{ES_{ion}} \cdot \frac{M_{NP}}{M_e} \qquad \text{(Equation 1)}$$

Given the assumptions of a spherical shape of the particles and a homogeneous particle density ρ of the corresponding bulk element, the particle size d_{NP} can be derived from Equation 2 as follows:

$$d_{NP} = \sqrt[3]{\frac{6}{\pi \cdot \rho} \cdot \frac{I_{NP} \cdot t_d \cdot \nu \cdot \eta}{ES_{ion}} \cdot \frac{M_{NP}}{M_e}} \qquad \text{(Equation 2)}$$

Since I_{NP} must be clearly distinguishable from the background signal, SDL is dependent on the limit of detection (LOD) of I_{NP}. The corresponding LOD signal intensity I_{LOD} was therefore defined as $3 \cdot I_{median}$,[6] whereas I_{median} represents the median of all the signal intensities throughout an entire measurement. I_{median} is in particular influenced by the signals derived from dissolved Ag(I) species and instrument noise. Therefore, SDL can be calculated as follows:

$$SDL = \sqrt[3]{\frac{18}{\pi \cdot \rho} \cdot \frac{I_{median} \cdot t_d \cdot \nu \cdot \eta}{ES_{ion}} \cdot \frac{M_{NP}}{M_e}} \qquad \text{(Equation 3)}$$

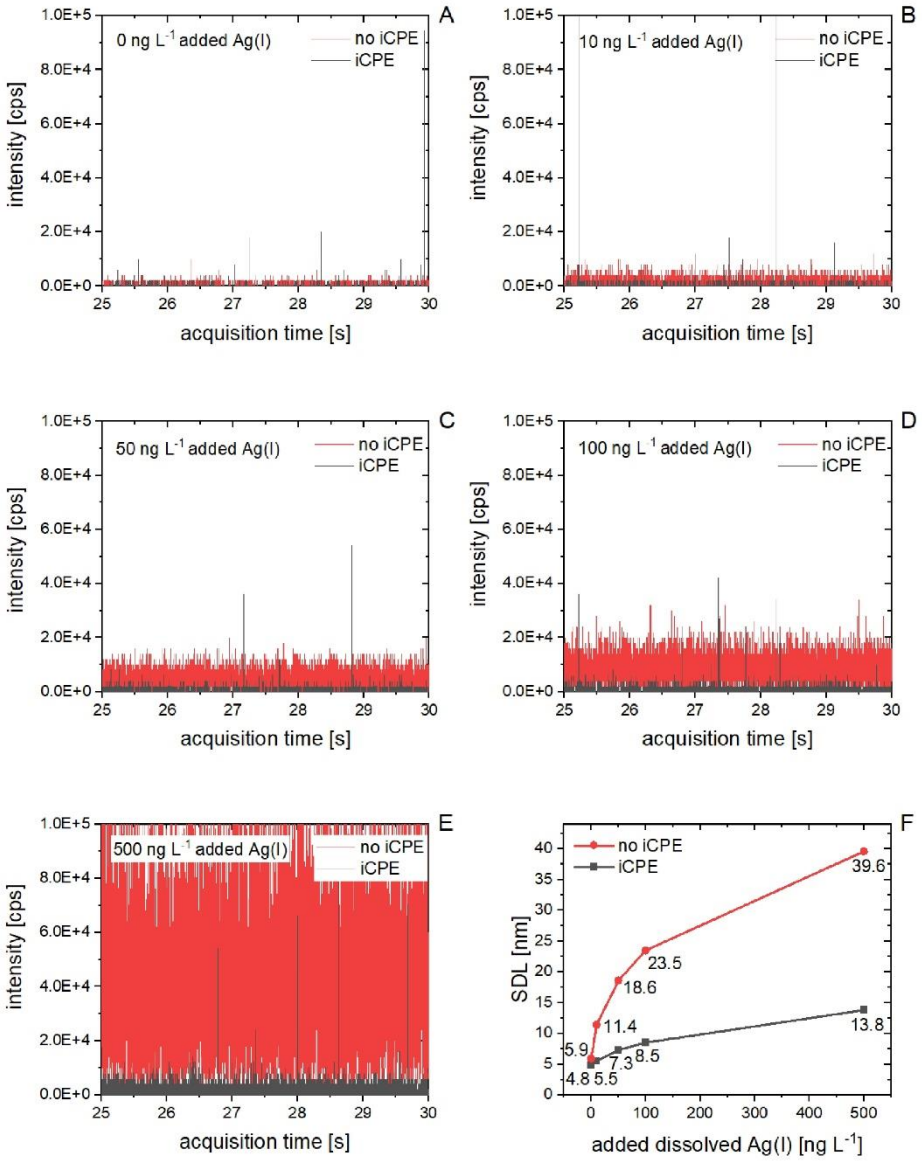

Figure A.11. Mass spectra obtained by sp-ICP-MS (t_d = 500 µs) in presence of increasing amounts of dissolved Ag(I) with and without CPE prior to measurement (A-E). SDL as function of Ag(I) added to samples (F).

References

1. Leung, B. O.; Jalilehvand, F.; Mah, V.; Parvez, M.; Wu, Q., Silver(I) Complex Formation with Cysteine, Penicillamine, and Glutathione. *Inorganic Chemistry* **2013,** *52* (8), 4593-4602.

2. Schmidbaur, H.; Schier, A., Argentophilic Interactions. *Angewandte Chemie International Edition* **2015,** *54* (3), 746-784.

3. Hartmann, G.; Hutterer, C.; Schuster, M., Ultra-trace determination of silver nanoparticles in water samples using cloud point extraction and ETAAS. *Journal of Analytical Atomic Spectrometry* **2013,** *28* (4), 567-572.

4. Wimmer, A.; Kalinnik, A.; Schuster, M., New insights into the formation of silver-based nanoparticles under natural and semi-natural conditions. *Water Research* **2018,** *141*, 227-234.

5. Pace, H. E.; Rogers, N. J.; Jarolimek, C.; Coleman, V. A.; Gray, E. P.; Higgins, C. P.; Ranville, J. F., Single Particle Inductively Coupled Plasma-Mass Spectrometry: A Performance Evaluation and Method Comparison in the Determination of Nanoparticle Size. *Environmental Science & Technology* **2012,** *46* (22), 12272-12280.

6. Lee, S.; Bi, X.; Reed, R. B.; Ranville, J. F.; Herckes, P.; Westerhoff, P., Nanoparticle Size Detection Limits by Single Particle ICP-MS for 40 Elements. *Environmental Science & Technology* **2014,** *48* (17), 10291-10300.

Crystallographic details

a) General information

The X-ray intensity data were collected on an X-ray single crystal diffractometer equipped with a CMOS detector (Bruker Photon-100), an IMS microsource with MoK_α radiation ($\lambda = 0.71073$ Å) and a Helios mirror optic by using the APEX III software package.[S1] The measurement was performed on single crystals coated with perfluorinated ether. The crystal was fixed on the top of a microsampler, transferred to the diffractometer and frozen under a stream of cold nitrogen. A matrix scan was used to determine the initial lattice parameters. Reflections were merged and corrected for Lorenz and polarization effects, scan speed, and background using SAINT.[S2] Absorption corrections, including odd and even ordered spherical harmonics were performed using SADABS.[S2] Space group assignments were based upon systematic absences, E statistics, and successful refinement of the structures. Structures were solved by direct methods with the aid of successive difference Fourier maps, and were refined against all data using the APEX III software[S1] in conjunction with SHELXL-2014[S3] and SHELXLE[S4]. Methyl hydrogen atoms were refined as part of rigid rotating groups, with a C–H distance of 0.98 Å and $U_{iso(H)} = 1.5 \cdot U_{eq(C)}$. Other H atoms were placed in calculated positions and refined using a riding model, with methylene and aromatic C–H distances of 0.99 and 0.95 Å, respectively, and $U_{iso(H)} = 1.2 \cdot U_{eq(C)}$. If not mentioned otherwise, non-hydrogen atoms were refined with anisotropic displacement parameters. Full-matrix least-squares refinements were carried out by minimizing $\Delta w(F_o^2-F_c^2)^2$ with SHELXL-97[S5] weighting scheme. Neutral atom scattering factors for all atoms and anomalous dispersion corrections for the non-hydrogen atoms were taken from International Tables for Crystallography.[S6] Images of the crystal structures were generated by Mercury.[S7-10]

b) Details for Ag(I)-EDTA

A clear colorless fragment-like specimen of $C_{10}H_{14}Ag_2N_2O_8$ that was crystallized from an aqueous solution, approximate dimensions 0.047 mm x 0.070 mm x 0.116 mm, was used for the X-ray crystallographic analysis.

A total of 1194 frames were collected. The total exposure time was 9.95 hours. The frames were integrated with the Bruker SAINT software package[S2] using a narrow-frame algorithm. The integration of the data using a monoclinic unit cell yielded a total of 11556 reflections to a

maximum θ angle of 25.02° (0.84 Å resolution), of which 1160 were independent (average redundancy 9.962, completeness = 100.0%, R_{int} = 4.18%, R_{sig} = 1.91%) and 995 (85.78%) were greater than $2\sigma(F^2)$. The final cell constants of a = 15.967(3) Å, b = 5.5779(8) Å, c = 15.342(3) Å, β = 106.428(7)°, volume = 1310.6(4) $Å^3$, are based upon the refinement of the XYZ-centroids of 128 reflections above 20 σ(I) with 5.262° < 2θ < 51.35°. Data were corrected for absorption effects using the multi-scan method (SADABS).[S4] The ratio of minimum to maximum apparent transmission was 0.885. The calculated minimum and maximum transmission coefficients (based on crystal size) are 0.7200 and 0.8710.

The final anisotropic full-matrix least-squares refinement on F^2 with 105 variables converged at R1 = 2.07%, for the observed data and wR2 = 4.53% for all data. The goodness-of-fit was 1.061. The largest peak in the final difference electron density synthesis was 0.511 $e^-/Å^3$ and the largest hole was -0.453 $e^-/Å^3$ with an RMS deviation of 0.102 $e^-/Å^3$. On the basis of the final model, the calculated density was 2.564 g/cm^3 and F(000), 984 e^-.

Table A.4: Sample and crystal data for **Ag(I)-EDTA**.

Identification code	WimAn1	
Chemical formula	$C_{10}H_{14}Ag_2N_2O_8$	
Formula weight	505.97	
Temperature	100(2) K	
Wavelength	0.71073 Å	
Crystal size	0.047 mm x 0.070 mm x 0.116 mm	
Crystal habit	clear colorless fragment	
Crystal system	monoclinic	
Space group	C 2/*c*	
Unit cell dimensions	a = 15.967(3) Å	α = 90°
	b = 5.5779(8) Å	β = 106.428(7)°
	c = 15.342(3) Å	γ = 90°
Volume	1310.6(4) $Å^3$	
Z	4	
Density (calculated)	2.564 g/cm^3	
Absorption coefficient	3.035 mm^{-1}	
F(000)	984	

Table A.5: Data collection and structure refinement for **Ag(I)-EDTA**.

Diffractometer	Bruker D8 Venture Duo IMS	
Radiation source	IMS microsource, Mo	
Theta range for data collection	2.66 to 25.02°	
Index ranges	-18<=h<=18, -6<=k<=6, -18<=l<=18	
Reflections collected	11556	
Independent reflections	1160 [R(int) = 0.0418]	
Coverage of independent reflections	100.0%	
Absorption correction	multi-scan	
Max. and min. transmission	0.8710 and 0.7200	
Refinement method	Full-matrix least-squares on F^2	
Refinement program	SHELXL-2014/7 (Sheldrick, 2014)	
Function minimized	$\Sigma\ w(F_o^2 - F_c^2)^2$	
Data / restraints / parameters	1160 / 54 / 105	
Goodness-of-fit on F^2	1.061	
Δ/σ_{max}	0.002	
Final R indices	995 data; $I>2\sigma(I)$	R1 = 0.0207, wR2 = 0.0429
	all data	R1 = 0.0284, wR2 = 0.0453
Weighting scheme	$w=1/[\sigma^2(F_o^2)+(0.0159P)^2+8.6992P]$ where $P=(F_o^2+2F_c^2)/3$	
Largest diff. peak and hole	0.511 and -0.453 eÅ^{-3}	
R.M.S. deviation from mean	0.102 eÅ^{-3}	

Supplementary References

[S1] *APEX suite of crystallographic software, APEX 3, version 2015.5-2,* Bruker AXS Inc., Madison, Wisconsin, USA (2015).

[S2] SAINT, Version 7.56a and SADABS Version 2008/1, Bruker AXS Inc., Madison, Wisconsin, USA (2008).

[S3] G. M. Sheldrick, "*SHELXL-2014*", University of Göttingen, Göttingen, Germany, (2014).

[S4] C. B. Huebschle, G. M. Sheldrick, B. Dittrich, *"SHELXLE"*, *J. Appl. Cryst.* **2011,** *44,* 1281.

[S5] G. M. Sheldrick, *"SHELXL-97"*, University of Göttingen, Göttingen, Germany, (1998).

[S6] A. J. C. Wilson, *International Tables for Crystallography*, Vol. C, Tables 6.1.1.4 (pp. 500-502), 4.2.6.8 (pp. 219-222), and 4.2.4.2 (pp. 193-199); Kluwer Academic Publishers: Dordrecht, The Netherlands (1992).

[S7] C. F. Macrae, I. J. Bruno, J. A. Chisholm, P. R. Edgington, P. McCabe, E. Pidcock, L. Rodriguez-Monge, R. Taylor, J. van der Streek, P. A. Wood, *J. Appl. Crystallogr.* **2008,** *41,* 466-470.

[S8] C. F. Macrae, P. R. Edgington, P. McCabe, E. Pidcock, G. P. Shields, R. Taylor, M. Towler, J. van de Streek, *J. Appl. Crystallogr.* **2006,** *39,* 453-457.

[S9] I. J. Bruno, J. C. Cole, P. R. Edgington, M. K. Kessler, C. F. Macrae, P. McCabe, J. Pearson, R. Taylor, *Acta Cryst.* **2002,** *B58,* 389-397.

[S10] R. Taylor, C. F. Macrae, *Acta Cryst.* **2001,** *B57,* 815-827.

8.3. Publikation 3

Looking at Silver-Based Nanoparticles in Environmental Water Samples: Repetitive Cloud Point Extraction Bridges Gaps in Electron Microscopy for Naturally Occurring Nanoparticles

Alexander Urstoeger,[§] Andreas Wimmer,[§] Ralf Kaegi, Simon Reiter and Michael Schuster[*]

* Corresponding author

E-Mail: michael.schuster@tum.de

[§] These authors contributed equally to the present study

Abdruck des Artikels mit Genehmigung von ACS Publications (siehe Kapitel 7.6) aus

Environmental Science & Technology, 2020, 54, 12063-12071.

Environmental Science & Technology

pubs.acs.org/est

Article

Looking at Silver-Based Nanoparticles in Environmental Water Samples: Repetitive Cloud Point Extraction Bridges Gaps in Electron Microscopy for Naturally Occurring Nanoparticles

Alexander Urstoeger,[§] Andreas Wimmer,[§] Ralf Kaegi, Simon Reiter, and Michael Schuster*

Cite This: *Environ. Sci. Technol.* 2020, 54, 12063−12071

Read Online

ACCESS | Metrics & More | Article Recommendations | Supporting Information

ABSTRACT: The growing use of silver-based nanoparticles (Ag-*b*-NPs) in everyday products goes hand in hand with their release into the environment, resulting in ng L^{-1} traces in natural water bodies. In order to assess their fate, possible transformations and ecotoxicology—essential information to proper risk assessment—particle size, shape, and chemical composition have to be determined. Transmission electron microscopy coupled with energy dispersive X-ray spectroscopy (TEM-EDX) is a powerful tool for determining these particle characteristics, but it requires high particle concentrations in order to produce statistically reliable results. In this study, we will present the extraction of Ag-*b*-NPs at environmentally relevant concentrations down to 5 ng L^{-1} from artificial as well as environmental water samples via cloud point extraction on a repetitive basis. The combination with an on-grid centrifugation technique ensures an efficient concentration and deposition of the extracted particles onto the TEM grid for subsequent TEM-EDX measurements. Furthermore, electron microscopy investigations were supplemented by single particle inductively coupled plasma mass spectrometry (sp-ICP-MS) measurements. Ag-*b*-NPs were successfully visualized and characterized at environmentally relevant concentrations of 5 ng L^{-1} with TEM-EDX and sp-ICP-MS measurements. Their size, shape, and chemical composition were not affected by the sample preparation.

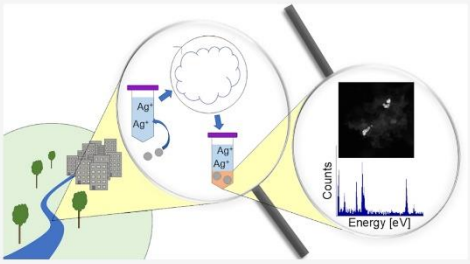

INTRODUCTION

The increasing use of silver nanoparticles (Ag-NPs) in everyday products like toiletries,[1,2] sportswear,[2] food packaging,[3,4] medical products,[4−7] cleaning products,[4] or even paint[8,9] leads to environmental exposure due to the washing, usage, and disposal of those goods.[2,8−11] Although wastewater treatment plants (WWTPs) are able to remove more than 90% of nanoparticulate silver material entering a WWTP, a small amount still reaches the environment via WWTP discharge, resulting in concentrations of 0.7−11.1 ng L^{-1} Ag in the effluent.[12,13] The major amount of nanoparticulate silver is retained in the sewage sludge and can also enter the environment via the sludge fertilization of fields.[12−15] In addition to discharges of Ag-NPs related to anthropogenic activities, Ag-NPs can also be formed via the reduction of dissolved silver by humic and fulvic acids in the environment.[7,16] Once in the environment, Ag-NPs are likely to interact with organisms and therefore pose a risk due to their biotoxicity.[7,15,17,18] Several studies have been carried out focusing on the toxicity of Ag-NPs on, e.g., freshwater invertebrates,[19] vertebrates,[20−22] bacteria,[23−25] algae, plants,[26,27] fungi,[26] and human cells.[28−30] A factor which greatly influences the toxicity of Ag-NPs is their size. It has been reported that smaller particles (<20 nm) are much more toxic than bigger ones due to their large specific surface area. In one respect, this high intrinsic surface increases the chance of interacting with biomolecules and subsequently entering the cell and, in a second respect, the release of silver ions.[21,31,32] Besides size, it is important to evaluate the ecotoxicity of Ag-NPs on the basis of chemical composition. Levard et al. reported a large decrease in toxicity toward killifish and duckweed by the sulfidation of Ag-NPs.[33] A general decrease in toxicity was reported for all organisms in a wide range of exposure media if the partial sulfidation was larger than 0.073 S/Ag molar ratio. This effect can be explained by the low solubility of Ag_2S. Fewer silver ions are released if an Ag_2S layer is formed around the Ag-NPs.[34] When released into the environment, Ag-NPs readily undergo several transformations, including the adsorption onto organic materials present in the environment, oxidation, (partial) dissolution, and reactions with dissolved species, which result in particles or coatings of,

Received: May 6, 2020
Revised: June 19, 2020
Accepted: August 26, 2020
Published: August 26, 2020

e.g., Ag_2S, the predominant species in the environment.[14,17,35−38] Also, Wimmer et al. found, that smaller Ag-*b*-NPs are dissolving much faster than bigger ones at environmentally relevant concentrations.[39] A factor, which also influences NP toxicity is their shape. Spherical particles enter cells much more likely than, e.g., nanotubes or fibers.[40] Also, the shape affects the size of NPs, therefore needing to be considered assessing nanoparticle toxicity. In order to address all kinds of silver nanoparticles, we will refer to them hereinafter as silver-based nanoparticles (Ag-*b*-NPs). As indicated above, their fate, possible transformations, and toxicological risks to the contaminated ecosystem predominantly depend on the size, shape, and chemical composition of Ag-*b*-NPs. Thus, these properties have to be investigated to allow for a comprehensive risk assessment. Transmission electron microscopy (TEM) equipped with energy-dispersive X-ray spectroscopy (EDX) is a powerful tool for determining these properties of Ag-*b*-NPs. However, particle-based TEM investigations require high particle concentrations which are well above the concentrations of environmentally occurring Ag-*b*-NPs. This limitation is actually intensified when looking at the conventional grid preparation of NP-containing samples. Only an aliquot of few μL of the whole sample is used for grid-preparation, further increasing detection limits. Screening the TEM grid for a disproportionate time range goes in hand with such high detection limits. Therefore, the present study follows the basic idea of concentrating the Ag-*b*-NPs in a sample of several mL onto a single TEM grid. As a result, detection limits are significantly reduced to environmentally relevant concentrations. One technique which greatly supports those efforts is cloud point extraction (CPE). CPE is capable of not only preconcentrating nanoparticles, but also separating them from dissolved and ionic species present in environmental samples without changing their size, shape, and composition. This technique was originally applied to the analysis of nonpolar organic substances and metal ions after complexation to nonpolar compounds in water.[41,42] Liu et al. were the first to use CPE for NP enrichment.[43,44] CPE for Ag-*b*-NP quantification has been thoroughly investigated and validated in our group.[13,45−47] However, preconcentration factors of CPE in view of environmentally relevant concentrations are not sufficient for subsequent TEM measurements. Thus, this study aims to present a novel method based on CPE in combination with a centrifugation technique for visualizing and characterizing silver nanoparticles in matrices comprising ultrapure water (UPW), as well as environmental water samples down to an environmental relevant concentration of 5 ng L^{-1} with TEM-EDX measurements. This approach covers (i) extracting and enriching Ag-*b*-NPs in environmental samples by CPE in a first step, followed by a second step of (ii) transferring the captured Ag-*b*-NPs onto a TEM grid. After extraction, Ag-*b*-NPs from an original 40 mL sample are present in some μL surfactant rich extract.

Further development of CPE was supported by inductively coupled plasma mass spectrometry (ICP-MS) measurements for Ag concentration analysis and single particle inductively coupled plasma mass spectrometry (sp-ICP-MS) measurements for particle number and size determination. sp-ICP-MS measurements were confirmed by TEM-EDX measurements.

MATERIALS AND METHODS

Materials. Acetic acid (glacial), Ag(I) ICP-standard ($AgNO_3$ in 3% HNO_3, β_{Ag} = 1000 mg L^{-1}), ethanol, ethylenediaminetetraacetate (EDTA) disodium salt, nitric acid (suprapure, 65%), silver(I) nitrate, sodium acetate anhydrous, and sodium dodecyl sulfate were purchased from Merck (Darmstadt, Germany). Indium ICP-standard ($In(NO_3)_3$ in 2−3% HNO_3, β_{In} = 1000mg L^{-1}), dispersions of citrate stabilized silver nanoparticles (CA@Ag-NPs) (β_{Ag} = 20 mg L^{-1}), D-penicillamine, and sodium sulfide (Na_2S) were purchased from Sigma-Aldrich (St. Louis, MO, U.S.A.). According to the supplier, CA@Ag-NPs should have a size of 40 nm. As indicated in the Results and Discussion, the average diameter was 36 nm. The mean particle sizes indicated in this study represent the mean value based on particle number frequency. Since CA@Ag-NP, silver sulfide nanoparticle (Ag_2S-NP (type I and type II)) dispersions contain impurities of dissolved Ag, the stock dispersions were purified from dissolved Ag species by dialysis (3.5 kDa regenerated cellulose membrane by ZelluTrans, Carl Roth, Karslruhe, Germany) prior to use. A citrate stabilized gold nanoparticle dispersion (CA@Au-NPs, NIST reference material RM 8013, 56 nm, β_{Au} = 52 mg L^{-1}) was purchased from the National Institute of Standards and Technology (Gaithersburg, MD, U.S.A.). Poly-L-lysine solution was obtained from Boster Biological Technology (Pleasanton, CA, U.S.A.). Triton X-114 (TX-114) was purchased from AppliChem (Darmstadt, Germany). All chemicals were of at least analytical grade and were checked for Ag contaminations by ICP-MS measurements before use. UPW (resistivity of 18.2 MΩ cm^{-1}) was obtained by a Milli-Q-Gradient System (Millipore GmbH, Schwalbach, Germany).

Instrumentation. A quadrupole mass spectrometer 7900 ICP-MS (Agilent, Santa Clara, CA, U.S.A.) equipped with an autosampler SPS4 (Agilent) and a MicroMist nebulizer (Glass Expansion, Melbourne, Australia) was used for Ag concentration and particle size determination. Ar 4.8 (Westfalen, Münster, Germany) was used as plasma gas. For Ag quantification, the analyte target mass was ^{107}Ag, and ^{115}In for the internal standard. The measurement time was set to 1 s for the analyte and 0.1 s for the internal standard. Each sample was measured five times. Measurements were carried out in He CCT mode to avoid isobaric and polyatomic interferences. The detection limit (DL) was 0.56 ± 0.25 ng L^{-1} (0.14 ± 0.06 ng L^{-1} after conduction of single CPE and 0.03 ± 0.01 ng L^{-1} after $rCPE_5$). Corresponding enrichment factors were taken into account in calculating the detection limit after CPE ($rCPE_5$). Calibration was performed in the range of 1 ng L^{-1} to 200ng L^{-1}. The nebulizer gas pressure was 429 kPa.

In single particle mode, ^{107}Ag was chosen as the target mass as well, and the dwell time was set to 500 μs. The pump rate was determined to be 0.310 mL min^{-1}. A CA@Au-NP (RM 8013) dispersion at an Au concentration of β = 52 ng L^{-1} was used to determine the transport efficiency η, which is the proportion of initial particles in the sample which finally reach the detector. η was determined to be 8% according to a previously approved procedure.[48,49] To prevent particle aggregation, the nanoparticle suspensions were ultrasonicated for 1 min in an ultrasonic bath—Ulsonix Proclean 3.0DSP (Ulsonix, Berlin, Germany). To obtain an element specific signal intensity for the sp-ICP-MS measurements, the signal sensitivity was calibrated using an Ag(I) solution at a concentration of 1 μg L^{-1}. Agilent MassHunter Workstation 4.4 software (version C.01.04) equipped with the Single Nanoparticle Application Module was used to evaluate particle

https://dx.doi.org/10.1021/acs.est.0c02878
Environ. Sci. Technol. 2020, 54, 12063−12071

size distributions. In sp-ICP-MS, transient, peak-like signals deriving from NP ionization events in the plasma are registered by the detector. The NP signal height and area are directly proportional to particle size. However, dissolved analyte species lead to a rather low yet constant signal. In sp-ICP-MS, it is essential to differentiate between the transient peak-like signals and the constant background. An excessive background covers small NP signals. In the event that no dissolved analyte species (β_{Ag} < DL) are present (such as after CPE), no background signal due to dissolved analyte species will be detected and, as a result, only the instrumental noise will limit the size detection limit (SDL). In our case, SDL was determined to be 8 nm.

A dedicated scanning transmission electron microscope (STEM, HD-2700-Cs, Hitachi, Japan) operated at an acceleration voltage of 200 kV was used for the TEM measurements. Images were recorded using either a secondary electron (SE) or a high angular annular dark field (HAADF) detector. Elemental analysis of individual particles was performed using an energy dispersive X-ray detector (EDAX, U.S.A.), and the spectra were recorded and processed using Digital Micrograph (v.1.85, Gatan Inc., U.S.A.).

The TOC content of river water samples was determined using a TOC-L analyzer (Shimadzu, Kyoto, Japan). Potassium hydrogen phthalate was used for calibration (Nacalai Tesque Inc., Kyoto, Japan).

Nanoparticle Synthesis and Characterization. Silver sulfide nanoparticles (Ag_2S-NPs) were synthesized according to a procedure previously published by Pettibone and Liu.[50] In brief, 0.16 mL of a 0.5 M Na_2S solution was added at once to 40 mL of a solution containing 2 mM $AgNO_3$. The mixture was stirred for 1 h in the dark at room temperature (RT). These nanoparticles are referred to as Ag_2S-NPs (type I) hereafter.

TEM-EDX measurements of the purified CA@Ag-NPs dialyzed in previously nonpurified dialysis membranes suggested that an Ag_2S layer formed around the silver core nanoparticles. The dialysis membranes probably contained small amounts of sulfide impurities and induced the sulfide formation for this reason. However, sulfidation might also have taken place during the storage or transport of the NPs. The molar ratio of Ag/S of the particles ranged from 3:1 to 5:1. These particles were used as Ag_2S-NPs (type II), suggesting a core−shell structure with an Ag core and an Ag_2S shell.

The CA@Ag-NP, Ag_2S-NP (type II), and synthesized Ag_2S-NP (type I) suspensions were dialyzed in the dark for 3 days. The water was changed twice a day. For CA@Ag-NPs, the dialysis membrane was put into UPW for several hours, whereas the water was changed twice to get rid of possible sulfide impurities before adding the NP suspension. Dialysis was carried out to separate the nanoparticles from the dissolved silver species and matrix constituents. After dialysis, the nanoparticle suspensions were stored in the dark at 5 °C and were stable for several weeks. The particle size, shape, and chemical composition were determined by TEM-EDX measurements. No sulfidation of CA@Ag-NPs could be detected.

Preconcentration and Separation of Ag-*b*-NPs from Aqueous Matrices. The UPW and river water samples were mixed with aqueous dispersions of CA@Ag-NPs, Ag_2S-NPs (type II), or synthesized Ag_2S-NPs (type I) to a total volume of 40 mL and a final Ag concentration of 5 ng L^{-1} and 50 ng L^{-1}, respectively. Afterward, CPE was conducted for the selective enrichment of Ag-*b*-NPs and separation from dissolved silver species.[45,46,51] For this purpose, 40 mL of each sample were mixed with 100 μL of 1.25 M acetic acid, 400 μL of a 1 M sodium acetate solution, 3 mL of a saturated aqueous solution of ethylenediaminetetraacetic acid disodium salt (EDTA), 1 mL of a 0.1 M D-penicillamine (D-PA) solution, and 1 mL of an aqueous solution of the surfactant TX-114 (10% (w/w)).[16,39,45,46] The mixture was shaken vigorously to ensure thorough mixing and incubated for 30 min at 40 °C. Centrifugation for 12 min at 4500 *g* was then conducted to enhance phase separation before cooling the sample for 10 min in an ice bath to increase the viscosity of the surfactant rich phase at the bottom of the vial. The aqueous supernatant was removed by means of decantation. For the repetitive CPE, the residual surfactant phase was again mixed with 40 mL of nanoparticle-containing aqueous sample, and CPE reagents were added as described above. In order to compensate for the surfactant loss in the preceding CPE, which was determined gravimetrically, 140 μL of a solution of the surfactant TX-114 (10% (w/w)) was added. Again, the mixture was shaken vigorously and incubated for 30 min at 40 °C. After incubation, the separation of the surfactant phase was enhanced by centrifugation as described above. After cooling the phase-separated mixture in an ice bath, the aqueous supernatant was again removed by decanting. This procedure was repeated until a total of 5 CPEs in a row ($rCPE_5$) were conducted. For sp-ICP-MS measurement, the remaining surfactant droplet containing the extracted and enriched Ag-*b*-NPs was diluted with 500 μL of ethanol and filled up with UPW to a total volume of 10 mL. To determine the Ag concentration with ICP-MS measurement, the CPE extract was, after carrying out above-mentioned dilution, mixed with HNO_3 yielding 1.625% (v/v) HNO_3 to dissolve extracted Ag-*b*-NP, thereby increasing the analyte stability and homogeneity. Recovery rates were calculated by dividing the Ag concentration after $rCPE_5$ through the initial Ag concentration in the sample.

Development and Optimization of a Centrifugation Technique for Subsequent Visualization of Ag-*b*-NPs with TEM-EDX. In order to transfer the Ag-*b*-NPs in a sample onto a TEM grid for investigation of the particles via TEM-EDX, a direct on-grid centrifugation procedure was used.[52] Several dispersions of 500 ng L^{-1} CA@Ag-NP in UPW were subjected to single CPE as described above. Each CPE extract was applied to a poly-L-Lysin functionalized TEM grid (the preparation is described in the following) − either with or without prior mixing with 500 μL of ethanol. Copper TEM grids (Micro to Nano, Haarlem, Netherlands) were functionalized with poly-L-lysine solution to enhance nanoparticle attachment to the carbon coating of the TEM grid.[53] For this purpose, the TEM grids were put into a droplet of poly-L-Lysin solution for 10 min and then in UPW for another 10 min. This procedure was repeated three times. After each step, the remaining liquid was blotted away with a filter paper. The dry TEM grid was then positioned on an (custom-made) aluminum cone within a micro reaction tube (Eppendorf, Hamburg, Germany). The aluminum cone was covered in Parafilm (Bemis Company Inc., Oshkosh, WI, U.S.A.) prior to positioning the TEM grid to enhance adhesion of TEM grid on the aluminum cone. Figure 1 shows a schematic of the setup. The detailed procedure for the TEM grid preparation is also described in a video.[54] In the following, the NP containing CPE extract was added to this tube. After centrifugation of the whole assembly of extract, aluminum cone, and TEM grid in

https://dx.doi.org/10.1021/acs.est.0c02878
Environ. Sci. Technol. 2020, 54, 12063−12071

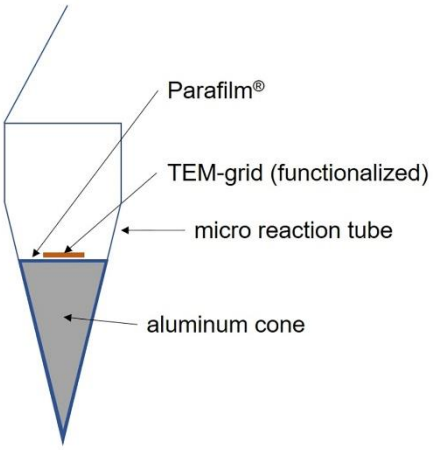

Figure 1. Poly-L-lysin functionalized TEM grid positioned onto an in Parafilm covered aluminum cone. The cone with adhered TEM grid is positioned into a micro reaction tube prior to addition of CPE extract for centrifugation.

the micro reaction tube at 10 000*g* for 30 min, the NPs from the original 40 mL sample were transferred onto the TEM grid. After centrifugation, the remaining surfactant rich phase was removed by pipetting. The fraction of particles deposited on the TEM grid corresponded to the volumetric fraction of the water column overlying the TEM grid compared to the total volume of suspension in the Eppendorf tube.

Several grid washing approaches using either ethanol or cyclohexane were evaluated to further reduce surfactant induced film formation during the grid preparation. Therefore, samples without added Ag-*b*-NP (to only observe the matrix effects) made from pure UPW or freshly sampled river water (without filtration) were subjected to a single CPE. As explained above, the extracts were mixed with 500 μL of ethanol in a first step and subsequently applied to the grid. After centrifugation was carried out and the residual surfactant rich phase was removed, the grids were covered with 500 μL of ethanol or cyclohexane. After incubation for 3 min, ethanol or cyclohexane, respectively, were carefully removed again via pipetting. This washing cycle was repeated six times in a row. After all six washing steps, the grid was dried in the reaction tube, gently removed from the aluminum cone, and stored in a TEM storage box until measurement.

In order to test the minimum detectable Ag-*b*-NP concentrations in environmental water samples, river water (without filtration) which did not contain any Ag traces above 0.56 ± 0.25 ng L^{-1} was mixed with 60 nm CA@Ag-NPs at concentrations ranging from 5 to 50 and to 500 ng L^{-1} nanoparticulate Ag. After performing CPE, all extracts were mixed with ethanol, and the grid was prepared as mentioned above, including the six washing steps with ethanol.

Investigation of Ag-*b*-NPs via TEM-EDX after Conduction of $rCPE_5$. For the TEM-EDX measurements, repetitive CPE was conducted 5-fold ($rCPE_5$), including experiments with six extractions in parallel (6 × $rCPE_5$) to lower the limit of detection for TEM measurements. The $rCPE_5$ extract—diluted with 500 μL ethanol and treated for 5 min in an ultrasonic bath and afterward for 1 min in an ultrasonic device UP200 St coupled to a VialTweeter (Hielscher Ultrasonics GmbH, Teltow, Germany) at half power to prevent particle aggregation—was transferred to a micro reaction tube. Afterward, centrifugation was carried out for 30 min at 10 000 *g*, resulting in a quantitative deposition of the Ag-*b*-NPs on the aluminum cone and a corresponding fraction on the TEM grid. After centrifugation, the CPE extract was removed by pipetting. For the experiments with 6 × CPE_5, another CPE extract, which was diluted again with 500 μL ethanol and treated in an ultrasonic bath and in the ultrasonic device as described above, was added to the micro reaction tube with the aluminum cone with adhered TEM grid in it, and the aforementioned centrifugation procedure was carried out again. This was done for all six consecutive CPE extracts. After the last centrifugation step and the subsequent removal of the CPE extract via a pipette, the TEM grid was washed six times with ethanol in the micro reaction tube as described above.

River Water Sampling. Surface water samples were taken from the Isarkanal river in Garching, Germany in July 2019 under dry weather conditions. All samples were taken from the same spot and collected in polyvinyl chloride (PVC) containers (0.5 L). Every container was rinsed three times with the sample before being filled with it. Surface water sample characteristics such as pH, TOC, and O_2 content are shown in the Supporting Information (SI, Table S1). For the TOC measurements, equal amounts of all samples were mixed together and subjected to TOC measurement. The samples were then filtered with a syringe filter (0.45 μm, cellulose acetate, VWR, Ismaning, Germany) and, after filtration, checked for Ag-*b*-NP content by single CPE hyphenated to (sp-)ICP-MS measurements. The samples were spiked with Ag_2S-NPs (type I) to a final concentration of β_{Ag} = 5 ng L^{-1} before performing $rCPE_5$ to mimic naturally occurring Ag-*b*-NPs in an environmental surface water matrix. Ag_2S-NPs were selected because they represent the majority of naturally occurring Ag-*b*-NPs.[14,17,35−38] For the sp-ICP-MS measurement, aliquots of all subsamples were mixed together, spiked with Ag_2S-NPs (type I), and subjected to $rCPE_5$ as described above and, subsequently, to sp-ICP-MS measurement. For characterization by TEM-EDX measurements, $rCPE_5$ was conducted with each sample, and the remaining surfactant droplets were centrifuged onto a single TEM grid as described above.

Error Calculations. Three independent sample replicates were prepared and measured individually for all measurements. Each sample was measured with five measurement replicates. The uncertainty was calculated via Gaussian error propagation, including pipetting uncertainties and standard deviations of the independently measured sample replicates. The Ag concentrations were blank corrected via measurement of blank samples.

■ RESULTS AND DISCUSSION

Characterization of Ag-*b*-NPs. In order to gain information about the size, shape, and chemical composition of Ag-*b*-NPs in their pristine state, TEM and EDX as well as sp-ICP-MS measurements were carried out for dispersions of freshly synthesized and purified CA@Ag-NPs, Ag_2S-NPs (type II), and Ag_2S-NPs (type I). In the following, unless stated otherwise, the particle size distributions determined by sp-ICP-

https://dx.doi.org/10.1021/acs.est.0c02878
Environ. Sci. Technol. 2020, 54, 12063−12071

MS measurements are presented on the basis of normalized particle number frequency.

CA@Ag-NPs showed a size range of approximately 16−74 nm (SI Figure S1) of nearly spherical particles (see the TEM image in SI Figure S2). The most frequent diameter of the particles determined by sp-ICP-MS measurement was 36 nm, while the average diameter was 35 nm. A TEM-SE image and the corresponding EDX spectrum of CA@Ag-NPs is shown in the SI, Figure S2.

TEM analyses revealed that the Ag_2S-NPs (type II) particles were spherical, with sizes between 20 and 80 nm (SI Figure S3). The most frequent diameter of the particles determined by sp-ICP-MS measurement was 44 nm, and the average diameter was 43 nm. EDX measurement revealed Ag to S ratios ranging from 3:1 to 5:1, suggesting the formation of an Ag_2S layer around an Ag core. A TEM-SE image of Ag_2S-NPs (type II) and the corresponding EDX spectrum is shown in the SI, Figure S4.

Ag_2S-NPs (type I) showed a size range of approximately 14−80 nm (SI Figure S5) of individual spherical particles, as well as particles which were possibly merged via Ag_2S nanobridges (see the TEM image in the SI Figure S6).[34] The most frequent diameter of the particles determined by sp-ICP-MS measurement was 16 nm, and the average diameter was 25 nm (SI Figure S5). EDX measurements revealed an Ag to S ratio of 2:1, which was consistent with the stoichiometry of acantite. A TEM-SE image of Ag_2S-NPs (type I) and corresponding EDX spectrum is shown in the SI, Figure S6.

Optimization of the Grid-Washing Procedure after the on-Grid Centrifugation for Subsequent TEM-EDX Measurement. In the development and optimization of the centrifugation technique for the subsequent visualization of Ag-*b*-NPs with TEM-EDX, dispersions of 500 ng L^{-1} CA@Ag-NP in UPW were subjected to CPE, and the extract was subsequently centrifuged onto a TEM grid, either with or without the addition of 500 μL of ethanol to the surfactant-rich extract prior centrifugation. As depicted in Figure S7, extracts mixed with ethanol resulted in less film formation, thus facilitating the identification of CA@Ag-NPs in the electron microscope.

TEM grids were washed after centrifugation with different washing reagents. Cyclohexane as a washing reagent led to an increased film formation both for samples made from UPW (Figure S8B) and river water (Figure S8D,F). Washing the prepared grids with ethanol resulted in less film formation (Figure S8A), even in the case of actual river water (Figure S8C,E). Therefore, grids were washed six times in a row using ethanol in all following experiments.

Considerations Regarding the Number of Nanoparticles on the Grid. After optimizing the grid preparation and the washing procedure for reducing film formation to an absolute minimum, the way was paved for the detection of traces of Ag-*b*-NPs in aqueous samples by means of TEM. We thus further investigated the lowest concentration of Ag-*b*-NPs in the samples prior to CPE, which were detectable with a reasonable effort. Theoretical considerations were factored into our experimental approaches. Assuming that the Ag-*b*-NPs exhibit a spherical shape and a density of 10.49 g cm^{-3} (such as the bulk material according to the GESTIS Substance Database, accessed in Mar. 2020 in the case of core Ag-NPs), it was possible to calculate the total number of particles present in a sample of a certain volume, e.g. a 40 mL aqueous sample. Ideally, all of these particles will be transferred onto the aluminum cone (8 mm diameter). A certain proportion of these particles reach the TEM grid (3.05 mm diameter) positioned on the aluminum cone. The imaging unit exhibits a resolution of, for instance, 1024 × 1024 pixels. In our case, 5 pixels were required to map the entire diameter of one nanoparticle. Given a 60 nm Ag-*b*-NPs, 1 pixel represents 12 nm. Considering said resolution, the area of each image section can be calculated accordingly and, in the following, also the number of image sections per total grid area. The average number of Ag-*b*-NPs on each TEM image section can then be calculated (see Table 1). This illustrates the expected effort for "finding Ag-*b*-NPs" on the grid by microscopy.

Table 1. Calculation of Average Number of Particles Detectable on Each TEM Image, Depending on NP Size and Concentration

Ag-b-NP size (nm)	Ag-b-NP concentration (ng L^{-1})	number of particles each TEM image section
10	5	8
10	50	80
10	500	800
20	5	4
20	50	40
20	500	400
60	5	1
60	50	10
60	500	100

These calculations reveal that, even at concentrations as low as 5 ng L^{-1} of nanoparticulate Ag, it is likely that at least one particle will be detected in each TEM image. However, it must be taken into consideration that these calculations are based on an 100% extraction efficiency during the CPE process. Therefore, the minimum detectable concentrations were also tested via actual experiments.

As depicted in Figure 2, Ag-b-NPs were detected by TEM for all three analyte concentrations, whereas the 5 ng L^{-1} analyte concentration required great effort to find Ag-b-NPs on the TEM grid. Therefore, it becomes necessary to further increase the enrichment factor during TEM grid preparation.

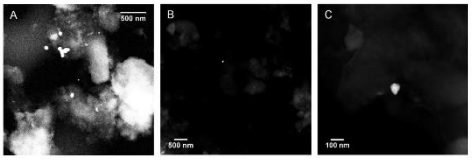

Figure 2. TEM-HAADF images of Ag-b-NPs after CPE of samples initially containing 500 ng L^{-1} (A), 50 ng L^{-1} (B), and 5 ng L^{-1} (C) nanoparticulate Ag from CA@Ag-NPs. Ag-b-NPs were detected in every sample and confirmed by EDX measurements (not shown).

Repetitive Cloud Point Extraction in Ultrapure Water. In order to further improve the enrichment factor during CPE, CPE was performed as a repetitive CPE (rCPE), in this case CPE was repeated five times ($rCPE_5$). The recovery rates of $rCPE_5$ of CA@AgNPs, Ag_2S-NPs (type II), and Ag_2S-NPs (type I) at a final silver concentration of β_{Ag} = 5 ng L^{-1} and β_{Ag} = 50 ng L^{-1}, respectively, in ultrapure water (UPW) are presented in Table 2. Both nanoparticulate Ag concentrations

https://dx.doi.org/10.1021/acs.est.0c02878
Environ. Sci. Technol. 2020, 54, 12063−12071

Table 2. Recovery Rates of Ag-b-NPs Conducting $rCPE_5$ at an Initial Concentration of β_{Ag} = 5 ng L^{-1} and 50 ng L^{-1}, Respectively

NPs	recovery rates (%)	
	β_{Ag} = 5 ng L^{-1}	β_{Ag} = 50 ng L^{-1}
CA@Ag-NPs	89 ± 4	100 ± 6
Ag_2S-NPs (type II)	83 ± 4	83 ± 4
Ag_2S-NPs (type I)	77 ± 2	73 ± 1

were extracted equally well. However, a higher degree of nanoparticle sulfidation showed slightly lower recovery rates than for core silver nanoparticles. The nanoparticle size and composition were not affected by the extraction method, as demonstrated by sp-ICP-MS and TEM-EDX measurements (Figures 3 and S9). The detailed procedure for the TEM grid preparation is described in a video[54] and in the Materials and Methods section (Development and optimization of a centrifugation technique for subsequent visualization of Ag-b-NPs with TEM-EDX). Particles of all sizes were extracted equally well. In order to achieve a further increase in the enrichment factors, which would be beneficial for visualizing Ag-b-NPs using TEM, $rCPE_5$ was run six times in parallel (6 × $rCPE_5$). However, the TEM measurements conducted on samples prepared after $rCPE_5$ and 6 × $rCPE_5$ (whereas all six extracts were centrifuged one after another onto a single TEM grid) were very comparable. Treating the grid several times with a CPE extract as described above may also lead to unproducible redispersion of Ag-b-NPs from the grid. This means that conducting only $rCPE_5$—without running it six times in parallel—ensures a preconcentration sufficient for visualizing Ag-b-NPs down to an environmentally relevant concentration of β_{Ag} = 5 ng L^{-1} using TEM (-EDX) measurements and without a major search effort.

Repetitive Cloud Point Extraction in River Surface Water. In order to investigate the robustness and applicability of $rCPE_5$ using actual environmental water samples, $rCPE_5$ was conducted with river surface water samples. Surface water sample characteristics such as pH, TOC, and O_2 content are shown in the SI (Table S1). The water samples revealed Ag-b-NP concentrations of β_{Ag} = 0.34 ± 0.04 ng L^{-1} (LOD was 0.03 ± 0.01 ng L^{-1} after $rCPE_5$). However, sp-ICP-MS measurements showed no particle signals, indicating that no particles >8 nm were present in the samples. The river water was spiked with Ag_2S-NPs (type I) at a final concentration of β_{Ag} = 5 ng L^{-1}. Subsamples of the aforementioned river water were subjected to $rCPE_5$, and subsequent ICP-MS measurements showed recovery rates of 65 ± 15%, indicating that most particles of the original sample were successfully extracted. The particle size and composition were not affected by the extraction technique (Figures 4 and 5). As with the model-systems in ultrapure water, particles of each size were extracted equally well, which shows that the environmental water matrix does not influence the extraction efficiency (Figure 5). These findings show the huge potential of this method for particle size and composition determination in environmental samples with sp-ICP-MS and TEM-EDX measurements, because it is able to provide this information at environmentally relevant concentrations and in complex environmental matrices. The size, shape, and chemical composition of nanoparticles are the key parameters in determining their environmental fate,

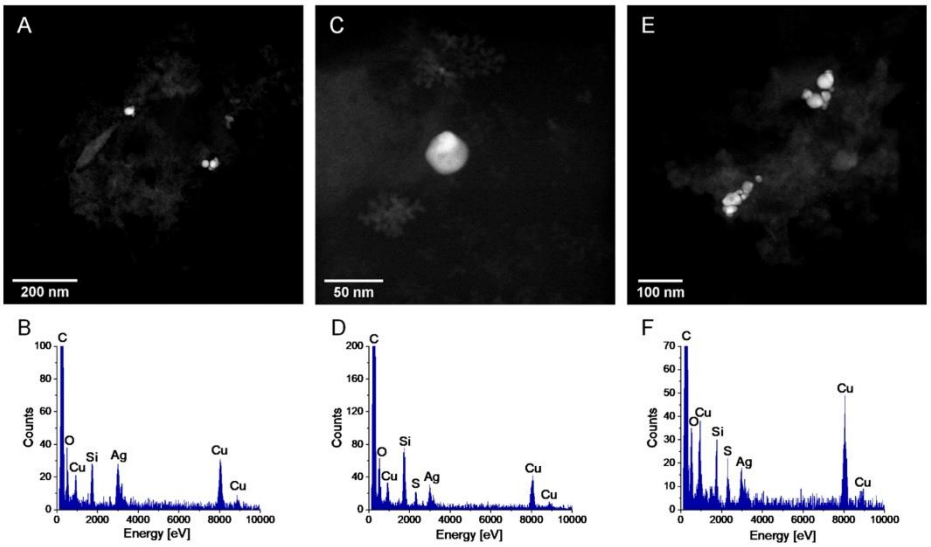

Figure 3. TEM-HAADF images and corresponding EDX spectra of CA@Ag-NPs (A, B), Ag_2S-NPs (type II) (C, D), and Ag_2S-NPs (type I) (E, F) at an environmental relevant silver concentration of β_{Ag} = 5 ng L^{-1} after $rCPE_5$ conducted in UPW. Additional C-, O-, Si-, and Cu-signals in the spectrum result from the sample carrier (copper grid with carbon film), and carbohydrate contamination during TEM measurement and residues from CPE chemicals.

https://dx.doi.org/10.1021/acs.est.0c02878
Environ. Sci. Technol. 2020, 54, 12063−12071

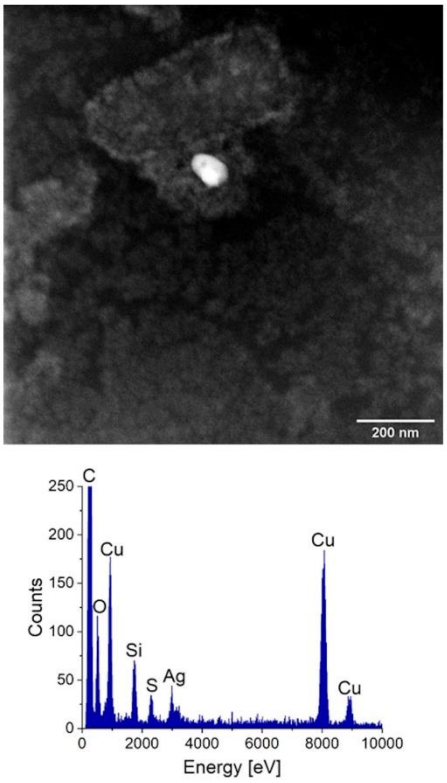

Figure 4. TEM-HAADF image and corresponding EDX spectrum of Ag_2S-NPs (type I) spiked to a river water sample (river Isarkanal) after $rCPE_5$ from samples originally containing 5 ng L^{-1} Ag. Additional C-, O-, Si-, and Cu-signals in the spectrum resulted from the sample carrier (copper grid with carbon film), carbohydrate contamination during illumination, residues from CPE chemicals and natural organic matter (NOM) residues from the environmental water sample.

possible transformations, and ecotoxicity, thus underlining the tremendous potential of the approach presented.

Environmental Impact. A proper risk assessment of the fate, transformations and ecotoxicity of NPs in the environment calls for essential information about particle size, shape, and chemical composition at environmentally relevant concentrations (ng L^{-1}) in complex environmental matrices. We hope that our presented approach can contribute to a comprehensive discussion on environmental concerns regarding the release, fate, possible transformations, and ecotoxicity of Ag-b-NPs in the environment. We hope the presented approach finds its way towards a standard procedure for the determination of nanoparticles in environmental samples, as it may also easily be adapted for the determination of other metal containing nanoparticles or even, e.g., micro- and nanoplastics.

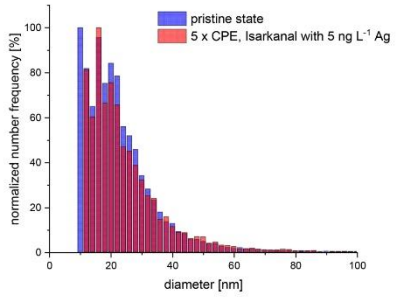

Figure 5. Comparison of particle size distributions of Ag_2S-NPs (type I) spiked to a river water sample (Isarkanal river) after $rCPE_5$ at a concentration of c(Ag) = 5 ng L^{-1} and of Ag_2S-NPs (type I) before $rCPE_5$ (pristine state). The size distributions presented are based on normalized particle number frequencies obtained by sp-ICP-MS measurements.

■ ASSOCIATED CONTENT

Supporting Information

The Supporting Information is available free of charge at https://pubs.acs.org/doi/10.1021/acs.est.0c02878.

Particle size distributions, TEM images, and EDX spectra of Ag-b-NPs; TEM images of the development of the centrifugation approach; and environmental water sample characteristics (PDF)

■ AUTHOR INFORMATION

Corresponding Author

Michael Schuster − *Division of Analytical Chemistry, Department of Chemistry, Technical University of Munich, Garching 85748, Germany*; Phone: +49 (0)89 289 13763; Email: michael.schuster@tum.de; Fax: +49 (0)89 289 14513

Authors

Alexander Urstoeger − *Division of Analytical Chemistry, Department of Chemistry, Technical University of Munich, Garching 85748, Germany*; orcid.org/0000-0003-1911-5070

Andreas Wimmer − *Division of Analytical Chemistry, Department of Chemistry, Technical University of Munich, Garching 85748, Germany*; orcid.org/0000-0002-1746-8932

Ralf Kaegi − *Eawag, Swiss Federal Institute of Aquatic Science and Technology, Dübendorf 8600, Switzerland*; orcid.org/0000-0002-2430-4733

Simon Reiter − *Division of Analytical Chemistry, Department of Chemistry, Technical University of Munich, Garching 85748, Germany*

Complete contact information is available at: https://pubs.acs.org/10.1021/acs.est.0c02878

Author Contributions

[$]These authors contributed equally to the present study. M. Schuster supervised the study. A. Urstoeger designed the study and its experimental setup. A. Urstoeger carried out the synthesis of the Ag-*b*-NPs, rCPE studies and river water sampling and all corresponding analytical measurements

assisted by S. Reiter. A. Urstoeger evaluated the acquired measurement data. R. Kaegi developed the on-grid centrifugation technique. A. Wimmer carried out the adjustment and optimization of the on-grid centrifugation technique to CPE and developed the washing procedure. R. Kaegi carried out TEM-EDX measurements. A. Urstoeger, assisted by A. Wimmer, and R. Kaegi evaluated and discussed TEM-EDX measurements. A. Urstoeger, A. Wimmer, R. Kaegi and M. Schuster wrote the manuscript.

Funding

This research project was financed by the Bavarian State Ministry for the Environment and Consumer Protection (TNT01NaT-73602)

Notes

The authors declare no competing financial interest.

■ ACKNOWLEDGMENTS

The authors gratefully acknowledge COST Action ES1205, supported by COST (European Cooperation in Science and Technology), and especially Dr. Lars Duester for triggering and enabling the international cooperation.

■ REFERENCES

(1) Kessler, R. Engineered Nanoparticles in Consumer Products: Understanding a New Ingredient. *Environ. Health Perspect.* **2011**, *119*, A120−A125.

(2) Benn, T.; Cavanagh, B.; Hristovski, K.; Posner, J. D.; Westerhoff, P. The Release of Nanosilver from Consumer Products Used in the Home. *J. Environ. Qual.* **2010**, *39*, 1875−1882.

(3) Duncan, T. V. Applications of Nanotechnology in Food Packaging and Food Safety: Barrier Materials, Antimicrobials and Sensors. *J. Colloid Interface Sci.* **2011**, *363*, 1−24.

(4) Kim, B.; Park, C.-S.; Murayama, M.; Hochella, M. F. Discovery and Characterization of Silver Sulfide Nanoparticles in Final Sewage Sludge Products. *Environ. Sci. Technol.* **2010**, *44*, 7509−7514.

(5) Soenen, S. J.; Parak, W. J.; Rejman, J.; Manshian, B. (Intra)cellular Stability of Inorganic Nanoparticles: Effects on Cytotoxicity, Particle Functionality, and Biomedical Applications. *Chem. Rev.* **2015**, *115*, 2109−2135.

(6) Stark, W. J.; Stoessel, P. R.; Wohlleben, W.; Hafner, A. Industrial Applications of Nanoparticles. *Chem. Soc. Rev.* **2015**, *44*, 5793−5805.

(7) Sharma, V. K.; Filip, J.; Zboril, R.; Varma, R. S. Natural Inorganic Nanoparticles - Formation, Fate, and Toxicity in the Environment. *Chem. Soc. Rev.* **2015**, *44*, 8410−8423.

(8) Mueller, N. C.; Nowack, B. Exposure Modeling of Engineered Nanoparticles in the Environment. *Environ. Sci. Technol.* **2008**, *42*, 4447−4453.

(9) Kaegi, R.; Sinnet, B.; Zuleeg, S.; Hagendorfer, H.; Mueller, E.; Vonbank, R.; Boller, M.; Burkhardt, M. Release of Silver Nanoparticles from Outdoor Facades. *Environ. Pollut.* **2010**, *158*, 2900−2905.

(10) Benn, T. M.; Westerhoff, P. Nanoparticle Silver Released into Water from Commercially Available Sock Fabrics. *Environ. Sci. Technol.* **2008**, *42*, 4133−4139.

(11) Glover, R. D.; Miller, J. M.; Hutchison, J. E. Generation of Metal Nanoparticles from Silver and Copper Objects: Nanoparticle Dynamics on Surfaces and Potential Sources of Nanoparticles in the Environment. *ACS Nano* **2011**, *5*, 8950−8957.

(12) Tiede, K.; Boxall, A. B. A.; Wang, X.; Gore, D.; Tiede, D.; Baxter, M.; David, H.; Tear, S. P.; Lewis, J. Application of Hydrodynamic Chromatography-ICP-MS to Investigate the Fate of Silver Nanoparticles in Activated Sludge. *J. Anal. At. Spectrom.* **2010**, *25*, 1149−1154.

(13) Li, L.; Stoiber, M.; Wimmer, A.; Xu, Z.; Lindenblatt, C.; Helmreich, B.; Schuster, M. To What Extent Can Full-Scale Wastewater Treatment Plant Effluent Influence the Occurrence of Silver-Based Nanoparticles in Surface Waters? *Environ. Sci. Technol.* **2016**, *50*, 6327−6333.

(14) Kaegi, R.; Voegelin, A.; Ort, C.; Sinnet, B.; Thalmann, B.; Krismer, J.; Hagendorfer, H.; Elumelu, M.; Mueller, E. Fate and Transformation of Silver Nanoparticles in Urban Wastewater Systems. *Water Res.* **2013**, *47*, 3866−3877.

(15) Kampe, S.; Kaegi, R.; Schlich, K.; Wasmuth, C.; Hollert, H.; Schlechtriem, C. Silver Nanoparticles in Sewage Sludge: Bioavailability of Sulfidized Silver to the Terrestrial Isopod Porcellio Scaber. *Environ. Toxicol. Chem.* **2018**, *37*, 1606−1613.

(16) Wimmer, A.; Kalinnik, A.; Schuster, M. New Insights into the Formation of Silver-based Nanoparticles under Natural and Semi-Natural Conditions. *Water Res.* **2018**, *141*, 227−234.

(17) Levard, C.; Hotze, E. M.; Lowry, G. V.; Brown, G. E. Environmental Transformations of Silver Nanoparticles: Impact on Stability and Toxicity. *Environ. Sci. Technol.* **2012**, *46*, 6900−6914.

(18) Wijnhoven, S. W. P.; Peijnenburg, W. J. G. M.; Herberts, C. A.; Hagens, W. I.; Oomen, A. G.; Heugens, E. H. W.; Roszek, B.; Bisschops, J.; Gosens, I.; Van De Meent, D.; Dekkers, S.; De Jong, W. H.; van Zijverden, M.; Sips, A. J. A. M.; Geertsma, R. E. Nano-Silver - a Review of Available Data and Knowledge Gaps in Human and Environmental Risk Assessment. *Nanotoxicology* **2009**, *3*, 109−138.

(19) Lekamge, S.; Miranda, A. F.; Abraham, A.; Li, V.; Shukla, R.; Bansal, V.; Nugegoda, D. The Toxicity of Silver Nanoparticles (AgNPs) to Three Freshwater Invertebrates With Different Life Strategies: Hydra Vulgaris, Daphnia Carinata, and Paratya Australiensis. *Front. Environ. Sci.* **2018**, *6* DOI: 10.3389/fenvs.2018.00152.

(20) Asharani, P. V.; Lian Wu, Y.; Gong, Z.; Valiyaveettil, S. Toxicity of Silver Nanoparticles in Zebrafish Models. *Nanotechnology* **2008**, *19*, 255102.

(21) Cho, Y.-M.; Mizuta, Y.; Akagi, J.-I.; Toyoda, T.; Sone, M.; Ogawa, K. Size-Dependent Acute Toxicity of Silver Nanoparticles in Mice. *J. Toxicol. Pathol.* **2018**, *31*, 73−80.

(22) Kumar, V.; Sharma, N.; Maitra, S. S. In Vitro and In Vivo Toxicity Assessment of Nanoparticles. *Int. Nano Lett.* **2017**, *7*, 243−256.

(23) Hajipour, M. J.; Fromm, K. M.; Akbar Ashkarran, A.; Jimenez de Aberasturi, D.; de Larramendi, I. R.; Rojo, T.; Serpooshan, V.; Parak, W. J.; Mahmoudi, M. Antibacterial Properties of Nanoparticles. *Trends Biotechnol.* **2012**, *30*, 499−511.

(24) Pal, S.; Tak, Y. K.; Song, J. M. Does the Antibacterial Activity of Silver Nanoparticles Depend on the Shape of the Nanoparticle? A Study of the Gram-Negative Bacterium Escherichia Coli. *Appl. Environ. Microbiol.* **2007**, *73*, 1712−1720.

(25) Shrivastava, S.; Bera, T.; Roy, A.; Singh, G.; Ramachandrarao, P.; Dash, D. Characterization of Enhanced Antibacterial Effects of Novel Silver Nanoparticles. *Nanotechnology* **2007**, *18*, 225103.

(26) Navarro, E.; Baun, A.; Behra, R.; Hartmann, N. B.; Filser, J.; Miao, A. J.; Quigg, A.; Santschi, P. H.; Sigg, L. Environmental Behavior and Ecotoxicity of Engineered Nanoparticles to Algae, Plants, and Fungi. *Ecotoxicology* **2008**, *17*, 372−386.

(27) Yan, A.; Chen, Z. Impacts of Silver Nanoparticles on Plants: A Focus on the Phytotoxicity and Underlying Mechanism. *Int. J. Mol. Sci.* **2019**, *20*, 1003.

(28) Asharani, P. V.; Low Kah Mun, G.; Hande, M. P.; Valiyaveettil, S. Cytotoxicity and Genotoxicity of Silver Nanoparticles in Human Cells. *ACS Nano* **2009**, *3*, 279−290.

(29) Haase, A.; Tentschert, J.; Jungnickel, H.; Graf, P.; Mantion, A.; Draude, F.; Plendl, J.; Goetz, M. E.; Galla, S.; Mašić, A.; Thuenemann, A. F.; Taubert, A.; Arlinghaus, H. F.; Luch, A. Toxicity of Silver Nanoparticles in Human Macrophages: Uptake, Intracellular Distribution and Cellular Responses. *J. Phys.: Conf. Ser.* **2011**, *304*, 012030.

(30) Lu, W.; Senapati, D.; Wang, S.; Tovmachenko, O.; Singh, A. K.; Yu, H.; Ray, P. C. Effect of Surface Coating on the Toxicity of Silver Nanomaterials on Human Skin Keratinocytes. *Chem. Phys. Lett.* **2010**, *487*, 92−96.

(31) Park, M. V. D. Z.; Neigh, A. M.; Vermeulen, J. P.; de la Fonteyne, L. J. J.; Verharen, H. W.; Briedé, J. J.; van Loveren, H.; de

Jong, W. H. The Effect of Particle Size on the Cytotoxicity, Inflammation, Developmental Toxicity and Genotoxicity of Silver Nanoparticles. *Biomaterials* **2011**, *32*, 9810−9817.
(32) Sotiriou, G. A.; Pratsinis, S. E. Antibacterial Activity of Nanosilver Ions and Particles. *Environ. Sci. Technol.* **2010**, *44*, 5649−5654.
(33) Levard, C.; Hotze, E. M.; Colman, B. P.; Dale, A. L.; Truong, L.; Yang, X. Y.; Bone, A. J.; Brown, G. E., Jr.; Tanguay, R. L.; Di Giulio, R. T.; Bernhardt, E. S.; Meyer, J. N.; Wiesner, M. R.; Lowry, G. V. Sulfidation of Silver Nanoparticles: Natural Antidote to their Toxicity. *Environ. Sci. Technol.* **2013**, *47*, 13440−13448.
(34) Levard, C.; Reinsch, B. C.; Michel, F. M.; Oumahi, C.; Lowry, G. V.; Brown, G. E. Sulfidation Processes of PVP-coated Silver Nanoparticles in Aqueous Solution: Impact on Dissolution Rate. *Environ. Sci. Technol.* **2011**, *45*, 5260−5266.
(35) Kaegi, R.; Voegelin, A.; Sinnet, B.; Zuleeg, S.; Hagendorfer, H.; Burkhardt, M.; Siegrist, H. Behavior of Metallic Silver Nanoparticles in a Pilot Wastewater Treatment Plant. *Environ. Sci. Technol.* **2011**, *45*, 3902−3908.
(36) Kaegi, R.; Voegelin, A.; Sinnet, B.; Zuleeg, S.; Siegrist, H.; Burkhardt, M. Transformation of AgCl Nanoparticles in a Sewer System - A field study. *Sci. Total Environ.* **2015**, *535*, 20−27.
(37) Nowack, B. Nanosilver Revisited Downstream. *Science* **2010**, *330*, 1054−1055.
(38) Nowack, B.; Ranville, J. F.; Diamond, S.; Gallego-Urrea, J. A.; Metcalfe, C.; Rose, J.; Horne, N.; Koelmans, A. A.; Klaine, S. J. Potential Scenarios for Nanomaterial Release and Subsequent Alteration in the Environment. *Environ. Toxicol. Chem.* **2012**, *31*, 50−59.
(39) Wimmer, A.; Urstoeger, A.; Funck, N. C.; Adler, F. P.; Lenz, L.; Doeblinger, M.; Schuster, M. What Happens to Silver-based Nanoparticles if They Meet Seawater? *Water Res.* **2020**, *171*, 115399.
(40) Champion, J. A.; Mitragotri, S. Role of Target Geometry in Phagocytosis. *Proc. Natl. Acad. Sci. U. S. A.* **2006**, *103*, 4930−4934.
(41) Stalikas, C. D. Micelle-mediated Extraction as a Tool for Separation and Preconcentration in Metal Analysis. *TrAC, Trends Anal. Chem.* **2002**, *21*, 343−355.
(42) Quina, F. H.; Hinze, W. L. Surfactant-mediated Cloud Point Extractions: An Environmentally Benign Alternative Separation Approach. *Ind. Eng. Chem. Res.* **1999**, *38*, 4150−4168.
(43) Liu, J.-F.; Chao, J.-b.; Liu, R.; Tan, Z.-q.; Yin, Y.-g.; Wu, Y.; Jiang, G.-b. Cloud Point Extraction as an Advantageous Preconcentration Approach for Analysis of Trace Silver Nanoparticles in Environmental Waters. *Anal. Chem.* **2009**, *81*, 6496−6502.
(44) Chao, J. B.; Liu, J. F.; Yu, S. J.; Feng, Y. D.; Tan, Z. Q.; Liu, R.; Yin, Y. G. Speciation Analysis of Silver Nanoparticles and Silver Ions in Antibacterial Products and Environmental Waters via Cloud Point Extraction-based Separation. *Anal. Chem.* **2011**, *83*, 6875−6882.
(45) Hartmann, G.; Hutterer, C.; Schuster, M. Ultra-Trace Determination of Silver Nanoparticles in Water Samples Using Cloud Point Extraction and ETAAS. *J. Anal. At. Spectrom.* **2013**, *28*, 567−572.
(46) Hartmann, G.; Baumgartner, T.; Schuster, M. Influence of Particle Coating and Matrix Constituents on the Cloud Point Extraction Efficiency of Silver Nanoparticles (Ag-NPs) and Application for Monitoring the Formation of Ag-NPs from Ag^+. *Anal. Chem.* **2014**, *86*, 790−796.
(47) Wimmer, A.; Ritsema, R.; Schuster, M.; Krystek, P. Sampling and Pre-Treatment Effects on the Quantification of (Nano)silver and Selected Trace Elements in Surface Water - Application in a Dutch Case Study. *Sci. Total Environ.* **2019**, *663*, 154−161.
(48) Peters, R. J.; Rivera, Z. H.; van Bemmel, G.; Marvin, H. J.; Weigel, S.; Bouwmeester, H. Development and Validation of Single Particle ICP-MS for Sizing and Quantitative Determination of Nano-Silver in Chicken Meat. *Anal. Bioanal. Chem.* **2014**, *406*, 3875−3885.
(49) Montaño, M. D.; Olesik, J. W.; Barber, A. G.; Challis, K.; Ranville, J. F. Single Particle ICP-MS: Advances Toward Routine Analysis of Nanomaterials. *Anal. Bioanal. Chem.* **2016**, *408*, 5053−5074.
(50) Pettibone, J. M.; Liu, J. In Situ Methods for Monitoring Silver Nanoparticle Sulfidation in Simulated Waters. *Environ. Sci. Technol.* **2016**, *50*, 11145−11153.
(51) Duester, L.; Fabricius, A. L.; Jakobtorweihen, S.; Philippe, A.; Weigl, F.; Wimmer, A.; Schuster, M.; Nazar, M. F. Can Cloud Point-based Enrichment, Preservation, and Detection Methods Help to Bridge Gaps in Aquatic Nanometrology? *Anal. Bioanal. Chem.* **2016**, *408*, 7551−7557.
(52) Mavrocordatos, D.; Perret, D. Non-artifacted Specimen Preparation for Transmission Electron Microscopy of Submicron Soil Particles. *Commun. Soil Sci. Plant Anal.* **1995**, *26*, 2593−2602.
(53) Prasad, A.; Lead, J. R.; Baalousha, M. An Electron Microscopy Based Method for the Detection and Quantification of Nanomaterial Number Concentration in Environmentally Relevant Media. *Sci. Total Environ.* **2015**, *537*, 479−486.
(54) How To Prepare a TEM Sample by Centrifugation. https://www.youtube.com/watch?v=PplBlJ7zCCA (accessed 2020).

https://dx.doi.org/10.1021/acs.est.0c02878
Environ. Sci. Technol. 2020, 54, 12063−12071

Supplementary Information

Looking at Silver-Based Nanoparticles in Environmental Water Samples: Repetitive Cloud Point Extraction Bridges Gaps in Electron Microscopy for Naturally Occurring Nanoparticles

Alexander Urstoeger,[†,§] *Andreas Wimmer,*[†,§] *Ralf Kaegi,*[‡] *Simon Reiter,*[†] *Michael Schuster*[*,†]

[†]Division of Analytical Chemistry, Department of Chemistry, Technical University of Munich, Lichtenbergstraße 4, Garching 85748, Germany

[‡]Eawag, Swiss Federal Institute of Aquatic Science and Technology, Überlandstrasse 133, Dübendorf 8600, Switzerland

[§]These authors contributed equally to the present study.

Corresponding author. *Tel: +49 (0)89 289 13763; fax: +49 (0)89 289 14513; email address: michael.schuster@tum.de

8 pages

9 figures

1 table

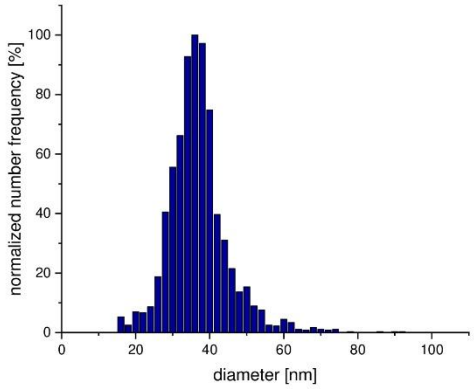

Figure S1. Particle size distribution of CA@Ag-NPs based on normalized particle number frequency obtained by sp-ICP-MS measurement. The most frequent diameter was 36 nm, and the average diameter was 35 nm.

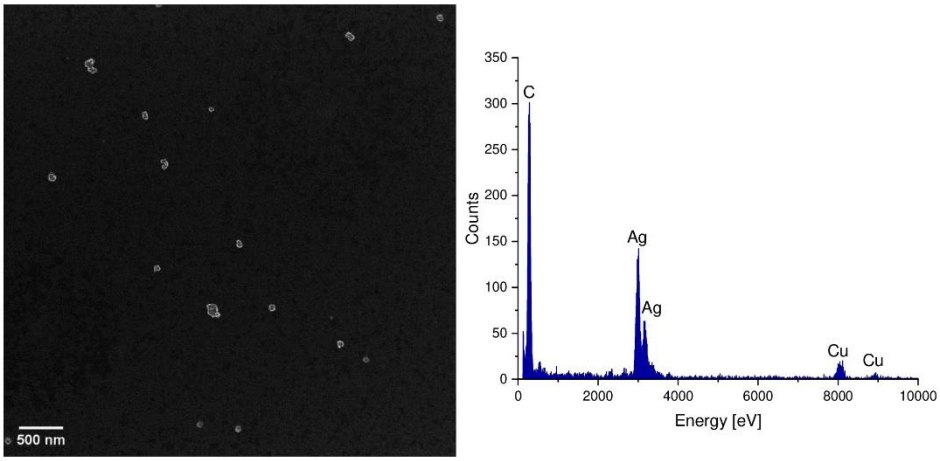

Figure S2. TEM-SE image of CA@Ag-NPs and the corresponding EDX spectrum. Additional C- and Cu-signals in the spectrum result from the sample carrier (copper grid with carbon film) and carbohydrate contamination during TEM measurements.

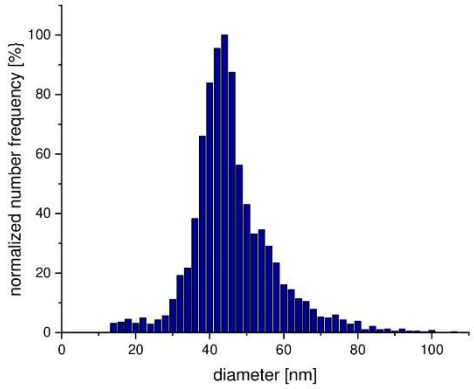

Figure S3. Particle size distribution of Ag2S-NPs (type II) based on normalized particle number frequency obtained by sp-ICP-MS measurement. The most frequent diameter was 44 nm, and the average diameter was 43 nm.

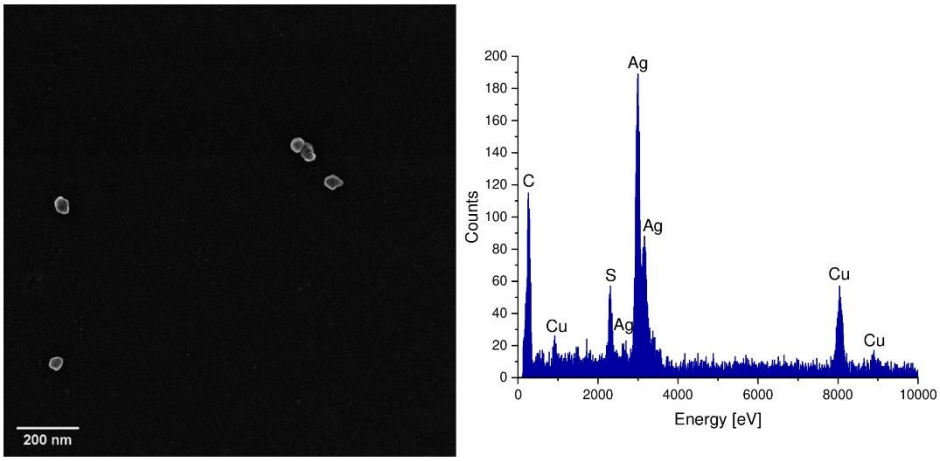

Figure S4. TEM-SE image of Ag_2S-NPs (type II) and EDX spectrum. Additional C- and Cu-signals in the spectrum result from the sample carrier (copper grid with carbon film) and carbohydrate contamination during TEM measurements.

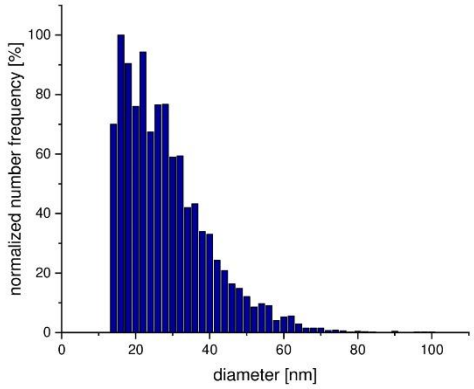

Figure S5. Particle size distribution of Ag_2S-NPs (type I) based on normalized particle number frequency obtained by sp-ICP-MS measurement. The most frequent diameter was 18 nm, and the average diameter was 25 nm.

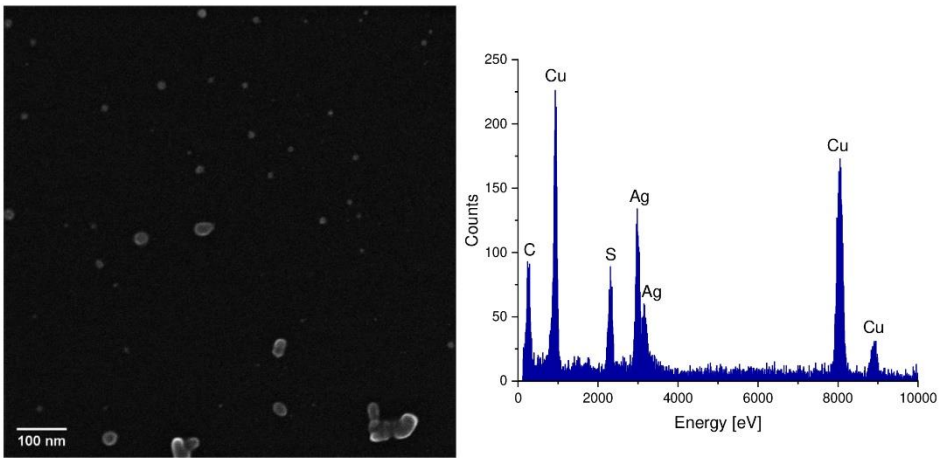

Figure S6. TEM-SE image of Ag2S-NPs (type I) and the corresponding EDX spectrum. Additional C- and Cu-signals in the spectrum result from the sample carrier (copper grid with carbon film) and carbohydrate contamination during TEM measurements.

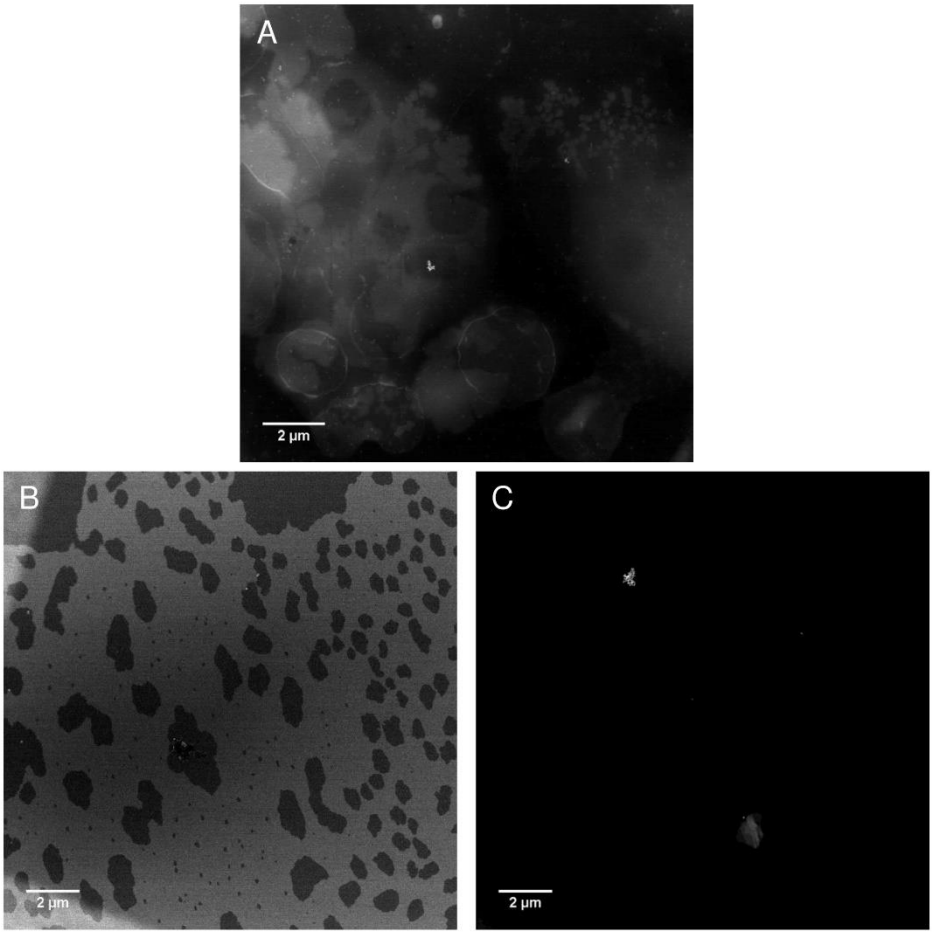

Figure S7: TEM-HAADF (A, C) and TEM-SE (B) images of samples containing CA@Ag-NPs in UPW. All samples were subjected to CPE, whereas the CPE extract was applied without added EtOH (A) and after mixing with EtOH (B, C) to the TEM grid. C represents the same sample as B but another image area and magnification. Particles visible in A and C represent Ag-b-NPs as confirmed by EDX measurements (not shown).

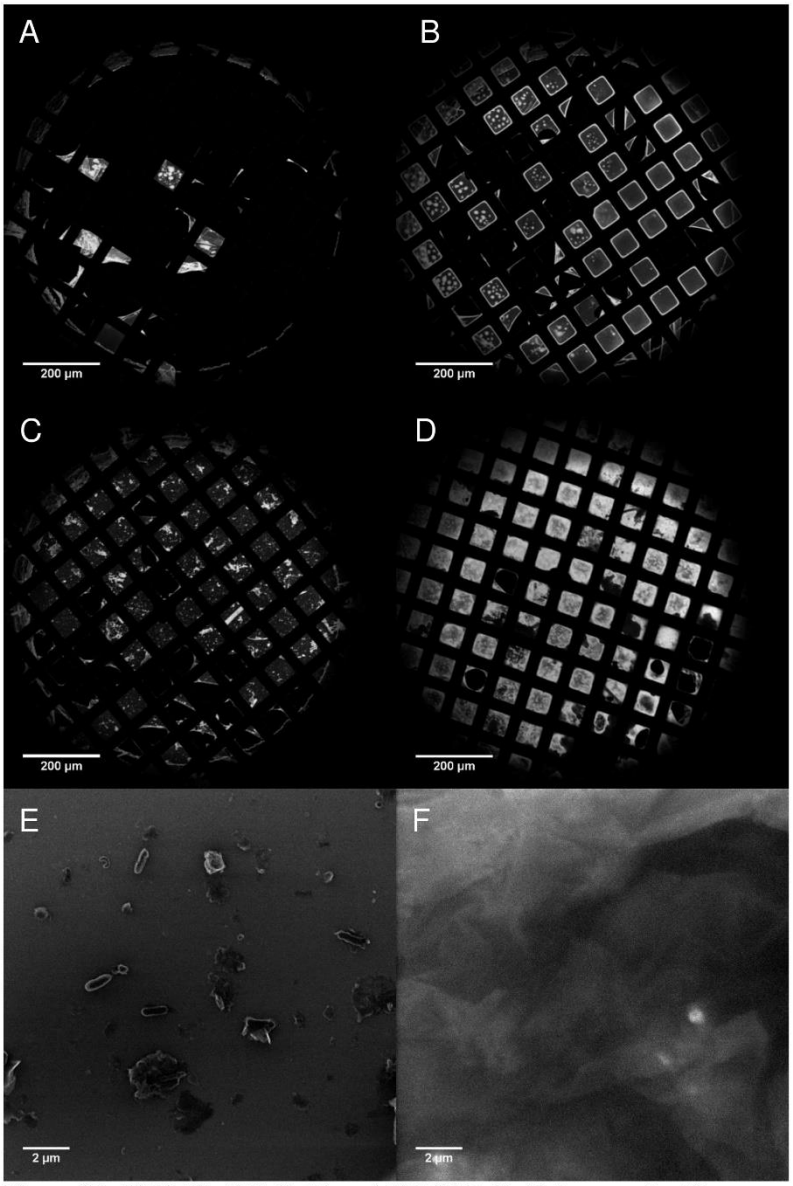

Figure S8: TEM-HAADF (A-D) and TEM-SE (E, F) images of grids prepared from CPE extracts of UPW (A, B) and river water samples (C-F). During grid preparation, washing was performed with EtOH (A, C, E) or cyclohexane (B, D, F), respectively.

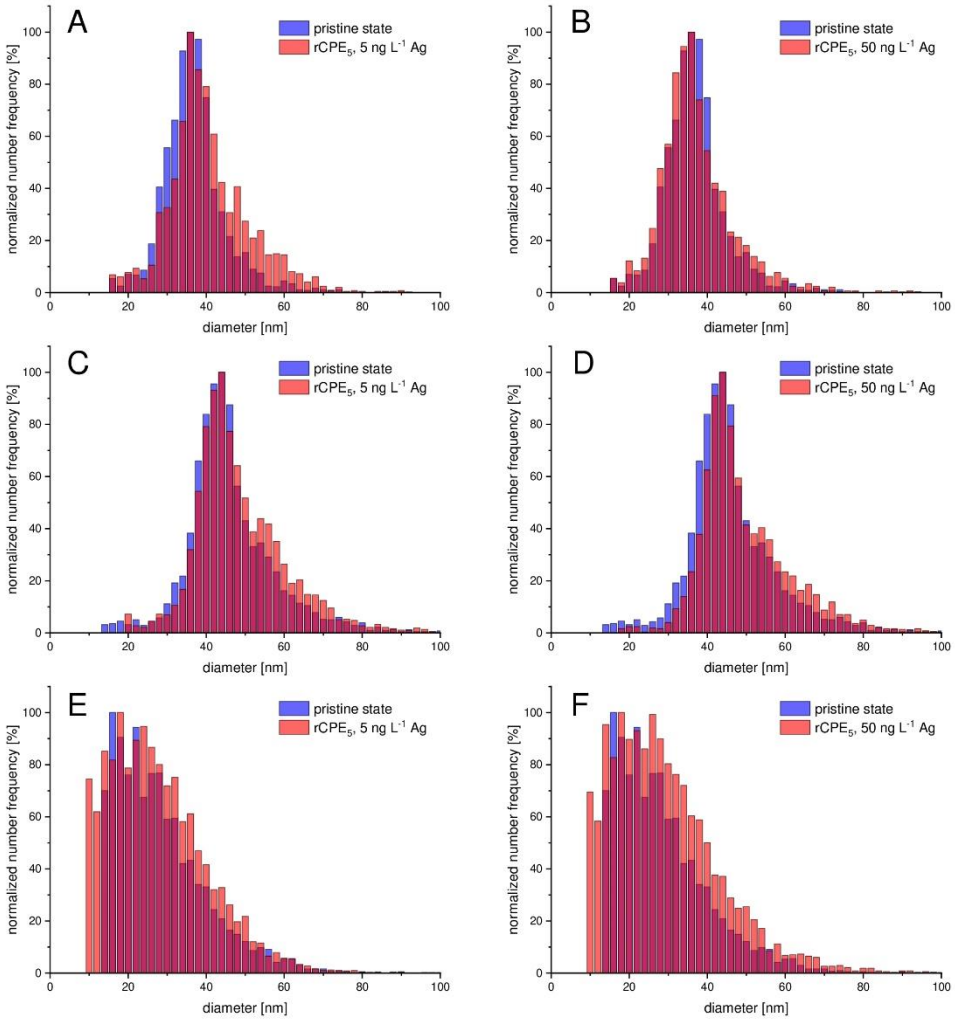

Figure S9. Comparison of particle size distributions of CA@Ag-NPs (A, B), Ag_2S-NPs (type II) (C, D), and Ag_2S-NPs (type I) (E, F) after rCPE5 with concentrations of c(Ag) = 5 ng L^{-1} as well as c(Ag) = 50 ng L^{-1} and the Ag-b-NPs before rCPE5 (pristine state). The size distributions presented are based on normalized particle number frequencies obtained by sp-ICP-MS measurements.

62 **Table S1. Characteristics of water samples collected from the Isarkanal river and TOC**
63 **content of a composite sample containing all samples to equal amounts.**

Sample number	pH	TOC [mg L^{-1}]	O_2 content [mg L^{-1}]
1	8.33		12.89
2	8.33		12.71
3	8.34		12.44
4	8.32		12.35
5	8.33		12.41
6	8.33		12.60
Composite sample		9.88 ± 0.38	

64

8.4. Publikation 4

What happens to silver-based nanoparticles if they meet seawater?

Andreas Wimmer [a,1], Alexander Urstoeger [a,1], Nils Christoph Funck [a], Franziska Petra Adler [a], Leonhard Lenz [a], Markus Doeblinger [b], Michael Schuster [a,*]

[a] Division of Analytical Chemistry, Department of Chemistry, Technical University of Munich, Lichtenbergstraße 4, 85748, Garching, Germany

[b] Department of Chemistry, Ludwig-Maximilians-Universität München, Butenandtstr. 5-13 (E), Munich, 81377, Germany

* Corresponding author

E-Mail: michael.schuster@tum.de

[1] These authors contributed equally to the present study

Abdruck des Artikels mit Genehmigung von Elsevier (siehe Kapitel 7.7) aus

Water Research, 2020, 171, 115399.

Water Research 171 (2020) 115399

Contents lists available at ScienceDirect

Water Research

journal homepage: www.elsevier.com/locate/watres

What happens to silver-based nanoparticles if they meet seawater?

Andreas Wimmer [a, 1], Alexander Urstoeger [a, 1], Nils Christoph Funck [a], Franziska Petra Adler [a], Leonhard Lenz [a], Markus Doeblinger [b], Michael Schuster [a, *]

[a] Division of Analytical Chemistry, Department of Chemistry, Technical University of Munich, Lichtenbergstraße 4, Garching, 85748, Germany
[b] Department of Chemistry, Ludwig-Maximilians-Universität München, Butenandtstr. 5–13 (E), Munich, 81377, Germany

ARTICLE INFO

Article history:
Received 1 September 2019
Received in revised form
18 November 2019
Accepted 14 December 2019
Available online 19 December 2019

Keywords:
Silver nanoparticles
Fate
Seawater
Cloud point extraction
Single particle inductively coupled plasma mass spectrometry
Electron microscopy

ABSTRACT

Silver based nanoparticles (Ag-b-NPs) in the environment are of current concern as they may pose risks to human and environmental health, even at low concentration levels. It is widely known that Ag-b-NPs, once released from products containing these particles for antimicrobial reasons, can pass through wastewater treatment plants to some extent. These particles are transported via running waterways and eventually reach the sea. However, the fate of environmentally relevant ng L^{-1} traces of Ag-b-NPs in seawater has not yet been sufficiently studied. Analytical techniques capable of determining these ultratraces of Ag-b-NPs in seawater are scarce and struggle furthermore with the high chloride content in highly saline matrices, such as seawater. In this study, we extracted Ag-b-NPs from matrices with varying salinity via cloud point extraction (CPE) and determined concentration and size of Ag-b-NPs in extracts with single particle inductively coupled plasma mass spectrometry (sp-ICP-MS). Applying this extraction and measurement technique, we were able to investigate the fate of Ag-b-NPs with different coatings (citrate and the predominant coatings in nature, silver sulfide and silver chloride) in matrices with increasing salinity and real seawater. All types of Ag-b-NPs were dissolved in all matrices almost independently of the chemical composition of the nanoparticles (NPs), whereas dissolution rates increased with increasing salinity due to the formation of soluble Ag(I) species and - in the presence of chloride - $AgCl_x^{1-x}$ ($x > 1$) complexes. After an incubation time of not more than 72 h, Ag-b-NPs were dissolved almost completely. During the dissolution process, NP shrinkage could be clearly observed by sp-ICP-MS. Supplementary electron microscopy measurements revealed that the sulfur content in silver sulfide nanoparticles (Ag_2S-NPs) increased during the dissolution process. Finally, we were able to investigate the dissolution process of real Ag-b-NPs in wastewater after increasing the salinity to seawater levels.

1. Introduction

Due to the growing use of silver nanoparticles (Ag-NPs) in commercially available products and applications, such as food storage containers, sporting goods, fabrics, food additives in animal feed, cosmetics, medical devices and many others (Kim et al., 2010; Peters et al., 2014), these nanoparticles are increasingly released into the environment. This has intensified the discussion about concerns regarding environmental compatibility of Ag-NPs. Several studies have dealt with the toxicity of silver nanoparticles in organs (Ahamed et al., 2010; Krug, 2014; Kumar et al., 2017; Wiemann et al., 2017) and metabolic pathways (Foldbjerg et al., 2009; Gopinath et al., 2010; Park et al., 2010; Ribeiro et al., 2015; Wise et al., 2010; Zhang et al., 2018). In addition to silver ions generated by dissolution of nanoparticles, Ag-NPs themselves are believed to negatively affect organisms (Asharani et al. 2008, 2009; Beer et al., 2012; Kim et al., 2009; Qian et al., 2013). Silver in this particulate form is believed to surpass even the ecotoxicological hazards of the corresponding bulk material (Hansen and Baun, 2012; Pettitt and Lead, 2013). Therefore, Ag-NPs should be monitored and analyzed in environmental samples in order to understand their fate and distribution in the environment, especially addressing the question of how environmental matrices influence particle dissolution and aggregation (Pasricha et al., 2012).

Once released into the environment, Ag-NPs interact readily with naturally occurring organic and inorganic substances and thus undergo a broad variety of surface modifications, which include adsorption of organic molecules present in the environment or

* Corresponding author.
E-mail address: michael.schuster@tum.de (M. Schuster).
[1] These authors contributed equally to the present study.

https://doi.org/10.1016/j.watres.2019.115399
0043-1354/

reactions with, e.g. dissolved species resulting in Ag_2S or AgCl coatings, whereas Ag_2S dominates environmentally relevant surface modifications (Kaegi et al. 2011, 2013, 2015). Therefore, Ag-NPs in the environment are described hereinafter as silver-based nanoparticles (Ag-b-NPs) so as to take every kind of surface modification into account.

Li et al. showed that over 94.6% of Ag-b-NPs were removed from wastewater treatment plant (WWTP) influent, but still resulted in an Ag-b-NP concentration ranging from 0.7 to 11.1 ng L^{-1} in the effluent released into the environment (Li et al., 2016).

These nanoparticles are transported in rivers and finally reach the sea, and the resulting fate of Ag-b-NPs can be characterized by two main processes: aggregation and dissolution. The Derjaguin–Landau–Verwey–Overbeak (DLVO) theory describes the stability of nanoparticle dispersions in aqueous matrices as an interplay of van der Waals interactions and electrostatic repulsion (Derjaguin and Landau, 1993; Lodeiro et al., 2016; Quik et al., 2014; Verwey, 1947). Once nanoparticles (NPs) are dispersed in matrices of high ionic strength, e.g. seawater, the net charge of the particles deriving from the corresponding electric double layer surrounding the particles is reduced. This results in an increase of remaining attractive forces encouraging attachment and thus aggregation of NPs (Lodeiro et al., 2016). Consequently, it is believed that Ag-b-NPs are not transported long distances in seawater. However, *Toncelli* et al. observed that the dissolution process dominates the fate of Ag-b-NPs in seawater at low concentrations (ng L^{-1} range) completely compensating for a DLVO-type aggregation effect (Toncelli et al., 2017). In general, the dissolution of Ag-b-NPs is best described by a widely accepted model established by Liu and Hurt, (2010). Ag-b-NPs in aqueous matrices undergo a cooperative oxidation process involving dissolved oxygen and protons forming peroxide intermediates and eventually water. Simultaneously, Ag(0) is readily oxidized to dissolved Ag(I), which is encouraged by a relatively low redox gap of −0.8 V (Liu and Hurt, 2010; Toncelli et al., 2017). Liu and Hart did not observe Ag-b-NP dissolution in deoxygenated seawater, and they were able to decrease it at a reduced pH due to an equilibrium shift (Liu and Hurt, 2010). Based on their observations and experiments, Liu and Hurt developed the following equation (Liu and Hurt, 2010):

$$2Ag_{(s)} + \frac{1}{2}O_{2(aq)} + 2H^{+} \leftrightarrow 2Ag^{+}_{(aq)} + H_2O_{(l)} \quad (1)$$

This dissolution process is furthermore influenced by the concentration of Ag-b-NPs and the constituents of natural water bodies like natural organic matter (NOM) and - in the case of seawater - high chloride contents. The dissolution rate is accelerated with decreasing Ag-b-NP concentration (Toncelli et al., 2017). NOM was reported to facilitate dissolution of Ag-b-NPs in aqueous matrices by complexation of Ag(I) and shifting of the equilibrium (Loza et al., 2014). Chloride present in aqueous matrices is able to eventually trap Ag(I) from the cooperative oxidation of Ag(0) to form soluble $AgCl_x^{1-x}$ ($x > 1$) complexes. According to the general rules of reaction equilibrium, this trapping process might accelerate the dissolution in seawater. However, *Liu* et al. reported that an incubation of Ag-b-NPs at mg L^{-1} range in seawater actually slowed down the dissolution process compared to an incubation in UPW. In reality, the higher pH of seawater in contrast to UPW inverts the equilibrium shift induced by the complexation of Ag(I) by Cl^- (Liu and Hurt, 2010). However, especially for low Ag-b-NP concentrations in seawater, this may no longer be the case.

There have been several studies focusing on the fate of Ag-b-NPs in seawater. *Teo* et al. found that the Ag-b-NP dissolution at an initial Ag-b-NP concentration of 0.1 mg L^{-1} was much faster in seawater than in ultra-pure (UPW) water or lake water (Teo and Pumera, 2014). Additionally, for nanoparticle concentrations of 200 ng L^{-1} and 2000 ng L^{-1}, a decrease in size and concentration with increasing time was observed when dispersed in seawater, with the dissolution rate being influenced by the thickness of the particles' coatings (Toncelli et al., 2017). Furthermore, it has been reported that, albeit to a very little extent, Ag-b-NPs can be freshly formed from an interaction of dissolved Ag(I) with NOM (Toncelli et al., 2017). However, the Ag-b-NP concentrations used in those studies were in the sub µg L^{-1} to upper µg L^{-1} range (Lodeiro et al., 2017; Teo and Pumera, 2014; Toncelli et al., 2017), which by far exceeds concentrations found in natural samples, which are typically in the pg L^{-1} to lower ng L^{-1} range (Li et al., 2016; Sun et al., 2016; Wimmer et al., 2018). Furthermore, previous studies on the fate of Ag-b-NPs in seawater used >200 ng L^{-1} of polyethyleneimine and polyvinylpyrrilidone coated Ag-NPs for their experiments (Toncelli et al., 2017), which do not exist in nature. On the contrary, *Kaegi* et al. were able to show that Ag-NPs entering a WWTP are sulfidized to a variable degree independent of their original coating (Kaegi et al. 2011, 2013).

For our work, we used naturally relevant silver nanoparticle modifications, such as silver sulfide, silver chloride and core silver nanoparticles at an environmentally relevant concentration of 50 ng L^{-1}. Our goal was to study the fate and stability of the nanoparticles once they were released into a seawater matrix. The salinity of seawater, which is the mass fraction of dissolved material in seawater, is 35.17 g kg^{-1}. The majority of the salinity is represented by Cl^- at a mass fraction of 19.35 g kg^{-1}, followed by Na^+ with a mass fraction of 10.78 g kg^{-1}, SO_4^{2-} with a mass fraction of 2.71 g kg^{-1} and Mg^{2+} (1.28 g kg^{-1}), Ca^{2+} (0.41 g kg^{-1}), and K^+ (0.40 g kg^{-1}) (Millero et al., 2008). The contribution of NaCl to the total Cl^- content calculated from this data is 85.9%. Such a high salt content causes instrumental problems in ICP-MS measurement, e.g. cone clogging and both spectral and non-spectral interferences. Dilution of the samples helps to avoid these problems, but it also leads to a significant loss of detection power.

We therefore used cloud point extraction (CPE), which is a highly selective separation and enrichment technique enabling Ag-b-NP extraction from complex aqueous solutions regardless of particle coating and without changing particle size and chemical composition (Hartmann et al. 2013, 2014). Dissolved silver, NOM and other particulate matter are tolerated in concentrations up to 100 µg L^{-1}, 100 mg L^{-1} and 0.1 mol L^{-1}, respectively. After CPE, the enriched and separated Ag-b-NPs can be forwarded to ICP-MS measurement for Ag concentration analysis and/or sp-ICP-MS for particle number and size determination.

Our experiments were furthermore supplemented by transmission electron microscopy (TEM) and energy-dispersive X-ray (EDX) spectroscopy to investigate the composition and possible transformation of the nanoparticles during incubation in seawater.

2. Materials and methods

2.1. Materials

Ag(I) ICP-standard ($AgNO_3$ in 3% HNO_3, β_{Ag} = 1000 mg L^{-1}), acetic acid (glacial), ethanol, ethylenediaminetetraacetate (EDTA) disodium salt, sodium chloride, sodium acetate anhydrous as well as ethanol and nitric acid (suprapure, 65%) were purchased from Merck (Darmstadt, Germany). Indium ICP-standard ($In(NO_3)_3$ in 2–3% HNO_3, β_{In} = 1000 mg L^{-1}), sulfur ICP-standard (H_2SO_4 in water, β_S = 1000 mg L^{-1}), dispersions of citrate stabilized silver nanoparticles (CA@Ag-NPs) (β_{Ag} = 20 mg L^{-1}), D-penicillamine, and sodium sulfide (Na_2S) were purchased from Sigma-Aldrich (St. Louis, MO, USA).

CA@Ag-NPs used in this study exhibited two different size

distributions, whereas sp-ICP-MS measurements (details are given in the Supporting Information (SI) Figs. S1 and S2) revealed maximum frequency particle sizes of 24 nm and 58 nm. It should be noted that throughout the entire study, particle sizes are given as maximum frequency sizes. We chose to use the maximum frequency sizes in order to enable comparison among widely varying particle types and size distributions. The maximum frequency size is the size that the most frequent particles comprising the entire distribution exhibit on the basis on number frequency. In all examined cases, this value was identical to the one determined on the basis of mass frequency. Therefore, particle size distributions themselves are usually presented as mass frequency unless otherwise specified.

Since CA@Ag-NP dispersions contain impurities of dissolved Ag, the stock dispersions were freed from dissolved Ag species by dialysis (3.5 kDa regenerated cellulose membrane by ZelluTrans, Carl Roth, Karlsruhe, Germany) prior to use. A citrate stabilized gold nanoparticle (CA@Au-NP) dispersion (NIST reference material RM 8013, 56 nm, $\beta_{Au} = 52$ mg L^{-1}, citrate stabilized) was purchased from the National Institute of Standards and Technology (Gaithersburg, MD, USA). Natural organic matter from the Suwannee River (SRNOM) - a reference material from the International Humic Substance Society (IHSS) - was used for all experiments investigating the influence of NOM on the stability of Ag-b-NPs in seawater. Triton X-114 was obtained from AppliChem (Darmstadt, Germany). All chemicals were at least of analytical grade and checked for silver contamination by ICP-MS prior to use. UPW (resistivity of 18.2 MΩcm) was obtained by a Milli-Q-Gradient-System (Millipore GmbH, Schwalbach, Germany). Solely filtrated natural sea water collected from the Gulf Stream in the Gulf of Mexico (S9148, 0.45 μm membrane-filtered, 3.5% salinity, 35 g L^{-1} salt including 89% NaCl (31 g L^{-1}) and 7% sulfate (2.4 g L^{-1})) was obtained from Sigma-Aldrich.

2.2. Instrumentation

A quadrupole mass spectrometer 7900 ICP-MS (Agilent, Santa Clara, CA, USA) equipped with an autosampler SPS4 (Agilent) and a MicroMist nebulizer (Glass Expansion, Melbourne, Australia) was used for Ag concentration and particle size determination. Argon 4.8 (Westfalen, Münster, Germany) was used as plasma gas (nebulizer gas pressure: $4.35 \cdot 10^2$ kPa). Ag quantification was carried out with the target masses ^{107}Ag (analyte) and ^{115}In (internal standard) in He CCT-mode (kinetic energy discrimination, He flow rate: 4.3 mL min^{-1}) to reduce isobaric and polyatomic interferences. Integration time for ^{107}Ag was set to 0.5 s. Data evaluation was performed using the Agilent MassHunter Workstation 4.4 software (version C.01.04, build 544.3).

In single particle mode, the dwell time was set to 500 μs, which results in 120,000 data points for an acquisition time of 60 s. ^{107}Ag was chosen as the target mass, and the pump rate was gravimetrically determined as 0.310 mL min^{-1}. Transport efficiency η describes the proportion of initial particles in the sample which finally reach the detector. The dispersion containing CA@Au-NP (RM 8103) at a Au concentration of $\beta = 52$ ng L^{-1} was used to determine η (~8%) according to a previously approved procedure (Montano et al., 2016; Peters et al., 2014). Before usage, the nanoparticle suspensions were ultrasonicated for 1 min in an ultrasonic bath of Ulsonix Proclean 3.0DSP (Ulsonix, Berlin, Germany) to prevent particle aggregation. Due to an element-specific signal intensity, elemental sensitivity was calibrated using an Ag(I) solution with a concentration of 1 μg L^{-1}. Particle size distributions were evaluated using the Agilent MassHunter Workstation 4.4 software (version C.01.04, build 544.3) equipped with the Single Nanoparticle Application Module.

(Scanning) transmission electron microscopy ((S)TEM) and energy-dispersive X-ray spectroscopy (EDX) measurements were conducted at 300 kV using a FEI Titan Themis electron microscope (Thermo Fischer Scientific, Waltham, MA, USA) equipped with a SuperX EDX detector. STEM was performed in annular dark field (ADF) mode. TEM samples were prepared on carbon film coated copper grids (S 162-6, Plano GmbH, Wetzlar, Germany). Before applying a small droplet of sample dispersion on the TEM grids, they were treated with a H_2/O_2 plasma for 5 s to make them hydrophilic. After an incubation period of 10 min, excess liquid was blotted away with filter paper. The samples were subsequently dried and inserted into the TEM.

TOC content of WWTP effluent samples was determined with a TOC-L-Analyzer (Shimadzu, Kyoto, Japan) following a standard protocol with potassium hydrogen phthalate as the calibrant. Therefore, aqueous solutions of potassium hydrogen phthalate containing 0.5–10 mg L^{-1} TOC were measured for calibration. Samples were measured without filtration and further acidified and thoroughly mixed shortly before the measurement started to ensure sample homogeneity and remove inorganic carbonates.

2.3. Nanoparticle synthesis and characterization

Silver sulfide nanoparticles (Ag_2S-NP) were synthesized according to a procedure published by Hartmann et al., (2014). For this purpose, 0.2 mL of a 10 mM Na_2S solution were added to 10 mL of a suspension containing 58 nm CA@Ag-NP ($\beta_{Ag} = 10$ mg L^{-1}). The mixture was stirred for 3 h in the dark at room temperature (RT). Silver chloride nanoparticles (AgCl-NPs) were prepared following a procedure proposed by Zhou et al., (2017). In this case, 8.5 mg $AgNO_3$ and 25 mg TX-114 were added to 50 mL of UPW. The solution was mixed dropwise with 1 mL of a 50 mM NaCl solution and was further stirred in the dark at RT for another 30 min. The synthesized Ag_2S and AgCl suspensions were dialyzed in the dark for three days, changing the water twice a day in order to separate the nanoparticles from the dissolved silver species and matrix constituents. The dialyzed NP suspensions were then stored in the dark at 5 °C and were stable for weeks. Particle size distribution, shape, and chemical composition of the synthesized Ag_2S-NPs and AgCl-NPs as well as CA@Ag-NPs were determined by (S)TEM-EDX.

2.4. Incubation and separation of Ag-b-NPs from highly saline matrices

Artificial seawater with 31 g L^{-1} NaCl and real seawater were mixed with aqueous dispersions of CA@Ag-NPs (24 nm, 58 nm maximum frequency size), synthesized AgCl-NPs and Ag_2S-NPs to gain dispersions with a volume of 40 mL and an Ag concentration of 50 ng L^{-1}. For reasons of comparability, similar NP dispersions were prepared in UPW. The influence of NOM on the stability of Ag-b-NPs in seawater was examined by adding 5 mg L^{-1} SRNOM to the aforementioned samples. WWTP effluent containing real Ag-b-NPs was collected from a plant in Southern Germany (WWTP Garching, capacity: 4'100 m^3 day^{-1}, building date: 1999) using disposable 500 mL PVC bottles, which were rinsed three times with the sample matrix prior to sampling. To obtain a final salt concentration of 31 g L^{-1}, NaCl was added in small portions while vigorously stirring to avoid localized salt overconcentration. All incubation experiments were prepared in triplicate, protected from light, shaken, and incubated for a certain period (1 h, 2 h, 3 h, 24 h, 48 h, 72 h).

During incubation, Ag-b-NPs may be partly or completely dissolved. CPE was used for selective enrichment of Ag-b-NPs from dissolved silver species and the highly saline matrix (Duester et al., 2016; Hartmann et al., 2013; Hartmann and Schuster, 2013). In brief, 40 mL of each sample were mixed with aqueous solutions of

ethylenediaminetetraacetic acid disodium salt, D-penicillamine, sodium acetate, acetic acid, and the surfactant TX-114 (Hartmann et al. 2013, 2014; Wimmer et al., 2018). After incubation at 40 °C for 30 min, separation of the surfactant phase was enhanced by centrifugation (12 min, 4500 g). The phase-separated mixtures were cooled (5 min, ice bath) and the aqueous supernatant was then removed by decanting. Details as well as the trueness and robustness of the CPE procedure are described by Hartmann et al. 2013, 2014. The remaining surfactant droplets containing the extracted and enriched Ag-b-NPs were diluted with ethanol (500 μL) and UPW to a total volume of 10 mL for the ICP-MS and sp-ICP-MS measurements. Samples are divided into further sub-samples. Those intended for sp-ICP-MS analysis are forwarded to measurement without further treatment. Sub-samples intended for conventional ICP-MS analysis are further mixed with HNO_3 yielding in a final acid concentration of 1.625% (v/v). HNO_3 is used to dissolve NPs in CPE extracts to increase sample homogeneity.

2.5. Determination of concentration and particle size of Ag-b-NPs in CPE extracts

Conventional ICP-MS was used to quantify total Ag concentration in the CPE extracts. In most cases, these measurements were supplemented by sp-ICP-MS measurements, which allow for the calculation of Ag-b-NP particle size in the CPE extracts by measuring the total mass of each single Ag-b-NP in the sample and, eventually, for the calculation of the total concentration of Ag-b-NPs by summation of each single Ag-b-NP mass. Calibration was performed with aqueous Ag(I) solutions of known concentration ranging from 5 to 200 ng L^{-1} (limit of detection, LOD = 0.2 ng L^{-1}; background equivalent concentration, BEC = 0.5 ng L^{-1}). Since these solutions underwent no CPE, they were prepared in a UPW matrix (acidified to 1.625% (v/v) HNO_3) including 5% (v/v) of TX-114 10% (w/w) and 5% (v/v) of ethanol (which is, e.g., 2.5 mL TX-114 10% (w/w) and 2.5 mL EtOH for a total volume of 50 mL) to mimic the matrix of the samples after CPE.

Quantitative sp-ICP-MS measurements were performed with non-acidified CPE extracts. Calibration samples (52 ng L^{-1} CA@AuNP dispersion and 1 μg L^{-1} Ag(I) solution) were prepared in a UPW matrix including 5% (v/v) of TX-114 10% (w/w) and 5% (v/v) of ethanol (which is, e.g., 2.5 mL TX-114 10% (w/w) and 2.5 mL EtOH for a total volume of 50 mL) to mimic the matrix of the samples after CPE. The calculations are subject to some uncertainties as they assume a spherical shape for all particles and require knowledge about the density ρ of the particulate materials (Peters et al., 2014), which is derived from the bulk materials Ag (ρ = 10.49 g cm^{-3}), AgCl (ρ = 7.23 g cm^{-3}) and Ag_2S (ρ = 5.56 g cm^{-3}) (according to the GESTIS Substance Database, Dec. 2018). In the case of Ag-b-NPs in real environmental samples (WWTP effluent), the NP modification is unknown but very likely Ag_2S (Kaegi et al., 2013). Despite its limitations, sp-ICP-MS is still the only method able to simultaneously determine concentration and particle size distribution of NPs at ng L^{-1} concentration levels, so it is the method of choice.

Size detection limit (SDL) for sp-ICP-MS measurement of Ag-b-NPs was determined to 8 nm. Transient signals deriving from nanoparticles being atomized in the plasma of the ICP-MS are registered during the measurement. The signal size corresponds to the size of the corresponding nanoparticle, i.e. small particles lead to only very little signals. Signals of smaller particles in the time resolved sp-mass spectra are not distinguishable anymore from signals derived from traces of dissolved Ag species or the instrument's background and are thus not applicable for data processing. Thus, concentrations measured by sp-ICP-MS represent the total Ag concentration of all particulate Ag species sized >8 nm.

2.6. Characterization of size, morphology and chemical composition of Ag-b-NPs incubated in real seawaters

Mass spectrometric analysis was supplemented by electron microscopy to investigate the fate of Ag-b-NPs in highly saline matrices. To meet limits of detection for TEM-EDX, Ag-b-NP dispersions were mixed 1:10 with real seawater, resulting in a total volume of 1.5 mL and incubated for 1 h. Afterwards, samples were filled in 3.5 kDa regenerated cellulose membranes surrounded by 1 L UPW to perform a dialysis for 24 h. UPW was replaced every 4 h. Dialysis can eliminate both Ag(I) deriving from potentially dissolved Ag-b-NPs and the high saline seawater matrix, which would otherwise cause incrustations on the TEM grid. A droplet of each prepared sample was examined by TEM-EDX as described in the "Instrumentation" section and compared to NPs which had not been in contact with seawater.

2.7. Error calculations

For all measurements, three independent subsamples were treated and measured individually. Each subsample was measured with three replicates n (U, n = 3). The uncertainty U was calculated via Gaussian error propagation based on pipetting uncertainties and standard deviations of the independently measured sub-samples. Blank samples were used to correct Ag concentrations in all incubation experiments.

3. Results and discussion

3.1. Nanoparticle characterization

The chemical composition, shape, and particle size of the commercially available and synthesized particles were analyzed to gain information about the pristine state of the particles prior to any incubation experiments. For this purpose, dispersions of the freshly synthesized and purified CA@Ag-NPs, AgCl-NPs and Ag_2S-NPs were prepared on copper grids and investigated with STEM and EDX.

STEM measurement of both types of CA@Ag-NPs showed spherical, sole particles with a particle size range of approximately 42–120 nm (SI, Fig. S1) and 14-100 nm (SI, Fig. S2). Maximum frequency particle sizes were determined by sp-ICP-MS as 24 nm and 58 nm, respectively. An examplary image of a particle sizing 53 nm and the corresponding EDX spectrum are given in Fig. 1. The particle related signals indicate that the core of the particle consists of pure silver.

The synthesized AgCl-NPs showed cubic non-aggregated particles with a broad size range of approximately 18–200 nm (SI, Fig. S3) with a maximum frequency particle size of 94 nm determined by sp-ICP-MS. Fig. 2 shows an example of a STEM-ADF image of a AgCl-NP cube with a side length of 100 nm and the corresponding EDX spectrum. The EDX spectrum reveals a Ag to Cl ratio of 1:1, which complies with the presence of AgCl particles.

Fig. 3 shows a TEM image of the synthesized Ag_2S-NPs and the corresponding EDX spectrum. In this case, some bridging between neighboring particles occurred and some particles show small cavities. A narrow particle size distribution was observed with a size range of 48–160 nm (SI, Fig. S4) and a maximum frequency particle size of 82 nm determined by sp-ICP-MS. EDX measurements revealed a Ag to S ratio of 2:1, which indicates the presence of Ag_2S-NPs. Obviously, the reaction of CA@Ag-NPs with sulfide resulted in the formation of fully sulfurized particles combined with an increase in the average size of the particles from 58 nm to 82 nm (SI, Fig. S4).

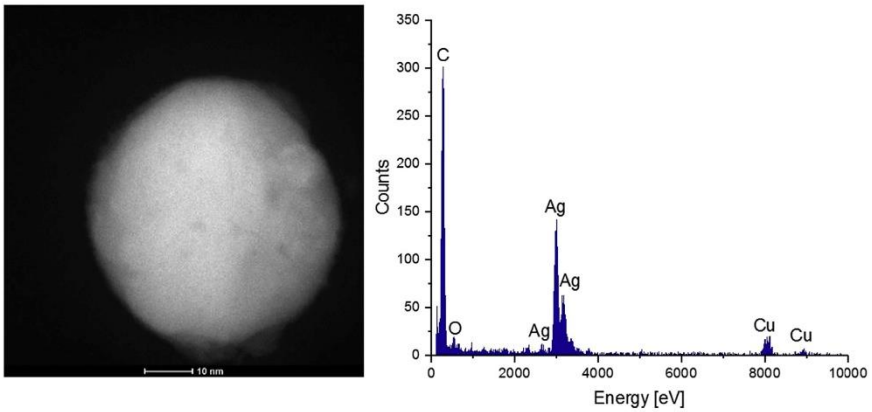

Fig. 1. STEM-ADF image and corresponding EDX spectrum of a citrate coated silver nanoparticle. Additional Cu-, O- and C-signals in the spectrum result from the sample support (carbon film on copper grid) and carbohydrate contamination during illumination.

3.2. Dissolution of differently coated and sized Ag-b-NPs incubated in UPW, artificial seawater, and real seawater

We examined the fate of differently coated and sized Ag-b-NPs in UPW, artificial seawater, and real seawater. Our preliminary tests prior to the incubation experiments confirmed the applicability of CPE to species selectively extract and enrich Ag-b-NPs from saline matrices. Extraction efficiency for Ag-b-NPs even increased from 88% in the UPW matrix to 94% in the highly saline matrix. Moreover, the co-extraction of soluble Ag(I) species from highly saline matrices into the organic phase amounted to less than one percent. Therefore, CPE is suitable to (i) quantitatively extract Ag-b-NPs from highly saline matrices into the organic phase and to (ii) perform this process species selectively. In other words, soluble Ag(I) species deriving from former Ag-b-NPs by means of dissolution in saline matrices are prevented from being transported into the organic phase.

We applied a dual approach for investigating the fate of Ag-b-NPs in UPW and highly saline matrices. First, we quantified the total concentration of Ag-b-NPs present after a certain incubation time, whereby these particles were thus able to resist an occurring NP dissolution process. Concentrations related to Ag for these remaining Ag-b-NPs in each incubation matrix (UPW, artificial, and real seawater) with increasing incubation time measured by CPE-ICP-MS are shown in Fig. 4 and Table S1 (see SI). Table S1 includes further concentration data measured for the same samples by CPE-sp-ICP-MS. These concentrations represent the concentration of particles $\geq$8 nm.

Second, we were able to display the change in sizes of Ag-b-NPs being incubated in the different matrices for increasing incubation time by CPE-sp-ICP-MS measurements (Fig. 5).

All experiments started with an initial Ag-b-NP concentration of ~50 ng L^{-1} (Fig. 4). As mentioned above, comparison of CPE-ICP-MS and CPE-sp-ICP-MS allowed differentiation between concentration of the total amount of particulate Ag species and those <8 nm (SI, Table S1). In most cases, CPE-sp-ICP-MS was not able to quantify all

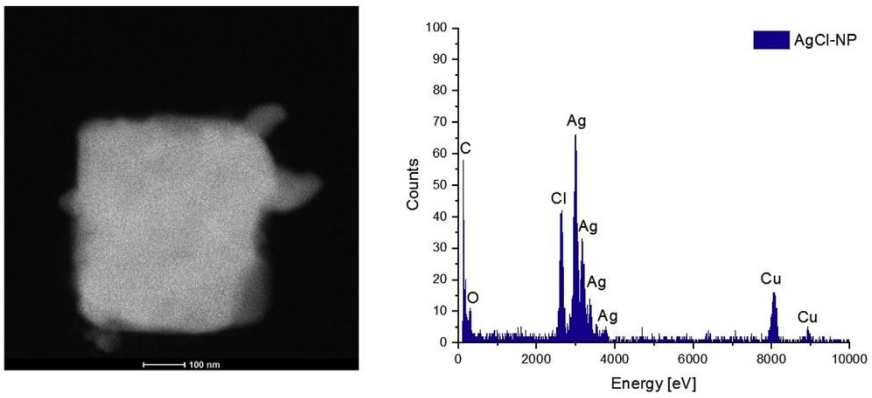

Fig. 2. STEM-ADF image and corresponding EDX spectrum of a silver chloride nanoparticle. Additional Cu-, O- and C-signals in the spectrum result from the sample support (carbon film on copper grid) and carbohydrate contamination during illumination.

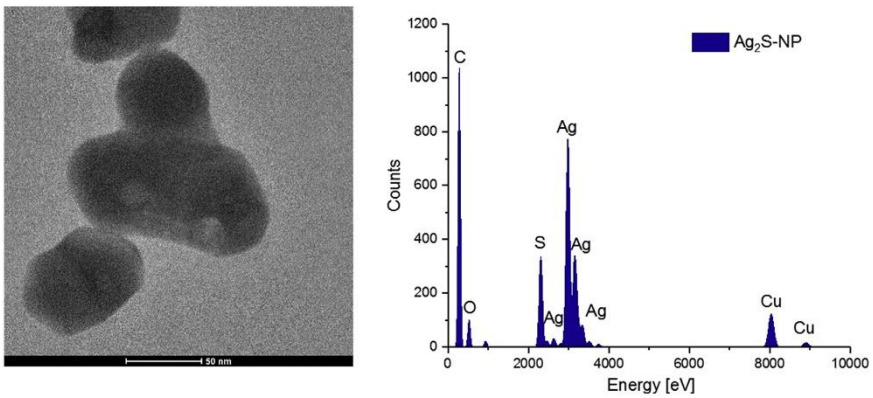

Fig. 3. TEM image and corresponding EDX spectrum of silver sulfide nanoparticles. Additional Cu-, O- and C-signals in the spectrum result from the sample support (carbon film on copper grid) and carbohydrate contamination during illumination.

particulate species since low concentrations of particles <8 nm were present. However, no correlation between the appearance of particles <8 nm and incubation time, matrix, and NP coating was detected.

As already described in the literature, cooperative oxidation processes transforming Ag(0) to soluble Ag(I) species followed by formation of soluble $AgCl_x^{1-x}$ (x > 1) in the presence of chloride (Levard et al., 2012; Liu and Hurt, 2010; Lodeiro et al., 2017) basically led to dissolution of all types of Ag-b-NPs in the three different matrices.

UPW establishes massive dilution pressure, readily transforming large parts of particulate Ag(0) into dissolved Ag(I) species by an equilibrium shift to dissolved Ag species (equation (1)), which is further promoted by the comparatively low pH of UPW (~5–6) compared to non-purified or natural water (~7–8) (Liu and Hurt, 2010). After an incubation period of 3 h in the UPW matrix, only 87% of the initially applied CA@Ag-NPs (58 nm pristine maximum frequency size) remained as particles. It should be noted that the sizes in brackets represent the mean pristine particle size before incubation, which is enclosed for the sake of clarity. After the same incubation time, only 1% of the initially applied CA@Ag-NPs (24 nm pristine maximum frequency size) remained. Due to the extremely large intrinsic surface of these small particles, oxidation to dissolved Ag(I) is massively promoted for smaller particles (Zhang et al., 2011). After 3 h of incubation in UPW, 26% of AgCl-NPs (94 nm pristine maximum frequency size) remained particulate. Since the AgCl particles initially exhibited a maximum frequency particle size of 94 nm, we would suggest a slow dissolution process.

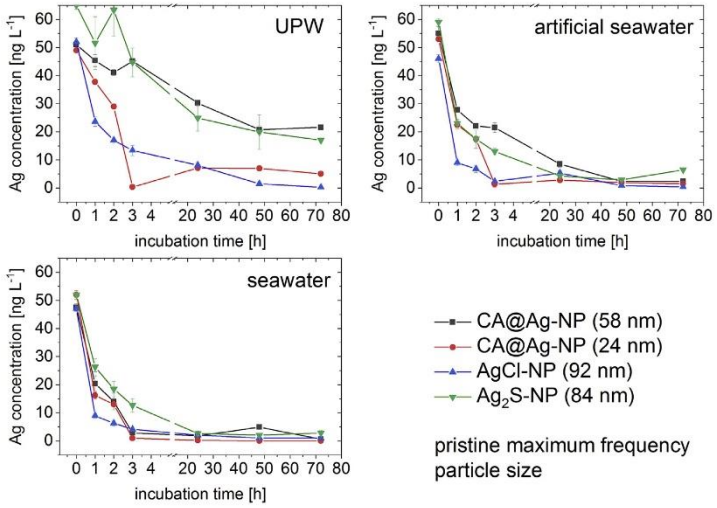

Fig. 4. Concentration of Ag present as nanoparticles for all four investigated Ag-b-NP types incubated in UPW, artificial seawater, and seawater with increasing incubation time. Measurements were performed by CPE-ICP-MS and, thus, concentrations correspond to the total amount of Ag-b-NPs (see SI, Table S1 for detailed measured values).

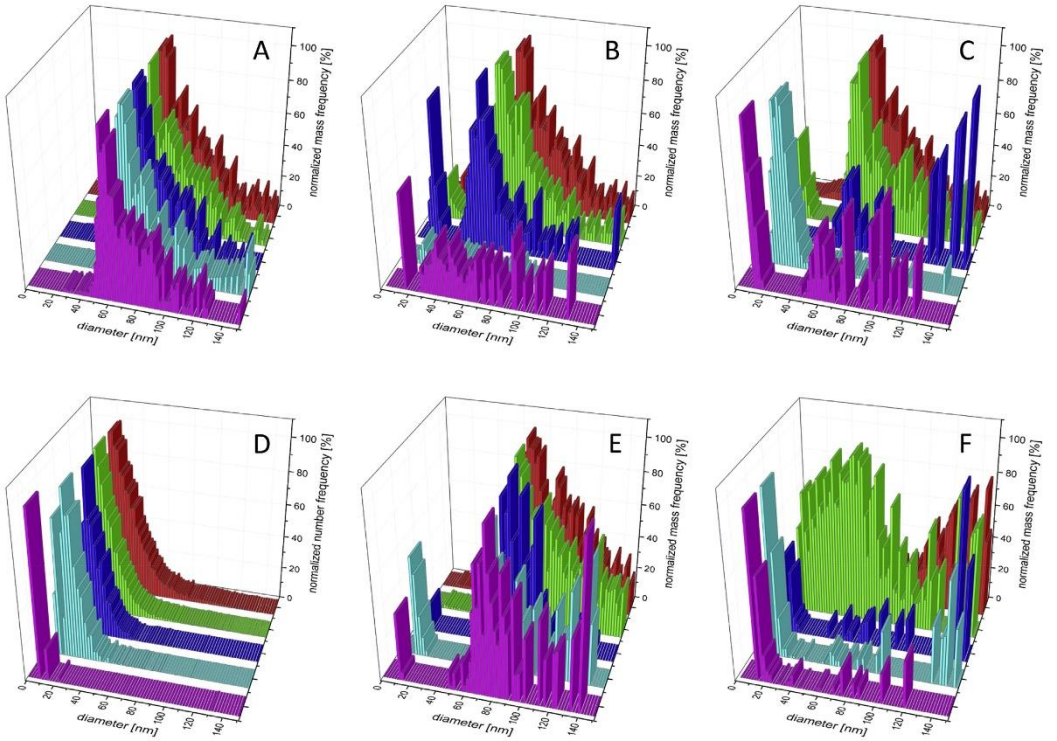

Fig. 5. Particle size distributions referred to normalized mass or number frequency of CA@Ag-NPs (58 nm pristine maximum frequency size) in UPW (A), CA@Ag-NPs (58 nm pristine maximum frequency size) in artificial seawater (B), CA@Ag-NPs (58 nm pristine maximum frequency size) in seawater (C), CA@Ag-NPs (24 nm pristine maximum frequency size) in seawater (D), Ag_2S-NPs (82 nm pristine maximum frequency size) in seawater (E), and AgCl-NPs (94 nm pristine maximum frequency size) in seawater (F). The four size distributions presented in each diagram are related to the pristine state (red), 1 h of incubation (green), 24 h of incubation (blue), 48 h of incubation (turquoise), and 72 h of incubation (purple). See also SI, Fig. S6 for another perspective of diagram F. Particles <8 nm were not detectable with sp-ICP-MS. Presented results are based on CPE-sp-ICP-MS measurements. (For interpretation of the references to color in this figure legend, the reader is referred to the Web version of this article.)

However, we observed quite high dissolution rates for AgCl-NPs, which can be explained by the fact that Ag in AgCl is already present in oxidation state I, accelerating the cooperative oxidation process responsible for the dissolution (Liu and Hurt, 2010). Since 69% of Ag_2S-NPs (82 nm pristine maximum frequency size) resisted dissolution after 3 h of incubation, the high insolubility of Ag_2S seems to compensate for the Ag oxidation state of I and thus prohibits these particles from fast dissolution. The general trend continued with increasing incubation time to 72 h, whereby 42% of the initially applied CA@Ag-NPs (58 nm pristine maximum frequency size), 26% of Ag_2S-NPs (82 nm pristine maximum frequency size), 10% of CA@Ag-NPs (24 nm pristine maximum frequency size), and 1% of AgCl-NP (94 nm pristine maximum frequency size) resisted dissolution. Overall, CA@Ag-NPs (58 nm pristine maximum frequency size) seemed to be the most stable modification of Ag-b-NPs in UPW, followed by Ag_2S-NPs (82 nm pristine maximum frequency size), CA@Ag-NPs (24 nm pristine maximum frequency size), and AgCl-NPs (94 nm pristine maximum frequency size). This is somewhat surprising since silver sulfide is one of the most insoluble salts. However, CA@Ag-NPs (58 nm pristine maximum frequency size) exceeded this insolubility, likely due to the fact that the coating reagent can slow down the oxidative dissolution process. Citrate coating has already been reported to be able to reduce Ag(I) to Ag(0), forming either new particles or being inserted into already existing particles (Kittler et al., 2010).

The presence of chloride, able to trap Ag(I) and thus shift the dissolution equilibrium (Liu and Hurt, 2010), leads to increasing dissolution rates for all types of Ag-b-NPs in artificial seawater. After an incubation of 3 h, only 3% of the initially applied CA@Ag-NPs (24 nm pristine maximum frequency size), 5% of AgCl-NPs (94 nm pristine maximum frequency size), 22% of Ag_2S-NPs (82 nm pristine maximum frequency size), and 39% of CA@Ag-NPs (58 nm pristine maximum frequency size) resisted dissolution and remained particulate. After 72 h, the dissolution process in seawater was almost finished, in contrast to incubation in UPW matrix, where 11% of Ag_2S-NPs (82 nm pristine maximum frequency size) and 1–4% of the other Ag-b-NPs were still present as particulate species. Again, small particle sizes encouraged dissolution, as CA@Ag-NPs (24 nm pristine maximum frequency size) were dissolved significantly faster than CA@Ag-NPs (58 nm pristine maximum frequency size). Again, CA@Ag-NPs (58 nm pristine maximum frequency size) and Ag_2S-NPs (94 nm pristine maximum frequency size) were more stable than CA@Ag-NPs (24 nm pristine maximum frequency size) and AgCl-NPs (94 nm pristine maximum

frequency size).

Dissolution rates reached their maximum in experiments involving real seawater as the incubation matrix. This observation is only partially reflected in the current literature. Liu et al. described that dissolution rates for Ag-b-NPs in the mg L^{-1} range incubated in seawater even decreased to some extent because the comparatively high pH (~8) in seawater shifts the equilibrium of the dissolution process at the expense of dissolved Ag(I) species (Liu and Hurt, 2010). However, reducing the Ag-b-NP concentration to an environmentally relevant level of some ng L^{-1} was reported to accelerate the dissolution process (Toncelli et al., 2017). In our experiment, the latter case seems to prevail, and it controls the dissolution process in real seawater. In general, we observed a dramatic drop in the concentration of remaining NPs in seawater within the first 3 h, whereas only 24% of the initially applied Ag_2S-NPs (82 nm pristine maximum frequency size), 9% of AgCl-NPs (94 nm pristine maximum frequency size), 6% of CA@Ag-NPs (58 nm pristine maximum frequency size), and 2% of CA@Ag-NPs (24 nm maximum frequency size) were still present as NPs in seawater. After incubation for 72 h, only 1–9% of Ag-b-NPs resisted dissolution in seawater. It is remarkable that some particles of all types of Ag-b-NPs could still be detected, indicating a certain stability of particle traces in seawater. This partial dissolution of Ag-b-NPs in aqueous matrices even after incubating for several days has also been described by Loza et al., (2014). Again, CA@Ag-NPs (24 nm pristine maximum frequency size) and AgCl-NPs (94 nm pristine maximum frequency size) showed only low stability during the incubation experiment in seawater for the aforementioned reasons. CA@Ag-NPs (58 nm pristine maximum frequency size) and Ag_2S-NPs (82 nm pristine maximum frequency size) displayed slightly higher stability. Very interestingly, Ag_2S-NPs (94 nm pristine maximum frequency size) even surpassed the stability of CA@Ag-NPs (58 nm pristine maximum frequency size) marginally, which could not be observed in any of the incubation experiments described above. This observation probably goes along with high concentrations of sulfate present in real seawater, which was not the case for UPW and artificial seawater, indicating the stability of silver sulfide coatings. However, the presence of sulfide coatings requires the reduction of S(VI) in sulfate to S(-II) in sulfide, which might take place to a small extent by integrating sulfate into the aforementioned cooperative oxidation reactions (Liu and Hurt, 2010).

CPE-sp-ICP-MS provides an even more detailed insight into the NP dissolution process (Fig. 5), as it describes the evolution of particle size distributions over time. Particle size distributions for CA@Ag-NPs (58 nm pristine maximum frequency size), Ag_2S-NPs (82 nm pristine maximum frequency size), and AgCl-NPs (94 nm pristine maximum frequency size) are given as normalized mass frequency. We chose this kind of presentation because very small particles <8 nm are present to a varying extent in all samples, but contribute only very little to the total particle mass. However, particles <8 nm would misleadingly affect the particle size distributions if presented as normalized number frequency. For CA@Ag-NPs (24 nm pristine maximum frequency size), presenting normalized number frequencies was feasible due to the narrow range of small particle sizes. In depth analysis of sp-ICP-MS data revealed additional information regarding particle numbers and their variation after incubation in aqueous matrices (Table 1).

Fig. 5A shows blank corrected particle size distributions of CA@Ag-NPs (58 nm pristine maximum frequency size) incubated in UPW for 1 h, 24 h, 48 h, and 72 h. As seen in Fig. 4 (SI, Table S1), the NP concentration was reduced by dissolution to 42% within 72 h. However, the NP size distribution did not change during the observed incubation period, so the maximum frequency size (Table 1) stayed constant during the experiment, which is due to the fact that primarily small particles were readily dissolved, thus not influencing the maximum frequency size of approximately 58 nm. We observed a rapid decrease of the total particle number within the first hour of incubation (Table 1), whereas particles ≤30 nm in particular were dissolved. Due to their high intrinsic surface, the small particle fraction was dissolved first. During the following days, almost all particles ≤30 nm were dissolved, whereas the number of particles >30 nm was reduced slightly, indicating their predominant stability.

Table 1
Compilation of the total number of NPs and numbers within a defined size range as well as the measured maximum frequency NP size; each measurement addresses a certain type of Ag-b-NP, incubation matrix and incubation time. Sizes in brackets represent the pristine maximum frequency size. Presented results are based on CPE-sp-ICP-MS measurements.

	0 h	1 h	24 h	48 h	72 h
	CA@Ag-NPs (58 nm) in UPW				
total number	10899	3716	1858	1019	1513
NP ≤30 nm	8098	988	256	7	86
NP >30 nm	2801	2728	1602	1012	1427
maximum frequency size [nm]	58	62	62	61	59
	CA@Ag-NPs (58 nm) in artificial seawater				
total number	10899	10374	8380	2433	1548
NP ≤30 nm	8098	8573	7692	2218	1291
NP >30 nm	2801	1801	688	215	257
maximum frequency size [nm]	58	57	46	10	10
	CA@Ag-NPs (58 nm) in seawater				
total number	3269	10206	2382	1852	3446
NP ≤30 nm	608	8977	2333	1801	3390
NP >30 nm	2661	1229	50	50	56
maximum frequency size [nm]	58	59	12	17	10
	CA@Ag-NPs (24 nm) in seawater				
total number	8695	9425	1879	288	1110
NP ≤16 nm	195	718	0	59	1077
NP >16 nm	8499	8708	1879	230	32
maximum frequency size [nm]	24	19	9	10	8
	Ag_2S-NPs (82 nm) in seawater				
total number	4929	4936	771	546	1486
NP ≤30 nm	2341	2446	623	530	1356
NP >30 nm	2588	2490	147	17	130
maximum frequency size [nm]	73	73	69	11	11
	AgCl-NPs (94 nm) in seawater				
total number	815	9240	2482	5170	4141
NP ≤30 nm	0	7593	2447	5145	4118
NP >30 nm	815	1647	35	25	23
maximum frequency size [nm]	70	15	12	12	12

Incubation of CA@Ag-NPs (58 nm pristine maximum frequency size) in artificial seawater (Fig. 5B) led to a reduction of the maximum frequency size of the particles from 58 nm to 46 nm within the first day of incubation, which goes along with a decrease in NP concentration (Figs. 4 and SI, Table S1). Table 1 shows that particles >30 nm in particular were dissolved, whereas the number of particles ≤30 nm stayed constant or increased. However, it is very likely that particles ≤30 nm were still dissolved, but the simultaneous dissolution of particles >30 nm also led to the formation of particles ≤30 nm. After 48 h of incubation, the maximum frequency particle size was reduced dramatically to 10 nm because a large proportion of particles was dissolved. In this case, the number of particles >30 nm and ≤30 nm was reduced equally.

In contrast to an incubation of CA@Ag-NPs (58 nm pristine maximum frequency size) in artificial seawater, the rapid concentration drop for an incubation in seawater occurred earlier after 24 h of incubation (Figs. 4 and SI, Table S1). This goes along with a

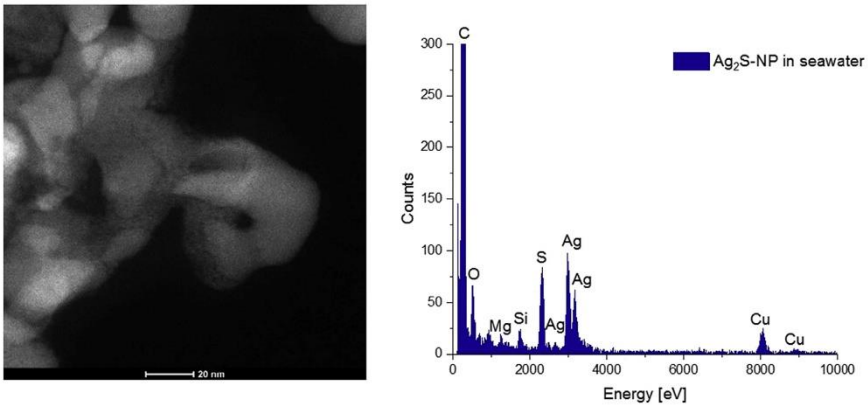

Fig. 6. STEM-ADF image of Ag_2S-NPs after incubation in seawater and corresponding EDX spectrum. Additional Cu-, O- and C-signals in the spectrum result from the sample support (carbon film on copper grid) and carbohydrate contamination during illumination.

strong decrease of the maximum NP frequency size from 58 nm to 12 nm after the same incubation period (Table 1, Fig. 5C). In Fig. 5C, particles exhibiting a maximum frequency particle size of 58 nm with a size range of approximately 14–100 nm were only observable until 1 h of incubation. Particles >30 nm were almost completely dissolved after 24 h of incubation (Table 1). Again, shrinking of particles >30 nm contributed to a constant number of particles ≤30 nm despite the accelerated dissolution of small particles taking place as well. This fast-shrinking process was enhanced at an increasing salinity of the incubation matrix.

For CA@Ag-NPs (24 nm pristine maximum frequency size), only traces of Ag-b-NPs were detectable after 24 h of incubation in seawater (Fig. 4, Table S1). The maximum frequency particle size was reduced from 24 nm to approximately 10 nm during the entire incubation period (Fig. 5D). Moreover, a fast drop in the NP number was observed after an incubation time of 24 h, whereas particles ≤16 nm accounted for the predominant particulate species (Table 1).

Particle size distributions of Ag_2S-NPs (82 nm pristine maximum frequency size) became narrower within the first 24 h of incubation (Fig. 5E), whereby maximum frequency particle sizes were hardly reduced from initially 73 nm to 69 nm. However, we observed a rapid drop in concentration (Fig. 4, Table S1) and particle number (Table 1), whereas NPs ≤30 nm and >30 nm were dissolved equally. As expected, smaller particles were dissolved faster due to their high intrinsic surface. Dramatically shrunk Ag_2S-NPs, formerly exhibiting sizes >30 nm, contributed as additional particles ≤30 nm. With decreasing proportion of particles >30 nm and the almost complete dissolution of initial 82 nm particles during the days of incubation, the concentration of smaller particles increased in Fig. 5E. Thus, particles of all sizes were affected by dissolution in seawater, whereas the dissolution of initial 82 nm particles resulted in a large number of remaining particles ≤30 nm.

After only 1 h of incubation, the mean particle size of AgCl-NPs (94 nm pristine maximum frequency size) incubated in seawater massively decreased from 94 nm to 15 nm, whereas the initial broad particle size distribution (approximately ranging from 60–150 nm) was completely reversed after 1 h (Fig. 5F; see also SI, Fig. S6 for another perspective). The experiment started with approximately 800 particles >30 nm (Table 1) and no measurable particles ≤30 nm. But, after only 1 h of incubation in seawater, the number of particles ≤30 nm increased dramatically to approximately 7'000, and the number of particles >30 nm doubled. This indicates that AgCl-NPs >30 nm were dissolved or even broken up, forming thousands of smaller particles with a broad size range from 8–120 nm. With an increasing incubation time of 24 h or longer, the concentration of particles >30 nm as well as the total concentration of AgCl-NPs still present in seawater was reduced to marginal values. Thus, NPs >30 nm were dissolved quickly in seawater in favor of residual smaller particles, which contribute only very little to the total concentration of NPs present in seawater.

Overall, CPE-sp-ICP-MS allows for the determination of particle sizes of Ag-b-NPs incubated in aqueous matrices at environmentally relevant concentration levels. Particle sizes were reduced, while this process depended on the particle coating and was accelerated by increasing salinity of the incubation media. Regarding long-term incubation of >72 h, no relevant Ag-b-NP concentrations sustained the most extreme conditions seawater constitutes for all kinds of investigated particles. For a short-term observation, however, our results show that larger Ag-b-NPs of >30 nm freshly released into seawater are transformed within 72 h to small particles <30 nm. This may lead to a short-term increase in the environmental (eco)toxicity and bioavailability of these particles, which are believed to be more critical in this respect than larger particles (Kittler et al., 2010).

In addition to the concentration and particle size of Ag-b-NPs, their surface modification and chemical composition influence the (eco)toxicology of these contaminants in the aqueous environment. As a result, we supplemented our examination of Ag-b-NPs in saline matrices with STEM-EDX measurements. No changes in the chemical composition of CA@Ag-NPs and AgCl-NPs after incubation for 1 h in sea water were detected by STEM-EDX. Rather small (d<20 nm) Ag_2S-NPs were detected using STEM after incubation in seawater (Fig. 6). Furthermore, TEM images show that Ag_2S-NP aggregate and form Ag_2S bridges to neighboring particles when being incubated in seawater (SI, Fig. S5, which is not the case for freshly prepared nanoparticle suspensions. This is a fully expected result based on the DLVO theory (Derjaguin and Landau, 1993; Lodeiro et al., 2016; Quik et al., 2014; Verwey, 1947): Increasing ionic strength in sea water reduces particles' stability and thus promotes aggregation. Some of the particles also have cavities. EDX measurement showed that a ratio of Ag:S of 1:1

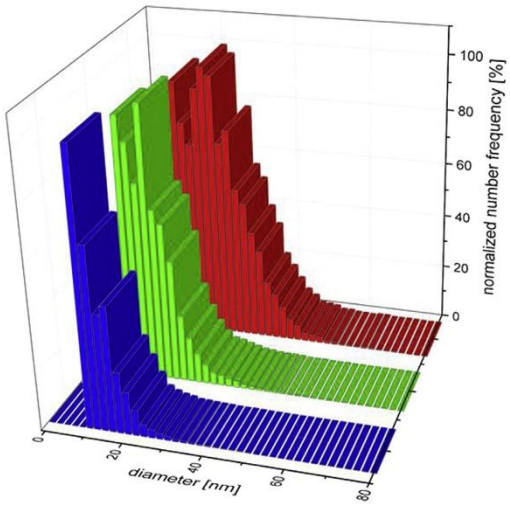

Fig. 7. Particle size distribution of Ag-b-NPs in WWT effluent before (red) and after incubation with (blue) and without (green) added NaCl. Incubation time was set to 72 h. Particles <8 nm were not detectable with sp-ICP-MS. Presented results are based on CPE-sp-ICP-MS measurements. (For interpretation of the references to color in this figure legend, the reader is referred to the Web version of this article.)

occurred in such particles. The signals arising from Mg, Si, among others, came either from the seawater matrix or TEM grids. The changing ratio of Ag:S from the initial 2:1 (Fig. 3) to 1:1 indicates that silver is dissolved while sulfur is accumulating around the particles when incubated in seawater.

3.3. Influence of incubation temperature and natural organic matter

Beyond the influence of nanoparticle coatings and matrix composition on the fate of Ag-b-NPs in seawater, we investigated the effect of increasing incubation temperature on the stability of Ag-b-NPs in real seawater (see SI, Table S2 for detailed measured values). Starting again with 50 ng L^{-1} CA@Ag-NPs (58 nm pristine maximum frequency size), we found that 55% of the initial NPs remained in the solutions after 1 h of incubation at a temperature of 23 °C and 61% at a temperature of 60 °C. After increasing the incubation time to 2 h, 49% of the initial NPs remained at a temperature of 23 °C, and 44% remained at a temperature of 60 °C. Comparable concentrations of remaining NPs independent of the applied incubation temperature indicates that there is no significant temperature effect on the dissolution of Ag-b-NPs in seawater. Similar observations were made for all other types of Ag-b-NPs.

NOM plays an important role in Ag-b-NP transformation processes in aqueous environments. On the one hand, NOM is able to decelerate Ag-b-NP dissolution effects in natural water bodies by blocking potential Ag oxidation sites of the NPs after adsorption, by serving as an oxidative sink in the cooperative redox system by NOM-oxidation, and, finally, by allowing a reversible reaction of formed Ag(I) to Ag(0) with NOM as the reductant (Liu and Hurt, 2010). The last point in particular is crucial for an environmentally relevant system containing dissolved Ag(I) species, since they are readily reduced to Ag(0) by NOM forming new Ag-b-NPs. *Wimmer* et al. have already reported on evidences that this process takes place in nature and is responsible for the existence of naturally formed Ag-b-NPs in the aqueous environment (Wimmer et al., 2018). As a result, we compared dispersions of CA@Ag-NPs (58 nm pristine maximum frequency size) and Ag_2S-NPs (82 nm pristine maximum frequency size) incubated in seawater for 1 h and 72 h with NOM (5 mg L^{-1}) and without NOM (see SI; Table S3 for detailed measured values). For CA@Ag-NPs (58 nm pristine maximum frequency size) after 1 h incubation, we found 74% (83% with NOM) remaining particles, which were reduced to 16% (4%) after 72 h. In the case of Ag_2S-NPs (82 nm pristine maximum frequency size), 87% (91% with NOM) of initially inserted NPs remained as particles after 1 h of incubation, whereas only 13% (2%) were left after 72 h. As these values illustrate, NOM did not protect Ag-b-NPs from dissolution in seawater. Within the first hour of incubation, there is no distinct effect of NOM observable, but, after 72 h, NOM increased the dissolved number of NPs for both types of Ag-b-NPs dramatically. In contrast to common expectations, NOM did support Ag-b-NP dissolution. The most likely explanation for this suprising behavior is that NOM forms complexes with dissolved Ag(I) species, removes them from the Ag(0)-Ag(I) equilibrium, and therefore accelerates the dissolution process (Liu and Hurt, 2010).

3.4. Dissolution of Ag-b-NPs in WWTP effluent

The main contamination source, respectively the main entry phase for Ag-b-NPs into the aquatic environment is wastewater released, e.g., by WWTPs. Ag-b-NPs in waste water are usually sulfidized to a large degree and most likely consist of Ag_2S (Kaegi et al., 2013). In addition to experiments with synthesized particles of known composition, we also investigated the fate of real particles in freshly sampled WWTP effluent with and without the addition of sodium chloride, which was added to the solutions prior to incubation to obtain a final salt concentration of 31 g L^{-1} NaCl. The initial total Ag-b-NP concentration in the effluent was 17.45 ± 1.19 ng L^{-1} measured with CPE-ICP-MS and 9.19 ± 0.02 ng L^{-1} measured with CPE-sp-ICP-MS, indicating that the solutions contained significant quantities of small particles <8 nm. The mean particle size (based on number frequency) for particles ≥ 8 nm measured by CPE-sp-ICP-MS was 22 nm (pristine maximum frequency size; see Fig. 7). After incubation for 72 h, the solutions contained a total Ag-b-NP concentration of 4.60 ± 0.41 ng L^{-1} and 3.70 ± 0.27 ng L^{-1} for particles ≥8 nm, with a mean particle size of 14 nm (16 nm maximum frequency size). Obviously, Ag-b-NPs contained in the effluent solutions were not stable in this matrix even under dark conditions and the data reveal that mainly small particles were dissolved. The addition of sodium chloride prior to incubation increased particle dissolution dramatically. After an incubation time of 72 h, a total Ag-b-NP concentration of 2.86 ± 0.42 ng L^{-1} and 1.51 ± 0.06 ng L^{-1} for particles ≥8 nm with a mean particle size of 11 nm (10 nm maximum frequency size) was observed. Ag-b-NPs that are present in real environmental samples obviously share the fate of particles investigated in the model experiments described above: Ag-b-NPs dissolve within 72 h to a large extent, whereas the dissolution is accelerated in the presence of chloride. Particle dissolution goes along with the reduced particle sizes presented in Fig. 7. However, dissolution took place more slowly than in the model experiments. A complex interrelation between NOM present in the WWTP effluent (TOC = 2.3 mg L^{-1}) trapping Ag(I) and shifting the equilibrium towards enhanced dissolution (Loza et al., 2014) and the ability of NOM to protect Ag-b-NP from dissolution by reduction of Ag(I) to Ag(0) forming new particles (Toncelli et al., 2017) is, among other things, responsible for decreased dissolution rates. Nevertheless, Ag-b-NPs initially contained in WWTP effluent and

transported by rivers to the sea can be expected to be dissolved within a short period of time.

4. Conclusion

All types of Ag-b-NPs were largely dissolved within a reasonable amount of time, whereby dissolution rates increased with the salinity of the incubation matrix. CA@Ag-NPs (24 nm pristine maximum frequency size) were dissolved significantly faster than CA@Ag-NPs (58 nm pristine maximum frequency size) due to their higher intrinsic surface. Additionally, we particularly examined environmentally more relevant Ag-b-NPs, namely Ag_2S- and AgCl-NPs because these particles are believed to be the most predominant species in the environment (Kaegi et al., 2013; Ma et al., 2014; Nowack et al., 2012; Sharma et al., 2015). Ag_2S-NPs (82 nm pristine maximum frequency size) displayed higher stability compared to AgCl-NPs (94 nm pristine maximum frequency size). All four examined particle types were dissolved almost completely in real seawater within three days.

Ag-b-NPs as a potential threat to marine environmental health is extensively discussed in the literature. However, our results confirm that CA@Ag-NPs in environmentally relevant concentrations are not stable in seawater for more than three days. AgCl-NPs and even Ag_2S-NPs share this fate despite the low solubility of the corresponding salts. Locally arising increased concentrations of soluble Ag(I) species caused by the dissolution of Ag-b-NPs may affect the health of the environment, but only for a limited time, and it may be compensated by a massive dilution effect of Ag(I) in the oceans. Once Ag-b-NPs reach the sea, they are dissolved and no longer constitute a significant risk to environmental health.

Funding

This research project was financed by the Bavarian State Ministry for the Environment and Consumer Protection (TNT01NaTFuE69458).

Author contribution

M. Schuster supervised the study. A. Wimmer designed the study and its experimental setup. A. Wimmer carried out incubation experiments and all corresponding analytical measurements assisted by N. Funk, F. Adler, and L. Lenz. A. Wimmer evaluated acquired measurement data. A. Urstoeger synthesized and characterized all types of Ag-b-NPs. M. Doeblinger carried out TEM measurements. A. Urstoeger, assisted by A. Wimmer, and M. Doeblinger evaluated and discussed TEM measurements. A. Wimmer, A. Urstoeger and M. Schuster wrote the manuscript.

Declaration of competing interest

The authors declare that they have no known competing financial interests or personal relationships that could have appeared to influence the work reported in this paper.

Appendix A. Supplementary data

Supplementary data to this article can be found online at https://doi.org/10.1016/j.watres.2019.115399.

References

Ahamed, M., Alsalhi, M.S., Siddiqui, M.K., 2010. Silver nanoparticle applications and human health. Clin. Chim. Acta 411 (23–24), 1841–1848.
Asharani, P.V., Lian Wu, Y., Gong, Z., Valiyaveettil, S., 2008. Toxicity of silver nanoparticles in zebrafish models. Nanotechnology 19 (25), 255102.
Asharani, P.V., Low Kah Mun, G., Hande, M.P., Valiyaveettil, S., 2009. Cytotoxicity and genotoxicity of silver nanoparticles in human cells. ACS Nano 3 (2), 279–290.
Beer, C., Foldbjerg, R., Hayashi, Y., Sutherland, D.S., Autrup, H., 2012. Toxicity of silver nanoparticles—nanoparticle or silver ion? Toxicol. Lett. 208 (3), 286–292.
Derjaguin, B., Landau, L., 1993. Theory of the stability of strongly charged lyophobic sols and of the adhesion of strongly charged particles in solutions of electrolytes. Prog. Surf. Sci. 43 (1), 30–59.
Duester, L., Fabricius, A.-L., Jakobtorweihen, S., Philippe, A., Weigl, F., Wimmer, A., Schuster, M., Nazar, M.F., 2016. Can cloud point-based enrichment, preservation, and detection methods help to bridge gaps in aquatic nanometrology? Anal. Bioanal. Chem. 408 (27), 7551–7557.
Foldbjerg, R., Olesen, P., Hougaard, M., Dang, D.A., Hoffmann, H.J., Autrup, H., 2009. PVP-coated silver nanoparticles and silver ions induce reactive oxygen species, apoptosis and necrosis in THP-1 monocytes. Toxicol. Lett. 190 (2), 156–162.
Gopinath, P., Gogoi, S.K., Sanpui, P., Paul, A., Chattopadhyay, A., Ghosh, S.S., 2010. Signaling gene cascade in silver nanoparticle induced apoptosis. Colloids Surfaces B Biointerfaces 77 (2), 240–245.
Hansen, S.F., Baun, A., 2012. When enough is enough. Nat. Nanotechnol. 7, 409.
Hartmann, G., Baumgartner, T., Schuster, M., 2014. Influence of particle coating and matrix constituents on the cloud point extraction efficiency of silver nanoparticles (Ag-NPs) and application for monitoring the formation of Ag-NPs from Ag+. Anal. Chem. 86 (1), 790–796.
Hartmann, G., Hutterer, C., Schuster, M., 2013. Ultra-trace determination of silver nanoparticles in water samples using cloud point extraction and ETAAS. J. Anal. Atomic Spectrom. 28 (4), 567–572.
Hartmann, G., Schuster, M., 2013. Species selective preconcentration and quantification of gold nanoparticles using cloud point extraction and electrothermal atomic absorption spectrometry. Anal. Chim. Acta 761, 27–33.
Kaegi, R., Voegelin, A., Ort, C., Sinnet, B., Thalmann, B., Krismer, J., Hagendorfer, H., Elumelu, M., Mueller, E., 2013. Fate and transformation of silver nanoparticles in urban wastewater systems. Water Res. 47 (12), 3866–3877.
Kaegi, R., Voegelin, A., Sinnet, B., Zuleeg, S., Hagendorfer, H., Burkhardt, M., Siegrist, H., 2011. Behavior of metallic silver nanoparticles in a pilot wastewater treatment plant. Environ. Sci. Technol. 45 (9), 3902–3908.
Kaegi, R., Voegelin, A., Sinnet, B., Zuleeg, S., Siegrist, H., Burkhardt, M., 2015. Transformation of AgCl nanoparticles in a sewer system - a field study. Sci. Total Environ. 535, 20–27.
Kim, B., Park, C.-S., Murayama, M., Hochella, M.F., 2010. Discovery and characterization of silver sulfide nanoparticles in final sewage sludge products. Environ. Sci. Technol. 44 (19), 7509–7514.
Kim, S., Choi, J.E., Choi, J., Chung, K.H., Park, K., Yi, J., Ryu, D.Y., 2009. Oxidative stress-dependent toxicity of silver nanoparticles in human hepatoma cells. Toxicol. In Vitro 23 (6), 1076–1084.
Kittler, S., Greulich, C., Diendorf, J., Köller, M., Epple, M., 2010. Toxicity of silver nanoparticles increases during storage because of slow dissolution under release of silver ions. Chem. Mater. 22 (16), 4548–4554.
Krug, H.F., 2014. Nanosafety research—are we on the right track? Angew. Chem. Int. Ed. 53 (46), 12304–12319.
Kumar, V., Sharma, N., Maitra, S.S., 2017. In vitro and in vivo toxicity assessment of nanoparticles. Int. Nano Lett. 7 (4), 243–256.
Levard, C., Hotze, E.M., Lowry, G.V., Brown, G.E., 2012. Environmental transformations of silver nanoparticles: impact on stability and toxicity. Environ. Sci. Technol. 46 (13), 6900–6914.
Li, L., Stoiber, M., Wimmer, A., Xu, Z., Lindenblatt, C., Helmreich, B., Schuster, M., 2016. To what extent can full-scale wastewater treatment plant effluent influence the occurrence of silver-based nanoparticles in surface waters? Environ. Sci. Technol. 50 (12), 6327–6333.
Liu, J., Hurt, R.H., 2010. Ion release kinetics and particle persistence in aqueous nano-silver colloids. Environ. Sci. Technol. 44 (6), 2169–2175.
Lodeiro, P., Achterberg, E.P., El-Shahawi, M.S., 2017. Detection of silver nanoparticles in seawater at ppb levels using UV-visible spectrophotometry with long path cells. Talanta 164, 257–260.
Lodeiro, P., Achterberg, E.P., Pampín, J., Affatati, A., El-Shahawi, M.S., 2016. Silver nanoparticles coated with natural polysaccharides as models to study AgNP aggregation kinetics using UV-Visible spectrophotometry upon discharge in complex environments. Sci. Total Environ. 539, 7–16.
Loza, K., Diendorf, J., Sengstock, C., Ruiz-Gonzalez, L., Gonzalez-Calbet, J.M., Vallet-Regi, M., Köller, M., Epple, M., 2014. The dissolution and biological effects of silver nanoparticles in biological media. J. Mater. Chem. B 2 (12), 1634–1643.
Ma, R., Levard, C., Judy, J.D., Unrine, J.M., Durenkamp, M., Martin, B., Jefferson, B., Lowry, G.V., 2014. Fate of zinc oxide and silver nanoparticles in a pilot wastewater treatment plant and in processed biosolids. Environ. Sci. Technol. 48 (1), 104–112.
Millero, F.J., Feistel, R., Wright, D.G., McDougall, T.J., 2008. The composition of standard seawater and the definition of the reference-composition salinity scale. Deep Sea Res. Oceanogr. Res. Pap. 55 (1), 50–72.
Montano, M.D., Olesik, J.W., Barber, A.G., Challis, K., Ranville, J.F., 2016. Single Particle ICP-MS: advances toward routine analysis of nanomaterials. Anal. Bioanal. Chem. 408 (19), 5053–5074.
Nowack, B., Ranville, J.F., Diamond, S., Gallego-Urrea, J.A., Metcalfe, C., Rose, J., Horne, N., Koelmans, A.A., Klaine, S.J., 2012. Potential scenarios for nanomaterial release and subsequent alteration in the environment. Environ. Toxicol. Chem. 31 (1), 50–59.
Park, E.J., Yi, J., Kim, Y., Choi, K., Park, K., 2010. Silver nanoparticles induce

cytotoxicity by a Trojan-horse type mechanism. Toxicol. In Vitro 24 (3), 872–878.
Pasricha, A., Jangra, S.L., Singh, N., Dilbaghi, N., Sood, K.N., Arora, K., Pasricha, R., 2012. Comparative study of leaching of silver nanoparticles from fabric and effective effluent treatment. J. Environ. Sci. 24 (5), 852–859.
Peters, R.J.B., Rivera, Z.H., van Bemmel, G., Marvin, H.J.P., Weigel, S., Bouwmeester, H., 2014. Development and validation of single particle ICP-MS for sizing and quantitative determination of nano-silver in chicken meat. Anal. Bioanal. Chem. 406 (16), 3875–3885.
Pettitt, M.E., Lead, J.R., 2013. Minimum physicochemical characterisation requirements for nanomaterial regulation. Environ. Int. 52, 41–50.
Qian, H., Peng, X., Han, X., Ren, J., Sun, L., Fu, Z., 2013. Comparison of the toxicity of silver nanoparticles and silver ions on the growth of terrestrial plant model Arabidopsis thaliana. J. Environ. Sci. 25 (9), 1947–1956.
Quik, J.T.K., Velzeboer, I., Wouterse, M., Koelmans, A.A., van de Meent, D., 2014. Heteroaggregation and sedimentation rates for nanomaterials in natural waters. Water Res. 48, 269–279.
Ribeiro, M.J., Maria, V.L., Scott-Fordsmand, J.J., Amorim, M.J.B., 2015. Oxidative stress mechanisms caused by Ag nanoparticles (NM300K) are different from those of AgNO(3): effects in the soil invertebrate enchytraeus crypticus. Int. J. Environ. Res. Public Health 12 (8), 9589–9602.
Sharma, V.K., Filip, J., Zboril, R., Varma, R.S., 2015. Natural inorganic nanoparticles - formation, fate, and toxicity in the environment. Chem. Soc. Rev. 44 (23), 8410–8423.
Sun, T.Y., Bornhöft, N.A., Hungerbühler, K., Nowack, B., 2016. Dynamic probabilistic modeling of environmental emissions of engineered nanomaterials. Environ. Sci. Technol. 50 (9), 4701–4711.
Teo, W.Z., Pumera, M., 2014. Fate of silver nanoparticles in natural waters; integrative use of conventional and electrochemical analytical techniques. RSC Adv. 4 (10), 5006–5011.
Toncelli, C., Mylona, K., Kalantzi, I., Tsiola, A., Pitta, P., Tsapakis, M., Pergantis, S.A., 2017. Silver nanoparticles in seawater: a dynamic mass balance at part per trillion silver concentrations. Sci. Total Environ. 601–602, 15–21.
Verwey, E.J.W., 1947. Theory of the stability of lyophobic colloids. J. Phys. Colloid Chem. 51 (3), 631–636.
Wiemann, M., Vennemann, A., Blaske, F., Sperling, M., Karst, U., 2017. Silver nanoparticles in the lung: toxic effects and focal accumulation of silver in remote organs. Nanomaterials 7 (12), 441.
Wimmer, A., Kalinnik, A., Schuster, M., 2018. New insights into the formation of silver-based nanoparticles under natural and semi-natural conditions. Water Res. 141, 227–234.
Wise, J.P., Sr, Goodale, B.C., Wise, S.S., Craig, G.A., Pongan, A.F., Walter, R.B., Thompson, W.D., Ng, A.K., Aboueissa, A.M., Mitani, H., Spalding, M.J., Mason, M.D., 2010. Silver nanospheres are cytotoxic and genotoxic to fish cells. Aquat. Toxicol. 97 (1), 34–41.
Zhang, J.L., Zhou, Z.P., Pei, Y., Xiang, Q.Q., Chang, X.X., Ling, J., Shea, D., Chen, L.Q., 2018. Metabolic profiling of silver nanoparticle toxicity in Microcystis aeruginosa. Environ. Sci.: Nano 5 (11), 2519–2530.
Zhang, W., Yao, Y., Sullivan, N., Chen, Y., 2011. Modeling the primary size effects of citrate-coated silver nanoparticles on their ion release kinetics. Environ. Sci. Technol. 45 (10), 4422–4428.
Zhou, X.-x., Li, Y.-j., Liu, J.-f., 2017. Highly efficient removal of silver-containing nanoparticles in waters by aged iron oxide magnetic particles. ACS Sustain. Chem. Eng. 5 (6), 5468–5476.

Supplementary Information

What happens to silver-based nanoparticles if they meet seawater?

Andreas Wimmer[1,#], Alexander Urstoeger[1,#], Nils Christoph Funck[1], Franziska Petra Adler[1], Leonhard Lenz[1], Markus Doeblinger[2], Michael Schuster[1,*]

[1] Division of Analytical Chemistry, Department of Chemistry, Technical University of Munich, Garching 85748, Germany

[2] Department of Chemistry, Ludwig-Maximilians-Universität München, Butenandtstr. 5–13 (E), 81377 Munich, Germany

[#] These authors contributed equally to the presented study.

[*] Corresponding author. Tel: +49 (0)89 289 13763; fax: +49 (0)89 289 14513; E-mail address: michael.schuster@ch.tum.de

8 pages

6 Figures

1 Table

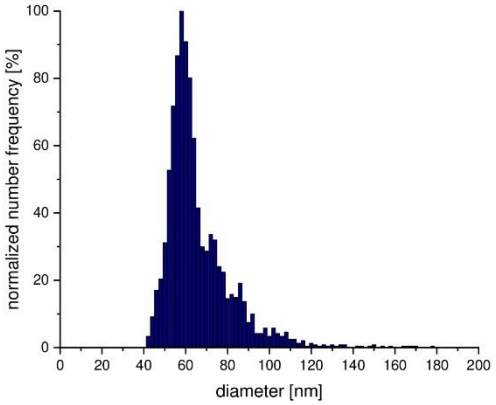

Figure S1: Particle size distribution based on particle number frequency of CA@Ag-NPs obtained from sp-ICP-MS measurement. The maximum frequency particle size is 58 nm.

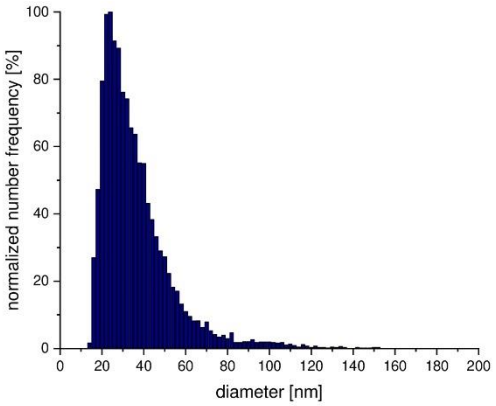

Figure S2: Particle size distribution based on particle number frequency of CA@Ag-NPs obtained from sp-ICP-MS measurement. The maximum frequency particle size is 24 nm.

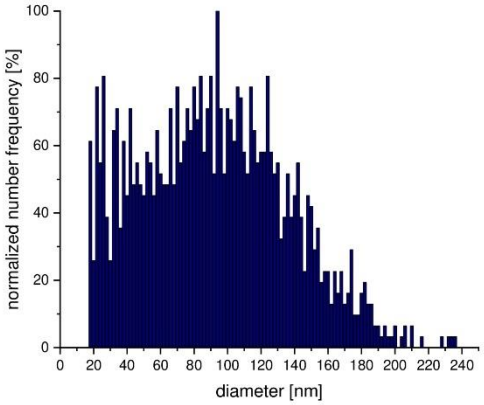

Figure S3: Particle size distribution based on particle number frequency of synthesized AgCl-NPs obtained from sp-ICP-MS measurement. The maximum frequency particle size is 94 nm.

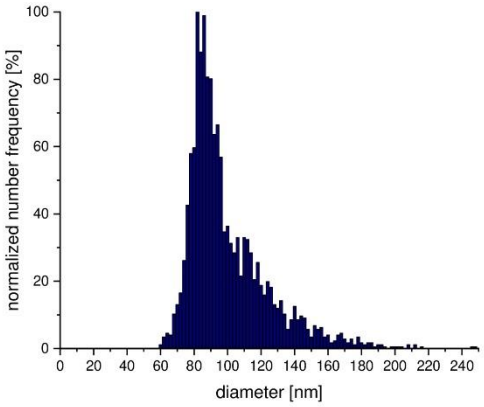

Figure S4: Particle size distribution based on particle number frequency of synthesized Ag_2S-NPs obtained from sp-ICP-MS measurement. The maximum frequency particle size is 82 nm.

Table S1: Compilation of measured Ag concentrations of total Ag-b-NPs (conventional ICP-MS) and Ag-b-NPs ≥ 8 nm (sp-ICP-MS) after incubation in ultra-pure water, artificial sea water and real sea water for a defined period of time supplemented by corresponding uncertainties U, the proportion of Ag-b-NPs < 8 nm in each sample and the proportion of remaining Ag-b-NPs in each incubation experiment. Given particle sizes represent the pristine maximum frequency particle sizes without incubation in the investigated media. "---" indicates measurements, in which no concentration beyond the limit of detection (LOD = 0.2 ng L^{-1}) could be detected.

incubation time [h]	Ag concentration of total Ag-b-NPs [ng L^{-1}]	U [ng L^{-1}]	Ag concentration of Ag-b-NPs ≥8nm [ng L^{-1}]	U [ng L^{-1}]	proportion Ag-b-NPs <8 nm [%]	proportion of remaining Ag-b-NPs [%]
CA@Ag 24 nm	**ultra-pure water**					
0	49.13	0.78	47.07	1.21	4.2	100
1	37.76	0.61	34.00	0.95	10.0	77
2	28.93	0.45	26.64	3.55	7.9	59
3	0.35	0.22	0.13	0.17	62.7	1
24	7.14	0.17	6.16	3.98	13.8	15
48	6.97	0.55	7.53	3.15	0.0	14
72	5.03	0.62	5.36	1.38	0.0	10
CA@Ag 58 nm	**ultra pure water**					
0	51.62	1.09	51.11	1.45	1.0	100
1	45.35	2.15	45.46	2.75	0.0	88
2	41.08	1.04	40.55	3.03	1.3	80
3	45.15	0.59	45.26	0.35	0.0	87
24	30.24	1.00	29.49	6.66	2.5	59
48	20.76	1.39	20.93	5.04	0.0	40
72	21.61	0.63	21.62	2.19	0.0	42
AgCl 94 nm	**ultra pure water**					
0	52.15	1.35	51.74	1.68	0.8	100
1	23.63	1.74	19.47	0.99	17.6	45
2	17.01	1.10	13.71	1.19	19.4	33
3	13.38	1.87	10.93	1.32	18.3	26
24	8.10	1.00	4.37	0.66	46.0	16
48	1.47	0.54	1.22	0.44	16.9	3
72	0.28	0.16	0.07	0.03	75.6	1
Ag_2S 82 nm	**ultra pure water**					
0	65.27	1.45	65.82	2.04	0.0	100
1	51.60	9.34	56.19	4.56	0.0	79
2	63.32	9.34	56.52	4.96	10.7	97
3	44.71	5.17	51.18	8.68	0.0	69
24	24.91	4.65	16.18	1.47	35.0	38
48	19.91	6.21	14.58	3.71	26.7	30
72	17.00	0.79	14.29	0.20	16.0	26

CA@Ag 24 nm	artificial sea water					
0	53.37	1.02	50.53	1.45	5.3	100
1	22.49	1.45	20.15	0.27	10.4	42
2	17.39	1.12	13.56	1.92	22.0	33
3	1.36	1.18	0.00	0.00	100.0	3
24	2.83	0.14	2.55	1.23	10.2	5
48	1.93	0.21	1.34	0.16	30.7	4
72	1.52	0.40	1.02	0.13	33.3	3
CA@Ag 58 nm	**artificial sea water**					
0	55.25	2.45	54.74	0.67	0.9	100
1	27.76	0.70	27.02	1.81	2.7	50
2	22.06	0.78	20.28	0.68	8.1	40
3	21.46	1.69	20.15	1.59	6.1	39
24	8.49	1.06	7.21	2.98	15.1	15
48	2.33	0.56	1.91	0.91	17.8	4
72	2.41	0.34	1.91	0.91	20.7	4
AgCl 94 nm	**artificial sea water**					
0	46.02	1.45	39.19	3.47	14.8	100
1	9.05	0.99	8.98	1.92	0.8	20
2	6.79	1.32	6.46	0.61	4.9	15
3	2.34	0.59	2.88	1.54	0.0	5
24	5.31	0.85	0.74	0.61	86.1	12
48	0.86	0.24	2.34	1.57	0.0	2
72	0.41	0.34	0.88	0.52	0.0	1
Ag_2S 82 nm	**artificial sea water**					
0	59.23	1.33	59.11	1.05	0.2	100
1	22.99	1.54	28.76	1.80	0.0	39
2	17.39	3.25	16.17	4.43	7.0	29
3	13.02	1.18	14.04	1.38	0.0	22
24	4.29	0.09	0.88	0.72	79.5	7
48	2.88	0.42	0.50	0.19	82.7	5
72	6.44	0.32	3.99	0.57	38.1	11
CA@Ag 24 nm	**sea water**					
0	52.04	1.56	50.23	1.23	3.5	100
1	16.21	0.34	13.12	0.64	19.1	31
2	12.98	0.24	10.54	1.34	18.8	25
3	0.98	0.12	0.42	0.52	56.9	2
24	---	---	0.14	0.06	---	0
48	---	---	0.25	0.07	---	0
72	---	---	0.17	0.07	---	0
CA@Ag 58 nm	**sea water**					
0	47.50	1.21	47.92	1.59	0.0	100
1	20.37	4.32	22.50	0.57	0.0	43
2	14.00	2.95	12.59	1.74	10.0	29
3	2.86	1.15	5.98	0.76	0.0	6
24	1.81	0.30	1.33	0.11	26.9	4

5

48	4.90	0.44	8.19	0.73	0.0	10
72	0.62	0.25	1.78	0.22	0.0	1
AgCl 94 nm	**sea water**					
0	47.98	0.92	47.34	1.34	1.3	100
1	8.99	0.82	5.60	0.62	37.7	19
2	6.29	0.99	0.29	0.22	95.4	13
3	4.14	0.73	0.11	0.08	97.3	9
24	2.09	0.79	0.43	0.19	79.5	4
48	1.01	0.18	0.26	0.07	74.2	11
72	0.96	0.50	0.26	0.07	72.8	2
Ag_2S 82 nm	**sea water**					
0	52.67	1.01	50.58	1.36	4.0	100
1	26.26	3.12	19.61	1.03	25.3	50
2	18.47	2.79	16.61	0.45	10.1	35
3	12.65	2.45	9.29	2.05	26.5	24
24	2.67	0.83	2.62	1.00	1.8	5
48	2.03	0.65	2.18	0.83	0.0	4
72	2.77	1.06	2.12	0.46	23.2	5

6

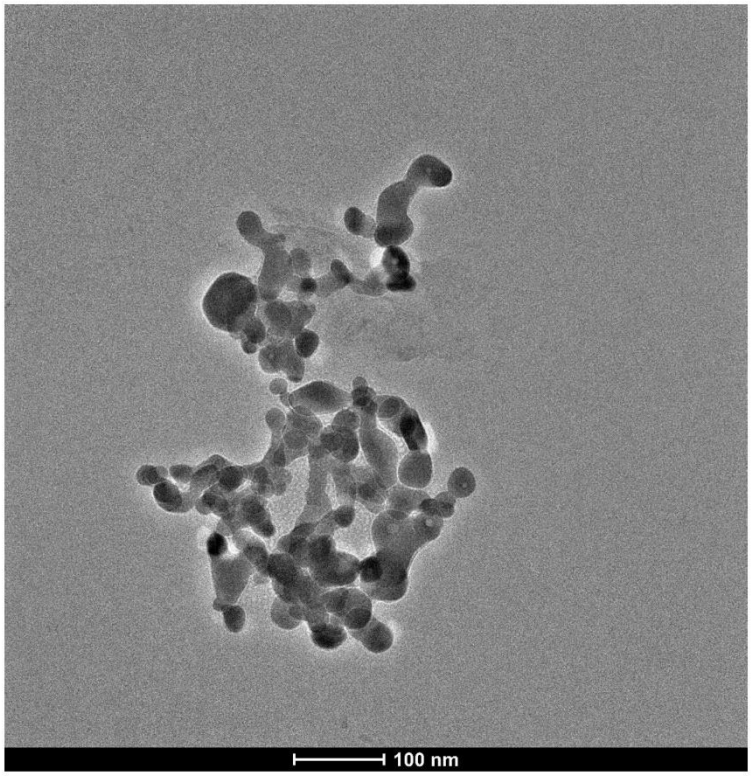

Figure S5: TEM image of an Ag_2S-NP aggregate after incubation in seawater for 1 h.

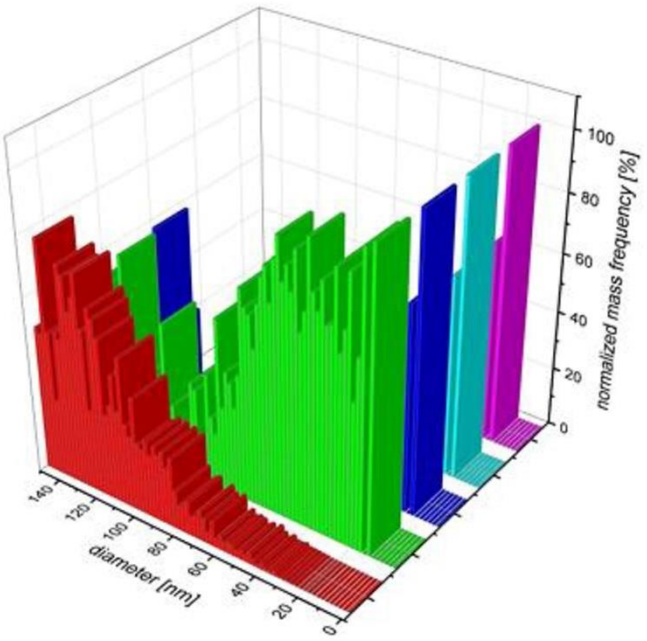

Figure S6: Particle size distributions of pristine (red) AgCl-NPs and incubated in seawater for 1 h of incubation (green), 1 day of incubation (blue), 2 days of incubation (turquiose), and 3 days of incubation (purple) presented as normalized mass frequency. Presented results are based on CPE-sp-ICP-MS measurements.

Table S2: Compilation of measured Ag concentrations of total Ag-b-NPs (conventional ICP-MS) after incubation in real sea water for a defined period of time at 23 °C and 60 °C supplemented by corresponding uncertainties U and the proportion of remaining Ag-b-NPs in each incubation experiment. Given particle sizes represent the pristine maximum frequency particle sizes without incubation in the investigated media.

incubation time [h]	**Ag concentration of total Ag-b-NPs [ng L^{-1}]**	**U [ng L^{-1}]**	**proportion of remaining Ag-b-NPs [%]**
CA@Ag 58 nm	**23 °C incubation temperature**		
0	48.45	0.33	100
1	26.59	0.44	55
2	23.64	0.21	49
CA@Ag 58 nm	**60 °C incubation temperature**		
0	49.62	0.82	100
1	30.19	1.05	61
2	22.05	0.45	44

Table S3: Compilation of measured Ag concentrations of total Ag-b-NPs (conventional ICP-MS) after incubation in aqueous solutions of NOM for an increasing incubation time supplemented by corresponding uncertainties U and the proportion of remaining Ag-b-NPs in each incubation experiment. Given particle sizes represent the pristine maximum frequency particle sizes without incubation in the investigated media.

incubation time [h]	Ag concentration of total Ag-b-NPs [ng L^{-1}]	U [ng L^{-1}]	proportion of remaining Ag-b-NPs [%]
CA@Ag 58 nm	**0 mg L^{-1} NOM**		
0	51.34	0.56	100
1	37.80	0.33	74
72	8.32	0.56	16
CA@Ag 58 nm	**5 mg L^{-1} NOM**		
0	49.88	0.41	100
1	41.54	0.65	83
72	1.98	0.09	4
Ag_2S 82 nm	**0 mg L^{-1} NOM**		
0	52.05	0.38	100
1	45.38	0.56	87
72	6.93	0.11	13
Ag_2S 82 nm	**5 mg L^{-1} NOM**		
0	47.79	0.36	100
1	43.65	0.26	91
72	1.08	0.08	2

9. Vollständige Publikationsliste

Publikationen

1. A. Urstoeger, L. Zacherl, M. Muhr, Y. Selic, M. Wenisch, M. Klotz, M. Schuster, Magnetic solid phase extraction of silver-based nanoparticles in aqueous samples: Influence of particle composition and matrix effects on its application to environmental samples and species-selective elution and determination of silver sulphide nanoparticles with sp-ICP-MS, Talanta, 2021, 225, 122028.
2. A. Wimmer, A. Urstoeger, T. Hinke, M. Aust, P.J. Altmann, M. Schuster, Separating dissolved silver from nanoparticulate silver is the key: Improved cloud-point-extraction hyphenated to single particle ICP-MS for comprehensive analysis of silver-based nanoparticles in real environmental samples down to single-digit nm particle sizes, Analytica Chimica Acta, 2021, 1150, 238198.
3. A. Urstoeger, A. Wimmer, R. Kaegi, S. Reiter, M. Schuster, Looking at Silver-Based Nanoparticles in Environmental Water Samples: Repetitive Cloud Point Extraction Bridges Gaps in Electron Microscopy for Naturally Occurring Nanoparticles, Environmental Science & Technology, 2020, 54, 12063-12071.
4. A. Wimmer, A. Urstoeger, N.C. Funck, F.P. Adler, L. Lenz, M. Doeblinger, M. Schuster, What happens to silver-based nanoparticles if they meet seawater?, Water Research, 2020, 171, 115399.

Poster

1. Stability of silver-based nanoparticles at environmentally relevant concentrations in seawater monitored by spICP-MS. A. Urstoeger, A. Wimmer, A. Schuster. European Winter Conference on Plasma Spectrochemistry 2019, Pau, Frankreich.

Vorträge

1. spICP-MS – en route to the perfect measurement. A. Urstoeger. A. Wimmer, M. Schuster, DAAS-Doktorandenseminar 2018, Geesthacht, Deutschland.
2. Stability of silver-based nanoparticles at environmentally relevant concentrations in seawater monitored by spICP-MS. A. Urstoeger. ANAKON 2019, Münster, Deutschland.

10. Literaturverzeichnis

[1] N. Taniguchi, On the basic concept of nanotechnology, Proceedings of the International Conference on Production Engineering, Part II, Japan Society of Precision Engineering, Tokyo, 1974.

[2] F. Gottschalk, T. Sun, B. Nowack, Environmental concentrations of engineered nanomaterials: review of modeling and analytical studies, Environmental Pollution, 2013, 181, 287-300.

[3] T.M. Benn, P. Westerhoff, Nanoparticle Silver Released into Water from Commercially Available Sock Fabrics, Environmental Science & Technology, 2008, 42, 4133-4139.

[4] T. Benn, B. Cavanagh, K. Hristovski, J.D. Posner, P. Westerhoff, The Release of Nanosilver from Consumer Products Used in the Home, Journal of Environmental Quality, 2010, 39, 1875-1882.

[5] R. Kaegi, B. Sinnet, S. Zuleeg, H. Hagendorfer, E. Mueller, R. Vonbank, M. Boller, M. Burkhardt, Release of Silver Nanoparticles from Outdoor Facades, Environmental Pollution, 2010, 158, 2900-2905.

[6] N.C. Mueller, B. Nowack, Exposure Modeling of Engineered Nanoparticles in the Environment, Environmental Science & Technology, 2008, 42, 4447-4453.

[7] B. Nowack, Nanosilver Revisited Downstream, Science, 2010, 330, 1054-1055.

[8] F. Gottschalk, T. Sonderer, R.W. Scholz, B. Nowack, Modeled environmental concentrations of engineered nanomaterials (TiO_2, ZnO, Ag, CNT, Fullerenes) for different regions, Environmental Science & Technology, 2009, 43, 9216-9222.

[9] L. Li, M. Stoiber, A. Wimmer, Z. Xu, C. Lindenblatt, B. Helmreich, M. Schuster, To What Extent Can Full-Scale Wastewater Treatment Plant Effluent Influence the Occurrence of Silver-Based Nanoparticles in Surface Waters?, Environmental Science & Technology, 2016, 50, 6327-6333.

[10] G. Hartmann, T. Baumgartner, M. Schuster, Influence of Particle Coating and Matrix Constituents on the Cloud Point Extraction Efficiency of Silver Nanoparticles (Ag-NPs) and Application for Monitoring the Formation of Ag-NPs from Ag^+, Analytical Chemistry, 2014, 86, 790-796.

[11] Europäische Kommission, Empfehlung der Kommission vom 18. Oktober 2011 zur Definition von Nanomaterialien, 2011. https://eur-lex.europa.eu/legal-content/DE/TXT/?uri=CELEX%3A32011H0696 (aufgerufen am 28.01.2021).

[12] J.N. Tiwari, R.N. Tiwari, K.S. Kim, Zero-dimensional, one-dimensional, two-dimensional and three-dimensional nanostructured materials for advanced electrochemical energy devices, Progress in Materials Science, 2012, 57, 724-803.
[13] K.L. Kelly, E. Coronado, L.L. Zhao, G.C. Schatz, The Optical Properties of Metal Nanoparticles: The Influence of Size, Shape, and Dielectric Environment, The Journal of Physical Chemistry B, 2003, 107, 668-677.
[14] Y.L. Hewakuruppu, L.A. Dombrovsky, C. Chen, V. Timchenko, X. Jiang, S. Baek, R.A. Taylor, Plasmonic "pump-probe" method to study semi-transparent nanofluids, Applied Optics, 2013, 52, 6041-6050.
[15] R.A. Taylor, P.E. Phelan, T.P. Otanicar, R. Adrian, R. Prasher, Nanofluid optical property characterization: towards efficient direct absorption solar collectors, Nanoscale Research Letters, 2011, 6, 225.
[16] R.A. Taylor, T. Otanicar, G. Rosengarten, Nanofluid-based optical filter optimization for PV/T systems, Light: Science & Applications, 2012, 1, e34.
[17] R.A. Taylor, T.P. Otanicar, Y. Herukerrupu, F. Bremond, G. Rosengarten, E.R. Hawkes, X. Jiang, S. Coulombe, Feasibility of nanofluid-based optical filters, Applied Optics, 2013, 52, 1413-1422.
[18] M. Amelia, C. Lincheneau, S. Silvi, A. Credi, Electrochemical properties of CdSe and CdTe quantum dots, Chemical Society Reviews, 2012, 41, 5728-5743.
[19] W.J. Stark, P.R. Stoessel, W. Wohlleben, A. Hafner, Industrial applications of nanoparticles, Chemical Society Reviews, 2015, 44, 5793-5805.
[20] I.L. Medintz, H.T. Uyeda, E.R. Goldman, H. Mattoussi, Quantum dot bioconjugates for imaging, labelling and sensing, Nature Materials, 2005, 4, 435-446.
[21] A. Puri, K. Loomis, B. Smith, J.-H. Lee, A. Yavlovich, E. Heldman, R. Blumenthal, Lipid-based nanoparticles as pharmaceutical drug carriers: from concepts to clinic, Critical Reviews in Therapeutic Drug Carrier Systems, 2009, 26, 523-580.
[22] M. Gujrati, A. Malamas, T. Shin, E. Jin, Y. Sun, Z.-R. Lu, Multifunctional Cationic Lipid-Based Nanoparticles Facilitate Endosomal Escape and Reduction-Triggered Cytosolic siRNA Release, Molecular Pharmaceutics, 2014, 11, 2734-2744.
[23] C.T. Shindu, Harshita, M. Pawan Kumar, T. Sushama, Ceramic Nanoparticles: Fabrication Methods and Applications in Drug Delivery, Current Pharmaceutical Design, 2015, 21, 6165-6188.
[24] R. Kessler, Engineered Nanoparticles in Consumer Products: Understanding a New Ingredient, Environmental Health Perspectives, 2011, 119, A120-A125.

[25] T.V. Duncan, Applications of Nanotechnology in Food Packaging and Food Safety: Barrier Materials, Antimicrobials and Sensors, J. Colloid Interface Sci., 2011, 363, 1-24.
[26] S.J. Soenen, W.J. Parak, J. Rejman, B. Manshian, (Intra)cellular Stability of Inorganic Nanoparticles: Effects on Cytotoxicity, Particle Functionality, and Biomedical Applications, Chemical Reviews, 2015, 115, 2109-2135.
[27] M. Bąkowski, B. Kiczorowska, W. Samolińska, R. Klebaniuk, A. Lipiec, Silver and Zinc Nanoparticles in Animal Nutrition – A Review, Annals of Animal Science, 2018, 18, 879-898.
[28] K. Balkis Ameen, K. Rajasekar, T. Rajasekharan, Silver Nanoparticles in Mesoporous Aerogel Exhibiting Selective Catalytic Oxidation of Benzene in CO2 Free Air, Catalysis Letters, 2007, 119, 289-295.
[29] H.-L. Jiang, T. Akita, T. Ishida, M. Haruta, Q. Xu, Synergistic Catalysis of Au@Ag Core−Shell Nanoparticles Stabilized on Metal−Organic Framework, Journal of the American Chemical Society, 2011, 133, 1304-1306.
[30] Q.H. Tran, T.M.H. Pham, L. Anh-Tuan, T. Matteo, Recent Advances of Silver Nanoparticles in Cancer Diagnosis and Treatment, Anti-Cancer Agents in Medicinal Chemistry, 2020, 20, 1276-1287.
[31] R. Ghosh Chaudhuri, S. Paria, Core/Shell Nanoparticles: Classes, Properties, Synthesis Mechanisms, Characterization, and Applications, Chemical Reviews, 2012, 112, 2373-2433.
[32] S. Prabhu, E.K. Poulose, Silver nanoparticles: mechanism of antimicrobial action, synthesis, medical applications, and toxicity effects, International Nano Letters, 2012, 2.
[33] A. Biswas, I.S. Bayer, A.S. Biris, T. Wang, E. Dervishi, F. Faupel, Advances in top–down and bottom–up surface nanofabrication: Techniques, applications & future prospects, Advances in Colloid and Interface Science, 2012, 170, 2-27.
[34] T.P. Yadav, R. Yadav, D. Singh, Mechanical Milling: a Top Down Approach for the Synthesis of Nanomaterials and Nanocomposites, Nanoscience and Nanotechnology, 2012, 2, 22-48.
[35] A.V. Kabashin, M. Meunier, Synthesis of colloidal nanoparticles during femtosecond laser ablation of gold in water, Journal of Applied Physics, 2003, 94, 7941-7943.
[36] D. Mijatovic, J.C.T. Eijkel, A. van den Berg, Technologies for nanofluidic systems: top-down vs. bottom-up—a review, Lab on a Chip, 2005, 5, 492-500.
[37] B. Malik, T.B. Pirzadah, M. Kumar, R.U. Rehman, Biosynthesis of Nanoparticles and Their Application in Pharmaceutical Industry, in: R. Prasad, V. Kumar, M. Kumar (Eds.), Nanotechnology: Food and Environmental Paradigm, Springer Singapore, Singapore, 2017, 235-252.

[38] R. Kaegi, A. Voegelin, C. Ort, B. Sinnet, B. Thalmann, J. Krismer, H. Hagendorfer, M. Elumelu, E. Mueller, Fate and Transformation of Silver Nanoparticles in Urban Wastewater Systems, Water Research, 2013, 47, 3866-3877.

[39] K. Tiede, A.B.A. Boxall, X. Wang, D. Gore, D. Tiede, M. Baxter, H. David, S.P. Tear, J. Lewis, Application of hydrodynamic chromatography-ICP-MS to investigate the fate of silver nanoparticles in activated sludge, Journal of Analytical Atomic Spectrometry, 2010, 25, 1149-1154.

[40] R. Kaegi, A. Voegelin, B. Sinnet, S. Zuleeg, H. Hagendorfer, M. Burkhardt, H. Siegrist, Behavior of Metallic Silver Nanoparticles in a Pilot Wastewater Treatment Plant, Environmental Science & Technology, 2011, 45, 3902-3908.

[41] S. Kampe, R. Kaegi, K. Schlich, C. Wasmuth, H. Hollert, C. Schlechtriem, Silver nanoparticles in sewage sludge: Bioavailability of sulfidized silver to the terrestrial isopod Porcellio scaber, Environmental Toxicology and Chemistry, 2018, 37, 1606-1613.

[42] A. Wimmer, A. Kalinnik, M. Schuster, New insights into the formation of silver-based nanoparticles under natural and semi-natural conditions, Water Research, 2018, 141, 227-234.

[43] S. Lekamge, A.F. Miranda, A. Abraham, V. Li, R. Shukla, V. Bansal, D. Nugegoda, The Toxicity of Silver Nanoparticles (AgNPs) to Three Freshwater Invertebrates With Different Life Strategies: Hydra vulgaris, Daphnia carinata, and Paratya australiensis, Frontiers in Environmental Science, 2018, 6.

[44] P.V. Asharani, Y. Lian Wu, Z. Gong, S. Valiyaveettil, Toxicity of silver nanoparticles in zebrafish models, Nanotechnology, 2008, 19, 255102.

[45] Y.-M. Cho, Y. Mizuta, J.-i. Akagi, T. Toyoda, M. Sone, K. Ogawa, Size-dependent acute toxicity of silver nanoparticles in mice, Journal of Toxicologic Pathology, 2018, 31, 73-80.

[46] V. Kumar, N. Sharma, S.S. Maitra, In vitro and in vivo toxicity assessment of nanoparticles, International Nano Letters, 2017, 7, 243-256.

[47] M.J. Hajipour, K.M. Fromm, A. Akbar Ashkarran, D. Jimenez de Aberasturi, I.R.d. Larramendi, T. Rojo, V. Serpooshan, W.J. Parak, M. Mahmoudi, Antibacterial properties of nanoparticles, Trends in Biotechnology, 2012, 30, 499-511.

[48] S. Pal, Y.K. Tak, J.M. Song, Does the Antibacterial Activity of Silver Nanoparticles Depend on the Shape of the Nanoparticle? A Study of the Gram-Negative Bacterium Escherichia coli, Applied and Environmental Microbiology, 2007, 73, 1712-1720.

[49] S. Shrivastava, T. Bera, A. Roy, G. Singh, P. Ramachandrarao, D. Dash, Characterization of enhanced antibacterial effects of novel silver nanoparticles, Nanotechnology, 2007, 18, 225103.

[50] E. Navarro, A. Baun, R. Behra, N.B. Hartmann, J. Filser, A.-J. Miao, A. Quigg, P.H. Santschi, L. Sigg, Environmental behavior and ecotoxicity of engineered nanoparticles to algae, plants, and fungi, Ecotoxicology, 2008, 17, 372-386.
[51] A. Yan, Z. Chen, Impacts of Silver Nanoparticles on Plants: A Focus on the Phytotoxicity and Underlying Mechanism, International Journal of Molecular Sciences, 2019, 20, 1003.
[52] P.V. AshaRani, G. Low Kah Mun, M.P. Hande, S. Valiyaveettil, Cytotoxicity and Genotoxicity of Silver Nanoparticles in Human Cells, ACS Nano, 2009, 3, 279-290.
[53] A. Haase, J. Tentschert, H. Jungnickel, P. Graf, A. Mantion, F. Draude, J. Plendl, M.E. Goetz, S. Galla, A. Mašić, A.F. Thuenemann, A. Taubert, H.F. Arlinghaus, A. Luch, Toxicity of silver nanoparticles in human macrophages: uptake, intracellular distribution and cellular responses, Journal of Physics: Conference Series, 2011, 304, 012030.
[54] W. Lu, D. Senapati, S. Wang, O. Tovmachenko, A.K. Singh, H. Yu, P.C. Ray, Effect of surface coating on the toxicity of silver nanomaterials on human skin keratinocytes, Chemical Physics Letters, 2010, 487, 92-96.
[55] S. Kim, J.E. Choi, J. Choi, K.-H. Chung, K. Park, J. Yi, D.-Y. Ryu, Oxidative stress-dependent toxicity of silver nanoparticles in human hepatoma cells, Toxicology in Vitro, 2009, 23, 1076-1084.
[56] C. Beer, R. Foldbjerg, Y. Hayashi, D.S. Sutherland, H. Autrup, Toxicity of silver nanoparticles—Nanoparticle or silver ion?, Toxicology Letters, 2012, 208, 286-292.
[57] M.V.D.Z. Park, A.M. Neigh, J.P. Vermeulen, L.J.J. de la Fonteyne, H.W. Verharen, J.J. Briedé, H. van Loveren, W.H. de Jong, The effect of particle size on the cytotoxicity, inflammation, developmental toxicity and genotoxicity of silver nanoparticles, Biomaterials, 2011, 32, 9810-9817.
[58] G.A. Sotiriou, S.E. Pratsinis, Antibacterial Activity of Nanosilver Ions and Particles, Environmental Science & Technology, 2010, 44, 5649-5654.
[59] J.A. Champion, S. Mitragotri, Role of target geometry in phagocytosis, Proceedings of the National Academy of Sciences of the United States of America, 2006, 103, 4930-4934.
[60] C. Levard, B.C. Reinsch, F.M. Michel, C. Oumahi, G.V. Lowry, G.E. Brown, Sulfidation Processes of PVP-Coated Silver Nanoparticles in Aqueous Solution: Impact on Dissolution Rate, Environmental Science & Technology, 2011, 45, 5260-5266.
[61] C. Levard, E.M. Hotze, G.V. Lowry, G.E. Brown, Environmental Transformations of Silver Nanoparticles: Impact on Stability and Toxicity, Environmental Science & Technology, 2012, 46, 6900-6914.

[62] R. Kaegi, A. Voegelin, B. Sinnet, S. Zuleeg, H. Siegrist, M. Burkhardt, Transformation of AgCl nanoparticles in a sewer system — A field study, Science of The Total Environment, 2015, 535, 20-27.
[63] B. Nowack, J.F. Ranville, S. Diamond, J.A. Gallego-Urrea, C. Metcalfe, J. Rose, N. Horne, A.A. Koelmans, S.J. Klaine, Potential scenarios for nanomaterial release and subsequent alteration in the environment, Environmental Toxicology and Chemistry, 2012, 31, 50-59.
[64] M.E. Schimpf, K. Caldwell, C. Giddings, Field-Flow Fractionation Handbook, 1 ed., Wiley-Interscience, New York, 2000.
[65] S. Dubascoux, I. Le Hécho, M. Hassellöv, F. Von Der Kammer, M. Potin Gautier, G. Lespes, Field-flow fractionation and inductively coupled plasma mass spectrometer coupling: History, development and applications, Journal of Analytical Atomic Spectrometry, 2010, 25, 613-623.
[66] A. Ulrich, S. Losert, N. Bendixen, A. Al-Kattan, H. Hagendorfer, B. Nowack, C. Adlhart, J. Ebert, M. Lattuada, K. Hungerbühler, Critical aspects of sample handling for direct nanoparticle analysis and analytical challenges using asymmetric field flow fractionation in a multi-detector approach, Journal of Analytical Atomic Spectrometry, 2012, 27, 1120-1130.
[67] E.P. Gray, T.A. Bruton, C.P. Higgins, R.U. Halden, P. Westerhoff, J.F. Ranville, Analysis of gold nanoparticle mixtures: a comparison of hydrodynamic chromatography (HDC) and asymmetrical flow field-flow fractionation (AF4) coupled to ICP-MS, Journal of Analytical Atomic Spectrometry, 2012, 27, 1532-1539.
[68] S. Brunauer, P.H. Emmett, E. Teller, Adsorption of Gases in Multimolecular Layers, Journal of the American Chemical Society, 1938, 60, 309-319.
[69] S. Mourdikoudis, R.M. Pallares, N.T.K. Thanh, Characterization techniques for nanoparticles: comparison and complementarity upon studying nanoparticle properties, Nanoscale, 2018, 10, 12871-12934.
[70] P.N. Njoki, I.I.S. Lim, D. Mott, H.-Y. Park, B. Khan, S. Mishra, R. Sujakumar, J. Luo, C.-J. Zhong, Size Correlation of Optical and Spectroscopic Properties for Gold Nanoparticles, The Journal of Physical Chemistry C, 2007, 111, 14664-14669.
[71] B.J. Berne, R. Pecora, Dynamic Light Scattering: With Applications to Chemistry, Biology, and Physics, Dover Publications Inc., Mineola, 2000.
[72] V. Filipe, A. Hawe, W. Jiskoot, Critical Evaluation of Nanoparticle Tracking Analysis (NTA) by NanoSight for the Measurement of Nanoparticles and Protein Aggregates, Pharmaceutical Research, 2010, 27, 796-810.

[73] D. Brucker, K. Leopold, Sizing silver nanoparticles in chicken meat using direct slurry sampling graphite furnace atomic absorption spectrometry, Analytical and Bioanalytical Chemistry, 2019, 411, 4551-4558.
[74] K. Leopold, A. Brandt, H. Tarren, Sizing gold nanoparticles using graphite furnace atomic absorption spectrometry, Journal of Analytical Atomic Spectrometry, 2017, 32, 723-730.
[75] T. Panyabut, N. Sirirat, A. Siripinyanond, Use of electrothermal atomic absorption spectrometry for size profiling of gold and silver nanoparticles, Analytica Chimica Acta, 2018, 1000, 75-84.
[76] M. Resano, E. Garcia-Ruiz, R. Garde, High-resolution continuum source graphite furnace atomic absorption spectrometry for the monitoring of Au nanoparticles, Journal of Analytical Atomic Spectrometry, 2016, 31, 2233-2241.
[77] L. Degenkolb, G. Metreveli, A. Philippe, A. Brandt, K. Leopold, L. Zehlike, H.-J. Vogel, G.E. Schaumann, T. Baumann, M. Kaupenjohann, F. Lang, S. Kumahor, S. Klitzke, Retention and remobilization mechanisms of environmentally aged silver nanoparticles in an artificial riverbank filtration system, Science of The Total Environment, 2018, 645, 192-204.
[78] M. Wierucka, M. Biziuk, Application of magnetic nanoparticles for magnetic solid-phase extraction in preparing biological, environmental and food samples, TrAC Trends in Analytical Chemistry, 2014, 59, 50-58.
[79] M. Mahmoudi, S. Sant, B. Wang, S. Laurent, T. Sen, Superparamagnetic iron oxide nanoparticles (SPIONs): Development, surface modification and applications in chemotherapy, Advanced Drug Delivery Reviews, 2011, 63, 24-46.
[80] J.-f. Liu, Z.-s. Zhao, G.-b. Jiang, Coating Fe_3O_4 Magnetic Nanoparticles with Humic Acid for High Efficient Removal of Heavy Metals in Water, Environmental Science & Technology, 2008, 42, 6949-6954.
[81] X. Zhou, J. Liu, C. Yuan, Y. Chen, Speciation analysis of silver sulfide nanoparticles in environmental waters by magnetic solid-phase extraction coupled with ICP-MS, Journal of Analytical Atomic Spectrometry, 2016, 31, 2285-2292.
[82] X.-x. Zhou, Y.-j. Li, J.-f. Liu, Highly Efficient Removal of Silver-Containing Nanoparticles in Waters by Aged Iron Oxide Magnetic Particles, ACS Sustainable Chemistry & Engineering, 2017, 5, 5468-5476.
[83] J.-f. Liu, J.-b. Chao, R. Liu, Z.-q. Tan, Y.-g. Yin, Y. Wu, G.-b. Jiang, Cloud Point Extraction as an Advantageous Preconcentration Approach for Analysis of Trace Silver Nanoparticles in Environmental Waters, Analytical Chemistry, 2009, 81, 6496-6502.

[84] F.H. Quina, W.L. Hinze, Surfactant-mediated Cloud Point Extractions: An Environmentally Benign Alternative Separation Approach, Industrial & Engineering Chemistry Research, 1999, 38, 4150-4168.
[85] C.D. Stalikas, Micelle-mediated Extraction as a Tool for Separation and Preconcentration in Metal Analysis, TrAC, Trends in Analytical Chemistry, 2002, 21, 343-355.
[86] E. Pramauro, E. Pelezetti, Surfactants in Analytical Chemistry: Applications of Organized Amphiphilic Media, Elsevier, Amsterdam, 1996.
[87] T.M. Schmitt, Analysis of Surfactants, 2 ed., CRC Press, London, 2019.
[88] D. Meyers, Surfactants in Solution: Monolayers and Micelles, Surfactant Science and Technology, 2005, 107-159.
[89] G. Hartmann, C. Hutterer, M. Schuster, Ultra-Trace Determination of Silver Nanoparticles in Water Samples Using Cloud Point Extraction and ETAAS, Journal of Analytical Atomic Spectrometry, 2013, 28, 567-572.
[90] P.G. Nilsson, H. Wennerstroem, B. Lindman, Structure of micellar solutions of nonionic surfactants. Nuclear magnetic resonance self-diffusion and proton relaxation studies of poly(ethylene oxide) alkyl ethers, The Journal of Physical Chemistry, 1983, 87, 1377-1385.
[91] L. Duester, A.-L. Fabricius, S. Jakobtorweihen, A. Philippe, F. Weigl, A. Wimmer, M. Schuster, M.F. Nazar, Can cloud point-based enrichment, preservation, and detection methods help to bridge gaps in aquatic nanometrology?, Analytical and Bioanalytical Chemistry, 2016, 408, 7551-7557.
[92] J.-f. Liu, R. Liu, Y.-g. Yin, G.-b. Jiang, Triton X-114 based cloud point extraction: a thermoreversible approach for separation/concentration and dispersion of nanomaterials in the aqueous phase, Chemical Communications, 2009, 1514-1516.
[93] H. Xie, Y. Gu, H.J. Ploehn, Dendrimer-mediated synthesis of platinum nanoparticles: new insights from dialysis and atomic force microscopy measurements, Nanotechnology, 2005, 16, 492-501.
[94] R. Reed, J. Weyers, A. Jones, Practical Skills in Biomolecular Science, 5 ed., Pearson Education Limited, Cham, 2016,
[95] A. de Haan, H. Bosch, Industrial Separation Processes, de Gruyter, Berlin, 2013.
[96] Agilent Technologies, Agilent 7900 Series ICP-MS Hardware Manual, 2014.
[97] R. Thomas, A Beginner's Guide to ICP-MS, Part II: The Sample-Introduction System, Spectroscopy, 2001, 16, 56-60.
[98] R. Thomas, A Beginner's Guide to ICP-MS, Part III: The Plasma Source, Spectroscopy, 2001, 16, 26-30.

[99] R. Thomas, A Beginner's Guide to ICP-MS, Part IV: The Interface Region, Spectroscopy, 2001, 16, 31-34.
[100] R. Thomas, A Beginner's Guide to ICP-MS, Part V: The Ion Focusing System, Spectroscopy, 2001, 16, 38-44.
[101] R. Thomas, A Beginner's Guide to ICP-MS, Part VI: The Mass Analyzer, Spectroscopy, 2001, 16, 44-48.
[102] R. Thomas, A Beginner's Guide to ICP-MS, Part X: Detectors, Spectroscopy, 2002, 17, 34-39.
[103] R. Thomas, A Beginner's Guide to ICP-MS, Part XII: A Review of Interferences, Spectroscopy, 2002, 17, 24-31.
[104] R. Thomas, A Beginner's Guide to ICP-MS, Part IX: Mass Analyzers: Collision/Reaction Cell Technology, Spectroscopy, 2002, 17, 42-48.
[105] C. Stephan, K. Neubauer, Single Particle Inductively Coupled Plasma Mass Spectrometry: Understanding How and Why, Single Particle ICP-MS Compendium, Perkin Elmer, 2014, 7-11.
[106] M.D. Montaño, J.W. Olesik, A.G. Barber, K. Challis, J.F. Ranville, Single Particle ICP-MS: Advances toward routine analysis of nanomaterials, Analytical and Bioanalytical Chemistry, 2016, 408, 5053-5074.
[107] H.E. Pace, N.J. Rogers, C. Jarolimek, V.A. Coleman, C.P. Higgins, J.F. Ranville, Determining Transport Efficiency for the Purpose of Counting and Sizing Nanoparticles via Single Particle Inductively Coupled Plasma Mass Spectrometry, Analytical Chemistry, 2011, 83, 9361-9369.
[108] G. Cornelis, M. Hassellöv, A signal deconvolution method to discriminate smaller nanoparticles in single particle ICP-MS, Journal of Analytical Atomic Spectrometry, 2014, 29, 134-144.
[109] F. Laborda, E. Bolea, J. Jiménez-Lamana, Single Particle Inductively Coupled Plasma Mass Spectrometry: A Powerful Tool for Nanoanalysis, Analytical Chemistry, 2014, 86, 2270-2278.
[110] D. Mavrocordatos, W. Pronk, M. Boller, Analysis of environmental particles by atomic force microscopy, scanning and transmission electron microscopy, Water Science and Technology, 2004, 50, 9-18.
[111] M. Hassellöv, J.W. Readman, J.F. Ranville, K. Tiede, Nanoparticle analysis and characterization methodologies in environmental risk assessment of engineered nanoparticles, Ecotoxicology, 2008, 17, 344-361.

[112] B. Fultz, J.M. Howe, The TEM and Its Optics, Transmission Electron Microscopy and Diffractometry of Materials, Springer-Verlag Berlin Heidelberg, Berlin, 2013, 59-115.
[113] B. Fultz, J.M. Howe, Transmission Electron Microscopy and Diffractometry of Materials, 4 ed., Springer-Verlag Berlin Heidelberg, Berlin, 2013.
[114] A.T. Hubbard, The Handbook of Surface Imaging and Visualization, CRC Press, Boca Raton, 1995,
[115] D.B. Williams, C.B. Carter, High-Resolution TEM, Transmission Electron Microscopy: A Textbook for Materials Science, Springer US, Boston, MA, 2009, 483-509.
[116] R. Kleiner, D. Koelle, F. Ludwig, J. Clarke, Superconducting quantum interference devices: State of the art and applications, Proceedings of the IEEE, 2004, 92, 1534-1548.
[117] J. Clarke, A.I. Braginski, The SQUID Handbook: Fundamentals and Technology of SQUIDs and SQUID Systems, 2004.
[118] R. Bosisio, F. Giazotto, P. Solinas, Parasitic effects in superconducting quantum interference device-based radiation comb generators, Journal of Applied Physics, 2015, 118, 213904.
[119] P. Atkins, J.D. Paula, Spectroscopy: molecular rotations and vibrations, Elements of Physical Chemistry, Oxford University Press, Oxford, 2013, 477-502.
[120] K. Cammann (Hrsg.), Instrumentelle Analytische Chemie, 1 ed., Springer Spektrum, Heidelberg, 2000.
[121] I.A. Mudunkotuwa, A.A. Minshid, V.H. Grassian, ATR-FTIR spectroscopy as a tool to probe surface adsorption on nanoparticles at the liquid–solid interface in environmentally and biologically relevant media, Analyst, 2014, 139, 870-881.
[122] S. Lee, X. Bi, R.B. Reed, J.F. Ranville, P. Herckes, P. Westerhoff, Nanoparticle Size Detection Limits by Single Particle ICP-MS for 40 Elements, Environmental Science & Technology, 2014, 48, 10291-10300.
[123] B. Kim, C.-S. Park, M. Murayama, M.F. Hochella, Discovery and Characterization of Silver Sulfide Nanoparticles in Final Sewage Sludge Products, Environmental Science & Technology, 2010, 44, 7509-7514.
[124] P. Lodeiro, E.P. Achterberg, J. Pampín, A. Affatati, M.S. El-Shahawi, Silver nanoparticles coated with natural polysaccharides as models to study AgNP aggregation kinetics using UV-Visible spectrophotometry upon discharge in complex environments, Science of The Total Environment, 2016, 539, 7-16.
[125] W.Z. Teo, M. Pumera, Fate of silver nanoparticles in natural waters; integrative use of conventional and electrochemical analytical techniques, RSC Advances, 2014, 4, 5006-5011.

[126] C. Toncelli, K. Mylona, I. Kalantzi, A. Tsiola, P. Pitta, M. Tsapakis, S.A. Pergantis, Silver nanoparticles in seawater: A dynamic mass balance at part per trillion silver concentrations, Science of The Total Environment, 2017, 601-602, 15-21.